Available online at www.sciencedirect.com
SCIENCE DIRECT®
PROGRESS IN ENERGY AND COMBUSTION SCIENCE
ELSEVIER
Progress in Energy and Combustion Science 30 (2004) 545–672
www.elsevier.com/locate/pecs

Pulse detonation propulsion: challenges, current status, and future perspective

G.D. Roy[a,*], S.M. Frolov[b], A.A. Borisov[b], D.W. Netzer[c]

[a]*Office of Naval Research, Ballston Centre Tower 1, Arlington, VA 22217, USA*
[b]*N.N. Semenov Institute of Chemical Physics, Moscow, Russia*
[c]*Naval Postgraduate School, Monterey, CA, USA*

Received 1 April 2003; accepted 11 May 2004
Available online 27 September 2004

Abstract

The paper is focused on recent accomplishments in basic and applied research on pulse detonation engines (PDE) and various PDE design concepts. Current understanding of gas and sprary detonations, thermodynamic grounds for detonation-based propulsion, principles of practical implementation of the detonation-based thermodynamic cycle, and various operational constraints of PDEs are discussed.
© 2004 Published by Elsevier Ltd.

Keywords: Gaseous and heterogeneous detonation; Pulse detonation engine; Design concepts; Propulsion; Thrust performance

Contents

Abbreviations: AI, air inlet; BR, blockage ratio; CJ, Chapman-Jouguet; CS, cross-section; DC, detonation chamber; DDT, deflagration to detonation transition; FAM, fuel—air mixture (−); HE, high explosive; HP, hydrogen peroxide; IPN, isopropyl nitrate; IR, infra red; NM, nitromethane; ON, octane number; PDE, pulse detonation engine; PDRE, pulse detonation rocket engine; PLIF, particle laser induced fluorescence; RFBR, Russian Foundation for Basic Research; SMD, sauter mean diameter; SWACER, shock wave amplification through coherent energy release; TEP, thermochemical equilibrium program; TJE, turbojet engine; TNT, trinitrotoluene; ZND, Zel'dovich—Neumann—Doering; 1D, one-dimensional; 2D, two-dimensional; 3D, three-dimensional.

* Corresponding author. Tel.: +1-703-696-4406.

0360-1285/$ - see front matter © 2004 Published by Elsevier Ltd.
doi:10.1016/j.pecs.2004.05.001

1. Introduction

The current focus in utilizing detonation for air-breathing propulsion has moved from the long-term studies of the possibility of fuel energy transformation in stabilized oblique detonation waves to investigations and practical development of propulsion engines operating on propagating detonations in a pulse mode. Contrary to the oblique-detonation concept that is applicable to hypersonic flight at velocities comparable or higher than the Chapman-Jouguet (CJ) detonation velocity of the fuel–air mixture (FAM), the concept of pulse detonation engine (PDE) is attractive for both subsonic and supersonic flight with PDE as a main propulsion unit or as an afterburner in turbojet or turbofan propulsion system. In particular, PDE-based propulsion is attractive for flight Mach number up to about 3–4 (see Section 2.4). Within this range of Mach number, solid rocket motors are known to be very efficient in terms of simplicity and high-speed capability, but they have a limited powered range. Turbojet and turbofan engines, due to their high specific impulse, provide longer range and heavier payloads, but at flight Mach number exceeding 2–3 they are getting too expensive. Ramjets and ducted rockets designed for flight Mach number up to 4 require solid rocket boosters to accelerate them to the ramjet take over speed, which increases the complexity and volume of a propulsion system. Combined-cycle engines, such as turborockets or turboramjets, are also very complex and expensive for similar applications.

In a PDE, detonation is initiated in a tube that serves as the combustor. The detonation wave rapidly traverses the chamber resulting in a nearly constant-volume heat addition process that produces a high pressure in the combustor and provides the thrust. The operation of multitube PDE configurations at high detonation-initiation frequency (about 100 Hz and over) can produce a near-constant thrust. In general, the near-constant-volume operational cycle of PDE provides a higher thermodynamic efficiency as compared to the conventional constant-pressure (Brayton) cycle used in gas turbines and ramjets. The advantages of PDE for air-breathing propulsion are simplicity and easy scaling, reduced fuel consumption, and intrinsic capability of operation from zero approach stream velocity to high supersonic flight speeds.

The global interest in the development of PDE for propulsion has led to numerous studies on detonations, particularly pertaining to its control and confinement. This is evident from the formation of collaborative teams by universities and industry worldwide. Dedicated technical meetings and special minisymposia and sessions on PDE in combustion-related conferences are becoming very popular. Several reviews have been already presented at various meetings [1–10] and published in archival journals [11–13].

During the period from 1998 to 2002, the US Office of Naval Research (ONR) and the Russian Foundation for Basic Research (RFBR) have jointly sponsored three International colloquia on detonations, in particular, those aspects of detonations that are directly relevant to the development of PDEs. In 1998, the International Colloquium on Advances in Experimentation and Computation of Detonations was held in St Petersburg with the participation of more than 60

Nomenclature

a	transverse detonation cell size
a_1	transverse size of primary detonation cell
a_2	transverse size of secondary detonation cell
A	amplitude or coefficient
A_1, A_2, A_3	constants
b	longitudinal detonation cell size
b_2	longitudinal size of secondary detonation cell
B	coefficient
c	speed of sound
c_p	specific heat at constant pressure
c_v	specific heat at constant volume
C	capacitance
d	diameter
D	shock wave, detonation, or flame front velocity
D'	nonideal detonation velocity
e	internal energy
E_s	energy flux
E	energy or activation energy
f	frequency
F	cross-section area
h	enthalpy
h°	formation enthalpy
H	flight altitude or total enthalpy
H'	dimensionless fluctuation of enthalpy
g	acceleration of gravity
I_s	momentum flux
I	impulse
$\tilde{I}_{sp}$	cycle-averaged specific impulse
I^0	impulse at fully filled conditions
$\tilde{I}^0_{sp}$	specific impulse at fully filled conditions
J	number or dimensionless heat release
k, K	constants
k'	kinetic energy dissipation
K'	dimensionless fluctuation of internal energy
L	length
l	distance
m	mass or temperature exponent
m_c	HE charge mass
$\dot{m}$	mass flow
$\tilde{\dot{m}}$	cycle-averaged mass flow
M_s	mass flux
M	Mach number
n	reaction order
N	power
p	pressure
P	thrust
$\tilde{P}$	cycle-averaged thrust
q	heat release
Q	mass flow rate
r	radius
$\bar{r}$	dynamic radius
R	radius or gas constant
R°	universal gas constant
Re	Reynolds number
S	entropy
v	specific volume
t	time
T	temperature
u	velocity
U	voltage
w	velocity
W	work
We	Weber number
u'	velocity fluctuation
X	distance
x	coordinate
Y	height
y	coordinate

Greek Symbols

α	oxidizer-to-fuel ratio
α_ν	parameter in strong explosion theory
β	reaction progress variable
γ	specific heat ratio
Δ	interval
δ	function or width/height
δ_D	dimensionless velocity deficit
ε	parameter in detonation cell model
ζ	coefficient
η	dimensionless energy loss
ϑ	temperature ratio
θ	function
θ_{rot}	rotation angle
κ'	coefficient of pressure loss in shock wave
λ	dimensionless distance
μ	molecular weight
ν	geometrical factor
ν_i	stoichiometric coefficient
ξ	number or nitrogen dilution coefficient
π	compression ratio
$\tilde{\Pi}$	cycle-averaged specific thrust
ρ	density
ρ_l^0	liquid density
σ	density ratio or normalized deficit of detonation velocity
τ	time or dimensionless time
τ_w	shear stress
τ^+	dimensionless duration of positive overpressure
Φ	equivalence ratio
φ	function or cone/wedge angle
ϕ	dimensionless kinetic energy dissipation
χ	thermodynamic efficiency
υ	cone half-angle
ψ	molar fraction
Ω	transmissibility parameter

Indices			
A	additive	m	mechanical
av	average	max	maximum
b	back	min	minimum
CJ	Chapman-Jouguet	N_2	nitrogen
c	cycle	na	without additive
cd	cell disappearance	nz	nozzle
cl	closed	O_2	oxygen
cp	combustion products	OD	overdriven detonation
cr	critical	p	plateau
D	detonation	pg	purging
DC	detonation chamber	pr	pressure recovery
DDT	deflagration-to-detonation transition	R	ram
di	diffuser inlet	r	reaction
de	diffuser exit	ri	reinitiation
d	droplet	rz	reaction zone
e	expansion	s	shock wave
eff	effective	sp	specific
er	energy release	st	stoichiometric
ex	exhaust	tr	traversing
exp	measured	ua	unit area
f	flame or fuel	w	wall
fd	feed	z	along z-axis
fl	filling	ν	symmetry (1, 2, or 3)
fr	fresh reactants	Σ	total
hs	hot spot	∞	undisturbed
i	ignition	0	initial conditions
in	initiation	1	planar
ind	induction	2	cylindrical
l	limit	298	standard temperature
		3	spherical

experts. In 2000, the International Colloquium on Control of Detonation Processes was organized in Moscow with more than 100 participants. The International Colloquium on Advances in Confined Detonations was held in Moscow in 2002 with more than 120 participants. As a result of these meetings, a number of books have been published containing extended abstracts of all presentations [14–16] and full edited manuscripts of selected papers presented at the colloquia [17–19]. The goal of this review paper is to provide, based primarily on the materials presented at the meetings mentioned above, a text or reference for those who are interested in recent accomplishments in basic and applied research on PDE and numerous PDE design concepts presented in review meetings and discussed in the literature.

In order to use propagating detonations for propulsion and realize the PDE advantages mentioned above, a number of challenging fundamental and engineering problems has yet to be solved. These problems deal basically with low-cost achievement and control of successive detonations in a propulsion device. To ensure rapid development of a detonation wave within a short cycle time, one needs to apply (1) efficient liquid fuel injection and air supply systems to provide fast and nearly homogeneous mixing of the components in the detonation chamber (DC); (2) low-energy source for detonation initiation to provide fast and reliable detonation onset; (3) cooling technique for rapid, preferably recuperative, heat removal from the walls of DC to ensure stable operation and avoid premature ignition of FAM leading to detonation failure; (4) geometry of the combustion chamber to promote detonation initiation and propagation at lowest possible pressure loss and to ensure high operation frequency; and (5) control methodology that allows for adaptive, active control of the operation process to ensure optimal performance at variable flight conditions, while maintaining margin of stability. In addition to the fundamental issues dealing with the processes in the DC, there are other issues such as (6) efficient integration of PDE with inlets and nozzles to provide high performance; and (7) efficient coupling of DCs in a multitube PDE configuration. Among the most challenging engineering issues, is the problem of durability of the propulsion system. As the structural components of PDE are subject to repeated high-frequency shock loading and thermal deformations, a considerable wear and tear can be expected within a relatively short period of operation. The other problems are noise and vibration.

The paper is organized in such a way that the reader first gets acquainted with a brief history of detonation research (Section 2.1) and with the current understanding of gas and spray detonation properties and dynamics (Sections 2.2 and 2.3). Then, based on this material, thermodynamic grounds for detonation-based propulsion are discussed in Section 2.4, followed by the principles of practical implementation of the detonation-based thermodynamic cycle in Section 2.5. As the main focus of this paper is the utilization of PDE for propulsion, various performance parameters of PDEs (e.g. specific impulse, thrust, etc.) are discussed in Section 2.6. Based on the analysis of detonation properties and dynamics, and on the requirements for practical implementation of the pulse-detonation cycle, various operational constraints of PDEs are described in Section 2.7.

Section 3 provides the reader with a detailed description of various PDE design concepts, including valved and valveless approaches (Sections 3.2 and 3.3), predetonator concept (Section 3.4), design solutions utilizing enhanced deflagration-to-detonation transition (DDT) (Section 3.5), concepts applying stratified fuel distribution in the PDE combustion chamber (Section 3.6), or using two fuels of different detonability (Section 3.7), several novel PDE concepts emphasizing on detonation initiation issues (Sections 3.8–3.10), and the PDE concept applying strong reactive shocks rather than detonations (Section 3.11). The PDE concepts described in Sections 3.2–3.10 imply the use of ducted combustors, either in single-tube or multitube configuration. Some specific features of multitube PDE design are discussed in Section 3.12. Resonator concept of Section 3.13 is somewhat different as it utilizes the cavity-induced resonant flow oscillations in the combustion chamber. Problems of integrating inlets and nozzles to the PDE design are discussed in Sections 3.14 and 3.15. Some issues dealing with control of repeated detonations in a PDE are considered in Section 3.16. The last Section 3.17 briefly describes application of PDEs for rocket propulsion.

2. Fundamentals

2.1. Historical review

Early attempts to utilize the power obtained from explosions for propulsion applications date back to late 17th–early 18th centuries and the contributions of Huygens and Allen are noteworthy. In 1729, Allen proposed a jet propelled ship [20] 'whose operation is owing to the explosion of gunpowder' in a proper engine placed within a ship. Before this archival contribution, gunpowder was predominantly used in artillery for destructive purposes.

First exposure of gaseous detonations dates back to 1870–1883 period when Berthelot and Vieille [21–25], and Mallard and Le Chatelier [26,27] discovered a combustion mode propagating at a velocity ranging from 1.5 to 2.5 km/s. This combustion mode arose when gas was ignited with a high-explosive charge. Later on it was observed in long tubes even when gas was ignited by nonexplosive means (spark or open flame). In this case, flame acceleration along the tube, often accompanied with flame speed oscillations, was detected prior to onset of detonation. The most impressive findings of those times indicated that the detected detonation velocity was independent of the ignition source and tube diameter and was primarily a function of the explosive mixture composition. The main distinctive feature of detonation was a severe mechanical effect implying the development of a high pressure in the propagating wave. The mechanism of detonation propagation has been identified as governed by adiabatic compression of the explosive mixture rather than by molecular diffusion of heat. During those times, the interest in detonation was basically associated with explosion prevention in coal mines.

A few years later, based on the shock wave theory of Rankine [28] and Hugoniot [29], Mikhelson in 1890 [30,31], Chapman in 1899 [32], and Jouguet in 1904 [33,34] provided theoretical estimates for the detonation parameters based on one-dimensional (1D) flow considerations and mass, momentum and energy conservation laws. In their theory, the detonation wave was considered as a pressure discontinuity coupled with the reaction front (instantaneous reaction). According to the theory, the detonation products possess density that is almost two-fold higher than the initial mixture density; temperature and pressure that are, respectively, 10–20% and two-fold higher than the corresponding values of constant-volume explosion; particle velocity that attains a value close to one half of the detonation velocity. Comparison of the theoretical predictions with experimentally observed detonation velocities showed fairly good agreement.

Since the end of the 19th–the beginning of the 20th century, significant progress has been made both in experimentation and analysis of detonations. In addition to explosion safety issues in coal mines and pits, other applications surfaced, in particular, those dealing with new technologies, balloon transportation, and reciprocating internal combustion engines. After the World War I, there was a considerable growth of interest to combustion in automotive and aircraft engines. Worth mentioning are the early contributions of Dixon, Nernst, Crussard, Woodbury, Campbell, Bone, Frazer, Egerton, Payman, Laffite, Townsend, and Lewis in understanding the mechanism of detonation onset and propagation (see corresponding references in Refs. [35,36]).

Two principal conditions required for detonation onset were observed, namely, (i) formation of a shock wave of intensity sufficient for explosive mixture to autoignite, and (ii) increase in the local rate of energy release up to the level sufficient for shock wave reproduction in the adjacent layer of the explosive mixture. Mixture autoignition was often detected ahead of the accelerating flame giving rise to blast waves propagating downstream and upstream. The former blast wave was attributed to detonation and the latter was called retonation. Apart from gasdynamic models of detonation, there were attempts to develop models based on the molecular mechanism of energy transfer in

the detonation wave. Lewis applied the theory of chain-branching reactions developed by Hinshelwood [37] and Semenov [38] to put forward the chemical mechanism of detonation propagation. Within this model, the detonation wave propagates due to energy transfer from detonation products to the fresh mixture with active molecules possessing the energy sufficient for self-sustained reaction propagation. Detailed experimental studies of the effect of initial mixture pressure and temperature, as well as tube length and diameter on the run-up distance to detonation were reported. The existence of concentration limits of detonation was identified. In 1926, Campbell and Woodhead [39] have discovered the spinning detonation propagating at oscillatory velocity. This discovery initiated numerous studies of the detonation wave structure.

In this period, many researchers (Ricardo, Edgar, Campbell, Midgley, Boyd, Brown, Watkins, Dumanois, Pye, Serruys, Schnauffer, Sokolik, Voinov and others, see corresponding references in Ref. [40]) were involved in studies of combustion control in internal combustion engines. It has been observed that at elevated compression ratios piston engines exhibited a sharp decrease in the effective pressure and, as a result—decrease in engine power. The term 'knocking' in combustion comes from the fact that the mentioned decrease in engine power is accompanied by a characteristic ringing noise. As knocking combustion restricted the allowable compression ratio, there was much effort to study the mechanism of 'knock'. Ricardo [41] attributed this mode of combustion in the engine to pre-flame autoignition of the end-gas in the cylinder. In his interpretation, autoignition of the end-gas results in a sharp pressure rise and formation of a blast wave that, similar to hammer, hits cylinder walls. In 1930, Aubert and Duchene applied photographic method to study combustion phenomena in engines. In a knocking engine they detected high-speed luminous fronts propagating both into fresh mixture and into combustion products—phenomena resembling detonation onset in a tube with a characteristic retonation wave. In 1934, Sokolik [40] substantiated the idea of Nernst [42] that detonation in tubes and knock in internal combustion engines are essentially the same phenomena. His comparative analysis of available evidence of detonation and knock onset revealed that physical conditions for these phenomena are completely similar. Experimental observations of autoignition in the preflame zone [43] revealed the existence of exothermic centers that give rise to fast flames and shock waves resulting in flame flashback. Apparently due to technical reasons, most of studies dealing with knocking combustion in piston engines were aimed at searching for effective anti-knock chemicals to inhibit preflame autoignition [44].

A considerable progress in understanding detonation physics occurred during the 1940–1950 s period. Experiments indicating a possibility of spherical flame acceleration and transition to detonation (i.e. DDT) were reported by Rakipova et al. [45] and Zel'dovich and Roslovsky [46]. The first comprehensive publication in which observations of spherical detonations were thoroughly discussed was by Ferrie and Manson [47]. Schelkin [48] reported pioneering results on the effect of wall roughness on the DDT distance and time, as well as on the detonation propagation velocity. By using various wire spirals inserted into the detonation tube, he controlled the DDT distance and time within a wide range. Of particular importance was Shchelkin's finding that detonation can propagate at velocities considerably less than the thermodynamic CJ velocity.

In 1940, Zel'dovich [49] developed a theory of detonation wave structure and detonability limits. The keystone of his theory is the necessity of close coupling between the lead shock wave and the finite-rate combustion chemistry. The lead shock wave provides adiabatic compression and heating of the fresh explosive mixture. The compressed mixture autoignites after a certain induction period and a part of the energy released is consumed to support constant-speed propagation of the lead shock. According to the theory, the structure and velocity of a detonation wave propagating along the tube is affected by heat and momentum losses at the tube walls via variation of the chemical induction time and momentum and energy fluxes behind the lead shock. At a certain level of losses (governed by tube diameter, dilution ratio, etc.) steady-state propagation of the detonation wave becomes impossible, as the lead shock and the reaction zone tend to decouple from each other. Later on, von Neumann [50] and Doering [51] have independently put forward similar models of a detonation wave comprising a lead shock followed by the reaction front, taking into account the finite-rate chemistry. At present, this model is known as Zel'dovich–Neumann–Doering (ZND) model of detonation.

Based on the theory, a number of important results have been obtained in 1940–1950s. For example, it was proved theoretically in Refs. [52–54] that (i) there exist nonplanar (cylindrical or spherical) detonation waves propagating at the same constant velocity as planar detonations, (ii) the critical initiation energy of detonation is proportional to t_i^{ν} (where t_i is the reaction induction time behind the lead shock front and ν is the geometry index equal to 1, 2, and 3 for plane, cylindrical, and spherical waves, respectively), (iii) there exists a critical radius of the blast wave produced by the initiator at which its amplitude drops to the value corresponding to the CJ detonation, and this critical radius depends on the reaction rate and defines both the critical energy of the initiation source and the minimum size of a cloud which can support detonation. The ZND model allowed reasonable predictions of concentration limits of detonations as well as dependencies of the limiting tube diameter on initial pressure, temperature and dilution ratio (see review articles [55,56]).

Although the ZND model is physically well-based and is a very helpful idealization of a real detonation wave, later on it has been clearly demonstrated both experimentally and theoretically that a detonation is essentially three-dimensional (3D) and steady-state only on average. Voinov [57], based on detailed observations of spinning detonations, discovered transverse waves behind the lead shock front.

Voitsekhovsky [58] and Denisov and Troshin [59] have discovered the multihead detonation and analyzed the flow patterns at the triple wave configurations with transverse shock waves and reaction fronts arising at the detonation front and changes in the flow patterns upon collisions of these configurations. Instability of realistic detonation waves and their 3D structure raised serious questions concerning the validity of the Arrhenius kinetics with an average temperature in 1D ZND modeling of detonation initiation and propagation. Direct photographs and soot imprints [60–62] showed unequivocally the fish-scales like cellular structure not only of CJ detonations but of the initial detonation kernel, which meant that the mixture was actually ignited behind the shock front in hot spots where temperature is significantly higher than the average temperature.

Based on this understanding numerous models of single-head (spinning) and multihead detonations have been suggested since 1950s (see review articles [63,64]).

With the growing availability of diagnostics with improved temporal and spatial resolutions and powerful computing resources, the progress in the detonation science after the 1960s has been overwhelming. First of all, it became possible to visualize the ignition process behind a reflected shock wave and discover two different modes of shock-induced ignition of a reactive gas, namely, 'strong' and 'mild' ignition [65,66]. Violent volumetric ignition of shock-compressed gas in which no local fluctuations of the ignition delays were resolved by the photographic technique was termed strong ignition in contrast to mild ignition of the shock-compressed gas in clearly visible exothermic centers (hot spots) giving rise to an accelerating flame fronts that run up to detonation in some cases. It has been unambiguously demonstrated that it is strong ignition mode that is relevant to detonation. However, the ignition process still remains dependent on flow fluctuations even in this case. As experimental evidence shows [67] the ignition front behind the lead shock is quite irregular. This is supported by the well-known nonuniform pattern of soot prints of multihead detonations. An analysis in Ref. [68] shows that the driving mechanism of ignition delay fluctuations are gasdynamic pulsations of the flow parameters due to collisions of weak acoustic and quasi-acoustic waves traveling behind the shock wave front and affecting it (because of the subsonic nature of the flow behind the shock wave). Interestingly, these fluctuations show up even in overdriven waves in which the heat release is relatively very low (the temperature rise due to the reaction not exceeding 400 K [69].

Numerous theoretical works on 1D and two-dimensional (2D) analysis of detonation wave instability predict that virtually all waves with realistic reaction kinetics are unstable and develop a spinning or multihead structure [70–76].

In the series of elaborate photographic studies, Oppenheim et al. [62,77–79] revealed various scenarios of detonation onset during DDT in tubes with smooth walls. Fast ejection of flame tongues and detonation kernel formation near the accelerating flame brush, as a result of collision of flame-driven shock waves, and as a result of shock wave reflection at contact discontinuities and tube walls were visualized.

Flame acceleration, DDT, and detonation propagation in rough-walled tubes were first visualized by Babkin and Kozatchenko [80,81]. It has been shown that the structures of detonations in rough and smooth tubes can differ considerably. In a tube with rough walls, mixture ignition is facilitated by roughness elements due to high local temperatures behind reflected shock waves. One-dimensional model predicts that due to this fact, detonations in rough tubes should exhibit higher stability and wider concentration limits [55,56]. However, experimental observations [82,83] show somewhat narrower concentration limits of low-velocity regimes as compared to detonation in smooth tubes and quite large wave velocity fluctuations and recovery of a detonation wave upon its entry from a rough tube into a smooth tube occurs within still narrower limits. This is evidently attributable to an essentially multidimensional nature of the reactive waves in rough tubes.

One of the questions of practical importance is, how a detonation wave originated in a narrow tube behaves when it enters a tube of a larger volume or unconfined mixture? The answer to this question should provide information about optimal ways of detonation initiation in large volumes, because a mixture in a narrow duct can be initiated much easier than in wide ones. Transition of detonation waves from narrow to wide ducts has been systematically studied by a number of investigators, starting as early as in 1956 [54]. Visualization of detonation transmission from a channel into an unconfined volume was probably first made by Mitrofanov and Soloukhin [84] in 1964.

Extensive experimental data on detonability of various fuels has been provided by research groups from all over the world [64,85–88]. Based on well-documented experimental data on detonation initiation, propagation and transition, several important empirical criteria have been extracted. The characteristic size in the fish-scales like structure of realistic detonation waves, referred to as the detonation cell size, was found to be a representative parameter to qualitatively grade detonability of the mixture: the larger the cell size the less sensitive is the mixture. The cell size was found to be a function of the initial pressure, temperature, mixture composition and tube diameter. The cell size was proved to be directly relevant to detonation transition from a channel to an unconfined volume [64], to the limiting tube diameter [89], and to the critical energy of detonation initiation [90].

Detonations in heterogeneous media containing gaseous oxidizer and liquid fuel spray or film, or solid fuel suspension is a topic of growing interest since the 1950s in view of industrial safety and military applications. Detonations in such media were extensively studied both experimentally [91] and theoretically [92]. It has been found that detonability of heterogeneous mixtures depends significantly on the fuel vapor concentration, in particular, for heavy hydrocarbon fuels.

A considerable progress has been made in understanding the mechanism of detonation initiation in the course of flame development. Two principal concepts are worth mentioning: Oppenheim's concept of predetonation point explosions giving rise to detonation 'bubbles' [62], and the Zel'dovich 'gradient' mechanism of detonation onset [93]. Somewhat of a mixed concept (shock wave amplification through coherent energy release (SWACER)) has been put forward by Lee and co-workers [94]. The Oppenheim's concept implies that, at attaining the autoignition conditions, shock-compressed gas explodes in several exothermic centers resulting in generation of spherical blast waves. Collision of the blast waves results in the onset of detonation kernels that give rise to detonation. Zel'dovich's gradient mechanism implies that self-ignition of shock-compressed gas, starting at location with the minimum ignition delay, then moves towards the locations with longer ignition delays (i.e. along the vector of ignition delay gradient). As the apparent velocity of the 'self-ignition wave' approaches the characteristic gasdynamic velocity (e.g. local speed of sound), a shock wave is formed in the compressible reactive mixture followed by spontaneous coupling of the shock with exothermic reaction and eventual transition to detonation. SWACER concept implies that localized microexplosion in the shock-compressed mixture gives rise to a blast wave (like in the Oppenheim's concept) that is further amplified according to the gradient mechanism. All these concepts differ only at first glance. Indeed, the detonation onset in the detonation kernels should essentially be based on Zel'dovich's mechanism of coupling between the compression wave and exothermic reaction, otherwise flame would never accelerate to velocities sufficient to drive a shock wave capable of self-igniting the mixture with delays inherent in detonation waves. On the other hand, as experiment shows, incipience of detonation waves never occurs throughout the whole mixture volume, thus supporting the idea of hot spot self-ignition. Thus, all the concepts are based on considering 'microexplosion(s)' in the exothermic center(s) formed in the shock-compressed gas. Zel'dovich's concept is less formal than the others because it includes the evolution of reaction inside the exothermic center, provides a complete physical explanation of the hot spot development and clear criteria for detonation origination, thus avoiding speculations on the strength of the blast wave produced by 'microexplosion'.

Historically, the two fundamental modes of combustion, namely flame and detonation, have found a wide variety of applications in human activities. It is a slow flame that has been extensively utilized in propulsion, power engineering, material science, and chemical technology, while detonations were used basically for military purposes. As the knowledge in detonation physics and chemistry is continuously advancing, one inevitably arrives at the time when this knowledge is to be used for constructive purposes as well to help humanity at large. Detonation is a very attractive phenomenon from the viewpoint of the thermodynamic efficiency of chemical energy conversion into thermal and kinetic energy. Once this advantage of detonation is capitalized properly, considerable benefits are expected to be achieved in terms of fuel consumption, manufacturing and operational costs, pollutant emissions, etc. It is the authors' profound belief that the existing knowledge and the on-going research will lead to the solutions of this challenging problem.

2.2. Gaseous detonations

2.2.1. General properties

In this section, steady reaction waves propagating at supersonic velocities are considered. This is necessary to understand the kind of unsteady regimes that can be anticipated in combustible mixtures. Steady-state analysis of gasdynamic equations, which predicts only restricted ranges of reaction wave velocities seems to be inconsistent with the experimental evidence of reactive waves propagation at any velocity between those of detonation and normal-flame. This contradiction is eliminated assuming that the observed waves that do not obey the steady equations are unsteady reactive waves (or quasi-detonations). Interestingly, the reaction zone velocity relative to the fluid immediately ahead of it never exceeds (even in unsteady waves) the maximum found from the slope of the Rayleigh line (actually Rayleigh–Michelson line [35,36], to give a tribute of respect to Michelson, who pioneered in the detonation theory [30,31]) tangent to the lower branch of the Hugoniot curve plotted for the initial state corresponding to the gas compressed in the precursor shock wave.

For applications, the dependence of detonation parameters on the initial conditions and their sensitiveness to the mixture equivalence ratio are of importance. Normally, this dependence is bell-shaped descending both towards lean and rich mixtures, except for hydrogen mixtures where the detonation velocity keeps rising far into the region of rich mixtures.

In homogeneous hydrocarbon–air mixtures, the detonation velocities peak in slightly rich mixtures. The maximum detonation velocity is attained in air mixtures with the equivalence ratio $\Phi \approx 1.2$ for saturated hydrocarbons, and $\Phi \approx 1.3$ for unsaturated hydrocarbons.

Fig. 1 shows the predicted dependencies of the detonation velocity D_{CJ} (*a*), temperature of detonation products T_{CJ} (*b*), dimensionless pressure of detonation products p_{CJ}/p_0 (*c*), and molecular mass of detonation products μ_{CJ} (*d*) on molar fraction of fuel in gaseous *iso*-octane–air (solid curve) and *n*-heptane-air (dashed curve) mixtures, calculated by using thermodynamic code SAFETY [95]. Here, indices 0 and CJ label quantities ahead of the detonation front and at the CJ plane, respectively. The dependencies of detonation velocity, temperature and pressure exhibit a characteristic bell shape, attaining detonability limits on both sides from the stoichiometric composition. *n*-Heptane and *iso*-octane mixtures show very similar properties.

Fig. 2 shows the calculated dependencies of the detonation velocity D_{CJ} (*a*), temperature T_{CJ} (*b*), dimensionless

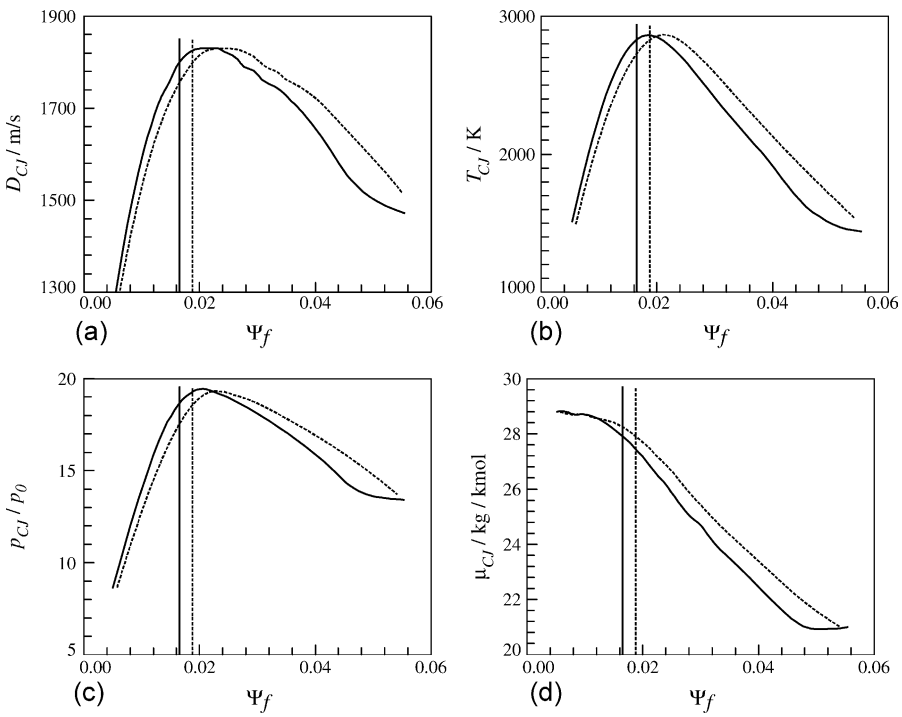

Fig. 1. Predicted dependencies of (a) detonation velocity D_{CJ}, (b) temperature T_{CJ}, (c) dimensionless pressure p_{CJ}/p_0, and (d) molecular mass μ_{CJ} of detonation products on fuel molar fraction in gaseous *iso*-octane–air (solid curves) and *n*-heptane–air (dashed curves) mixtures [95]. Vertical lines correspond to stoichiometric fuel molar fraction $\psi_{f,st}$.

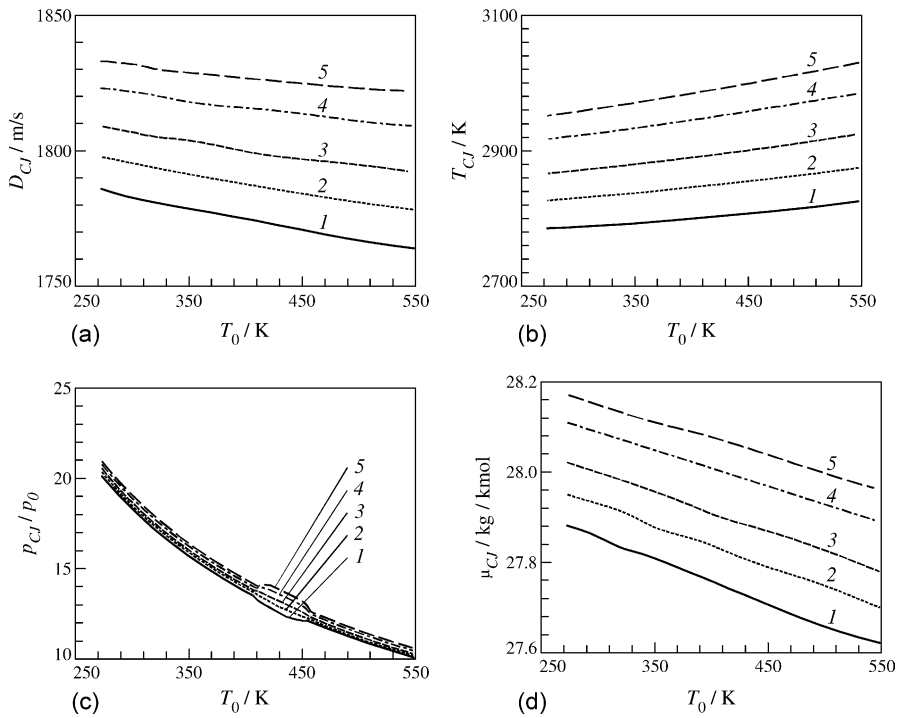

Fig. 2. Calculated dependencies of (a) detonation velocity D_{CJ}, (b) temperature T_{CJ}, (c) dimensionless pressure p_{CJ}/p_0, and (d) molecular mass of detonation products μ_{CJ} on the initial temperature and pressure for stoichiometric *iso*-octane–air mixture [95]; 1—$p_0 = 0.5$ atm, 2—1.0, 3—2.0, 4—5.0, and 5—10.0 atm.

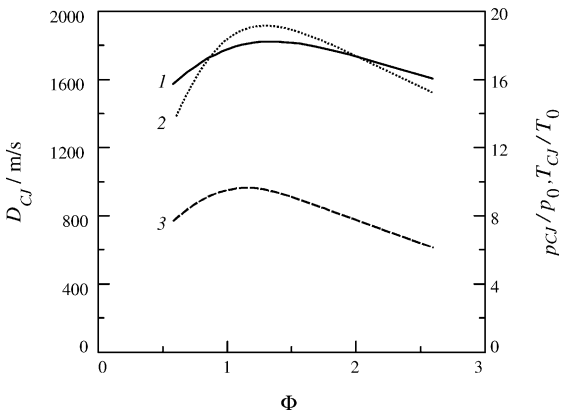

Fig. 3. Detonation properties of homogeneous JP-10-air mixture obtained by using thermodynamic code TEP [96,97]; 1—D_{CJ}, 2—p_{CJ}/p_0, 3—T_{CJ}/T_0.

pressure p_{CJ}/p_0 (*c*), and molecular mass μ_{CJ} (*d*) on the initial temperature T_0 and pressure p_0 of a stoichiometric homogeneous *iso*-octane–air mixture [95]. The effect of the initial temperature on the detonation velocity is insignificant (Fig. 2a). According to elementary considerations, the initial internal energy is just added to the reaction heat and an increase in the initial temperature should slightly increase the detonation velocity. However, the actual influence of the initial temperature on the detonation velocity is more complex since due to dissociation the reaction heat drops as the final temperature in the products rises. This partly compensates for the initial energy increase, so that the detonation velocity is virtually independent of the initial temperature. In line with this logic, the temperature of detonation products increases only slightly with the initial temperature (Fig. 2b). An important parameter such as the detonation pressure (Fig. 2c) decreases with temperature because the pressure ratio is proportional to the initial fluid density. Due to dissociation, the molecular mass of detonation products decreases, however, insignificantly.

At the low end, the initial pressure should not affect the detonation velocity, but at higher pressures the equilibrium in the reaction products is shifted towards polyatomic molecules, which lie at lower energy levels. Hence, reduced dissociation of the products increases slightly the detonation velocity (Fig. 2a), temperature (Fig. 2b), and molecular mass (Fig. 2d). Dimensionless detonation pressure is almost insensitive to the initial pressure (Fig. 2c). It should be noted that at very low initial pressures the detonation parameters are affected by losses to the walls of even quite wide tubes (this effect is not taken into account in thermodynamic calculations of Fig. 2). All the features of Fig. 2 are confirmed by the measurements and are typical for detonations of high hydrocarbons.

As JP-10 is considered as one of prospective fuels for PDE applications, Fig. 3 shows the calculated detonation properties of homogeneous JP-10–air mixture [96] that are very similar to those presented in Fig. 1. The properties presented in Fig. 3 were obtained by using thermochemical equilibrium code TEP [97] which does

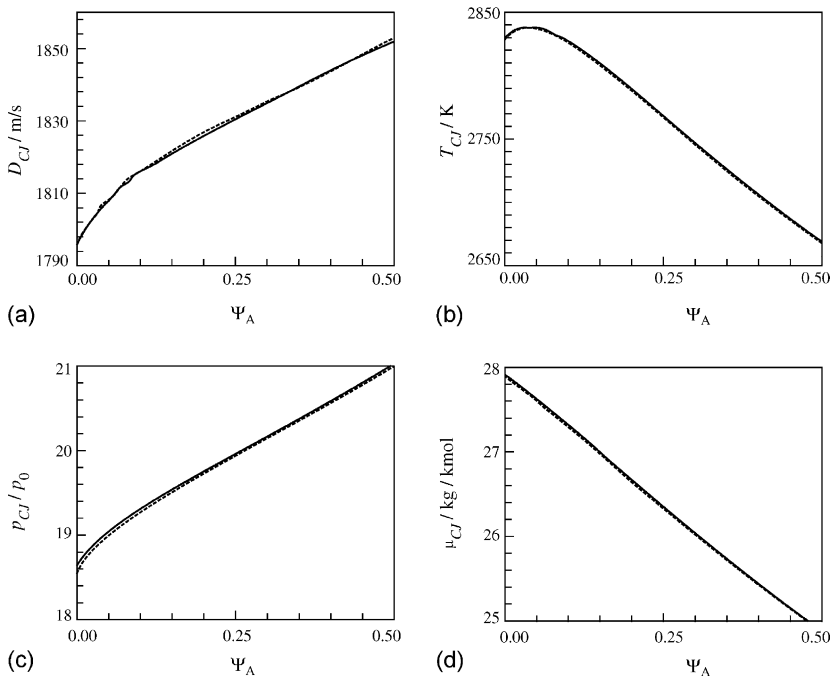

Fig. 4. Predicted dependencies of (a) detonation velocity D_{CJ}, (b) temperature T_{CJ}, (c) dimensionless pressure p_{CJ}/p_0, and (d) molecular mass μ_{CJ} of detonation products on the molar fraction of HP vapor ψ_A admixed to the stoichiometric homogeneous *iso*-octane–air (solid curves) and *n*-heptane–air (dashed curves) mixtures [95].

not account for finite-rate chemical kinetics and assumes that all of the fuel is in a vaporized state.

Of importance is the effect of relatively small fuel additives (up to 20%) on the detonation parameters. It is anticipated that small additives can hardly influence the characteristics of steady CJ detonation waves. Indeed, thermodynamic calculations performed in Ref. [95] for the *iso*-octane–air and *n*-heptane–air mixtures with admixed hydrogen peroxide (HP) vapor (see Fig. 4) reveal a weak dependence of detonation velocity (Fig. 4a), as well as temperature (Fig. 4b), pressure (Fig. 4c), and molecular mass (Fig. 4d) of detonation products on the molar fraction of the additive, ψ_A.

A great body of the experimental data on detonation parameters reveals that, for overwhelming majority of mixtures and shapes of charges, the measured wave velocities and pressures are fairly well consistent with the ideal thermodynamic calculations. It should be emphasized that recorded pressure profiles exhibit intense oscillations and, therefore, a comparison of calculations with experiment in this case is often uncertain to a large extent.

Usually, in compliance with the thermal theory of detonation limits [98], deviations of the measured detonation wave velocities in mixtures with Arrhenius reaction kinetics from those calculated do not exceed about 10% even for marginal detonations. However, there are exceptions for special types of detonations heavily affected by energy and momentum losses in which heat release kinetics senses only little variations of the gas parameters. These waves require special consideration (see Section 2.2.5).

Detonation parameters that are measured involving (intrinsically) integration over the duct cross-section (such as density measured by absorption of X-rays) exhibit profiles subject to less pronounced oscillations [99]. The averaged density at the end of the zone where the reaction keeps going and transverse waves are still intense is indeed consistent with thermodynamic calculations. Recent detailed measurements of temperature and pressure histories behind a detonation front [100], using advanced laser diagnostics, revealed that trends in measurements agree with simulations [101] although certain discrepancies in the profiles are apparent (Fig. 5).

This certainly makes the 1D ZND theory very useful even though it does not adequately describe peculiarities of the detonation wave structure. There are several reasons for the detonation parameters to deviate from ideal thermodynamic calculations: wave instability, incomplete reaction at the sonic (CJ) plane (if it exists in multidimensional waves), and momentum and energy losses. Therefore, a reasonably good agreement between the calculated and measured detonation parameters is observed only in long ducts of a diameter exceeding the limiting value. At short distances from the initiator (of about 1 or 2 m) and in narrow ducts, the deviations can be quite significant as obvious even from 1D calculations with finite reaction kinetics.

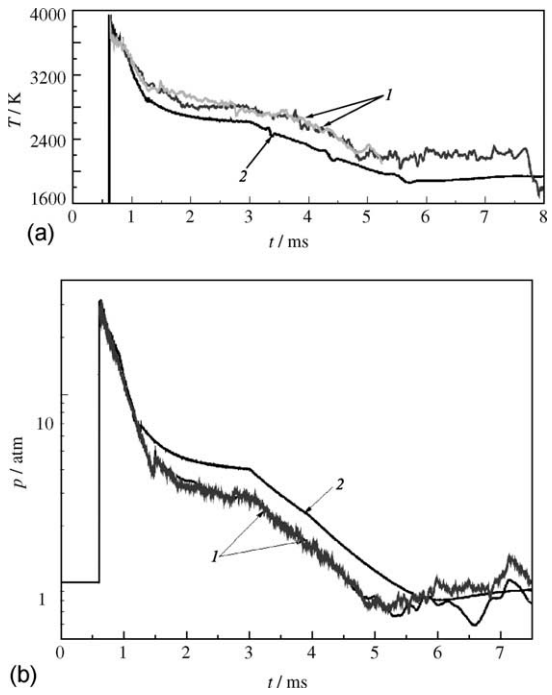

Fig. 5. Measured 1 [100] and computed 2 [101] gas temperatures (a) and pressures (b) for detonation of stoichiometric C_2H_4–O_2 mixture at normal conditions. Peaks on temperature and pressure curves correspond to CJ conditions: $T_{CJ} = 3937$ K and $p_{CJ} = 33.3$ atm, respectively.

One of the most important features of detonation waves in homogeneous mixtures is the instability that results in their essentially 3D and unsteady nature. A major feature of detonation wave propagation is shown in Fig. 6a and b. Fig. 6a shows a typical footprint of detonation on the sooted foil mounted on the tube wall [102], Fig. 6b [103] in terms of a series of pressure maps at evenly spaced intervals. The connection of the paths of triple points produces the cellular structure that has become a characteristic feature of gaseous detonations. The dimensions of the cellular structure—longitudinal size *b* and transverse size *a*—are related to the properties of the material and the chemical reaction mechanism. Long chemical reaction times or induction times correlate with large detonation cells.

The structure of most propagating detonations is usually much more complex than that shown in Fig. 6, sometimes there are substructures within a detonation cell, and sometimes the structures are very irregular. Moreover, some detonations exhibit essentially 3D structure [104]. In Ref. [104], detailed measurements of the detonation structure in a square-section tube were made. The schematics of transverse motion of front shocks in cases of 2D and 3D detonation structures are shown, respectively, in Fig. 7a and b.

Modeling of detonation waves initiated and propagating in real combustion chambers is an efficient method for

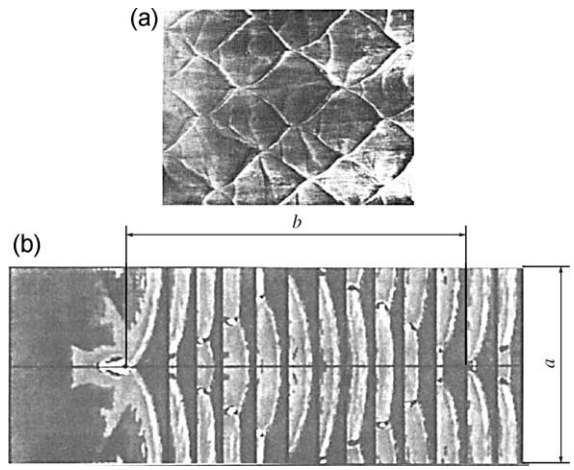

Fig. 6. (a) Soot footprint of $2CO + O_2$ detonation [102]. (b) Computed sequence of pressure contours from a computation of a detonation cell for a mixture of H_2:O_2:Ar/2:1:7. The cell length b is about 77 mm and the ratio of the width a to the length of the cell, $a/b \approx 0.61$. The computed detonation velocity is 1623 m/s (CJ velocity is 1619 m/s). The black lines superimposed on the contours trace the paths of the triple points [103].

optimizing the performance of a propulsion device. Taking into account the realistic detonation (or reactive shock) structure in modeling codes would necessitate prohibitively fine 3D computational grids, normal simulations are not attempted to resolve the fine wave structure, yielding parameters averaged over the spatial computational cells. In order to understand how adequate the simulation results are, consider the wave parameters averaged over the coordinate normal to the wave propagation direction (analog of the 1D ZND model).

Most of the measurements with detonation waves, except those intended to study their structure, are performed treating them as a 1D phenomenon. It is necessary to know what correspondence these measurements have in relation to the averaged parameters in detonation waves. Below, one of the feasible models is considered that is general enough to be capable of explaining the physical meaning of averaged measured detonation parameters and their behavior in time behind the detonation front. It is a good supplement to any numerical solution of 3D or 2D detonation problems since unlike numerical results, this approach provides the means of easy access to the general properties of detonation waves.

Following Voitsekhovsky et al. [105], assume that the flow behind the detonation front can be represented by 'turbulent' motion including pressure, density, entropy, and velocity fluctuations, which is specified by some averaged fluctuation parameters and by the averaged unidirectional flow. Since this formulation of the problem remains 1D (no lateral flux of mass, momentum and energy) one can write the conservation equations in the following form:

$$D/v_0 = M_s$$

$$p_0 + D^2/v_0 = I_s$$

$$(D/v_0)(h_0 + D^2/2) = E_s$$

where v is the specific volume, h is the enthalpy, M_s, I_s, and E_s are, respectively, the mass, momentum, and energy fluxes averaged over the tube cross-section. The detonation wave is assumed to propagate along the z-axis and integration is performed over the flow cross-section. As a steady detonation wave is considered, the integrands are time independent (which implies that they are averaged over some time which is much longer than the characteristic pulsation time equal to b/D).

To make the equations more convenient for further qualitative analysis they are presented in the form:

$$D/v_0 = u_{z,av}/v_{av}$$

$$p_0 + D^2/v_0 = p_{av} + (u^2_{z,av}/v_{av})(1 + K')$$

$$[\gamma/(\gamma - 1)]p_{av}v_{av} + D^2/2 = [\gamma/(\gamma - 1)]p_0v_0 + u^2_{z,av}/2 - [q(1 - \beta) - H']$$

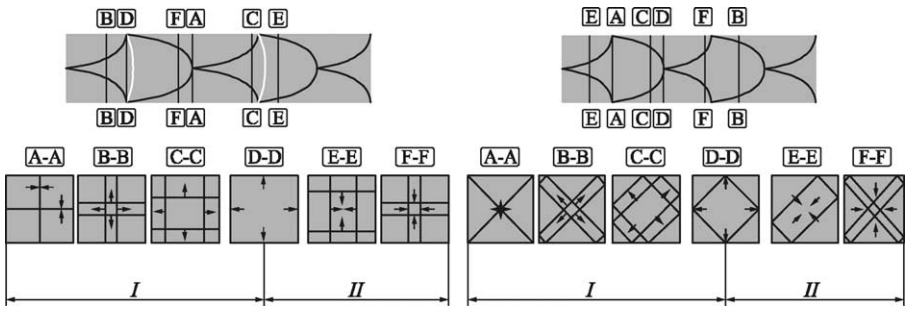

Fig. 7. Schematic diagram of the front shocks at different locations of the cycle of the detonation cell [104]. (a) The case represented here is 'in phase' (rectangular type). The arrows show the motion of the four triple point lines generating the central octahedron faces. I—development of Mach stem inside the central octahedron, II—development of incident wave inside the central octahedron. (b) The case represented here exhibits no slapping waves (diagonal type) and the shocks are canted at an angle of 45° to the tube wall. The arrows show the motion of the four out of eight triple point lines generating the central octahedron faces. For clarity, the motion of the other four triple point lines is not shown. I—development of Mach stem inside the central octahedron, II—development of incident wave inside the central octahedron.

Here, $K' = u'^2_{av}/u^2_{z,av}$ and H' are the fluctuations of kinetic energy and enthalpy, respectively, u' is the velocity fluctuation, β is the reaction progress variable, and γ is the ratio of specific heats, subscript 'av' signifies averaging.

The Rayleigh–Michelson line in this case is no longer a straight line because it depends on K', and the Hugoniot has in general a usual shape, although it depends on both K' and H'. Thus, the governing equations differ from the conventional ZND ones by the presence of K' and H', which characterize the momentum and energy fractions contained in the fluctuations. Both the Hugoniot and the Rayleigh–Michelson lines depict not only the final state but intermediate ones as well, for each state there exist its own values of β, K', and H'. These three quantities vary more or less independently since they characterize different processes (chemical reaction, mechanical equilibration, and mixing of the gases). Although K' and H' seem to be interdependent, their variation with departure from the lead front (or leading control surface) may differ. Unfortunately, at present it is inexpedient even to try to specify their dependence on the distance from the lead front, because this would necessitate the exact solution of the 3D unsteady problem. The only thing which is definite about these quantities is that all of them vanish as the system approaches equilibrium (but certainly at different rates).

The only curves, which one can plot in the p/p_0 vs. v/v_0 diagram, are the planar-shock and final-detonation Hugoniots. The shock Hugoniot does not represent any real state since it is never reached, because within the framework of the averaged approach the curved lead fronts (as in Fig. 6), first, spread the discontinuity in space, and, second, start locally the reaction virtually at the instant when the first portions of the lead front touch the control surface, i.e. K', 1-β, and H' are finite from the very beginning. An analysis of the equations shows that the fluid keeps gaining some energy (either from the reaction or, which is much more likely, due to conversion of the excess kinetic and thermal energy of fluctuations into average internal energy and kinetic energy of the unidirectional flow) downstream of the averaged CJ plane. Since this heat deposition occurs in the supersonic region of the steady flow it chokes partially the flow and should generate a compression wave in it.

It follows from the above considerations that real multifront detonations propagating in tubes may be treated on average as plane ones but one has to take into account the peculiarities of the energy evolution profiles which now should also include various types of energy and momentum conversions in the flow. Both experiment and numerical calculations [106,107] show that there is some unburnt mixture that escapes the zone attended by strong pressure waves, thus burning of these mixture pockets (although small in the volume fraction) downstream of the CJ plane must also be taken into account. Characteristic of multifront detonations, treated as 1D waves, are low parameters at the lead shock front (von Neumann spike). The effect of transverse waves and spatial inhomogeneity of multifront detonations may result in both lower and higher detonation velocities as compared to the plane CJ state depending on the ratio of the equilibration rates for all the three major components governing interconversions of the momentum and energy within the zone between the lead front and the effective CJ plane, where mean flow velocity is sonic.

The above qualitative model allows one to explain experimental observations [99] that seemed to be somewhat surprising (Fig. 8). The first observation (see Fig. 8a) is the averaged-density variation behind the detonation front. Numerous measurements of X-ray absorption by heavy noble gases (Xe or Kr) revealed the following characteristic features of the density profiles: (i) the density everywhere behind the lead shock front (peak marked 1) is significantly lower than that predicted for the von Neumann spike, ρ_s, (ii) the minimum density (between peaks marked 1 and 2) is always slightly below (10–15%) the ideal CJ value, ρ_{CJ}, and (iii) after the minimum, the density grows

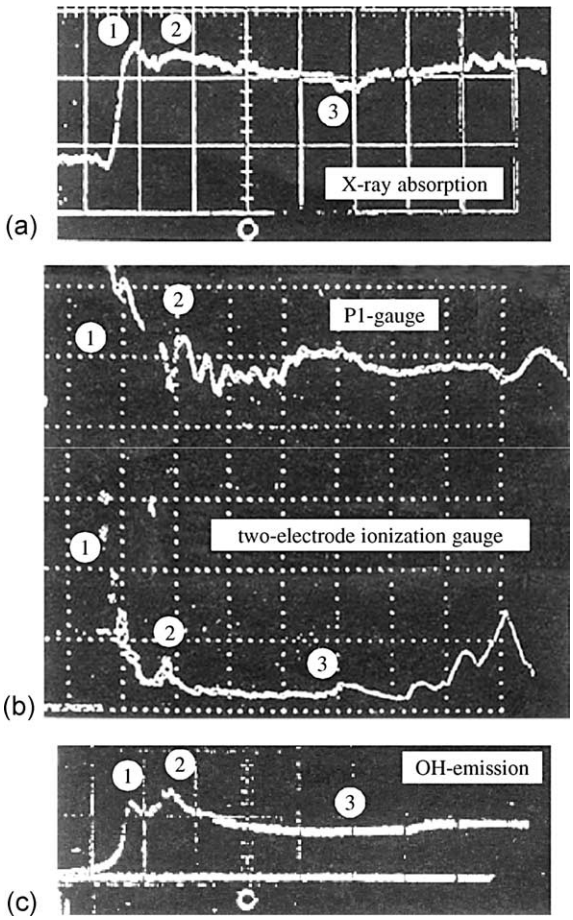

Fig. 8. Records of X-ray absorption (a), pressure and ionization current (b), and OH-emission (c) behind a detonation wave in 6% propane + 30% O_2 + 29% N_2 + 35% Kr mixture; $D = 1569$ m/s, the longitudinal cell size $b = 20–25$ mm [99]. Time interval between peaks 1 and 2 (14–18 μs) characterizes the maximum duration of chemical energy deposition behind the detonation wave.

slightly again (peak marked 2) and then decays in the Taylor rarefaction wave. The farther away is the detonation wave from the spinning mode the less pronounced is the von Neumann spike.

The second observation concerns the averaged pressure (see Fig. 8b, upper beam). It should be noted that the pressure fluctuations are more pronounced therefore the accuracy with which the average profile is drawn is less satisfactory, but nevertheless, the pressure recorded within the von Neumann spike (marked 1) is definitely lower than that predicted by the ZND model and the minimum pressure (marked 2) is 10–15% lower than the ideal CJ pressure, p_{CJ}. Thus, the two types of measurements ascribe unequivocally the real detonation wave to the weak (underdriven) branch of the equilibrium Hugoniot. This behavior finds a simple explanation within the framework of the above model.

Furthermore, measurements of the ionization current and the OH emission (Fig. 8b, lower beam, and Fig. 8c), as well as recent PLIF measurements [108] (Fig. 9) are also consistent with the above model.

Indeed, the model states that the major chemical reaction is completed within a zone which is smaller than the cell size, and in conformity with this, both the OH emission and the ionization current peak at the very beginning of the cell size thus indicating that the reaction rate passed its maximum. It is worth noting that OH emission is most likely due to the recombination of O and H atoms and the ionization, although close to the thermal one, still can be influenced by chemi-ionization within the zone with intense chemical reaction. That is why it is believed that the first peaks (marked 1) in Fig. 8b (low beam) and c reflect the behavior of the chemical reaction. The next peaks (marked 2) that are present in all the signals are presumably due to the collision of the tails of the transverse waves behind the reaction zone. This collision raises the temperature of the reaction products to a very high value, which increases the thermal luminosity and the ionization. Hence, the time interval between the peaks (14–18 μs in Fig. 8b and c)

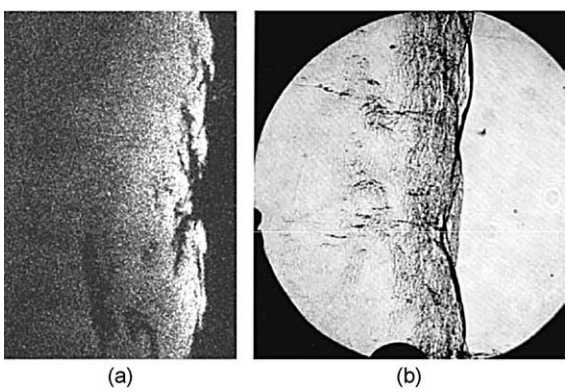

Fig. 9. OH PLIF (a) and Schlieren (b) images in H_2–N_2O–$3N_2$ mixture at initial pressure 20 kPa [108]. Chemical activity nearly ceases at a distance of about one detonation cell size.

characterizes approximately the maximum duration of chemical energy deposition behind the detonation front. In terms of distance, this is the time representative of the longitudinal detonation cell size b.

Purely gasdynamic studies of the effective sonic plane [64], indicate that the CJ plane is positioned at a distance of several cell sizes from the lead shock front. The effective CJ plane is defined as a site where either the attached oblique shock wave at a sharp wedge, over which a detonation wave propagated started to depart from the tip, or as a cross-section in a tube covered with a thin film (destroyed by the detonation wave) at which the lateral rarefaction wave ceased to affect the detonation wave velocity.

It is remarkable that the third rise in the density signal in Fig. 8a (marked 3) also coincides with analogous rises (also marked 3) in all the signals, which means that this rise is accompanied by an increase in the average internal energy of the reaction products, i.e. it signifies an effective energy gain. This energy gain was discussed in the above model. The possibility of detonation wave velocities higher or lower than D_{CJ} predicted by the model is also confirmed by experiment.

Thus, in spite of a very qualitative treatment of the problem in the model, it provides quite reasonable and logical explanations of many experimental findings. The weakest point of the model is the relative rates of change of longitudinal, b, or transverse, a, cell size and D, since it just states that they may vary, but not specifying how. Since this variation is very important for the structure of detonation waves, the model calls for further development. Probably the measurements of the average parameters behind the detonation waves will help one to specify these rates and ascribe them to one or another hydrodynamic or chemical processes.

The marginal spinning detonations are known to show good consistency with the acoustic modes in the detonation products [109,110]. It is expedient to note that not only spinning detonation exhibits such a consistency, but the real multifront detonations show also a resonance behavior with the higher acoustic modes. This is not surprising because as in spinning modes, finite-amplitude waves in the products generated by the transverse waves near the lead front degenerate very rapidly into acoustic or quasi-acoustic ones because of the high (as compared to the transverse wave) velocity of sound in the products. Moreover, the shock waves in the products dissipate their energy at a high rate just by transferring it to dissociation of the highly heated gas and thus approach rapidly the acoustic velocity. Experimental photographs show quite clearly that the waves in the products can propagate at a velocity slightly higher than the acoustic one only near the detonation front, further downstream they rapidly are converted into the conventional acoustic modes. Thus the close coupling between the two types of waves supporting each other is inherent in all detonation waves.

From the aforesaid, it may be inferred that although the average chemical reaction time certainly affects directly

both the detonation cell size and the distance between the lead shock front and the effective CJ plane, the relation between these characteristic parameters is not unique. The only definite statement that can be made at this stage of our knowledge of the process is the relative order of the magnitudes of these times: the average length of the chemical reaction zone is less than the detonation cell size, while the separation of the lead shock wave and the average CJ plane is longer than the cell size. It should be, however, noted that the maximum (local) energy conversion zone (meaningful for the ZND model) size can be commensurate with the cell size.

Since the cell size a (or b) as the most readily measurable quantity is often used as the kinetic characteristic of both the reaction zone length ($L_{rz} = k_1 a$) and the CJ plane position ($L_{CJ} = k_2 a$), it should be emphasized that the proportionality coefficients k_1 and k_2 are functions of many parameters and therefore the relations which are derived for a restricted number of mixtures are applicable only to them and not necessarily should hold for other mixtures. This can be illustrated, for example, by the dependence of transverse cell size a on the reciprocal temperature at the lead shock front, T_s. A typical Arrhenius plot of a is shown in Fig. 10, from which it is obvious that unlike the ignition delays the cell size a exhibits a definitely nonArrhenius behavior with a too high effective activation energy in multihead detonation waves and too low energy when only few heads are present in the front. Hence the exact relations between the cell size a, reaction zone length L_{rz}, and the physical detonation front thickness L_{CJ} (that is the zone where a detonation wave is vulnerable to any external perturbations) still await more sophisticated and detailed numerical and analytical studies.

After analyzing steady-state modes of propagation of supersonic reaction waves one may formulate the definition of detonations in order to distinguish them from other regimes. When defining detonation it is appropriate to proceed essentially from the ZND model since despite over-idealization of the process it nevertheless reflects all its

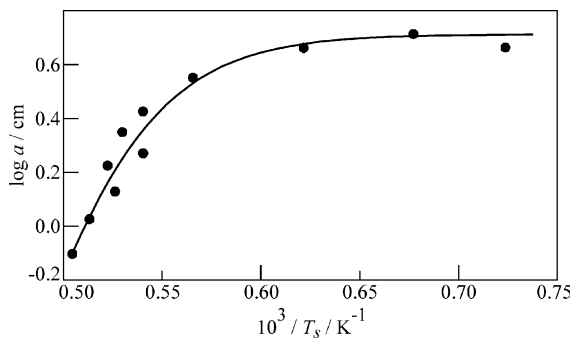

Fig. 10. Arrhenius plot of the transverse size a of the detonation cell in propane–oxygen mixtures diluted by various amounts of nitrogen and krypton at normal initial pressure and temperature [99]. T_s is the post-shock temperature.

principal features. That is why it is still used almost without any modifications by the specialists. Thus, it is expedient to apply the term detonations to supersonic reactive waves in which the exothermic reaction is coupled with the shock wave supported by the heat released behind it and which, in the absence of external energy sources, approach in the final run a steady state characterized by a plane (or zone) positioned downstream of the lead wave front nonpermeable for weak gasdynamic perturbations. This definition relies on the physical model of the wave and therefore defies misinterpretation.

Unfortunately, the complexity of the gasdynamic pattern in real detonation waves and the absence (for this reason) of simple analytical relations capable of predicting the behavior of detonations under various conditions that may be encountered in practice shifts the emphasis towards finding empirical or semi-empirical correlations. Especially this concerns marginal and unsteady detonation waves, which are of the greatest practical importance since they define the conditions for onset and propagation of detonation. This is the wave type, which is expected to be normally observed in combustion chambers of PDEs. Detonation wave instability is inherent not only in gaseous mixtures but heterogeneous systems as well. Therefore deriving reliable expressions that relate the heat release kinetics in detonation waves to the wave structure and parameters easily recorded in experiment and specify the averaged parameters appearing in the equations of the above model is the goal of future experimental and theoretical investigations.

The basic quantitative characteristics of any reactive mixture are the detonation limits, limiting diameters of detonation propagation, the minimum energy of direct detonation initiation, and the critical diameter of detonation transmission to unconfined charge. The knowledge of the detonation wave structure allows one to understand the nature of the detonation limits and correctly predict behavior of detonation waves under various conditions and detonability of FAMs.

2.2.2. Detonability limits

One of the major practical problems is classification of combustible mixtures with respect to their detonability. The problem is not simple since the critical conditions for detonation depend on several initial conditions that the nondetonability criterion may be used only as applied to a particular situation. However, there are some general experimental approaches that provide sufficient information to assess, at least relatively, the detonability of various mixtures. These are the approaches based on the concepts of octane number (ON) dating back to late 1920s [111–113], concerning detonation run-up distance [40], critical initiation energy [54,114], and limiting tube diameter [54–56,115]. Contrary to other approaches, the ON concept is usually applied to a test fuel in a piston engine to assess the detonability in terms of the percentage of *iso*-octane (by volume) in the *n*-heptane–*iso*-octane blend that matches

the test fuel in the allowable compression ratio. Since there are definite reasons for considering engine 'knock' to be identical to the detonation phenomenon [116], the ON concept is sometimes attractive for at least qualitative analyses [117,118].

The most important parameter defining detonability of various mixtures irrespective of the detonation wave geometry are ranges of the initial conditions under which detonation can be self-sustaining. These conditions comprise: concentrations at the fuel-lean and rich limits, the limiting initial pressure and size of the duct or unconfined cloud, critical diameters for detonation transition between volumes of various geometry, and permissible concentration variations in an inhomogeneous initial mixture.

Most of the detonation studies are performed in tubes since detonation can be most easily initiated in ducts. Therefore, it is reasonable to start the analysis with consideration of limiting parameters for detonations in tubes.

Analysis of the experimental observations pertaining to marginal detonations reveals that a decrease in the concentration of one of the mixture components, mixture dilution by an inert gas, or pressure reduction results in an increase of the characteristic reaction time or detonation cell size. As an example, Fig. 11 shows the comparison of predicted and measured transverse detonation cell size a [120] for hydrogen–oxygen mixtures with different dilution with argon at different initial pressure.

In a tube of fixed diameter, it means that the number of cells on the detonation front tends to one, when detonation propagates in the spinning mode. All the available experimental data suggest that this is the last quasi-steady-state mode of detonation propagation. Hence, one may state that detonation decay always passes through the spinning

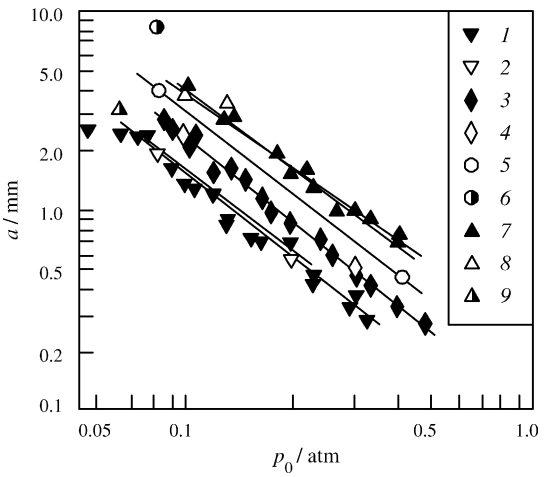

Fig. 11. Comparison of the calculated detonation cell size a with experimental data [63,119] for $H_2 + O_2 + X$Ar mixtures (1, 3, 7). 1, 2—$X = 0\%$ Ar, 3, 4—50% Ar, 5, 6—60% Ar, 7, 8, 9—70% Ar, 2, 4, 5, 8—calculated in Ref. [120], 6—[107], and 9—[121,122].

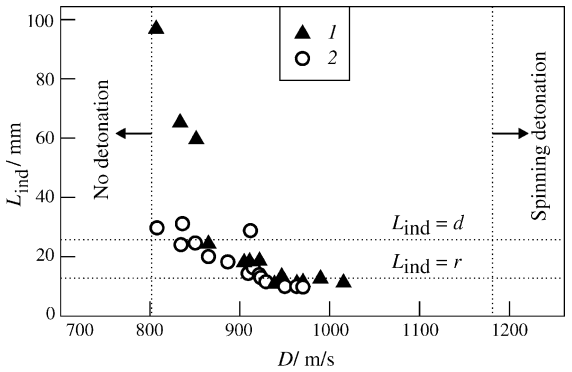

Fig. 12. Measured induction zone length vs. velocities of the lead shock front of decaying acetylene–oxygen–diluent (Ar) detonations [123]: 1—induction time and 2—smoked foil measurements. Normal initial temperature. The detonation limits were found in terms of initial pressure.

mode. Fig. 12 [123] presents the measured induction zone length L_{ind} vs. velocities of the lead shock front D of decaying acetylene–oxygen–diluent (Ar) detonations. In the experiments [123], most of the data falls in the region where the induction zone length ($L_{ind} = t_{ind}D$, t_{ind} is the reaction induction time behind the shock wave) is less than the tube diameter d and slightly larger than the tube radius r.

As the shock velocity approaches the limiting velocity of spinning detonation, D_{CJ}, the induction length tends to the value of $0.8r$. The extrapolation of this data gives the criterion for detonation propagation in round tubes:

$$t_{ind}D \leq 0.8r \quad (1)$$

Although this correlation is stated to be a detonation limit, the conditions under which the experiments have been conducted can hardly qualify to substantiate that this statement applies for detonation propagation in long ducts. It is commonly recognized that the realistic relation between the induction zone length and the tube diameter is:

$$L_{ind} = t_{ind}u \approx d$$

where u is the particle velocity in the front-fixed frame of reference and d is the tube diameter, rather than Eq. (1). It should be emphasized that this relation is only approximate because depending on the mixture composition and fuel type the ratio between the induction zone length and tube diameter may vary. Moreover, it depends on the accuracy of induction periods used in the comparison (experimental spread of ignition delays of nondilute detonable mixtures measured in shock tubes is at least off by a factor of 2) and the temperature behind the lead shock wave, which varies in a wide range behind the nonplanar front inherent in spinning waves. According to geometrical considerations, the $t_{ind}u/d$ ratio should be close to 3 because the spin pitch nearly equals to πd and certainly the maximum induction zone length should be less that the spin pitch, otherwise detonation would not propagate in a quasi-steady mode. However, as observations of soot prints left by marginal

spinning detonation show [124], the maximum induction zone length intensely and irregularly fluctuates due to the hot spot nature of ignition, which naturally drastically reduces the aforesaid ratio and renders it fairly uncertain.

What would happen if the conditions for detonation are worsened still further? The irregular fluctuations of the induction zone increase local heat and momentum losses from this zone, which may eventually result in complete decoupling of the reaction front from the lead shock front and its conversion into the flame front governed by the convective or conductive energy transfer. Such local separation of the two fronts was recorded quite clearly on smoked foils [124]. A local separation can be followed by complete decoupling of the flame front and shock wave throughout the tube cross-section.

There is still a possibility for the mixture between the two fronts to self-ignite in a hot spot (or multiple hot spots) and develop a secondary detonation wave (or strong reactive wave) that then catches up with the lead shock front and gives rise to an overdriven detonation. This overdriven detonation will certainly decay and, thus, the process enters the next cycle of detonation wave decay. Hence, the spinning mode should be adjacent to the region of so-called galloping propagation mode. This latter mode exhibits sometimes rather regular velocity jumps and for this reason may be thought of as being quasi-steady, but it is much more sensitive to even minor changes in the initial conditions than the spinning mode is, therefore it would be proper to refer it to unsteady propagation modes of supersonic reactive waves. The larger the tube diameter and the more sensitive is the reaction rate to temperature variations, the greater is the scale of the pulsations. Usually, as the conditions depart from those required for the stable spinning mode, the velocity pulsations become greater and of a larger scale, until the detonation wave degenerates completely into a flame and a shock wave. Normally the galloping regime is observed within a very narrow concentration range [124]. For unstable, near-limit phenomena in some particular mixtures, like galloping detonations, the existence criterion [123] is (see Fig. 12):

$$0.8r \leq t_{\mathrm{ind}}D \leq d \tag{2}$$

Thus, one can define the detonation limit in a tube as a boundary between the regions of existence and failure of the spinning detonation mode. Although very approximate and applicable to mixtures studied, the criteria of types (1) and (2) incorporate chemical properties of the mixture, particle velocity, and characteristic dimensions of the channel, and can be very useful in analysis of near-limit and failure modes of detonation propagation. It is worthy to note that the Zel'dovich theory of detonability limits predicts a similar relationship between the induction zone length of the near-limit detonation and the tube diameter [115].

Of course, the procedure of measuring detonation limits should be standardized somehow (like that for flammability limits), since the detonation limits should depend on the following major factors: the initiation energy (too small energies will lead to underestimation of the limits, whereas an excessively strong initiator in a tube of a limited length will overdrive the wave and thus overestimate the mixture detonability), the tube diameter and length.

The distance required to reach steady-state detonation at the limits increases as compared to that far from the limits, therefore quite long tubes are needed when measuring the limiting concentrations. For example, Pawel et al. [125] found out that a 7 m long tube 16 or 26 mm in diameter was insufficient for the marginal fuel-lean hydrogen–air detonation to establish. It was possible to obtain the lean limit of detonation in tubes 14 m long with 17.3% (vol.) H_2 in a 16 mm diameter tube and 15.3% (vol.) H_2 in a 26 mm diameter tube.

Another factor that may affect the results of measurements is the quality of the mixture: imperfect mixing narrows the limits markedly.

Experiments show that the lean limits for hydrocarbons and both limits for hydrogen are independent of the tube diameter after it reaches a certain value, which is close to 70–100 mm [124]. However, the rich limits for hydrocarbons increase continuously with the diameter. The limiting diameters for FAMs range from about 6 mm for hydrogen–air and 20–30 mm for hydrocarbon–air mixtures. For methane–air mixtures, the limiting diameter is estimated at 100 mm (in a 70 mm inner diameter tube detonation propagated only in a stoichiometric mixture and only in an unstable mode). Fuel–oxygen mixtures have smaller limiting diameters (for hydrogen–oxygen and methane–oxygen mixtures it is about 2 mm, while for a more detonable acetylene–oxygen mixture it is even less than 1 mm).

Initial temperature T_0 affects the detonability limits as clearly shown by Pawel et al. [125] who investigated the influence of initial temperature ($T_0 = 135$, 195, and 295 K) on the detonability of CH_4–O_2, H_2–O_2, and H_2–air mixtures. Fig. 13 shows the results of their measurements. For all the systems under investigation in Ref. [125], the concentration limits of stable detonation were found to become narrower for lower initial temperatures. This is partly confirmed by detonation cell measurements of Tieszen et al. [126] shown in Table 1. As follows from the table, stoichiometric propane–air mixture shows the opposite trend: detonation cell size tends to increase with T_0 and detonability limits should be narrower at higher T_0. Note, that based on the classical theory of detonation, one could expect the effect of initial temperature T_0 similar to that shown by propane. The temperature behind the shock wave front leading detonation is nearly independent of T_0 but the chemical kinetics behind the shock is affected by density. Because the reaction time is inversely proportional to the gas density to power n (where n is the reaction order), the detonation limits should become narrower at higher T_0. Here, however, it is worth noting that the effects associated with initial temperature (in its range studied) are too

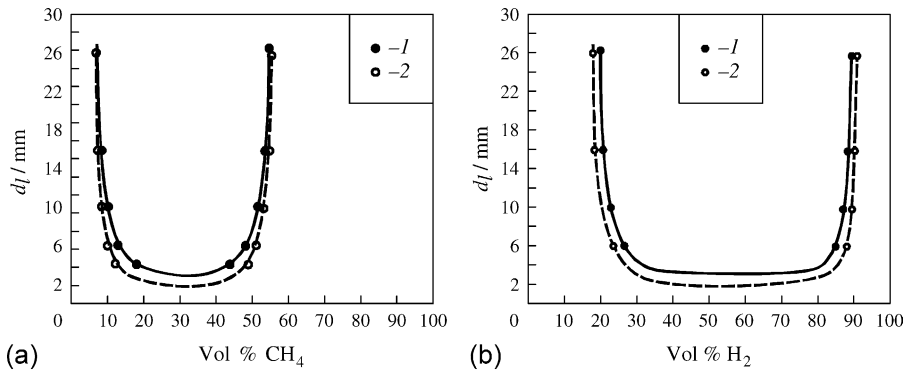

Fig. 13. Measured dependencies of the limiting tube diameter on the molar fraction of fuel in CH_4–O_2 (a) and H_2–O_2 (b) mixtures at pressure 1 atm and different initial temperatures [125]: (a) 1—T_0 =195 K, 2—295 K; (b) 1—T_0 =135 K, 2—295 K.

insignificant and can be concealed by the uncertainty in measured cell size to make any definite conclusions. Based on general reasoning one can expect extension of the detonation limits when the temperature approaches self-ignition temperature.

Auffret et al. [127], based on their experimental studies, have proposed the following correlation of the detonation cell size a for C_2H_2–O_2 mixtures:

$$a \sim p_0^{-n} T_0^m$$

Within the initial temperature range $T_0 = 293$–500 K, and initial pressure range p_0 =0.05–1 bar, $n \approx 1.1$–1.3, and $m \approx 0.9$ for the stoichiometric mixtures tending to $m \approx 0$ for fuel-lean mixtures. Contrary to Ref. [125], the findings of Ref. [127] indicate that the detonability of near-stoichiometric mixtures is deteriorated by increasing the initial temperature. Thus, the effect of initial temperature on detonability limits is still a controversial issue.

Reduction of the initial pressure affects significantly both the limiting diameter and concentration limits of detonation increasing the former and making narrower the latter. For example [124], propane–air mixtures are detonable within the range of C_3H_8 molar concentration from 3 to 6% at 0.7 atm, and only from 3.5 to 5.7% at 0.2 atm; at 0.15 atm detonation does not propagate in the 70 mm inner diameter tube. Fig. 14 shows the measured pressure dependencies of the concentraion limits of CH_4–O_2–N_2 detonations in a tube 16 mm in diameter [128]. Clearly, the limiting pressure depends on mixture sensitivity: it is 200 Torr for pure CH_4–O_2 mixture and about 360 Torr for CH_4–O_2–N_2 mixture with 33% N_2. It is interesting that at pressure exceeding 600 Torr the fuel-rich limits were found to be wider for less sensitive mixtures.

The state of the tube walls also affects the limiting conditions for detonation propagation. In rough tubes, the detonation limits (for detonation waves spreading at high velocity close to the ideal CJ value) are usually narrower than in smooth ones [124]. This is because the loss of the momentum at the roughness elements reduces the detonation velocity, and thereby increases significantly the bulk reaction zone (although shock wave reflections at

Table 1
Comparison between measured transverse cell size a at 25 and 100 °C for stoichiometric fuel–air mixtures of some gaseous hydrocarbons (initial pressure 1 bar) [126]

Fuel	a (mm)		a (100 °C)/a (25 °C)
	25 °C	100 °C	
C_2H_2	5.3	4.0	0.75
C_2H_4	19.5	16	0.82
C_2H_6	50	48	0.96
C_3H_8	50	52	1.04
CH_4	305	260	0.85

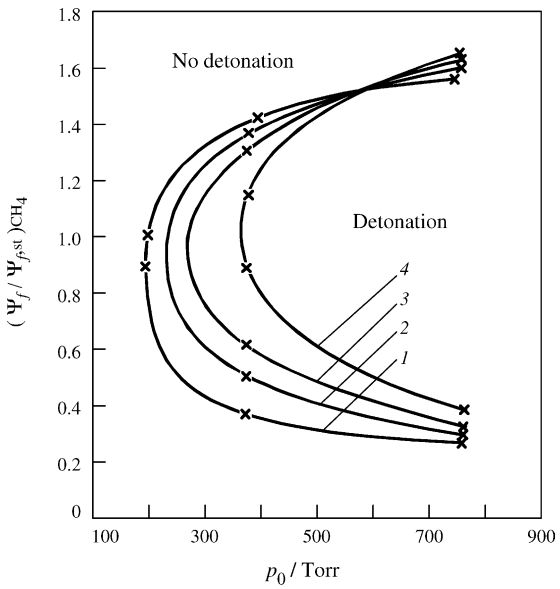

Fig. 14. Measured pressure dependencies of the concentration limits of CH_4–O_2–N_2 detonations in a tube 16 mm in diameter (normal initial temperature) [128]: 1—molar fractions of N_2 and O_2 equal to 0 and 100%, 2—10 and 90%, 3—18 and 82%, and 4—33 and 67%.

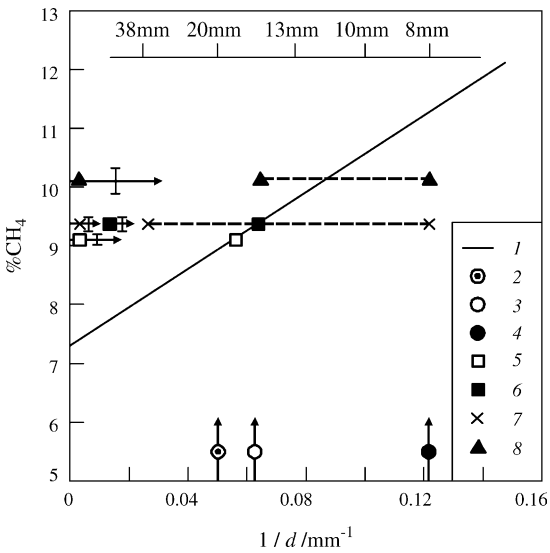

Fig. 15. Summary of experimental results of Ref. [129] on the detonability limits of CH_4–O_2 mixture in tubes of different shape of cross-section. Solid line 1 represents limits for tubes with circular cross-section with points 2–4 corresponding to round tubes 20, 16, and 8 mm in diameter, points 5–8 correspond to tubes of rectangular cross-section: 5—18 × 18 mm, 6—16 × 16 mm, 7—38 × 8 mm, and 8—16 × 8 mm. Dashed lines indicate reciprocal values of the short and the long side of the rectangular tubes. They are plotted at the measured limit concentration value.

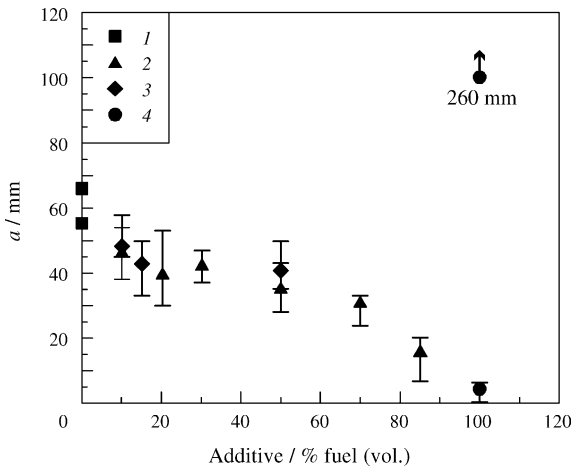

Fig. 16. Measurements of transverse detonation cell size a in JP-10–additive–air mixture at p_0 =100 kPa, T_0 =353 K. All data points for hydrocarbon–air mixtures are from Ref. [126], cell size for CH_4–air mixture is 260 mm [130]; 1—no additive, 2—C_2H_2-additive, 3—CH_4-additive, and 4—C_2H_4-additive.

the roughness protrusions on the walls facilitate attaching the reaction zone to the shock front).

Tubes used in practice are not necessarily round, therefore a question arises, how the shape of the channel affects the critical conditions for detonation propagation. Jost and Wagner [129] investigated detonability limits of CH_4–O_2 mixture in tubes with circular, square, and rectangular cross-section. Fig. 15 shows the summary of their experimental findings in terms of the limiting methane concentration vs. hydraulic diameter plot. Following Jost and Wagner, an estimate of the limits of detonability based on hydraulic diameters gives a reasonable value as long as one side of a rectangular cross-section is larger than a certain lower limit. The concept of limiting hydraulic diameter does not take into account real processes behind the detonation front. Nevertheless, it was found that in tubes of rectangular and even triangular cross-section the last mode of stable detonation propagation was quite similar to spinning detonation with a single transverse wave. Of course, the flow pattern at the tube periphery is somewhat different from that in round tubes, but the general features of the marginal detonation are similar. In rectangular tubes the single-head mode is still the last one before detonation failure, provided the ratio of the channel width to its height does not exceed 2. With larger ratios, the marginal detonation mode is multiheaded.

Additives of more reactive fuels even in small amounts extend markedly the detonation limits and reduce the limiting tube diameter. According to experimental data of Borisov et al. [124], ethylene added to methane in amount of 10% reduces the critical diameter below 70 mm (detonation propagates in the 70 mm inner diameter tube stably within the 9–11% CH_4 concentration range). With 20% ethylene additives to methane, the mixture is detonable within the 8–12% CH_4 range. Such active additives as acetylene-, organic-nitrates-, and NF_2-containing compounds extend the detonation limits and reduce the limiting diameter even to a greater extent. Fig. 16 [130] shows the effect of various hydrocarbon additives (C_2H_2, C_2H_4, and CH_4) on the detonation cell size of stoichiometric JP-10–additive–air mixtures. The experiments were conducted in the heated 280 mm diameter detonation tube. Similar data on the effectiveness of adding low-molecular weight fuels as sensitizers to hexane–air mixture was reported in Ref. [131].

In situ mixing of hydrocarbon fuel with HP can also be used to significantly widen detonability limits [95]. Fig. 17 shows the predicted dependencies of the transverse detonation cell size in *iso*-octane–air–HP (solid curve) and *n*-heptane–air–HP (dashed curve) mixtures on HP molar fraction. Addition of HP (up to 20%) results in decreasing the cell size by a factor of 20. As HP is commercially available in the form of concentrated aqueous solutions, it is interesting to evaluate the effect of water. Fig. 18 shows the predicted detonation cell size as a function of molar fraction of water ψ in the aqueous solution of HP for the systems *iso*-octane—20% HP and *iso*-octane—60% HP. Clearly, the detonation cell size is affected by water but if highly concentrated HP solutions are used (e.g. 85–95%), the detonability of the blend remains much higher than that of pure hydrocarbon fuel.

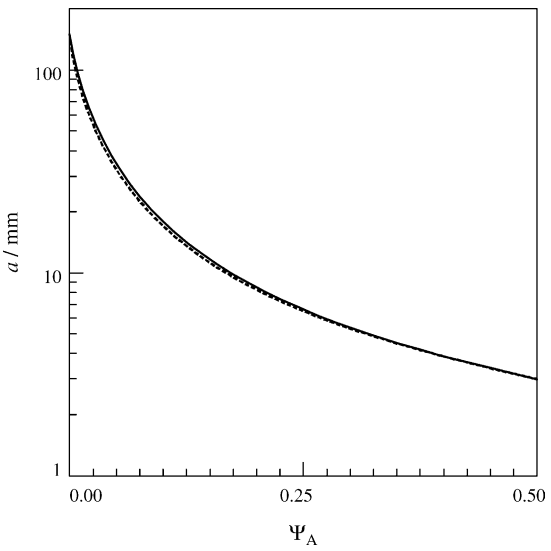

Fig. 17. Predicted dependencies of the transverse detonation cell size a in stoichiometric *iso*-octane–air–HP (solid curve) and *n*-heptane–air–HP (dashed curve) mixtures on HP molar fraction ψ_A [95].

This section focuses on the effect of chemically active additives mostly on the parameters pertaining to a critical behavior of detonation waves. It has been discussed in Section 2.2.1 that small additives can hardly influence the characteristics of steady CJ waves. Indeed, a change in the rate of a chemical reaction can affect only the detonation cell size, which, in multihead detonation waves has nothing to do with the averaged detonation parameters. The chemical kinetics becomes a crucial factor only when the critical phenomena are concerned (minimum initiation energies, limiting diameter, concentration limits of detonation, etc.). As is well established, the major mechanism governing the heat release in detonation waves is self-ignition of the mixture. This mechanism is also responsible for direct onset of detonation in the course of DDT. Therefore, to assess the effect of additives on detonation processes, one has to find out how the additives affect the basic self-ignition stages. Before analyzing the effect of additives, we consider the peculiarities of spontaneous ignition in shock-preheated gases under conditions relevant to those existing in detonation waves or DDT processes. A great body of experimental data and numerical modeling show that the range of characteristic times inherent in the processes at issue is sub-milliseconds, at longer times normally no strong coupling between the shock (or compression wave) and chemical reaction has ever been observed. This range is covered by the shock tube experiments, which provide much more reliable kinetic data than do direct measurements in detonation waves, moreover, the conditions for ignition in shock tubes are similar to those in detonation waves, except the absence of traveling transverse waves in the shocked mixture.

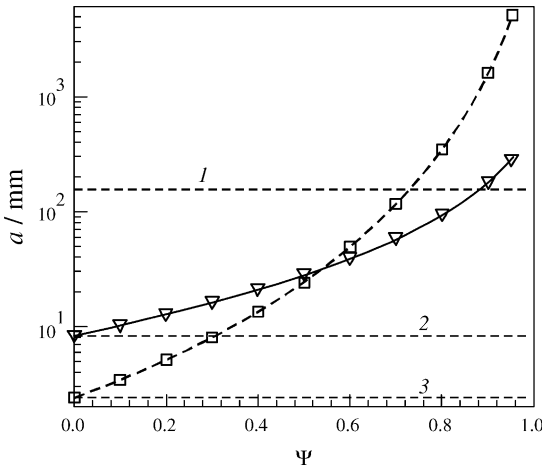

Fig. 18. Predicted transverse detonation cell size a as a function of molar fraction of water ψ in the aqueous solution of HP for the *iso*-octane—20% HP (solid curve) and *iso*-octane—60% HP (dashed curve) systems. Horizontal dashed lines 1, 2, and 3 correspond to the predicted cell sizes in the corresponding systems with 0% H_2O_2, 20% H_2O_2, and 60% H_2O_2, respectively, at $\psi = 0$ [95].

Although a detonation wave is characterized by a great variety of representative chemical reaction times, its marginal behavior is controlled by the longest of them, therefore there is no need to analyze the effective heat release profiles throughout the wave and restrict consideration only to local self-ignition process, which can be adequately characterized by shock-tube data. The basic conclusion drawn from these data is that ignition never occurs simultaneously throughout the preheated mixture volume. Ignition in exothermic centers ('hot spots') arising due to gasdynamic fluctuations is a well-established fact in shock tubes, and this ignition seriously affects the time history of heat release. As experience suggests, hot spot ignition is inherent in all techniques used to study self-ignition.

How does the hot-spot mechanism affect the overall heat release in a shocked mixture? A comparison of the data on spontaneous ignition with kinetic modeling of adiabatic chain-thermal explosions reveals that hot spots reduce the effective ignition delay, however, not drastically. But when the overall heat release profile (which is the result of averaging the reaction course in many elementary mixture volumes subjected to various fluctuations) is considered, asynchronous mixture ignition in these volumes would significantly extend the time range within which the reaction runaway is observed, affecting the overall ignition delay only little, except when the ignition delay becomes commensurate with the runaway time. An analysis of kinetic measurements in a wide range of reaction times shows that for hydrocarbon–air mixtures the runaway time is close to 100 μs and only insignificantly depends on temperature and initial pressure [132]. It is also affected only little by chemical additives. Global kinetic heat release equations often used in 1D simulations must take into account this peculiarity of the thermal explosion development (which is reflected in

the popular two-stage kinetics of hydrogen–oxygen reaction). Thus, one should anticipate the effect of additives on the induction period alone. Therefore, the effect of additives on the parameters of marginal detonations is much less pronounced than their effect on ignition delays.

With respect to the effect of additives on the ignition delays, various kinetic mechanisms of chain-thermal reactions taking place under adiabatic or isothermal conditions have been analyzed in detail [133]. This study has demonstrated that the promoter effects depend on the type of the ignition reaction and the nature of the additive. The production of active species from the promoter must be adjusted to the oxidation reaction of the basic fuel: it must be fast but not too fast, otherwise, the active species would recombine faster rather than they enter in the chain propagation reactions. The promoter effect levels off as the promoter concentration increases, therefore, as follows from various estimates, there is no reason to add more than 15 or 20% of promoters to fuels. The reduction of ignition delays is less when the temperature is higher. The larger the hydrocarbon molecule, the lower the promoting effect. Table 2 illustrates the effect of various additives (introduced in amount of 1% with respect to fuel) on the ignition delays of $6CH_4 + 12O_2 + 82Ar$ mixture at 1000 K and 1 atm.

The most efficient promoters for hydrocarbons are those that serve as homogeneous catalysts. Among them are organic nitrates and fluoronitrates. In the case of nitrates, pseudo-radicals NO react with the fuel or oxygen to produce radicals or atoms, and then recover to their initial state. In the case of tetrafluorohydrazine, radicals react with HO_2 radicals to produce fluorine atom, hydroxyl, and FNO. Then reactions $F + H_2O = HF + OH$, $OH + CO = CO_2 + H$, and $FNO = F + NO$ follow that introduce the NO pseudo-radical in the system. The effect of most efficient additives on self-ignition of a 3.6% C_3H_8 + 16.4% O_2 + Ar mixture is shown in Fig. 19.

As far as the influence of additives in promoting the detonation parameters is concerned, experiment shows that both the minimum energies of direct initiation of detonation and limiting diameters of detonation can be reduced by a factor usually not exceeding two.

It is of interest to compare the detonation and flammability limits under the same conditions. All the early experimental data furnished evidence that not all of the flammable mixtures could detonate, and only quite recently it has been discovered that this is not always true. For instance, for ethane–air and propylene–air mixtures

Table 2
Effect of various additives (introduced in amount of 1% with respect to fuel) on the ignition delays of $6CH_4 + 12O_2 + 82Ar$ mixture at 1000 K and 1 atm [133]

Additive	Cl_2	CH_3I	H_2	$(CH_3)_2N_2$	N_2F_2	C_4H_{10}	CH_3CHO
$\tau_{i,na}/\tau_i$	1.2	1.2	1.2	2.5–3.0	3.0	1.5–2	2

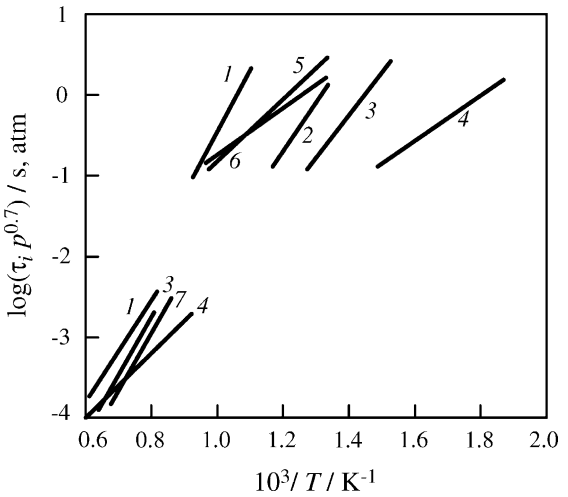

Fig. 19. Arrhenius plots of measured ignition delays for 3.6% C_3H_8 + 16.4% O_2 + Ar mixture (1) and the same mixture with 0.036% *iso*-$C_3H_7ONO_2$ (2), 0.18% *iso*-$C_3H_7ONO_2$ (3), 0.54% *iso*-$C_3H_7ONO_2$ (4), 0.036% N_2F_4 (5), 0.036% CH_3ONO_2 (6), and 0.18% N_2F_4 (7) [133].

both the rich and lean detonation limits are very close to their flammability counterparts, whereas hydrocarbon–air mixtures with inhibitor additives (tetrafluoro-dibromo-ethane) detonate in a much wider range of the inhibitor concentration than they burn [134]. This is not surprising, because the reaction mechanism governing propagation of flames and detonations is quite different. Reactions in detonation waves are essentially of the self-ignition type, whereas in flames they start in the preheat zone at relatively low temperatures due to radical (mostly H atoms) diffusion to this zone. Inhibitor additives suppress these reactions by scavenging the radicals, and that is why the flame is quenched. In as much as in detonation waves the reaction starts at a high temperature in the shocked gas, at which the inhibitor molecules decompose very fast, it is not affected by the additives (or sometimes can even be enhanced by the radicals formed in the course of inhibitor decomposition). This conclusion is supported by the data on self-ignition of hydrocarbon–air mixtures with additives behind reflected shock waves in shock tubes [135].

It is worth to mention one experimental fact indicating that the maximum velocity deficit (as compared to the CJ detonation velocity) for the essentially 3D spinning mode does not exceed ten percent, which is in good agreement with the available theories of detonation limits (e.g. Zel'dovich theory [55,56,98]). It is not unexpected, since this model is applicable to real detonations, but with a slight modification that the longest reaction zone influencing the limit is located near the walls just in front of the transverse detonation wave. This zone is most sensitive to the flow fluctuations due to the largest Arrhenius exponent E/RT. The fact that the local decoupling may dramatically affect the detonation wave is clearly shown by experimental runs,

suppressed by liquid films [136]. The shadowgraphs demonstrate that the local reaction zone destruction is followed by a very quick disappearance of the reaction front all over the tube cross-section.

Thus, the models proposed for planar detonation waves describe at least qualitatively the marginal behavior of 3D detonation waves. The exact solution of the 3D unsteady problem for the marginal detonation is extremely time consuming. Therefore, for practical purposes a very simple relation may be suggested. The spinning wave can be quasi-steady solely when the spin pitch is larger than the maximum length of the reaction zone. Otherwise, the amount of the energy released behind the detonation front will fluctuate, leading to periodical (or aperiodical) decay of the lead shock wave and, hence, to instantaneous lengthening of the reaction zone beyond the limit where the reaction completely decouples with the shock front. Thus, one may write for the limiting detonation diameter $\pi d_l > ut_r$ (u is the particle velocity in front-fixed frame of reference and t_r is the characteristic reaction time), where in accordance with many measurements, the angle of the helical spin trajectory is assumed to be close to 45°. Analysis of many spin tracks shows that because of the fluctuation of the reaction zone length the above inequality should be changed to $d_l = ut_r$ at the limit.

This simple formal model of detonation limits allows explaining the virtual independence of the lean detonation limits in lean hydrocarbon–air mixtures and the two limits in hydrogen–air mixtures from the tube diameter when it exceeds a certain value. The above limiting condition suggests a logarithmic extension of the limits with tube diameter (indeed, as tube diameter, d, increases, the temperature behind the lead shock wave can drop as $\log d$, since $t_r \sim \exp(E/RT)$, this in turn means that the energy loss from the mixture increases also logarithmically). However, in reality this dependence is significantly weaker. In real waves, instability generates not only transverse waves but longitudinal waves as well. These oscillations cause periodical fluctuations of the reaction zone length. In tubes of large diameter, these oscillations affect the reaction zone more substantially. This is because, first, the wavelength of the dominant longitudinal oscillations becomes comparable with the reaction zone length, and, second, when the mixture approaches the limit inherent in large-diameter tubes, the temperature behind the lead shock wave drops and the E/RT factor gets so high that the reaction zone cannot tolerate even very small perturbations (because it will tend to infinity at the elongation stage). This implies that the actual reaction zone length should be much shorter than that permitted by the Zel'dovich theory. One-dimensional numerical calculations of detonation initiation with heat losses taken into account show that the widening of the detonation limits with diameter occurs much slower than logarithmically.

It should be emphasized that the sharp transition from detonation go to no-go condition must occur only when the temperature sensitivity of the reaction rate is high enough. The Zel'dovich theory is essentially based on this assumption. A comparison of the two components of the reaction time (induction time t_{ind} and energy release time t_{er}) shows that for many hydrocarbon–air mixtures they become equal to each other in the direct vicinity of the limits. This is just confirmation of the above statement. Indeed, the temperature sensitivity of t_{ind} is very high whereas that of t_{er} is very low, therefore, when t_{er} dominates, gasdynamic fluctuations do not strongly change the overall reaction zone length. As calculations of initiation of 1D detonation by a point explosion demonstrate, the minimum initiation energy also corresponds to the situation at which t_{ind} becomes less than t_{er} after the first dip of the initiating-wave velocity (during this dip their relation reverses).

In some practical situations the reactive-gas charge can be stratified, i.e. a nonreactive gas would serve as its outer boundary, instead of solid walls. The critical diameter for detonation propagation in this case should be much greater. Experiments with unconfined cylindrical mixture charges support this assertion. Rarefaction waves spreading inward the charge result in a peculiar gasdynamic pattern of the flow with various types of transverse and longitudinal perturbations. The detonation cell size and velocity change periodically in the radial and axial directions, the average velocity is 20–30% lower than its CJ value. Interestingly, the critical diameter of unconfined charges for hydrocarbon–air mixtures is nearly identical [135] with the critical diameter for detonation transition from a narrow tube into a wider tube (see Section 2.2.4). Experiments also show that even light confinement, like a wire spiral, significantly reduces the critical diameter [136].

In previous discussions, the issues dealing with limits of detonability in single-shot studies were considered. One more issue extremely important for pulse detonation propulsion is the limits of detonability in a pulse mode, which is recently investigated by Baklanov et al. [137]. For detonation experiments with gaseous mixtures, a 3 m long tube was used. The tube was water-cooled, and the pulse frequency was varied from 0.5 to 10 Hz. Mixtures of methane with oxygen-enriched air at normal pressure were studied. Predetonation distances and detonation velocities were measured as functions of oxidizer-to-fuel ratio, α. The effect of different vortex generators on shortening the predetonation distance was also studied. It has been shown that the predetonation distance is very sensitive to α and exhibits a well-known U-shaped behavior. An example of measured dependence of the predetonation length on α for the methane–oxygen-enriched air mixture is given in Fig. 20.

Presented in the same figure is the measured dependence of the predetonation distance on α for the case when a vortex generator is inserted in the detonation tube. The vortex generator is the inverted Schelkin spiral: on a part of the inner surface of the tube the thread was machined. It follows from the figure, that for fuel-rich mixtures ($\alpha < 1$) the dependence of L_{DDT} on α is not affected by the vortex generator while for fuel-lean mixtures ($\alpha > 1$) the vortex

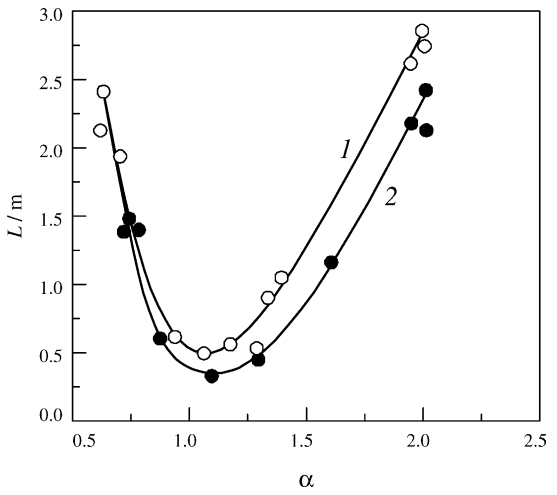

Fig. 20. Measured predetonation length vs. oxidizer-to-fuel ratio α for methane–oxygen-enriched air mixture without (1) and with (2) vortex generator [137].

generator provides a noticeable effect on the predetonation length. A number of experiments have been performed to reveal the dependencies of detonability limits and predetonation length on the Reynolds number of the inflow of unburned combustible mixture in a detonation tube. Reynolds number was varied by means of changing the pulse frequency and overall mass flow rate. It has been shown that an increase in the flow velocity inside the chamber results in widening detonability limits.

2.2.3. Direct initiation

The energy required to initiate detonation directly should certainly be evolved at a high rate and in the amount capable of generating a blast wave with an amplitude at least close to that of the shock wave propagating at the CJ velocity and with duration of the pressure pulse comparable or longer than that of the reaction induction time. Since the heat behind the detonation front is evolved within a finite time, the critical energy for detonation initiation should exceed some finite value determined as

$$E_1 \geq \int_0^{r_{cr}} \left(\rho e + \rho \frac{u^2}{2}\right) \mathrm{d}r \qquad \text{for plane geometry} \tag{3}$$

$$E_2 \geq \int_0^{r_{cr}} 2\pi r \left(\rho e + \rho \frac{u^2}{2}\right) \mathrm{d}r \tag{4}$$

for cylindrical geometry

$$E_3 \geq \int_0^{r_{cr}} 4\pi r^2 \left(\rho e + \rho \frac{u^2}{2}\right) \mathrm{d}r \tag{5}$$

for spherical geometry

where r_{cr} is a certain critical radius which specifies the rear boundary of the zone behind the lead front of the blast wave possessing an energy sufficient to support further propagation of the detonation wave and e is the internal energy of the gas within this zone. For convenience, the gas parameters can be related to the steady CJ detonation wave with the finite reaction zone because, as it will be shown below, usually r_{cr} is markedly larger than the detonation cell size. This is accounted for by the fact that the distance between the lead shock front and the effective CJ plane, L_{CJ}, in multifront detonations is greater than the longitudinal cell size b, and, since the rarefaction wave that follows the blast wave produced by the initiator is very steep, the energy deposited to the mixture must support the reactive wave even for a longer distance in order to preclude its decay. Thus, physical considerations suggest that r_{cr} should be significantly longer than L_{CJ}. If the total energy averaged over the $[0, r_{cr}]$ interval is removed from the integral sign in Eqs. (1)–(3) one arrives at the following simple relations:

$$E_1 = k_1 r_{cr,1}, \qquad E_2 = k_2 r_{cr,2}^2, \qquad E_3 = k_3 r_{cr,3}^3$$

where indices 1, 2, and 3 denote planar, cylindrical, and spherical cases, respectively, and k_ν ($\nu = 1$, 2, and 3) are the corresponding constants. If one goes further assuming that there exists an approximate proportionality between the induction zone length, $L_{ind} = t_{ind} u$, and r_{cr}, the above relationships can be rewritten as follows:

$$E_\nu = k L_{ind}^\nu$$

where k is constant. This latter equation was derived first by Zel'dovich et al. [54].

Of course, the above relationships are quite far from the exact ones and are only capable of predicting the general trends, because they still are based on the concept of a smooth 1D wave and do not take into account the real structure of detonation waves. Moreover, the flow conditions behind detonation waves of various geometry are different, therefore the averaged total energies also will slightly depend on r_{cr}. For this reason a direct experimental study was undertaken to verify the validity of these relations [138].

Fig. 21 presents the results of measurements of critical energies of detonation initiation in fuel–oxygen (filled symbols) and fuel–air (open symbols) mixtures. The measured energies in the graph are grouped near a straight line with a slope equal to 3.0, which is in line with the Zel'dovich relation $E_\nu = k L_{ind}^\nu$. According to this relation, the critical energy for spherical detonation initiation, E_3, is proportional to the reaction time to the third power and the critical energy for plane detonation initiation, E_1, is proportional to the reaction time to the first power. Hence, in logarithmic coordinates $\log E_3 - \log E_1$ the slope of the $E_3(E_1)$-dependence should be 3.0. Although this relationship follows from the dimensional analysis, this consistency is somewhat surprising, because the conditions for reaction progress behind the lead shock front (e.g. the temperature gradient in the reaction zone) in both geometries are different. Anyway, this empirical correlation supporting the general theoretical model is very helpful in assessing

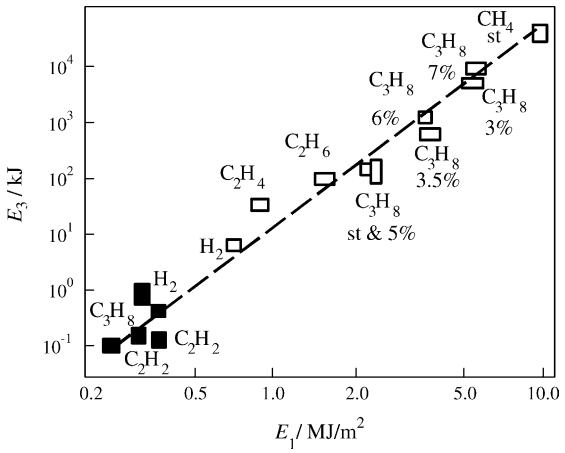

Fig. 21. Critical energy of direct initiation of spherical detonation (E_3) vs. the critical energy of plane detonation initiation (E_1) for various fuel–oxygen (filled symbols) and fuel–air (open symbols) mixtures at normal initial pressure [138].

the detonability of low-reactivity combustible mixtures. For example, the available data on the critical energy of detonation initiation in unconfined methane–air mixtures lack consensus, ranging from 1 kg TNT to more than 100 kg TNT. Based on the presented correlation, a value of about 10 kg TNT is most reasonable.

The minimum energy of direct detonation initiation is a very attractive criterion for calculating it numerically using the ZND model. However, the first calculations showed a dramatic discrepancy between the calculated and measured energies (sometimes up to 10^4 for spherical detonations). The calculated energies were always higher than the measured ones. This was ascribed to the three-dimensionality of the real process of detonation onset. This explanation is quite plausible. First, there is a direct experimental evidence of formation of strong gasdynamic perturbations on the incipient detonation front. A single strong transverse wave arises when the blast wave front area is small, and then the number of perturbations grows quickly as the wave front departs from the initiation site. Second, the transverse waves shorten appreciably the overall reaction zone attaching it to the lead shock wave and thereby stabilizing the detonation wave. Thus, the transverse waves, on the one hand, make the initiation of the reaction in the detonation wave easier but, on the other, they extend the overall reaction time and, what is particularly important, the distance from the lead shock front to the effective CJ surface. As the calculations show, the initiation process is characterized by detonation velocity pulsations of a very high-amplitude due to longitudinal instability caused by the rarefaction waves traveling between the initiation centre and the detonation front. These pulsations naturally increase periodically the length of the reaction zone (if the detonation wave is treated as a ZND one) and at the beginning may be a reason of detonation failure due to the too rapid decay of the blast wave being only insignificantly supported by the energy evolved in the reaction zone of a very small radius at the maximum reaction zone length in the end of the pulsation (in the case of plane initiation, the heat transfer may cause detonation failure during the pulsations). The presence of the transverse waves generating hot spots that do not allow large reaction zone pulsations makes the blast wave–reaction zone complex less vulnerable to longitudinal fluctuations and thereby facilitates the initiation process (despite the larger overall thickness of the detonation front).

It should be also noted that the discrepancy between the calculated and measured E_3 is ascribed partially to the incorrectness of the global reaction rate equation used in many studies. More detailed reaction schemes improved the agreement, although it still remained insufficient to consider such calculations as a quantitative method for evaluating the critical energy of direct detonation initiation.

Calculations using the ZND model with inclusion of the detailed kinetics reveal [134] that there are three characteristic ranges of the blast wave Mach number within which the nature of the process is different. In the vicinity of an initiator, with almost instantaneous energy release, the blast wave initiates a reaction with extremely short ignition delays but the overall energy release is negative due to dissociation of the reaction products. In the second stage, the reaction, which is already exothermic on the whole, becomes weakly coupled with the lead blast wave, i.e. these two fronts depart from each other in time. This departure may continue until a minimum wave velocity is reached which, depending on the energy of the source and on the thermodynamic and kinetic parameters of the mixture, can drop even to $0.6D_{CJ}$, where D_{CJ} is the thermodynamic detonation velocity. The cell size during this stage of the initiation process grows and sometimes disappears (or to be more precise, the traces of the triple points become illegible) for a short period when the energy is close to the critical one, thus indicating that the transverse waves may attenuate (but not vanish). The third stage is reinitiation of the detonation (if it has been converted for a while into a decoupled nonsmooth shock wave and reaction front) or its acceleration. The CJ state is usually attained after one or several oscillations of the detonation velocity. The deeper the dip of the detonation velocity, i.e. the closer the source energy to the critical value, the larger is its overshoot that follows the minimum. The nature of the overshoot is quite clear, after decoupling a large mass of the gas between the two fronts, self-ignites in hot spots and this generates a compression wave within this zone which then overtakes the lead shock wave and amplifies it.

It is natural to connect the position of the minimum on the D vs. distance curve with the critical radius introduced earlier, because anyway there is no strict definition of r_{cr}. The experimental data indicate that final transition to the CJ state occurs approximately at $r = 2r_{cr}$.

Numerical calculation cannot provide quite reliable data on the critical energy of detonation initiation because of

the uncertainty of the heat release kinetics, therefore semi-empirical approaches seem to be most attractive. That is why a large number of studies are devoted to derivation of such semi-empirical relations.

One of the first approaches was suggested by Troshin [139]. He defined r_{cr} as a radius at which two conditions are satisfied simultaneously, namely, the velocity of the blast wave generated by a strong point explosion with the energy E_3 equals D_{CJ}, and the chemical energy released within this region equals that deposited by the source. The following expression was then derived for E_3 :

$$E_3 = \frac{4}{3}\pi r_{cr,3}^3 \left[0.31 \frac{\rho_{CJ} u_{CJ}^2}{2} + \frac{0.59 p_{CJ}}{\gamma_{CJ} - 1} - \frac{p_0}{\gamma_{CJ} - 1} - \rho_0 q \right]$$

where q is the heat effect of chemical reactions. For a stoichiometric hydrogen–oxygen mixture the critical radius was expressed through the length of the induction zone, L_{ind}, as

$$R_{cr,3} = 40 \frac{L_{ind}}{\gamma_{CJ} - 1}$$

Thus, it has been shown that the critical radius must be much larger than the induction zone length L_{ind} and longer that the longitudinal detonation cell size b.

The above expression is not conducive to be used for quick estimation of E_3. Therefore, it has been suggested to assume that the above relation between L_{ind} and $r_{cr,3}$ derived for oxygen–hydrogen mixtures holds for other mixtures as well. The coefficient of proportionality relating E_3 and t_{ind}^3 varies from mixture to mixture within a factor of 1.4, which is less than the spread of the experimental data on t_{ind}. Therefore an average value of this proportionality coefficient, 4.2×10^{20} J/s^3, was chosen for practical use [135]. The data presented in Table 3 demonstrate quite a good agreement of the estimates with measured E_3.

More sophisticated studies based on the analysis of the detonation wave structure lead also to relations that are essentially one version of the Zel'dovich formula or another.

Some authors attempted to estimate E_3 for spherical detonations from the data on the critical diameter of detonation transition from a tube into the unconfined mixture (see Section 2.2.4) or from the limiting diameter of detonation propagation in a tube.

Table 3
Comparison of calculated and measured values of E_3 for various stoichiometric fuel–air mixtures [135]

Fuel in air (stoich.)	Ethane	Ethylene	Propane	Methane
E_{3calc} (kg TNT)	0.018	0.007	0.07	120
E_{3exp} (kg TNT)	0.035	0.015	0.08	10–100 (estimates)

The numerical calculations for gaseous mixtures within the framework of a 1D detonation model [140,141] describe in detail a qualitative pattern of 1D initiation: attenuation of an initiating wave at initiator energy $E < E_\nu$ ($\nu = 1, 2,$ or 3) and formation of a detonation wave at $E \geq E_\nu$. In Ref. [142], a quantitative approach for calculating E_3 with a parameter taken from experiments is suggested and implemented for stoichiometric hydrogen–air mixture within the framework of detailed kinetics model. Other mixtures needed new calculations.

About 20 approximate models for a 1D detonation initiation in gaseous mixtures are known so far. All were analyzed previously in Refs. [143,144]. Such models allow the estimation of a value of E_ν with some accuracy.

In a multifront detonation wave, at any instant of time, the induction zone differs significantly (up to two orders of magnitude) for various elements of the detonation wave front. In this case, the use of a uniform ignition delay for the entire front (as in 1D models) can strongly misrepresent the initiation conditions. The reason for this is that ignition event is governed by a local temperature in the hot spots rather than by the average temperature. Such spots in a real detonation wave are the sites of collisions of transverse waves. The account of nonone-dimensional collisions of shock-wave configurations in a realistic detonation front allows the level of the critical initiation energy to be significantly lowered (in comparison with 1D models). Such a model of multipoint initiation was suggested in Ref. [145] and then modified in Refs. [146,147].

According to the latest version of the model, the energy of individual hot spots, E_{hs}, and the critical initiation energies (for $\nu = 1, 2, 3$), are defined by the following formulae:

$$E_{hs} = 4\varepsilon^2 \alpha_\nu \rho_0 D_{CJ}^2 b^2$$

$$E_1 = \frac{\pi (d_{cr}/a)}{4b} E_{hs} = A_1 \rho_0 D_{CJ}^2 b$$

$$E_2 = \frac{\pi (d_{cr}/a)}{2} E_{hs} = A_2 \rho_0 D_{CJ}^2 b^2$$

$$E_3 = 2\pi \tan\varphi (d_{cr}/a)^2 b E_{hs} = A_3 \rho_0 D_{CJ}^2 b^3$$

where $\tan\varphi = a/b$, ε is a parameter in the detonation cell model [148], d_{cr} is the critical diameter for reinitiation of spherical detonations under diffraction (see Section 2.2.4), α_ν is the parameter of the strong explosion model, and A_ν is the constant.

Other approximate models for estimating E_ν are worth noting. In Refs. [149,150], the following relationships are suggested:

$$r_{cr} \approx 8\nu\gamma^2 (\sigma_s + \sigma_s^{-1} - 2) \frac{L_{ind} R T_s}{3E}$$

$$E_\nu = \alpha_\nu p_0 \left(\frac{8 r_{cr}}{\nu} \right)^\nu$$

where E is the effective activation energy of the induction period (within the framework of the average description

using the Arrhenius equation), $\sigma = \rho/\rho_0$ is the density ratio, $\alpha_\nu (\nu = 1, 2, 3)$ are the constants, and index s labels properties at the lead shock wave.

In Ref. [151], the critical energy of spherical detonation initiation is defined as:

$$E_3 = \frac{2197\pi\gamma_0 J M_{CJ}^2}{16} p_0 a^3$$

where M_{CJ} is the Mach number of the CJ detonation and $J \approx q/(\nu D_{CJ}^2)$.

In Ref. [152], the critical energy of spherical detonation initiation is considered to be proportional to the induction zone length, L_{ind}, which is calculated on the basis of a detailed kinetic mechanism:

$$E_3 = BL_{ind}^3$$

where the coefficient B is determined from a measured value of E_3 for a fixed mixture composition and then considered constant for other mixtures of the given fuel.

The formulas of other available models show a much greater discrepancy when compared with experimental data and therefore are not discussed here.

Fig. 22 [153] shows the comparison of predicted and measured critical explosive charge mass, m_c, required for initiation of spherical detonations of ethylene–air and hydrogen–air mixtures depending on fuel concentration. The correlation between m_c and E_3 is given by:

$$m_c[\text{kg TNT}] = \frac{E_3[\text{J}]}{4.520 \times 10^6}$$

In general, the agreement between the predicted and measured results can be treated as satisfactory.

Thus, the energy of direct detonation initiation can be estimated from measured detonation cell sizes, ignition delays (or more precisely reaction times that include also the heat evolution stage), from various critical diameters, and from energies of direct detonation initiation in tubes. All these semi-empirical methods suffer significant errors associated with uncertainty of the measured cell sizes (because in most of practically important mixtures the cell structure is quite irregular) and with rather too approximate equations that do not take into account all the gasdynamic and chemical factors and nonuniqueness of the relation between the detonation front thickness, cell size, and reaction time. The method based on measurements of the initiation energy of plane detonation (as illustrated by Fig. 21) has some advantages since it does not require measurements of poorly reproducible parameters and admits measuring initiation energies of mixtures with very low reactivity in the laboratory-scale equipment. The limiting diameter of detonation propagation in tubes is the lowest of all the types of critical diameters usually measured in detonation studies, and a length of the tube which limits r_{cr}, can be taken as large as required to make measurements with mixtures possessing very low detonability.

The measured minimum initiation energies for some fuel–oxygen mixtures are listed in Table 4 [155]. For the FAMs, the values of E_3 (in kg of Tetryl) were measured in Ref. [156] (see Table 5).

Another serious problem, which arises in detonation initiation experiments and may cause misleading inferences, is the rate of heat deposition by the initiation source. In this respect, all the sources can be divided into two groups: the first one represents sources where the blast wave with the maximum amplitude at the front is formed already within the source and the second comprises sources with energy deposition distributed in time. High explosives and detonating gases are typical representatives of the first group, while electrical devices can be related to the second one. For the first group, the governing parameter is

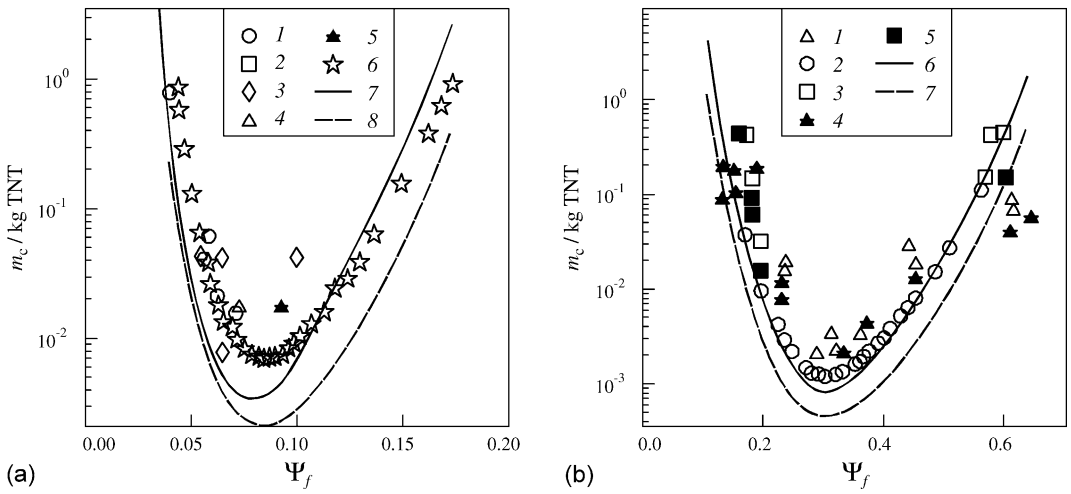

Fig. 22. Critical explosive charge mass, m_c, for initiation of spherical detonations vs. molar fraction of fuel, ψ_f (a) C_2H_4–air mixture. Symbols—experiments [143]: 1–5—detonations, 6—deflagration. Curve 7—models [143,144], curve 8—models [150,154]; (b) H_2–air mixture. Symbols—experiments [143]: 1–5—detonations. Curve 6—models [143,144], curve 7—models [150,154].

Table 4
Measured minimum initiation energies for some fuel–oxygen mixtures [155]

Fuel	Fuel % in the most detonable mixture	E_3 (J)
Acetylene	40.0	<0.11
Ethylnitrite	31.0	0.31
Allene	28.6	0.31
Methyacetylene	28.6	0.31
Ethylene oxide	40.0	0.31
Vinylmethyl ether	28.6	0.62
Cyclopropane	25.0	0.62
Ethylene	33.0	0.62
Vinylfluoride	40.0	0.88
Propylene	25.0	1.25
Diethyl ether	40.0	2.50
Propane	22.2	2.50
Ethane	28.6	8.75
Acetaldehyde	40.0	12.50

the energy released due to detonation of a charge, provided that the blast wave entering the mixture to be initiated has the parameters higher than those of the lead shock wave of CJ detonation. It is shown [157] that detonating gases give the same energy of direct detonation initiation as high explosives do solely when the shock amplitude produced by the initiating mixture ('donor') is not lower than the shock pressure in the wave leading the CJ detonation in the test mixture ('acceptor').

For the sources of the second group (e.g. electrical discharges), both experiments and calculations show that there is one parameter on which the critical energy depends, this is the source power or characteristic time of energy evolution. Fast energy evolution means that all the energy of the electrical discharge has been released before the onset of detonation so that this energy deposition can be approximately treated as an instantaneous explosion on the time scale relevant to detonation initiation. At longer times, or lower source power, a part of the energy deposited does not contribute to the blast wave production and therefore is lost, so that more energy should be introduced during the first stage of the electrical discharge, which is most important for detonation initiation.

In practice, initiation of detonation can be achieved even with energy sources somewhat weaker than the critical one.

Table 5
Measured minimum initiation energies E_3 (in kg of Tetryl) for some fuel–air mixtures [156]

Methane	Ethane	Propane	*n*-Butane	*i*-Butane	Ethylene
22[a]	0.04 (0.03)[b]	0.08 (0.05)	0.08 (0.05)	0.1 (0.08)	0.015 (0.010)

[a] Extrapolated.
[b] Insufficient to cause gas detonation.

This can be done by varying the geometry of the confinement, for example, by initiating the detonation in a tube and then letting it enter an unconfined cloud, or placing obstacles on the way of the blast wave (with a low blockage ratio), or else by HE charges with shells (dense shells allow the blast wave generated by the primary explosion to decay more slowly). Even in semi-confined areas, one can reduce substantially the minimum charge capable of initiating semi-spherical detonation just by varying the charge geometry, for example, by spreading the same amount of HE over a solid surface. Two conditions are to be met here in order to get reliable initiation with the same amount of HE. First, the layer should not be thinner than that providing the critical energy for plane detonation initiation, and the second, the lateral rarefaction wave should not merge at the charge axis until the blast wave travels beyond the critical radius.

Detonation can also be initiated by sources, which do not produce strong shock waves. A promising technique for detonation initiation with relatively weak sources has been suggested and validated experimentally by Frolov et al. [158,159]. Here, distributed external energy sources are used to artificially induce exothermic reactions behind a relatively weak shock wave in order to stimulate strong coupling between the shock wave and energy deposition. In the experiments, a weak shock wave was accelerated in the reactive mixture by means of in-phase triggering of seven electrical discharges in the course of shock wave propagation along the tube. Detonation-like regimes have been obtained at a distance of 0.6–0.7 m in the stoichiometric gaseous propane–air mixture under normal conditions in a smooth-walled 2 in.-diameter tube. Moreover, it has been found that the total critical detonation initiation energy was significantly less than that required for direct detonation initiation with a single electric discharge.

In Ref. [160], this technique has been applied to spray detonation initiation (see Section 2.3.3). Here, spontaneous or stimulated (e.g. by electrical discharge) ignition of reactive mixture is used to amplify the shock wave. Frolov et al. explain the approach by means of simple 1D calculations shown in Fig. 23a–d. Case (*a*) presents the primary (attenuating) shock wave produced by initiator located at the closed end-wall of the tube. Case (*b*)) shows the situation when the external ignition source mounted at a certain distance from the end-wall (shown as a horizontal bar with an arrow) is triggered somewhat prior to the primary shock arrival. The external ignition source facilitates ignition of the mixture producing a local pressure peak, and the primary shock wave is slightly amplified. Case (*c*) shows nearly 'resonant' conditions, when the external ignition source is triggered nearly in phase with primary shock arrival. Finally, case (*d*) corresponds to resonant conditions, when the external ignition source is triggered just in phase with primary shock arrival. Clearly, in case (*d*) external stimulation of reaction results in detonation initiation. With increasing the time delay of triggering

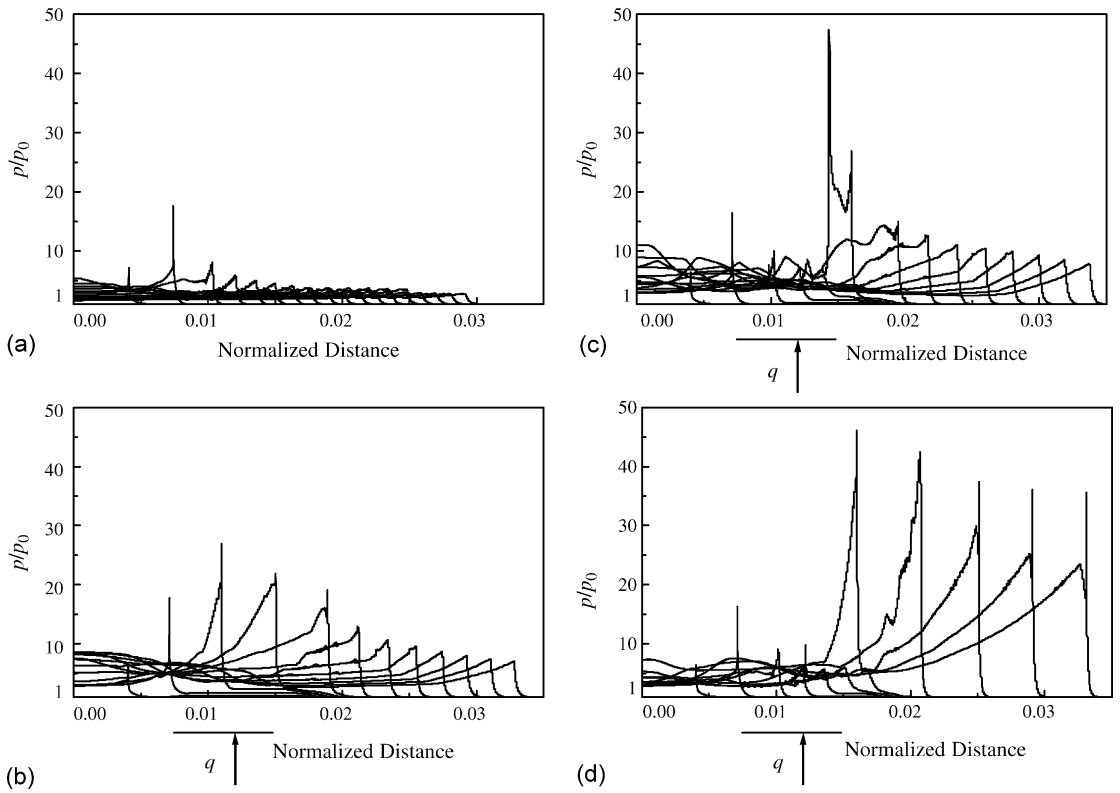

Fig. 23. Calculated temporal evolution of pressure waves generated by a hot spot and external energy deposition in a reacting gas: (a) hot spot ignition of reactive mixture, (b) hot spot ignition followed by triggering of external energy source (shown with a bar and arrow) far prior to shock wave arrival; (c) hot spot ignition followed by triggering of external energy source nearly resonant with shock wave arrival; and (d) resonant triggering of energy source resulting in detonation initiation [159,160].

the external ignition source, the situation becomes again very similar to that shown in Fig. 23b and a. The important feature of the phenomenon is that the dynamics of the system is very sensitive to the triggering time of the external igniter, other parameters kept unchanged. Note that, in fact, the idea of using a sequence of external igniters to initiate detonation goes back to Zel'dovich and Kompaneetz [98]. A 1D computational study of shock-wave amplification by energy deposition from external sources in the inert medium was reported by Thibault et al. [94].

There are examples available in the literature of direct detonation initiation by injecting hot turbulent jets [161] or some chemical compounds [162], as well as by irradiating the photosensitive gas [163], leading to mixture self-ignition. The mechanism of detonation initiation in these cases is essentially based on the idea first put forward by Zel'dovich et al. [93] and then developed in many theoretical studies [164,165]. This is self-ignition or flame (at some stage of the process) front acceleration and shock wave amplification in mixtures with temperature or concentration gradients. These produce a gradient of ignition delays, which affects energy release behind a weak compression wave, formed due either to the initial pressure disturbance or to very intense reaction in a certain volume at the initial stage of the process. Since the pressure rise near the travelling compression wave front shortens the ignition delays in this region, this wave initially driven by the self-ignition front propagating due to natural termination of induction periods in subsequent mixture layers converts gradually into a self-supporting wave and no longer needs the ignition delay gradient. This type of detonation initiation may turn out much more convenient in many practical applications than the direct initiation of detonation.

Chemical additives may also reduce the energy required to initiate detonation by blast waves. This effect may be readily estimated from the Zel'dovich formula. Indeed, since the energy of direct initiation depends on the reaction time reduction of either t_{ind} or t_{er} will reduce E_ν. There are many chemical additives capable of reducing t_{ind} at high temperatures within an order of magnitude, but t_{er} is almost insensitive to additives studied, therefore E_ν is reduced by additives to a much lesser extent than the induction time (usually within a factor of less or only slightly higher than 10, instead of several orders as would be expected from the Zel'dovich formula). But nevertheless, as experiment shows, small amounts of organic nitrates, nitrites, or compounds containing NF_2 groups, as well as of unsaturated or higher hydrocarbons being added (in concentrations not

higher than 15–20% with respect to the fuel) to simple hydrocarbon gases (like propane, methane, ethane) do reduce E_3 for initiation of spherical detonation by factors quite suitable for practical purposes. It should be emphasized that the effect of promoters is strongly dependent on the nature of both the fuel and the additive, and therefore the optimum concentration and the type of promoter should be sought for individually for each fuel.

Thus, the critical initiation energy is heavily affected by the 3D structure of detonation waves, which implies that its calculation should be based not only on reliable chemical kinetic data, but on the 3D unsteady computer codes. Therefore, at present, there is not much hope that numerical modeling will furnish quite reliable and easily accessible information on E_ν. The semi-empirical relations based on measured parameters relevant to the heat evolution kinetics are almost the only source for estimating E_ν (although the results obtained using these relations exhibit uncertainty within an order of magnitude for spherical detonations). The overwhelming majority of these semi-empirical procedures use the only reliably measured parameter relevant to the kinetics of heat evolution in detonation waves, namely, the detonation cell size, which unfortunately is not uniquely related to the real reaction zone length in detonation waves.

The most reliable direct measurements of E_ν is a time consuming and very expensive procedure, particularly for FAMs, therefore it is relatively seldom used. It should be emphasized that E_ν can be varied within a limited range by both physical and chemical means.

Mixture preconditioning can substantially reduce the initiation energy. The most illustrative examples of this preconditioning are initiation of detonation after reflection of weak shock waves from concave end-plates, after imploding shock waves, and in an expanding flow. Incident shock waves preheat the mixture and generate after reflection a hot spot (a region of finite size with a temperature gradient and high temperature at the center capable of self-igniting the mixture). The temperature gradient favors fast coupling between the compression wave generated by mixture self-ignition at the hot spot center and heat release in the adjacent mixture layers which ends up in detonation onset. Depending on the fuel type and end-plate geometry, the shock Mach number needed to initiate detonation in a FAM initially at room temperature can be reduced to about 2, which means a significant reduction of the energy to be deposited for generating detonation. As an example, Fig. 24 shows the results of computer simulation [166] of detonation initiation behind a shock wave reflected from the lateral wall of cylindrical cavity filled with stoichiometric hydrogen–oxygen mixture at $T_0 = 300$ K, $p_0 = 0.1$ bar. The initial intensity of the shock wave in the channel attached to the cavity is as low as $M_s = 2.2$. The local pressure and temperature peaks in the gasdynamic focus formed after shock reflection are sufficient to ignite the mixture and give rise to detonation as indicated in Fig. 24c and d.

A device capable of creating a collapsing toroidal detonation wave front has been designed and manufactured in Ref. [130] (Fig. 25). The goal is to generate pressures and temperatures at the focal point of the collapsing detonation wave that will be sufficient to initiate detonations in insensitive FAMs inside a detonation tube without blocking the flow path. This toroidal initiator uses a single spark and an array of small-diameter channels to generate and merge many detonation waves to create a single detonation wave with a toroidal front. Testing was performed with stoichiometric propane–oxygen mixtures at $p_0 = 1$ bar. Images of the detonation front show a nearly circular wave front (Fig. 26). To determine the pressure increase achieved by toroidal focusing, pressure transducers were mounted on a radial line with the central transducer located on the central axis of the initiator tube. A typical set of pressure traces is shown in Fig. 27. The outermost three pressure transducers show a gradually decreasing pressure wave as the radius of the imploding torus decreases. The central pressure transducer, however, recorded a value above its maximum reliable operating range. This value was four times larger than the CJ pressure for the mixture.

2.2.4. Detonation transition

Since the energy required to initiate detonation, particularly in FAMs, is so large that it is extremely difficult to generate the conditions where direct initiation can result from a typical energy source. Detonation is known to arise most readily in long narrow ducts. Hence, in practice, it is important to estimate the probability of transition of detonation to unconfined or semi-confined large mixture volumes from where it can be excited by weak sources. For this reason, numerous investigations were conducted to study critical conditions for detonation transition from a tube to an unconfined mixture cloud or to a tube of a much larger diameter. Here a parameter controlling the transition is the critical diameter of the narrow tube, d_{cr}. The values of this critical diameter were estimated for many fuel–oxygen and FAMs. They range from millimeters to more than one meter. It is natural to expect that d_{cr} should depend on the distance between the lead shock front and the effective CJ plane, L_{CJ}, which can be expressed through the transverse cell size, a, of the detonation front. Experiments show that usually the ratio of d_{cr} to the cell size, d_{cr}/a, is close to 13 for round tubes and 7 for slots [84]. Although there are some mixtures where the ratio reaches even 46.

Fig. 28a–c present three series of Schlieren photographs relevant to detonation transition (superctitical case), detonation reignition (near-critical case) and detonation decay (subcritical case) in hydrogen–oxygen–argon mixture [167].

To understand the reason why the ratio d_{cr}/a is nearly constant and why it is close to the above numbers, it is necessary to analyse the flow pattern near a step-wise

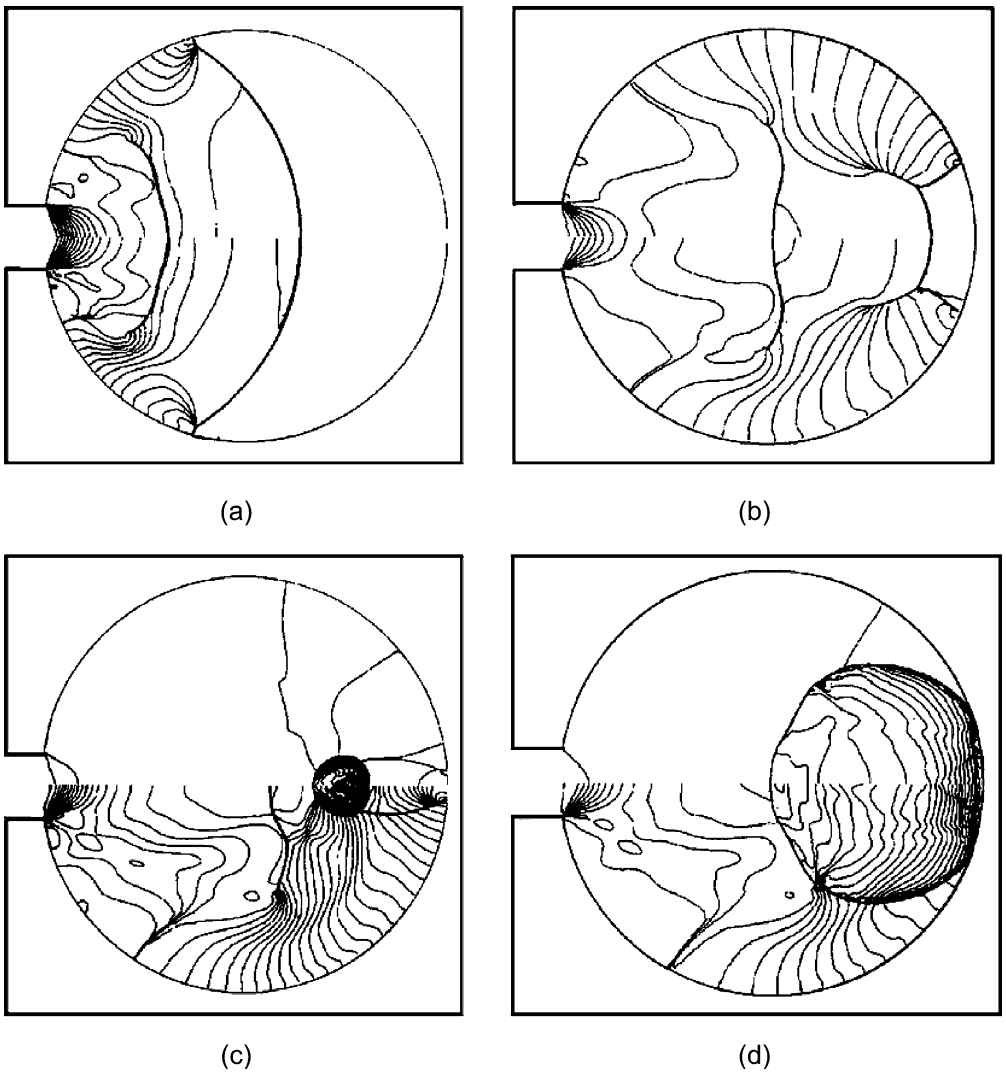

Fig. 24. Numerical simulation of initiation of detonation in stoichiometric H_2–O_2 mixture behind a shock wave reflected from the lateral wall of cylindrical cavity [166]. Initial shock Mach number in the channel attached to the cavity is 2.2. Upper halves of figures show predicted isobars, lower—isochors for different time instants relative to the time of spontaneous ignition: (a) −33 μs, (b) −8 μs, (c) +11 μs, and (d) +39 μs.

change of the tube cross-section (Fig. 29a [55,168]). When detonation wave 1 exits from a channel it generates a diffracted shock front 2 at the periphery (Fig. 29b [169]). The temperature drop in this wave portion is so large that ignition ceases behind it. Thus, transverse waves 3 travelling over the detonation front meet no partners to collide with at the periphery. The soot tracks show clearly (Fig. 29a) that a kind of a phase wave of cell disappearance originates at the tube rim and propagates toward the tube axis. This wave propagates at the velocity of transverse wave motion (which is approximately $0.6D_{CJ}$). Lateral expansion of the gas at the tube rim produces a rarefaction wave fan, the head of which (curve 4 in Fig. 29b) spreads toward the tube axis. It spreads through the unburnt mixture compressed by the lead shock front of the detonation wave, since it is this wave which can

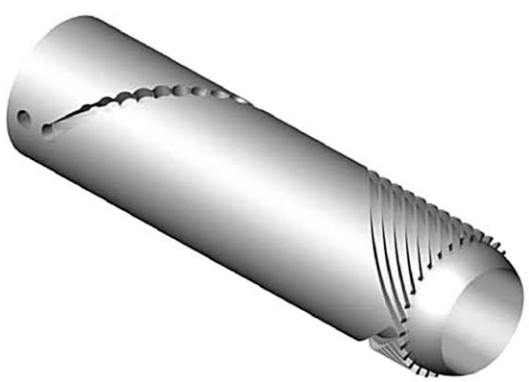

Fig. 25. Schematic of annular detonation wave initiator (covering shell omitted for clarity) [130].

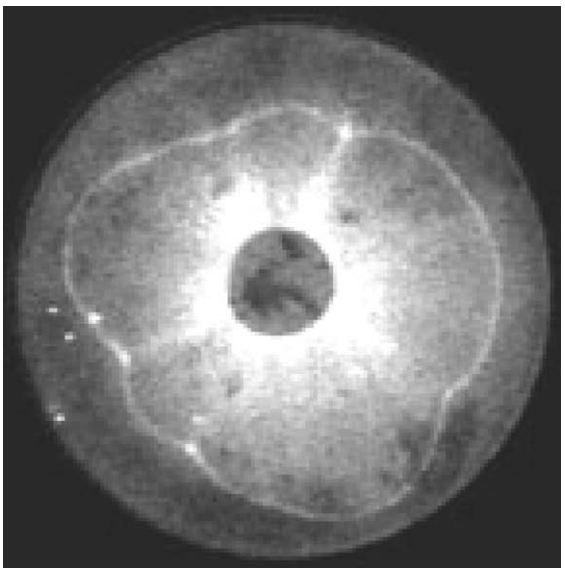

Fig. 26. Chemiluminescence image of imploding detonation wave. Irregular secondary wave is thought to be due to interaction with window [130].

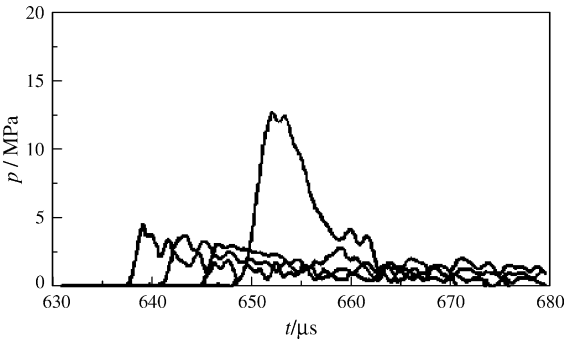

Fig. 27. Pressure traces obtained in the initiator shown in Fig. 25.

be responsible for reaction suppression. The velocity of this rarefaction wave is equal to $\sqrt{c_s^2 - (D^2 - u_s^2)}$. Here, c_s is the speed of sound in the shocked gas. As the analysis of multicell detonations shows, the reaction front 5 tends to decouple from the lead shock front (curve 6) within the second part of the detonation cell, i.e. when the blast wave generated by the transverse wave collisions attenuates. This means that the disappearance of collisions of the transverse waves (triple points 7) extends the reaction zone to such an extent that one can hardly expect any reaction behind the lead shock front at the periphery (where no collisions occur). The detonation wave will decay if, after the rarefaction wave arrival at the tube axis, no ignition occurs within the zone between the attenuated detonation wave (with no collisions) and the rarefaction wave trajectory. This ignition (if at all it occurs) will restart the cell structure in the zone between the trajectories of the two waves. It is clear that for restarting to occur the distance between the above two trajectories should be no less that the transverse size of the newly formed cell (which should be larger than the cell of the unperturbed detonation wave). This yields a simple relation for the height δ_{ri} at which this reinitiation occurs:

$$\delta_{ri} > \frac{b_2}{2} + \frac{Aa_1 D}{u_{cd} - u_e}$$

where b_2 is the longitudinal size of the secondary cell, $A = a_2/a_1$ is the ratio of the transverse sizes of the primary and secondary cells, and u_{cd} and u_e are velocities of the cell disappearance and rarefaction waves, respectively. Thus δ_{ri} measured from the soot tracks can be used to estimate A. Reinitiation is a stochastic process since it involves ignition, which occurs with a certain spread of the ignition delays (see dense regions in Fig. 29a). Furthermore, for both round tubes and slots this reinitiation must occur simultaneously throughout the cross-section near the duct axis. This imposes a more severe condition on the critical diameter and the minimum permissible reinitiation zone width ($d = \xi a_2$, where $\xi > 1$). This finally yields:

$$d_{cr} = \frac{2\xi A u_{cd}}{u_{cd} - u_e}$$

The values obtained for the coefficients in the equation for d_{cr} are presented in Table 6.

A comparison of this relation with experimental data on d_{cr} gives values of ξ ranging between 1.6 and 2.3 for round tubes, which seems quite reasonable. The presence of

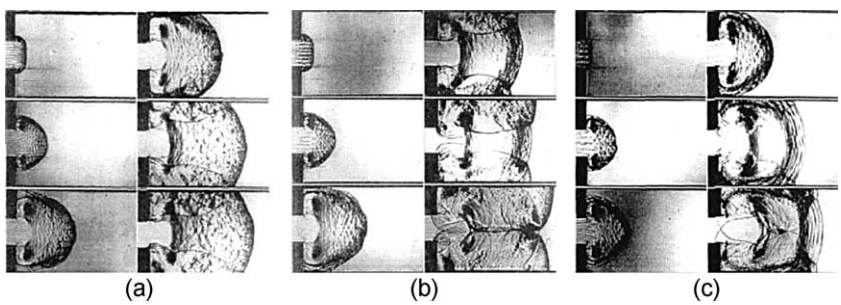

Fig. 28. Three series of Schlieren photographs relevant to (a) detonation transition (superctitical case), (b) detonation reignition (near-critical case) and (c) detonation decay (subcritical case) in a stoichiometric hydrogen–oxygen–argon mixture. (a) 60% Ar, (b) 70% Ar, and (c) 73% Ar [167].

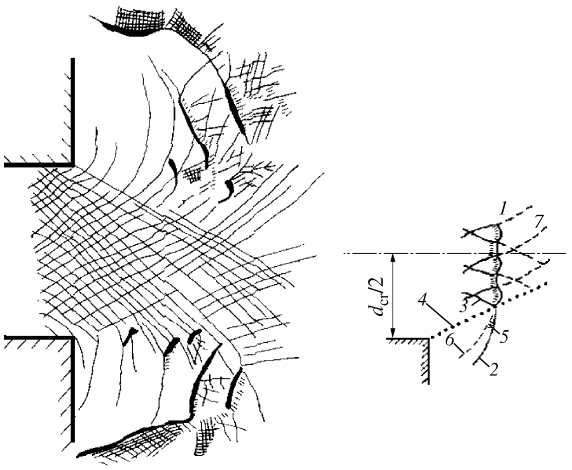

Fig. 29. (a) Sketch of a soot track record of the reestablishment of a $2C_2H_2 + 5O_2$ detonation propagating through a suddenly expanding channel [55,168]. (b) Critical diameter model [169]. 1—detonation wave, 2—diffracted shock wave, 3—transverse wave, 4—head of rarefaction wave, 5—reaction front, 6—decoupling of reaction front from the diffracted shock wave, 7—trajectories of triple points.

detonation cells of various sizes and fluctuation of ξ may account for the large d_{cr} values reported for some mixtures.

Experiments with different mixtures show that the critical diameter of a duct, at which detonation sustains in the unconfined cloud, is a function of the angle of the cone through which detonation waves travel from the duct to the cloud. This dependence is shown in Fig. 30 [138]. As seen from the figure, the critical diameter ceases to depend on the cone angle φ when its value exceeds 60°. This means that at greater cone angles a part of the mixture at the periphery does not contribute to detonation reinitiation, because the amplitude of the diffracting wave is too low for the mixture to self-ignite within a reasonable time interval. The results of Fig. 30 can also be explained in another way: decreasing the transition

Table 6
Coefficients for evaluating d_{cr}

Mixture	u_{cd}/D	u_e/D	c_s/D	c_{CJ}/D	δ_{ri}/a_1	A	ξ
$2H_2 + O_2$	0.59	0.42	0.44	0.56	7.0	1.1	1.6
$2H_2 + O_2 + 1.17N_2$	0.57	0.38	0.43	0.56	6.5	1.1	1.8
$CH_4 + 2O_2$	0.64	<0.45	0.35	0.56	3.8	>0.7	1.6
$CH_4 + 2O_2 + 1.17N_2$	0.64	<0.45	0.35	0.54	5.8	>1.0	1.6
$C_3H_8 + 2O_2$	0.62	0.36	0.26	0.56	7.5	1.7	2.3
$C_3H_8 + 4.4O_2$	0.68	0.41	0.30	0.54	7.5	1.8	2.2
$C_3H_8 + 5O_2$	0.53	0.34	0.31	0.54	8.0	1.4	2.0
$C_2H_2 + 2.5O_2$	0.56	0.36	0.35	0.57	3.7	0.7	2.0
$C_2H_2 + O_2$	0.54	0.35	0.31	0.55	–	–	1.9

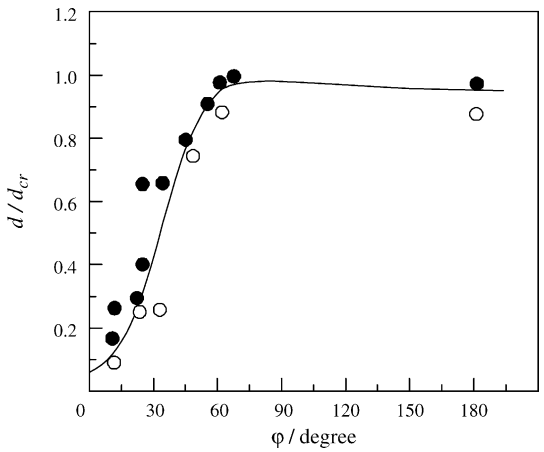

Fig. 30. The critical diameter for detonation transition from a tube into a large volume as a function of the transition cone angle φ [138]. Open and filled circles pertain to no go and go runs, respectively. Mixtures: hydrogen–oxygen and methane–oxygen.

cone angle below 60° promotes transition of detonation from the duct to the cloud or large volume. Of course, the transition conditions depend on the initial pressure. This is illustrated by Fig. 31 [170] showing smoked foil records for detonation in $C_2H_2 + 2.5O_2$ mixture propagating through conical expansions with different angles at near-critical initial pressures.

There are two other principal means to enhance transition of detonations. The first is to increase the power of the driver, for example, to use a more energetic (e.g. fuel–oxygen) mixture in the duct [171]. It has been shown that initiation of a nitrogen-diluted propane–oxygen mixture in a large vessel is more readily accomplished by a driver containing undiluted propane–oxygen mixture rather than the same dilute test gas. In terms of the value of d_{cr}/a, the enhancement of driver power resulted in decreasing d_{cr}/a value by a factor of 1.75 (from 21 to 12), where a is the transverse cell size for the mixture being initiated. Thus, the propane–oxygen driver was capable of initiating a considerably less sensitive mixture. In order to increase the power of the driver one can use an overdriven rather than regular CJ detonation wave. To overdrive detonation in the driver, Vasil'ev [172] applies a divergent conical nozzle. In this case, it is possible to decrease the value of d_{cr}/a for initiating a stoichiometric acetylene–oxygen mixture by a factor of 1.8 at overdrive ratio of $D/D_{CJ} = 1.3$.

Desbordes [88] and Desbordes and Lannoy [173] have investigated the effects of overdriving a detonation wave during diffraction from a smaller combustion tube to a larger volume. In both studies it was found that a definite benefit could be obtained when a detonation wave was allowed to propagate into a less reactive mixture immediately before diffraction occurred, thus creating an overdriven condition in the less reactive mixture.

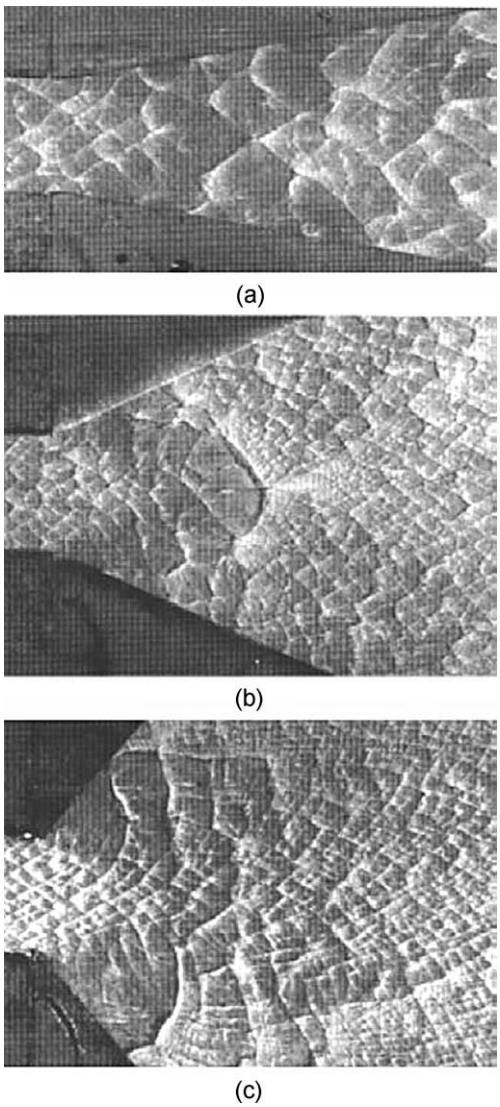

Fig. 31. Smoked foil records for detonation in $C_2H_2 + 2.5O_2$ mixture propagating through conical expansions with different angles at near-critical initial pressures [170]. (a) $\varphi = 10°$, p_0 =4.0 kPa, (b) 25°, 8.0 kPa, and (c) $\varphi = 45°$, p_0 =10.6 kPa.

A second means of promoting transmission is to use various shock reflection and focusing techniques. Vasil'ev studied detonation transmission through the plate with several orifices [174]. He found that distributed initiation sources were more efficient than a single orifice of the same overall exit area. The reason for such an effect is lengthening of the overall energy liberation time and formation of hot spots due to shock collisions after passing through the distributed orifices.

Murray et al. [175] studied transition geometries shown in Fig. 32. For comparison purposes, they introduced the 'transmissibility' parameter $\Omega = d_{cr}/d_0$, where d_0 is the actual tube diameter with transition enhancing elements.

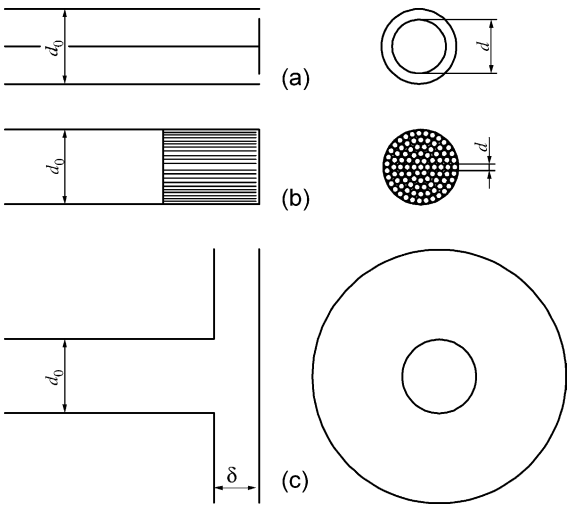

Fig. 32. Transmission geometries in experiments [175]: (a) annular orifice, (b) tube bundle, and (c) cylindrical gap.

Defined in this manner, values of Ω greater than unity indicate that transition is enhanced relative to that from a simple tube, while values less than unity signify that transition is inhibited. In experiments with annular orifices (Fig. 32a), a maximum value of $\Omega = 2.2$ was observed in acetylene–air mixtures and $\Omega = 1.8$ in acetylene–oxygen mixtures. This means that a driver tube 2.2 times smaller than the critical tube diameter can be used to initiate detonation in the unconfined region outside of the tube when the appropriate orifice plate is present at the exit. In contrast, tube bundles (Fig. 32b) were found to be relatively inefficient transition promoters. In the case of transition to a cylindrical gap, the transmissibility was a function of δ/d_0, where δ is the gap width. Experiments employing acetylene–oxygen mixtures have shown that $\Omega = 2.4$ for the largest gap used ($\delta/d_0 = 1.12$).

Teodorczyk et al. [176] and Oran et al. [177,178] have analyzed the reinitiation mechanisms associated with Mach reflections at a rigid wall of a quasi-detonation wave propagating in an obstacle-laden channel and of a spherical blast wave, respectively. Both studies stress the importance of the rapid reignition sites immediately behind the generated Mach stems at the wall. Murray et al. [175] also demonstrated the importance of shock–shock and shock–wall collisions for different exit conditions at the diffraction plane, including tube bundles, annular orifices, and cylindrical diffraction. The reinitiation mechanism associated with the Mach reflections observed in the above-mentioned studies is extremely important for the initiator concept utilized in PDEs. It also becomes particularly important as the combustor diameter approaches the cell size of the mixture and few transverse waves exist to assist with adjusting the spreading wave to the conditions in the expanding flow near the diffraction plane. The reinitiation process under such conditions appears to be a very local

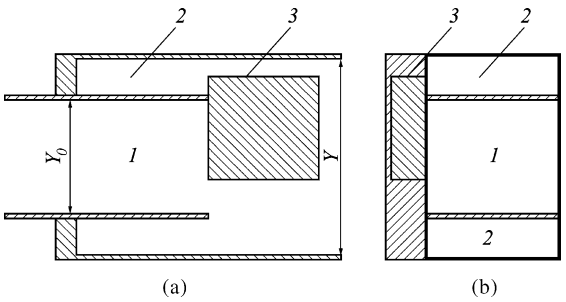

Fig. 33. Optical access 2D test section used for imaging studies in detonation transition experiments [179]; (a) side view, (b) end view; 1—initiator tube, 2—test tube, and 3—window.

process and the influence of the wave front structure and reflection cannot be ignored during the analysis.

It is natural that all the approaches that allow one to enhance the detonation transition can be combined. Below, two recent examples are presented that combine different tools for improving the transition conditions.

Brophy et al. [179] have conducted detailed experiments aimed at better understanding of the mechanisms responsible for successful detonation transition in a 2D geometry shown in Fig. 33. Fig. 34 summarizes the successful and unsuccessful test conditions for which detonation transmission occurred in the ethylene–air mixtures. With the exception of an occasional reignition due to a localized explosion some distance behind the leading shock, it appears that the shock reflection at the confining surface of the outer wall to be the primary mechanism for reinitiation in this geometry. Primarily, the increased heating and associated chemical activity behind the arising Mach stem provide the rapid energy release required for reinitiation. It is believed that if the detonation wave exiting from the initiator can be tailored to possess a very large Mach number, the transition via the diffraction will be substantially enhanced.

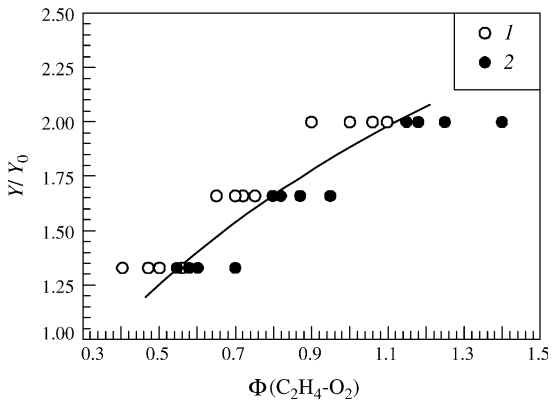

Fig. 34. Results for the 2D diffraction geometry [179]. Y_0 =50.8 mm, p_0 =100 kPa, T_0 =283 K. Test mixture—C_2H_4–air; initiator mixture—C_2H_4–O_2. 1—unsuccessful and 2—successful initiation.

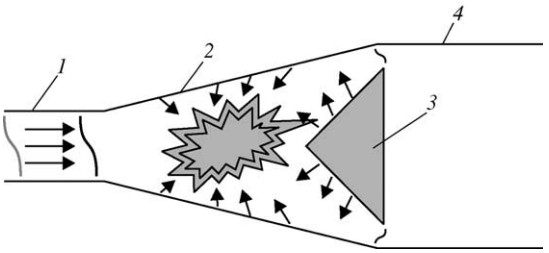

Fig. 35. Schematic representation of the initiation of detonation transition from narrow tube 1 to wide tube 4 via transition cone 2 and shock-focusing obstacle 3 [180].

Santoro et al. [180], to enhance ethylene–oxygen–nitrogen detonation transition, installed shock-focusing obstacles in the transition cone (with a 10° divergence angle) at different locations downstream of the transition cone exit. Shock-focusing obstacles (in the form of disks of 50 and 78% blockage ratio (BR) or 45° cone of 78% BR) were found to improve the conditions for detonation transition from the narrow tube (33.3 mm in diameter) to the main tube (105 mm in diameter). In particular, their results indicate that a conical obstacle is superior to the flat disk obstacles of comparable BR. Fig. 35 depicts a schematic representation of the process. The key phenomena include the propagation of overdriven detonation occurring in the end region of narrow tube 1, which is followed by a significant energy release in the volume of gases located in transition section 2. The enhancement observed with the addition of transition obstacles 3 is postulated to be a result of shock focusing as compression waves are reflected from the obstacle and walls. In the final stages of the process, localized explosion occurs and the resulting detonation wave is characterized by a high degree of overdrive. Thus, the overdriven detonation wave enters the transition section before it decays back to the CJ state. It is believed that within the transition section, further interaction of the decaying detonation with the shock-focusing obstacle generates hot spots where localized explosion occurs. Again, this phenomenon sustains the detonation and allows it to successfully transition into main tube 4.

Thus, a combination of Mach reflections, shock focusing, and overdriven conditions are the mechanisms which appear to dominate detonation transition and are likely to be the apparatus for application in detonation-based propulsion systems.

Detonation limits and critical distances are certainly affected by the quality of the mixture, i.e. by how thoroughly and homogeneously the components are mixed. There is direct experimental evidence of extension of the detonability limits and critical diameters just by better mixing of the components. In practice, highly homogeneous mixtures are very seldom encountered. Therefore, it is of interest to evaluate how the concentration gradients may affect both propagation and critical conditions of detonations.

There could be several configurations of the concentration fields. The typical situation for fuel spills or injectors (for example, in a liquid propellant combustion chambers) is detonation propagation along a stratified mixture. Usually the most detonable layer is situated somewhat above the surface from which the fuel is supplied to the oxidizing atmosphere, and once initiated, it propagates interacting either with less detonable or inert layers (fuel-rich on the injector side and fuel-lean at the ambient gas side). The critical conditions in this case are similar to those in unconfined mixture layers, except the reaction in the less detonable mixture would partially support the main detonation wave.

Investigations on transition of detonation through the regions of nonuniform composition were also reported [181–184]. For example, Thomas et al. [181] produced gradients of concentration by allowing molecular diffusion to take place between the $C_2H_2 + 2.5O_2$ mixture and argon, for varying times after the removal of a special slide initially separating the gases. Fig. 36 shows the measured velocity vs. distance plots. The solid curves at some plots represent the calculated CJ values appropriate to the particular mixture composition. From a knowledge of the concenteration gradients at the velocity–distance record, velocity–dilution dependence can be obtained that is shown in Fig. 37. It is seen that the detonation velocities in the gradient concentration fields agree well with the corresponding measured steady state detonation velocities shown by solid circles in Fig. 37. The difference between measured and calculated velocities can be attributed to wall effects not taken into account in thermodynamic calculations. Hence, one may conclude from this agreement that the velocity at any plane in a concentration gradient adjusts very rapidly to the value appropriate to the dilution. As the spacing of the transverse waves in a detonation, and hence the cell size, is very sensitive to the degree of departure of the wave velocity from the CJ value, an additional test of the validity of the above finding was made by smoked-foil method [181]. Fig. 38 shows the results of such measurements obtained with carbon dioxide as a diluent gas. The solid line presents the longitudinal cell size b for a steady-state detonation as a function of CO_2 dilution. Thus, taken together, the velocity (Fig. 37) and cell size (Fig. 38) data indicate that the cell structure is likely to adjust

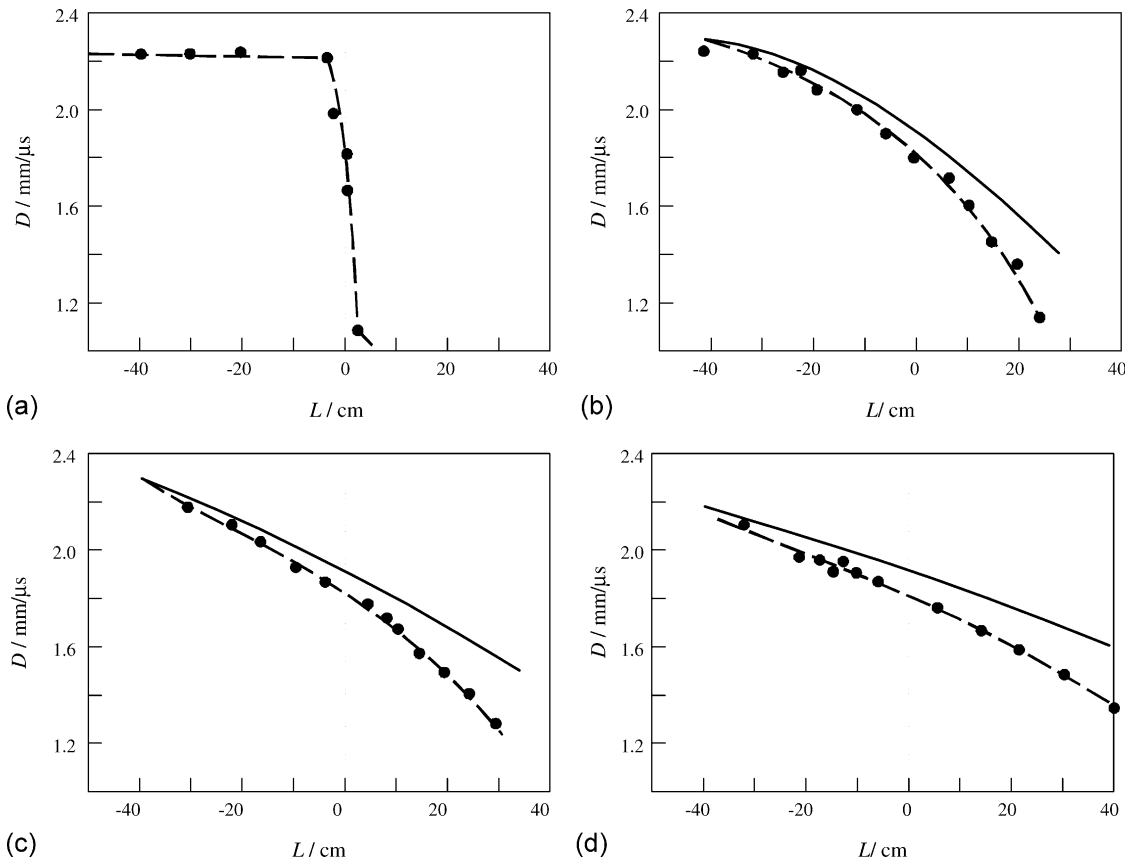

Fig. 36. Velocity D vs. distance L plots for a range of diffusion times for $C_2H_2 + 2.5O_2$ mixture into argon, $p_0 = 100$ Torr, rectangular tube 22×10 mm; (a) 0 s, (b) 120, (c) 240, and (d) 600 s. Solid lines are calculated CJ velocities corresponding to the local gas composition [181].

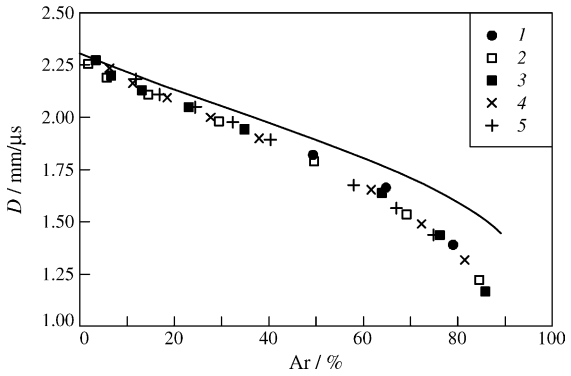

Fig. 37. Measured velocities as a function of local composition of $C_2H_2 + 2.5O_2 + Ar$ mixture. Solid curve is calculated CJ velocity. 1—measured steady state velocities at the corresponding compositions. Other symbols correspond to different diffusion times: 2—120 s, 3—240, 4—360, and 5—600 s [181].

rapidly to the local concentration conditions. This is in general agreement with the conclusion first established by Strehlow et al. [185].

One of the situations often encountered in practice is propagation of detonation through a nondetonable gap. Experiments have demonstrated that there is a reinitiation stage between detonation initiation and passage of detonation through the gap: the wave velocity drops in the gap and then builds up again in the detonable mixture and interestingly enough, like in the case of initiation the minimum velocity observed at the critical gap width is about $0.6D_{CJ}$. No detonation transmission occurs, if the velocity drops below this value. Numerical simulation [186] reveals a similar behavior of transient detonation (see Fig. 39).

2.2.5. Nonideal detonations

The term nonideal detonations relates to detonation processes in which only a fraction of the available heat is released upstream of the sonic plane and that are influenced

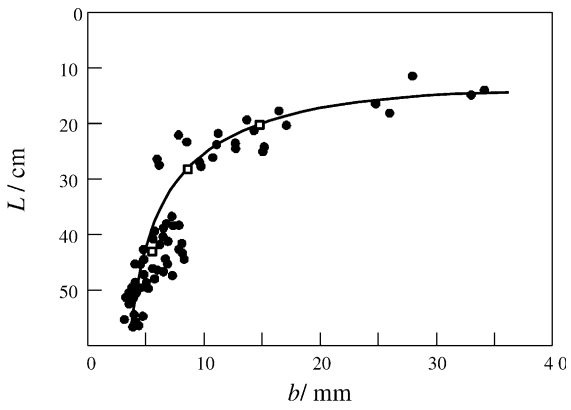

Fig. 38. Variation of measured longitudinal cell size b with distance L after 6 min diffusion time at a $C_2H_2 + 2.5O_2/CO_2$ interface. Open points are from measurements of steady state detonations at the corresponding compositions [181].

by various types of losses. The list of intrinsic losses includes:

I. Losses involving nonequilibrium processes in the reaction zone:

- losses due to nonuniform distribution of the thermodynamic parameters, concentration and velocity fields across a tube;
- losses caused by turbulence in the core flow;
- losses induced by nonstationary processes in the reaction zone;

II. Irreversible losses of energy:

- friction losses involving:
  (a) viscous losses in boundary layers;
  (b) eddy losses due to flow separation on obstacles;
- bow shock losses at obstacles;
- losses arising from divergence of streamlines in the reaction zone;
- heat losses to the tube walls and obstacles;
- losses connected with incomplete burning of the combustible mixture.

One may estimate the approximate magnitude of the losses included in the first group from the following observations. Detonation velocities of most reactive mixtures (e.g. $C_2H_2 + 2.5O_2$, $2H_2 + O_2$) measured in smooth-walled tubes of a diameter up to 75 mm are smaller than thermodynamic values calculated without taking into account the losses [98]. The detonation velocity deficit due to nonuniformity of the flow in the reaction zone is greater than that caused by relaxation phenomena [187]. Clearly, some types of losses can be neglected. If there are irreversible losses caused by external forces (losses of the second group) one may disregard the losses of the first group and use relations of equilibrium thermodynamics. At high magnitude of the second-group losses, nonequilibrium effects become significant and the problem of correct formulation of the equation of state arises. In this case, gradients of the flow parameters must be included in the equation of state. As long as the detonation parameters are close to the calculated ones, there is no grounds to doubt that the losses are much less than the energy and momentum flux in the wave caused by the exothermic reaction.

The traditional analysis of the so-called thermal model of steady detonations with losses performed for the first time by Zel'dovich [49] led to a conclusion that for a reaction kinetics obeying the Arrhenius law the losses can reduce the detonation velocity only insignificantly. Significunt losses result in detonation failure. However, losses from a detonation wave may cause not only its failure, but may change radically the mode of its propagation. Early experiments by Shchelkin [48] revealed that in rough tubes reaction waves could propagate at constant velocities that were much below

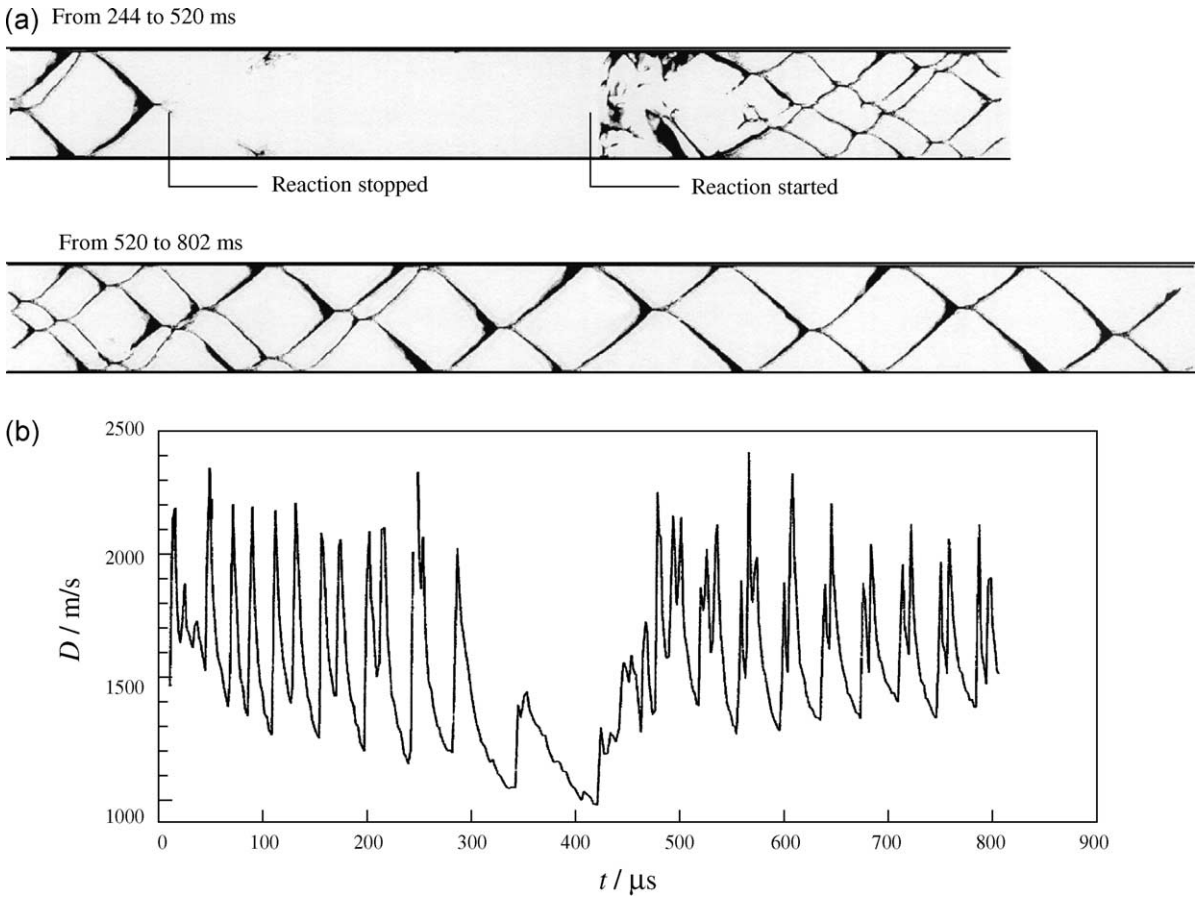

Fig. 39. Two-dimensional simulation of a reactive wave propagating in a hydrogen–oxygen–argon (2/1/7) mixture. The chemical reaction has been cut off at 283 μs and reignited after 140 μs. (a) Detonation imprints for a wave. (b) Evolution of the detonation velocity [186].

the limiting ones predicted by the Zel'dovich theory. Later investigations showed that the reaction zone in such steady waves was essentially 3D and very long as compared to those found in ordinary detonation waves. Moreover, it was also discovered that the reaction started near the walls immediately behind the lead shock front. All these findings allowed Zel'dovich to put forward a physical model of this wave comprising two essential elements: ignition of the mixture at the wall by the shock wave reflected at the roughness elements and subsequent mixture burning in a turbulent flame front formed in the boundary layer. This detonation mode is called differently by various authors: low-velocity detonations, quasi-detonations, and nonideal detonations. All the terms, except 'quasi-detonations', reflect adequately the nature of this phenomenon, because all the features of the ZND model, namely, shock initiation of the reaction, supersonic velocity, and incapability of the rarefaction wave to overcome a certain plane behind it (i.e. the self-sustaining nature of the wave) are inherent in this wave. Term quasi-detonations is, in this respect somewhat conventional, and is used often because of its brevity.

First, consider the losses associated with the effect of confinement, because, in practice, unconfined detonations are encountered much less frequently than detonations in various forms of ducts. This is due to the fact that initiation of detonation and spontaneous transition from deflagration to detonation in ducts impose much less severe restrictions on the ignition source and reactivity of the mixture. No data on successful DDT independent of the influence of the vessel walls or the ignition source are available in the literature. Special experiments [188] in which precautions were made to preclude formation of a boundary layer, strong initial shock waves, and possible reflections of the compression waves produced by the flame showed that even in hydrogen–oxygen and acetylene–oxygen mixtures at initial pressures up to 80 atm detonation never originated as a consequence of spherical-flame acceleration within a distance of 10 cm from a very weak ignition source. The mixtures detonated only when some flow turbulizers

were mounted in the vessel (a simple rod 3 mm in diameter sufficed to cause the transition due to formation of a boundary layer and flame acceleration along it).

The discussion here is restricted to steady phenomena in order to show how the losses may influence the detonation wave parameters and structure. It is not difficult to estimate how insignificant a role conductive or convective heat and momentum transfer play in detonation waves propagating in relatively large tubes with smooth walls. Thus the governing mechanism of heat evolution behind detonation waves is self-ignition of the shocked gas (it cannot be due to flame propagation), and the heat and momentum losses due to build up of the boundary layer within the zone between the shock and CJ planes cannot directly affect the flow in the core. Nevertheless, they can affect the course of the reaction behind the detonation front indirectly through rarefaction waves generated by these losses. Indeed, deceleration of the flow near the wall and cooling of a thin gas layer 'sucks' some gas mass, its momentum, and energy to the wall thereby producing a rarefaction wave which propagates at an acoustic velocity towards the tube axis and decelerates the lead shock wave since this occurs within the zone with $M < 1$ where any perturbation may overcome the shock front. Decreasing the tube diameter or introducing wall roughness will evidently result in loss enhancement.

These qualitative considerations imply that the rarefaction waves spreading at velocities of the order of 1 km/s may more or less normalize the flow parameters over the tube cross-section and thereby make the 1D approach applicable to treating the averaged flow parameters behind the lead shock front, at least for qualitative analysis.

As shown by Frolov [56] kinetic energy dissipation in the detonation wave can result in the detonation velocity decrease and attaining detonability limits. Depending on the mechanism of momentum loss (e.g. drag force, turbulence generation and dissipation, expansion, shock reflections, etc.) detonation velocity deficit differs. In principle, if the dissipation mechanism is weakly coupled with the flow (as is the case with detonations in rough tubes) the theory predicts a continuous spectrum of detonation velocities. In the case of strong coupling between the kinetic energy dissipation and flow properties (as is the case with detonations in smooth tubes) there exists a finite tolerable drop in the detonation velocity manifesting detonability limit.

As a matter of fact, a simple form of the energy conservation equation for the flow behind the steady, planar, self-sustained detonation front propagating at the CJ detonation velocity D_{CJ} is:

$$h_{CJ} - h_s + \frac{u_{CJ}^2}{2} - \frac{u_s^2}{2} = q$$

where h is the static enthalpy, u is the velocity in the frame of reference attached to the lead shock, q is the chemical effect of reaction, and indices s and CJ correspond, as before, to flow properties immediately behind the lead shock and at the CJ plane, respectively.

This equation indicates that the chemical effect of reaction is consumed to increase the static enthalpy of the post-shock flow from h_s to h_{CJ} and the kinetic energy from $u_s^2/2$ to $u_{CJ}^2/2$. Based on the strong shock approximation, it is easy to estimate the relative distribution of chemical energy among those components:

$$\frac{h_{CJ} - h_s}{q} = \frac{2\gamma(2-\gamma)}{\gamma+1}$$

$$\frac{u_{CJ}^2 - u_s^2}{2q} = \frac{(\gamma-1)(2\gamma-1)}{\gamma+1}$$

where γ is the specific heat ratio (assumed constant).

Let us assume that a part of kinetic energy of the post-shock flow, $k' > 0$, is dissipated into heat due to momentum loss. In terms of the above equations, this can be written as:

$$\frac{h'_{CJ} - h'_s}{q'} = \frac{2\gamma(2-\gamma)}{\gamma+1} + \Delta \tag{6}$$

$$\frac{u'_{CJ}2 - u'_s 2}{2q'} = \frac{(\gamma-1)(2\gamma-1)}{\gamma+1} - \Delta$$

where prime denotes the disturbed solution, and $\Delta = k'/q'$. As a result of such redistribution of energy, one can expect variation of parameters in the CJ plane. First, it can be shown that the CJ condition $u'_{CJ}/c'_{CJ} = 1$ does not hold any more at a given detonation velocity $D = D_{CJ}$ (c_{CJ} is the speed of sound at the CJ plane). Indeed, as in this case $q' = q, h'_s = h_s$, and $u'_s = u_s$, the perturbed values of flow velocity and sound speed at the CJ plane are given by:

$$u'_{CJ} = u_{CJ}\sqrt{1 - \frac{2k'}{u_{CJ}^2}}$$

$$c'_{CJ} = c_{CJ}\sqrt{1 + \frac{(\gamma-1)k'}{c_{CJ}^2}}$$

In the undisturbed CJ detonation wave, $u_{CJ} = c_{CJ}$; therefore the above equations clearly indicate that $u'_{CJ}/c'_{CJ} < 1$. This means that the steady solution is violated at any finite k'. Since the disturbed flow becomes subsonic, the rarefaction waves enter the reaction zone and decrease the detonation velocity. The normalized deficit of the detonation velocity:

$$\sigma_D = \frac{D_{CJ}^2 - D'^2}{D_{CJ}^2}$$

can be readily found. As, in general, $q' \neq q, h'_s \neq h_s$, and $u'_s \neq u_s$, Eqs. (6) result in:

$$u'_{CJ} = u_{CJ}\sqrt{1 - \frac{2k'}{u_{CJ}^2} - \frac{\sigma_D u_s^2}{u_{CJ}^2} - \frac{(\gamma-1)(2\gamma-1)}{\gamma+1}\frac{2\eta q}{u_{CJ}^2}}$$

$$c'_{CJ}=c_{CJ}\sqrt{1-\frac{(\gamma-1)k'}{c^2_{CJ}}-\frac{(\gamma-1)\sigma_D h_s}{c^2_{CJ}}-\frac{(\gamma-1)(2-\gamma)}{\gamma+1}\frac{\eta q}{c^2_{CJ}}}$$

where $\eta=1-q'/q>0$ is the dimensionless energy loss due to incomplete burnout of mixture at the CJ plane. The CJ condition $u'_{CJ}/c'_{CJ}=1$ can be then satisfied only if

$$\sigma_D=\frac{\gamma-1}{2}\left[\frac{2k'}{u_s^2}+\frac{\gamma(\gamma-1)}{\gamma+1}\frac{2\eta q}{u_s^2}\right]$$

or, in terms of the detonation velocity:

$$D'=D_{CJ}\sqrt{1-\frac{(\gamma+1)^2}{\gamma-1}\frac{k'}{D^2_{CJ}}-\gamma(\gamma+1)\frac{\eta q}{D^2_{CJ}}} \quad (7)$$

As seen from Eq. (7), any mechanism of kinetic energy dissipation results in the detonation velocity deficit, i.e. $D'<D_{CJ}$.

Eq. (7) was derived without specifying a particular dissipation function k'. Clearly, if k' is decoupled from flow properties and the mechanism of chemical energy deposition is insensitive to decrease in the detonation velocity, then, theoretically, depending on dissipation k', there exists a continuous spectrum of detonation velocities below $D=D_{CJ}$. In this context, detonation in rough tubes can be considered as an example with dissipation nearly decoupled from the flow. A shock wave propagating over rough surface undergoes multiple reflections forming short-lived hot spots whose temperature exceeds substantially that to which the gas is heated after reflection of a shock wave travelling with the detonation velocity from a plane surface. Thus even incident shock waves with Mach numbers slightly above 2 may ignite even methane–air mixture with ignition delays of the order of 10 μs. This has been shown by experiments on fuel–air detonations spreading in a rough tube. The delays between shock front arrival and first rise of the ionisation current witnessing the onset of chemical reaction measured in these tests never exceeded 10 μs. The multiple reflections provide a reliable ignition source tying tightly the beginning of the reaction zone to the shock front. The first and the most important factor of detonation stability in this case is that this source shows no critical sensitivity to shock wave variations as does the delay of bulk ignition at the detonation limit. The second factor of detonation stability is that the flame once ignited propagates as a highly turbulent reaction zone with the effective reaction zone length nearly insensitive to the detonation velocity. In addition, the rate of kinetic energy dissipation is determined by the drag coefficient of mechanical obstructions in a tube. The third important factor of detonation stability is that in a wide range of flow Reynolds number, the drag coefficient is known to be nearly constant and dependent only on obstruction shape. It is noteworthy that 1D analysis of the averaged detonation parameters reveals the other important feature of the flow pattern—quite high unburnt fraction η at the CJ plane.

Experimentally, by introducing mechanical obstructions, one can continuously decrease the detonation velocity by a factor of 5 [189]. A series of experiments were carried out in a tube 12 m long and 174 mm in diameter equipped with orifice-plate obstacles spaced at one tube diameter with BR of 0.3, 0.6, and 0.9. Fig. 40 shows typical data on a quasi-steady detonation propagation velocity in stoichiometric hydrogen–air mixtures diluted with nitrogen as a function of hydrogen content, nitrogen dilution coefficient ξ, and BR.

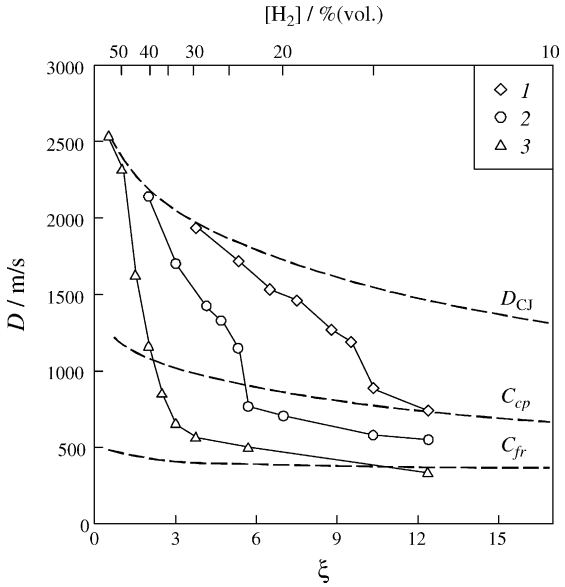

Fig. 40. Effect of BR on the characteristic quasi-steady detonation velocity in the tube with orifice-plate obstructions filled with the stoichiometric $2H_2+O_2+\xi N_2$ mixtures ($\xi=[N_2]/[O_2]$): 1—BR = 0.3, 2—0.6, and 3—BR = 0.9 [189].

Based on the data presented in Fig. 40 various detonation propagation modes can be distinguished. In the high-speed mode, the detonation velocity is somewhat below the CJ velocity $D=D_{CJ}$ (dashed curve marked D_{CJ}). This propagation mode is usually referred to as quasi-detonation mode. In the second mode, referred to as 'choking' mode, the detonation velocity is close to the speed of sound in the combustion products (dashed curve marked c_{cp}). The largest velocity deficit was observed for BR = 0.9 when the wave propagated with a quasi-steady velocity close to the sonic velocity in the fresh reactants (dashed curve marked c_{fr}). It is doubtful that this latter mode is consistent with the definition of detonation given in Section 2.2.1.

If the mechanism of kinetic energy dissipation is significantly coupled with the post-shock flow one can expect the existence of detonability limits. Let us consider the case when kinetic energy dissipation is provided with skin friction in a tube with smooth walls [56]. It can be shown that for a tube of circular cross-section in this case:

$$k'\approx\frac{4(L_{CJ}/d)\bar{\tau}_w}{\rho_0}=f(D') \quad (8)$$

where $\bar{\tau}_w$ is the mean shear stress in the reaction zone. Clearly, the dissipation k' is strongly coupled with the flow, in particular due to exponential dependence of the reaction zone length L_{CJ} on the post-shock temperature. By taking into account the dependencies of all parameters entering Eq. (8) on D', Eq. (7) for this case can be rewritten as:

$$D' = D_{CJ}\sqrt{1 - \frac{\varphi(D')}{D_{CJ}^2}\exp\left(\frac{\theta}{D'^2}\right)} \tag{9}$$

where $\varphi(D')$ is some algebraic function of D' and $\theta = (\gamma+1)^2E/2(\gamma-1)$. The exponential term can be approximated in the form:

$$\exp\left(\frac{\theta}{D'^2}\right) \approx \exp\left(\frac{\theta}{D_{CJ}^2}\right)\exp\left(-\frac{\theta(D'^2 - D_{CJ}^2)}{D_{CJ}^4}\right)$$

and rewrite Eq. (9) as

$$\delta_D = \phi\exp(\delta_D)$$

where $\phi = \varphi\theta D_{CJ}^{-4}\exp(\theta/D_{CJ}^2)$ is the nondimensional parameter representing kinetic energy dissipation, and $\delta_D = -\theta D_{CJ}^{-4}(D'^2 - D_{CJ}^2)$ is the dimensionless velocity deficit. Differentiating δ_D with respect to ϕ gives

$$\frac{d\delta_D}{d\phi} = \frac{e^{\delta_D}}{1-\delta_D}$$

and, obviously, $\delta_D \le 1$, as the velocity deficit should increase with dissipation. The limiting value of the detonation velocity deficit is attained at $\delta_D = 1$, i.e. the lowest value of the detonation velocity D_l' is given by:

$$D_l' = D_{CJ}\left(1 - \frac{2(\gamma-1)}{(\gamma+1)^2}\frac{D_{CJ}^2}{E}\right)^{1/2}$$

As $2(\gamma-1)D_{CJ}^2/(\gamma+1)^2 = RT_s$, one arrives at the Zel'dovich formula for the tolerable drop in the detonation velocity:

$$\frac{D_{CJ} - D_l'}{D_{CJ}} \approx \frac{RT_s}{2E} \tag{10}$$

Similar solutions can be obtained for some other dissipation functions determined by momentum loss due to lateral expansions of the reaction zone and inert mass addition due to interphase mass transfer [190].

Experimentally, the velocity deficit of detonations propagating in narrow channels was studied by Ishii et al. [191]. Fig. 41 shows the measured relationship between the normalized detonation velocity deficit, $\Delta D/D_{CJ} = (D_{CJ} - D')/D_{CJ}$, and normalized gap size, δ/a, obtained from experiments with hydrogen–oxygen mixture at initial pressure of 88 kPa (points 1, detonation cell size 1.7 mm) and 39 kPa (points 2, detonation cell size 4.5 mm).

As the velocity deficit exceeds 20%, the limiting galloping mode of detonation was observed with velocity fluctuations attaining ± 1000 m/s. These findings correlate, in general, with the predictions based on Eq. (10).

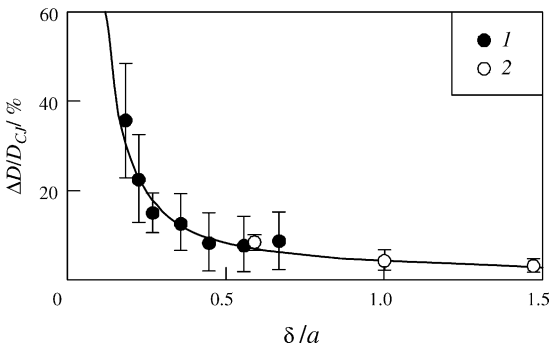

Fig. 41. Measured relationship between the normalized detonation velocity deficit $\Delta D/D_{CJ}$ and normalized gap size δ/a : 1—initial pressure of 88 kPa and transverse detonation cell size a =1.7 mm; 2—39 kPa and 4.5 mm [191].

2.2.6. Transient deflagration and DDT

Initiation by weak sources implies that detonation onset includes a stage of burning. Though the DDT problem has repeatedly been tackled theoretically, so far there has been no successful closure. But the pattern of this transition is clearly understood qualitatively. It includes the stages of:

(i) acceleration of the laminar flame due to the growth of its surface area;
(ii) turbulent flame wrinkling and generation of intense transverse and longitudinal quasi-acoustic waves;
(iii) formation of a shock wave with an inhomogeneous temperature distribution behind its front;
(iv) mixture self-ignition in hot spots arising due to collisions of transverse compression waves behind the main shock front; acceleration of the flames originating at these hot spots and spreading along the temperature gradients around the hot spots up to local onset of detonation; the average temperature of the shock-compressed gas is still lower than that required to ignite the whole mixture with reasonably short induction periods; and
(v) coalescence of the locally born reactive shocks and detonation waves with each other and with the leading shock front to produce an overdriven detonation throughout the duct section area which decays to the CJ state.

Stages (ii)–(iv) are least amenable to computer simulation because they require adequate models of turbulence to calculate flame acceleration and generation of compression waves and very fine computational grids to resolve hot spot ignition and flame acceleration. There have been some attempts to simulate DDT with low-order turbulence models [192] and initial DDT stages with high-order models [193]. The classical DDT scheme provides very long predetonation distances unsuitable for practical applications. It is efficient only in the presence of surfaces inducing turbulence.

In view of application to PDEs, flame acceleration and DDT in semi-open tubes are of most importance. There exist several recent studies [194,195] where the interaction of the first pressure wave generated by flame motion on the process of flame acceleration during the early part of propagation has been studied. A compression wave originating at the closed tube end at the time the flame is ignited is reflected at the tube open end as a rarefaction wave and propagates backward. The trajectory of this initial pressure wave is linked to the flame trajectory in Ref. [194] deduced from video records of flame propagation, and the pressure evolution recorded at the closed tube end. It has been found, that the initial flame development can be divided in three consecutive stages:

1. The flame first develops spherically around the ignition point and reaches the tube wall;
2. The flame then accelerates due to the increase in flame surface; and
3. The increasing contact surface and heat losses between the flame and the walls then lead to a decrease in the flame velocity. Given sufficient time, the flame then starts to accelerate again.

The interaction of the first pressure wave generated by flame motion and the flame front itself can have different consequences, depending on the stage at which this interaction occurs. If the flame is still at the first or second stage of its development (i.e. the flame velocity is low as compared to the sound velocity), then the first pressure wave has no significant influence on the flame trajectory. On the contrary, this interaction is a strong promoter of flame acceleration if takes place when the flame has reached the third stage of its initial development. In this last case, transition to detonation at a subsequent stage of flame propagation is most likely to occur.

Typical diagrams of the measured flame front trajectory are shown in Fig. 42 for three tube lengths for the $C_2H_2 + 2.5O_2 + 16.76N_2$ mixture [195]. One readily

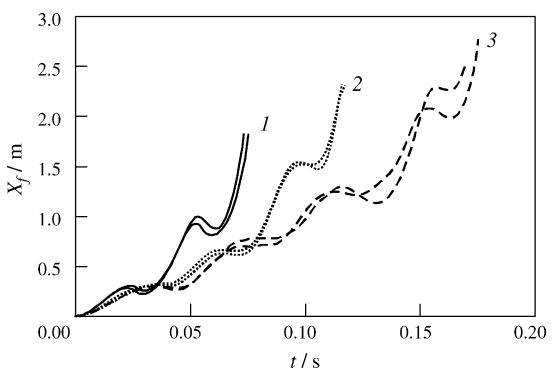

Fig. 42. Time histories of flame front position X_f in $C_2H_2 + 2.5O_2 + 16.76N_2$ mixture for different tube lengths: 1—$L = 2.1$ m, 2—2.6 m, and 3–3.1 m. Tube of square cross-section 40 × 40 mm [195].

observes that the first stage of flame propagation (before its first stop) is virtually independent of the tube length. This is in line with the results of the authors obtained in stoichiometric propane–air mixtures and corresponds to the development of the flame in the tube before it is perturbed by acoustic waves. Then it is seen that the number of flame oscillations increases with increasing the tube length. At the same time, the average flame front speed tends to diminish when the tube length increases. Thus increasing the tube length not necessarily leads to flame acceleration when it is subject to oscillations.

At the initial stage of flame propagation, an important role is also played by the igniter [196]. With ignition occurring at a closed end of the tube, the laminar flame will quickly become turbulent due to various instability mechanisms. Since, for a FAM, the laminar flame propagates at speeds of 30–50 cm/s, the time required for the flame to reach the tube wall and make the transition to a turbulent flame feasible normally comprises the largest portion of the time required for the entire DDT process. If a sufficiently powerful igniter is used it may be possible to avoid the laminar to turbulent flame transition process entirely. This is illustrated in Fig. 43a, where DDT in a propane–oxygen–nitrogen mixture at 1 bar initial pressure occurs in a 15 cm-diameter 2.2 m long tube (closed at both ends) with regularly spaced orifice partitions. If the typical spark plug igniter is replaced with a small precombustion chamber in which the combustion products eject outward, the time required for DDT is reduced nearly by a factor of two: from about 24 to 14 ms. However, the distance required for DDT (about 0.4 m) remains unaffected. At the velocity–distance diagram (see Fig. 43b), the results obtained with the two different igniters are indistinguishable. This is because, while the ignition chamber succeeds in creating a turbulent flame earlier, the turbulent flame must still propagate through the same distance before reaching velocities sufficient for the onset of detonation. This result is in contrast to the often-repeated statement found in the PDE-related literature: that a powerful igniter is necessary for short DDT distance. While the laminar to turbulent flame transition comprises the majority of the time required for DDT, it is shorter in the length scale required for DDT. (The above-mentioned statement is true if in parallel with increasing the igniter power one undertakes precautions to perturb the flow and enhance the turbulence, e.g. by producing long jets distributing the ignition source along the duct, or else by increasing the source power to a level ample to generate intense compression waves from the very beginning.)

The key objective of this section is to discuss the methods of shortening the DDT distance, rather than to analyze the whole DDT process. There are a few experimental methods for reducing predetonation distances. The most popular approach is to introduce the so-called Shchelkin spiral which turbulizes the flow near the duct walls. Another approach is to use small-diameter tubes

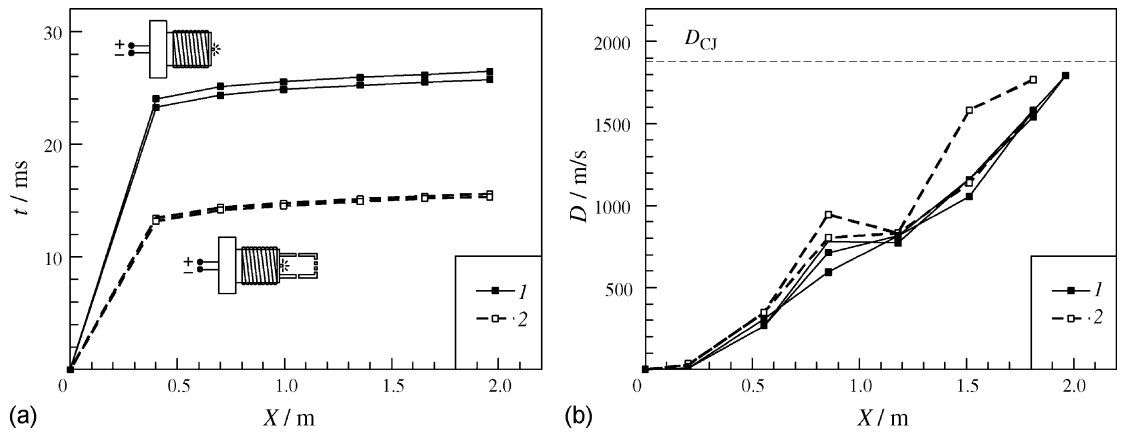

Fig. 43. Time vs. distance (a) and velocity vs. distance (b) data for a $C_3H_8 + 5(O_2 + 3N_2)$ mixture undergoing DDT in a 15 cm-diameter tube with regularly spaced obstacles, as measured by ionization probes on the tube wall. Two different igniters (spark plug (1) and flame jet from precombustion chamber (2)) are shown (initial pressure 1 bar) [196].

(predetonation distances are known to diminish with decreasing tube diameters) and a transition cone to let the detonation wave enter ducts of a larger size without decaying. But even with these approaches, one is incapable of reducing predetonation distances to lengths reasonably short for practical devices.

Experiments [135] have proved that an efficient approach is installation of perforated discs in a duct with a blockage area decreasing and the disc spacing increasing with distance from the ignition source. The main idea behind this method is to use jet ignition of the mixture in the compartments between the discs. It is hot jets that pass through perforations in the discs rather than flame fronts. They increase the burning rate drastically. With this method it was possible to produce a detonation in a hydrogen–air mixture at the distance of about 1 m in a tube 120 mm in diameter, and at the distance of 1.5 m in a propane–air mixture in a tube of the same diameter. In a smooth tube of the same diameter, the expected predetonation distance would exceed 100 m.

Turbulent jet ignition is very efficient in transforming mixture burning into detonation or detonation-like modes of reaction propagation, no matter what kind of a jet is used: jet of reactive oxidizer, e.g. fluorine [162], jet of hot reaction products [130,161,197], supersonic jets of inert gas [197], and different combinations of jets.

Murray et al. [162] suggested an interesting hypothetical scheme of the detonation initiation process which includes formation of shock waves in the vortex arising at the leading jet edge. Interaction of these waves produces a Mach disc, which in the final run serves as a detonation precursor.

Achasov and Penyazkov [197] conducted experiments on detonation initiation by a weak spark plug (0.8 mJ) in acetylene–oxygen mixtures diluted with nitrogen in rectangular 10×10 mm channel 143 mm long. Fig. 44 (curve 1) shows the transition distance (L_{DDT}) vs. nitrogen concentration in the channel. The transition distance is expressed in terms of the specific length L_{DDT}/δ, where δ is the channel height. As follows from Fig. 44, dilution of a stoichiometric acetylene–oxygen mixture with nitrogen heavily alters the transition length when nitrogen molar fraction, ξ, exceeds 18.5%. The onset of detonation at $\xi \leq 18.5$ is observed at a distance less than 17 mm from the spark plug. As the nitrogen content increases, the transition length rises rapidly.

To promote detonation initiation, a turbulence generating perforated steel plate with 0.62 mm diameter holes and an open area ratio of 0.077 has been utilized [197]. The plate (3 mm thick) was mounted at a distance of 27 mm from the ignition spark. Thus, the channel was divided into two parts, namely, the prechamber and the combustion chamber. As seen from Fig. 44, the perforated plate significantly shortens the predetonation distance. The critical nitrogen molar fraction increases from 18.5% (without plate) to 60% (with plate).

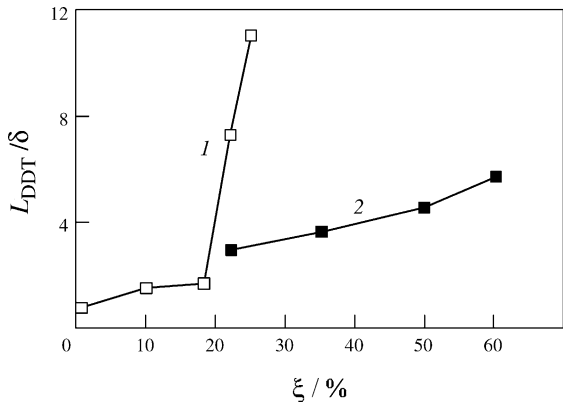

Fig. 44. Normalized DDT distance L_{DDT}/δ vs. nitrogen dilution ξ for stoichiometric acetylene–oxygen–nitrogen mixtures at initial pressure 0.1 MPa in the channel without (1) and with (2) a perforated plate [197].

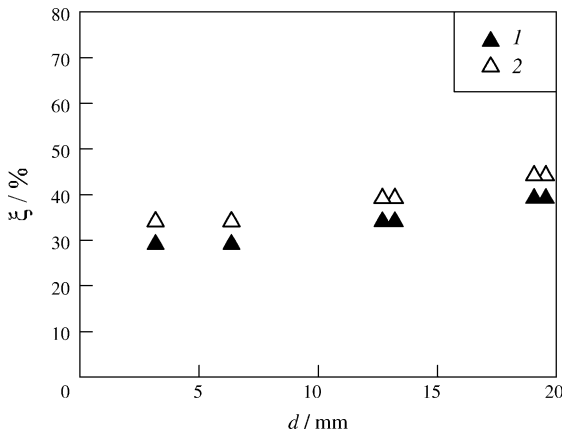

Fig. 45. Effect of orifice diameter d on the critical nitrogen molar fraction ξ required for detonation initiation in propane–oxygen–nitrogen mixture at pressure of 0.1 MPa [130]. 1—detonation and 2—no detonation.

The effectiveness of using a hot turbulent jet to initiate a detonation in a short distance was recently investigated experimentally [130]. A turbulent jet of combustion products, passing from a driver section through an orifice into a test section (1 m long, 76.2 mm i.d.), was used to initiate a turbulent flame in the test gas. The driver was filled with stoichiometric propane–oxygen mixture and the test section was filled with stoichiometric propane–oxygen mixture with varying nitrogen dilution. Fig. 45 shows the dependence of the critical (maximal) N_2 dilution vs. orifice diameter with the initial driver pressure at 0.1 MPa. Increasing the orifice diameter from 3 to 19 mm increases the critical dilution level from 30 to 40% N_2. Experiments were also carried out with an array of orifices to examine the role of jet mixing. For a given open area, the multiple hole geometry resulted in only a 5% increase in the critical dilution level over the equivalent single hole geometry.

Vasil'ev [198] utilized multiple orifice plates and a 100 mm diameter tube to construct an efficient DDT accelerator (Fig. 46a). With this accelerator, a stoichiometric methane–air mixture was detonated (under normal conditions) at a distance of 2.5–3.0 m, i.e. the DDT distance L_{DDT} was about 25–30 tube diameters. The arising detonation wave propagated in the marginal spinning mode. In the experiments with large tubes a special device was used to expedite formation of a planar flame. This device was placed in front of the DDT-accelerator (section A-A in Fig. 46a). Fig. 46b shows the measured dependencies of the DDT distance vs. initial pressure of stoichiometric hydrogen–air and acetylene–air mixtures in the large-diameter tube (250 mm in diameter). The DDT distance in Fig. 46b includes the length of the DDT-accelerator. As seen from Fig. 46b, at normal pressure, the DDT distance is about two tube diameters for the specified mixtures.

Another investigation [199] applies porous materials (mesh, bed of steel balls, and foamed ceramics) to shorten

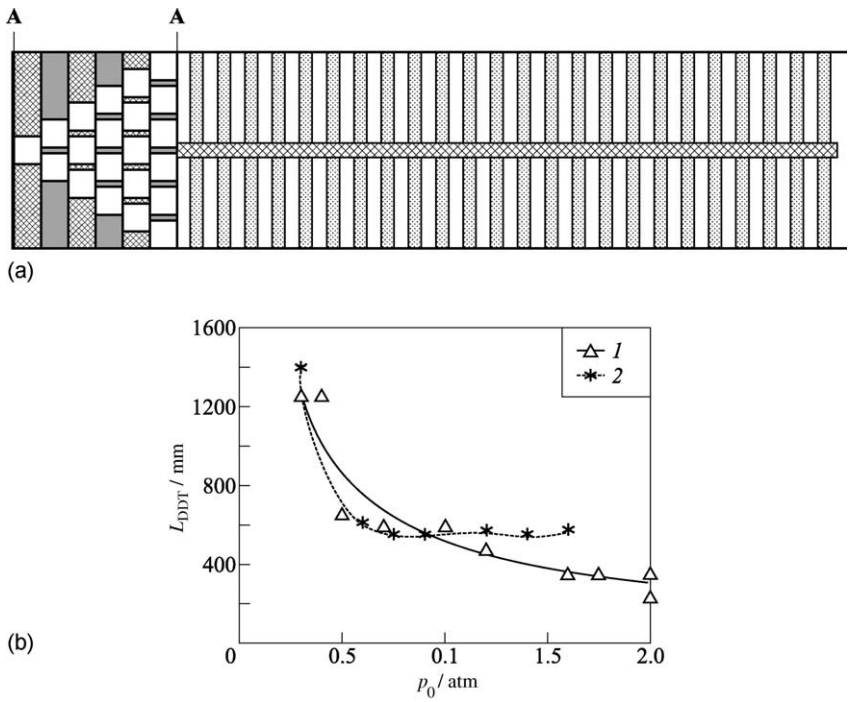

Fig. 46. Sketch of the DDT accelerator (a) and effect of initial pressure p_0 on DDT length L_{DDT} in stoichiometric hydrogen–air (1) and acetylene–air (2) mixtures in a tube 250 mm in diameter [198]. A–A is the device aimed at faster formation of a planar flame.

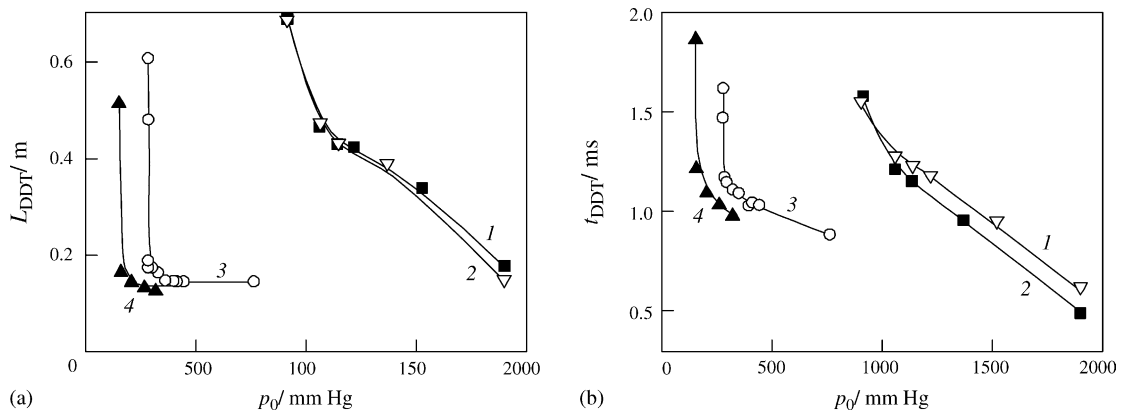

Fig. 47. Measured DDT length L_{DDT} (a) and time t_{DDT} (b) in $C_2H_2 + 2.5(O_2 + 1.4N_2)$ mixture vs. initial pressure p_0: 1—tube with no inert porous filling, 2—tube with steel mesh (permeability 0.36), 3—tube with complex porous filling 60 mm thick: mesh + inert porous filling (5.5 mm steel balls); and 4—tube with foamed ceramics (porosity 0.66) 50 mm thick [199].

the predetonation distance. Fig. 47 shows measured DDT length and time in $C_2H_2 + 2.5(O_2 + 1.4N_2)$ mixture vs. initial pressure p_0. As seen, the mesh does not produce any significant effect on transition length and leads only to slight acceleration of the flame front. Porous medium greatly decreases the DDT length and time.

Extensive research at McGill University [200,201] on DDT in tubes with large-scale obstacles have identified an optimum obstacle BR (~40%) and an optimum obstacle spacing of roughly one tube diameter that result in minimum length scales required for DDT.

Whatever the particular gasdynamic pattern of the transition process, jet ignition seems to have a common manifestation—generation of blast waves (due to fast mixture burning in the turbulent mixing layer) followed by their possible acceleration in the medium with temperature and/or concentration gradients which ends up in close coupling between the shock wave and the heat release front [93,164,165]. The physical nature of detonation development in inhomogeneous mixtures is quite obvious. Shock waves can be augmented by heat release in the gas behind its front when the gas temperature (or radical concentration) and chemical reaction rate is high enough for any changes in the wave amplitude to significantly affect the heat release, and when reaction time gradient in the medium is small enough for a small perturbation arising due to a local reaction to be capable of inducing reaction in neighboring layers. The criterion for coupling suggested in Ref. [164] reflects this idea: the reaction front should propagate at a velocity approximately equal to the representative velocity of perturbations

$$\frac{dt_i}{dl} \sim (\gamma RT)^{1/2}$$

where t_i is the ignition delay time, l is the distance, and R is the gas constant.

The best method of detonation initiation by weak sources most suitable for practical purposes is mixture preheating to a preignition state or sending a weak shock wave through a burning heterogeneous mixture. Experimental observations vividly illustrate the efficiency of this approach. Numerous shock tube experiments and observations of destruction patterns after accidental gas explosions in long ducts demonstrate that detonation onset in precompressed and shock-preheated combustible gases takes place within very short distances (even without involvement of the flow interaction with the walls) leading in practical cases to excessively severe damage of the tube portions near closed ends.

2.3. Heterogeneous detonations

2.3.1. General properties

In general, two-phase systems dealing with fuel–air explosion studies are *gas–droplet*, *gas–film (layer)*, and *dust* mixtures. A review of works devoted to *gas–droplet* and *gas–film* detonations can be found, for example, in Refs. [91,138,202]. The state-of-art and most important problems of *dust* explosion research are described in Ref. [203], where about a thousand references relevant to dust explosions have been covered, and measures preventing dust explosions and detonations in industry or mitigating their effect have been discussed. The number of works in the field of multiphase detonations is rapidly increasing. It is due to safety requirements in different industries utilizing powders of combustible materials.

The lack of knowledge of the nature of two-phase detonations can be partly ascribed to the fact that two- and multiphase mixtures cannot be characterized by the same number of governing parameters as a gaseous mixture. Indeed, apart from the chemical composition and initial pressure and temperature of the mixture, one should take into account particle size and its distribution, particle shape, temporal and spatial uniformity of the particle concentration field, vapor-phase distribution, etc. The latter effects may essentially promote explosion initiation in reactive

mixtures. Moreover, depending on the average particle size, the detonation zone thickness in two-phase mixtures is at least a few times larger than that in homogeneous mixtures (even for nearly the same composition), hence, shock tubes used in two-phase detonation studies must be essentially longer than tubes employed in gas detonation studies. This fact and sedimentation of particles essentially complicate the problem of qualitative preparation of homogeneous two-phase mixtures. All these features make the problem of two-phase detonation much more complicated than that of gas detonations. As a result, the current knowledge of the nature of two-phase detonations is considerably less complete than the theory of gaseous detonations.

The wave structure problem is traditionally considered in two classes of approaches: (i) global 1D approaches dealing only with parameters averaged over the cross-section normal to the direction of wave propagation, and (ii) multidimensional approaches in which the parameters measured locally are analyzed. The first approach is most suitable for practical purposes because it is the averaged parameters that determine the wave properties relevant to practical combustion devices.

Despite the fact that the actual wave structure is 3D, approach (i) still remains the main focus in all detonation studies.

The wave profiles were examined extensively resulting in the following basic findings: First, the pressure oscillates as in gaseous detonation weaves with a frequency identical with those of luminosity oscillations on the streak photographs, which indicates that the 3D structure of detonation waves is similar in both cases, at least for spinning and two- or three-head waves. The von Neumann spike is clearly seen on the pressure records for mixtures with particles larger than a few microns indicating that the rate of heat evolution in heterogeneous mixtures is much slower than in gases. Preevaporation of a fuel or addition of volatile components to the fuel drastically reduces the von Neumann spike duration making the pressure records similar to those observed in gaseous mixtures and drastically enhances detonability of the mixture. This is true both for liquid and solid particles. Efficient are even very low concentration of reactive gaseous components. The additives sharply reduce the ignition stage but only slightly influence the burning rate; therefore the detonation wave parameters still are dependent on the particle size, in particular for solid particles. Even suspensions of dust of high explosives in detonating gases do not support steady-state detonation with enhanced parameters (much higher than those in the gas mixture) until the particle size is below ten microns. In contrast to gaseous mixtures, heterogeneous detonation waves, both air–vapor (gas fuel)–solid, air–vapor (gas fuel)–liquid and air–nonvolatile condensed particles with wide size distribution readily form the so-called multifront detonation waves (in which two or more successive wave fronts propagate one after another) due to complicated heat exchange and reaction processes that result in nonmonotonic heat release behind the lead shock wave front. Other parameters measured in the reaction zone of heterogeneous mixtures also show that the pulses are long and that reaction keeps going even behind the averaged CJ plane. This is particularly obvious in the ionization current records that last up to 10 ms at a very high level.

The velocity of detonation waves spreading in heterogeneous mixtures with fine droplets are usually about 100–200 m/s lower than the calculated CJ velocity. For relatively large droplets, the detonation velocity deficit may attain 700–800 m/s. Table 7 shows the comparison of measured detonation velocities with the predicted CJ velocities based on experimental data of Refs. [96,137,160,204–210].

The distance to onset of the steady CJ regime after initiation of detonation in heterogeneous mixtures is much longer than in gaseous mixtures. Also, the comparative effect of confining walls on the parameters of gaseous and heterogeneous detonations is different.

Thus, the structure of heterogeneous detonation waves in many respects is similar to that in gaseous mixtures, but there are also some specific features that should be taken into account in modeling these waves. Many of these features are not properly understood yet.

As was discussed in Section 2.2, the detonation front in gaseous mixtures is never plane and smooth and consists of a number of detonation cells formed by interaction of transverse shock waves. The behavior of a two-phase explosive mixture becomes similar to that of gaseous mixture as particle size decreases and the fuel volatility rises. Hence, it is natural that detonation fronts in two-phase mixtures have a cellular structure resembling that inherent in homogeneous mixtures [211]. Ingignoli et al. [212] were apparently the first to report about cellular structure of aluminum (particles)–oxygen detonation. Fig. 48 shows their photograph of the detonation structure recorded on a soot plate. In the experiments, aluminum particles in the form of flakes with a thickness less than 1 μm and longitudinal size up to 25 μm were used. The footprint of Fig. 48 corresponds to the conditions when a leading front velocity in the cloud was as large as 1650 m/s (corresponding CJ velocity is 1493 m/s). Only part of detonation cells can be observed as is explained with the limited dimension of experimental setup used. The characteristic cell width would be about 50–100 mm.

In droplet–gas systems, the cellular structure was observed in Ref. [213] for suspensions of very fine decane drops (5 μm in diameter) in nitrogen-diluted oxygen (with $[N_2]/[O_2] \leq 2$). It has been found that for the stoichiometric decane aerosol–oxygen system the measured cell size is about five times greater than the computed cell size based on homogeneous-phase kinetics. This result indicates that physical processes are present in heterogeneous detonations substantially increasing the induction zone length.

As far as the detonation wave instability and resulting front pattern are concerned, there is not very much

Table 7
Two-phase gas-droplet detonation velocities in tubes at initial pressure $p_0 = 1$ atm

Gas	Liquid fuel	Mean drop diameter (μm)	Equivalence ratio	Detonation velocity (calc.) (m/s)	Detonation velocity (meas.) (m/s)	Tube diameter (mm)	Ref.
O_2	$C_{10}H_{20}$	200	1.0	2320	1620–1740	50.8	[204]
O_2	$C_{10}H_{20}$	940	0.5	2030	1200–1550	41 × 41	
O_2	$C_{10}H_{20}$	2600	0.23	1780	970–1250	41 × 41	
O_2	$C_{10}H_{20}$	2600	1.0	2320	1520 ± 150	41 × 41	
O_2	$C_{10}H_{20}$	290 and 940	0.2	1670	1520	41 × 41	
O_2	$C_{10}H_{20}$	290	0.3	1830	1680	41 × 41	
O_2	$C_{10}H_{20}$	290	0.5	2030	1920	41 × 41	
O_2	$C_{10}H_{20}$	290	1.0	2380	2130	41 × 41	
O_2	$C_{10}H_{20}$	750	0.914	2260	1830 ± 20	41 × 41	[205]
O_2	$C_{10}H_{22}$	2 (0.5–10)	0.65	2150	2100	22.2	[206]
O_2	$C_{10}H_{22}$	2 (0.5–10)	0.65	2150	2050	14.2	
O_2	$C_{10}H_{22}$	2 (0.5–10)	0.65	2150	2000	8.2	
O_2	$C_{10}H_{22}$	2 (0.5–10)	0.65	2150	1850	4.9	
O_2	$C_{10}H_{22}$	2 (0.5–10)	0.25	1770	1900	14.2	
O_2	$C_{10}H_{22}$	2 (0.5–10)	0.1	1390	1710	14.2	
O_2	Kerosene	2350	0.1–1.5	1360–2500	1300–1700	70	[207]
O_2	JP-10	1–12	1.25	–	1925–2010	38	[96]
Air (425 K)	JP-10	2–3	1.5	1800	1800	127	
Air (375 K)	JP-10	2–3	1.5	1800	1890	127	
O_2	C_6H_{14}	40–60	0.3	1850	1630	102.5	[208,209]
O_2	C_6H_{14}	40–60	0.35	1910	1650	102.5	
O_2	C_6H_{14}	40–60	0.41	1950	1670	102.5	
O_2	C_6H_{14}	40–60	0.49	2040	1720	102.5	
O_2	C_6H_{14}	40–60	0.56	2090	1700	102.5	
O_2	C_6H_{14}	40–60	0.68	2170	1780	102.5	
Air	C_6H_{14}	5	≈1.0	1850	1700 ± 100	50.8	[210]
Air	C_7H_{16}	5	≈1.0	1850	1700 ± 100	50.8	
Air	C_6H_{14}	5	≈1.0	1850	1620 ± 40	27	[160]
Air	Gasoline (≈70 °C)	–	1.0	–	1900	36	[137]

difference between the gas and two-phase mixtures, because a stability analysis shows that the shock front–exothermic reaction complex is unstable irrespective of what parameter in the expression for the heat evolution rate is responsible for its variation (temperature, pressure, or relative velocity of the particles and gas) and for the feedback between the reaction zone and the lead shock front.

Indeed, in suspensions of fine decane droplets (diameter about 2 μm) in oxygen (equivalence ratio in a range of 0.2–0.65), reaction zone length, L_{rz}, was about 12 mm at detonation velocity of about 2000 m/s [206]. Estimates show that for such fine droplets relaxation of the particle velocity is terminated within a distance of about 1 mm, and the zone where droplets are deformed, shattered and evaporated is less than 1 mm, and the induction zone length is about 0.1 mm. These estimates mean that the reaction zone length L_{rz} (which appears to be an order of magnitude longer) is controlled by other processes [202]. The behavior of such detonations has very much in common with detonations of gaseous systems. Namely, transition from deflagration to detonation is accompanied by spinning phenomena, self-supported detonation parameters oscillate with a frequency corresponding to longitudinal detonation cell size $b = 4.5 - 6.7$ mm. Hence, L_{rz} is about $2b$, that is, the reaction zone length is comparable with the cell size like in gaseous systems, and the ratio between L_{rz} and b has a value not very much differing from that inherent in gas

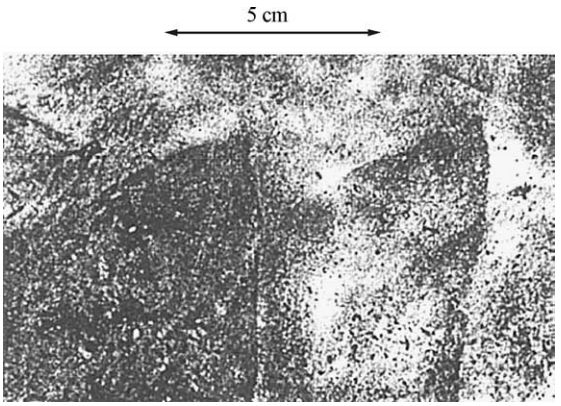

Fig. 48. Photograph of structures recorded on a soot plate in the case of detonating an unconfined cloud of aluminum particles in oxygen atmosphere [212]. The particles had a form of flakes with a thickness less than 1 μm and longitudinal size up to 25 μm.

detonations. Thus, the two-phase detonation structure can be very similar to that of gaseous detonation waves, but the cell size is few times larger due to longer heat evolution times (that includes many physical processes together with chemical ones).

The fundamental difference between the structures of detonation waves in two-phase and gaseous FAMs consists in the pattern of heat evolution behind the lead shock front. As distinct from gaseous mixtures, heat release in two-phase mixtures is smoother and always has a long tail where fuel burns in the diffusion-controlled regime. The long heat-release tail in sprays is a result of two-phases of fuel burning. The droplet break-up process is normally completed within a time period, which is much shorter than the overall heat release time. The mixture at the periphery of the cloud formed after break-up self-ignites. Thus, the fuel-rich mixture in the cloud core surrounded by the hot self-ignition products burns at a rate controlled by oxidizer diffusion into it. This results in longer reaction zones than in gases, higher energies of direct initiation of detonation, high unburnt fraction downstream of the averaged CJ plane, and therefore—lower detonation velocities, strong dependence of the critical characteristics of detonation on fuel volatility and the initial vapor pressure, smearing of the cell structure as the cell size decreases, and higher overpressures and impulses of heterogeneous detonation waves. Indeed, experimental studies reveal that the so-called von Neumann spike in all heterogeneous detonation waves is clearly seen (in contrast to gaseous waves, where it is usually unresolved by the conventional pressure gauges). The reaction zone length grows in the following order: gas–droplets–dust particles.

A comparison with calculations by various models demonstrates that 1D approaches yield more adequate results for heterogeneous detonations than for gaseous ones. Unfortunately, virtually all the studies modeling heterogeneous detonations consider only the droplet break-up and self-ignition stages, ignoring the diffusion-controlled stage.

2.3.2. Detonability limits

As mentioned above, the overall reaction zone in heterogeneous detonation waves is longer than that in gases, therefore, the linear scales inherent in two-phase detonation waves are large.

Detonability of two-phase fuel–oxygen mixtures is undoubtedly higher than that of FAMs, and this is why fuel–oxygen mixtures were mainly studied in laboratory-scale experiments. Detonations in oxygen–droplet systems were observed in a wide range of droplet size (from 1 to 10 mm) for a variety of liquid fuels (kerosene, decane, hexane, etc.). Steady dust detonations were observed in cornstarch and wheat particles–oxygen mixtures [211,214,215]. A special attention was paid also to steady detonation of aluminium–air and aluminium–oxygen systems [216,217].

However, the situation with concentration limits of two-phase detonations is more complicated than in the case of gaseous mixtures. In the first place, the rich concentration limit of two-phase *gas–droplet* detonation exists only in the case of very fine and volatile droplets: in these mixtures the rich limit approaches the upper concentration limit of gas detonation. Otherwise, detonation can propagate in a very rich two-phase gas–droplets mixture with an equivalence ratio of about 10. (Similar situation exists in detonation waves propagating in tubes with a layer of liquid or powder fuel on the tube walls—in this case, detonation wave consumes only as much fuel as suffices for detonation to propagate.) The existence of self-supported detonations in very rich mixtures is due to shattering and stripping of larger droplets by a high-velocity gas flow behind the shock front. As a result, only small newly generated microdroplets participate in the burning process and liberate their chemical energy in the detonation wave. The remaining larger droplets may burn out behind the averaged CJ plane of the detonation wave in the unsteady expansion wave. The rich concentration limit in dust systems may also be larger than that in gaseous mixtures due to more rapid ignition and burning of smaller particles that are present in a real polydisperse powder [218].

There is no doubt about existence of the lean concentration limit of two-phase detonation. If the particles or droplets are small (< 10 μm) then this limit is quite close to the lean concentration limit of gaseous detonation.

Concentration limits of two-phase detonations strongly depend on the particle or droplet size, the concentration of oxygen or nitrogen in the gas, and fuel vapor pressure. Sensitivity of the concentration limits of detonation propagation to nitrogen content in the mixture is particularly high [207]. Namely, the range of fuel concentration, within which detonation propagation is possible, rapidly decreases when nitrogen concentration increases. As a result, FAMs are detonable only when particles or droplets are small. For example, lean detonation concentration limit of aluminum suspensions in air is between 110 and 140 g/m^3 for a mean particle size below 1 μm and between 150 and 200 g/m^3 for flake particles of an equivalent diameter of 6 μm and thickness of about 1 μm (flaked aluminum powder) [216].

Fig. 49 shows the measured velocity profile of a marginally stable detonation in *n*-hexane spray–oxygen mixture [209]. The velocity is detected by using multiple ionization probes and pressure transducers mounted along the detonation tube. The detonation tube with 102.5 mm inside diameter and 5.8 m length has been fitted with 40 pairs of fuel injectors (modules) mounted equidistantly along the tube. The fuel injectors of each pair were positioned directly opposite one another, and were fired under identical conditions to ensure homogeneous mixing of liquid fuel with oxygen. Marginal conditions for detonation propagation in the experiments of Ref. [209] arose at the overall equivalence ratio as low as 0.2.

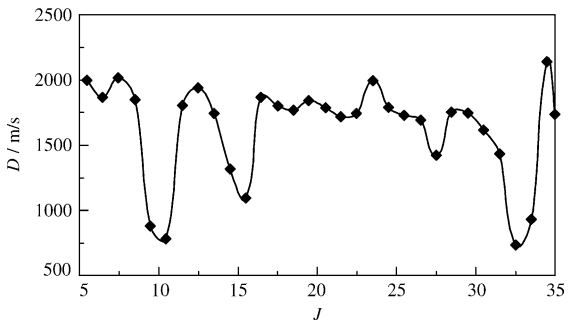

Fig. 49. Velocity profile for a marginally stable *n*-hexane spray—oxygen detonation measured by ionisation probes in a 102.5 mm diameter and 5.8 m length tube of modular configuration [209]. *J* is the fuel injector module number. Single module length is 100 mm.

As seen from Fig. 49, the detonation propagates in the mode resembling the galloping mode of gaseous detonation.

Detonation stability was found to vary with fuel injection pressure (droplet diameter) and equivalence ratio. As can be seen in Fig. 50, the range of equivalence ratios for which stable detonation was achieved grew wider as droplet Sauter mean diameter (SMD) decreased. For the experiments with the largest mean droplets (those performed with a fuel pressure of 300 Psi = 20.7 bar), stable detonation was never obtained. However, there was a large range of stable equivalence ratios when using smaller droplets. In all cases, stability degraded as the mixture became either too lean or too rich.

Although the concentration limits of two-phase detonations were determined in tubes, it turns out that for larger droplets the detonability window may be even wider than those in homogeneous systems because (as mentioned above) the rich detonability limit for larger drops is higher. The same trend is also observed in dust suspensions but it is not so prominent as in liquid fuels because of the very severe constraints imposed on the particle size in these mixtures (as mentioned above, the lack of the shattering mechanism in detonation of solid particles in air is the reason why only extremely tiny particles (less than 10 μm) can form detonable mixtures).

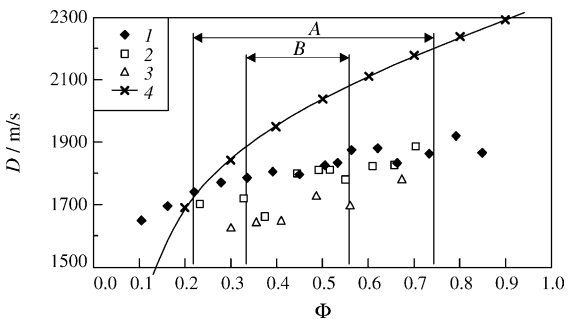

Fig. 50. Two-phase *n*-hexane–oxygen mean detonation velocity *D* and stability vs. fuel injection pressure (drop diameter) and equivalence ratio *Φ* [209]. 1—fuel injection pressure 700 psi (48.3 atm), 2—500 psi (34.5 atm), 3—300 psi (20.7 atm), and 4—gas-phase CJ detonation velocity; ranges *A* and *B* correspond to stability limits for fuel injection pressure of 700 and 500 psi, respectively. Detonation is never stable with fuel injection pressure of 300 psi.

As in case of gaseous detonations (see Section 2.2.2), the concentration limits of two-phase detonations should be independent of the tube diameter, provided it is sufficiently large as compared to the limiting tube diameter. Despite the fact that the von Neumann spike in heterogeneous detonations is usually much thicker than that in gaseous mixtures, the effect of the tube diameter on the detonability limits in them should be less pronounced than in gaseous mixtures, because the heat release rate is less sensitive to temperature, pressure, and overall equivalence ratio (see Section 2.2.5).

In liquid sprays, smearing of the time histories during the reaction runaway arises naturally because of the long diffusion-controlled stage of burning the cloud formed after droplet breakup. In addition, the induction period in heterogeneous mixtures includes some physical processes, such as formation of bow shocks attached to droplets of droplet ensembles, droplet breakup, particle preheating, and gasification. This undoubtedly would reduce the sensitivity of the global heat release kinetics to chemically active additives. Nevertheless, similar to homogeneous mixtures, detonability limits of heterogeneous mixtures can be affected by additives. The delays of ignition of drops suspended in air behind shock waves exhibit three major types of behavior of blends in heterogeneous mixtures, which are displayed in Fig. 51 [219]. Thus, fuel blends can be considered as possible ways of influencing the heat release kinetics in sprays.

Because of different reaction mechanisms governing flame propagation and detonation, there are systems where the ratio between the detonation and flammability limits is inverse to those commonly believed. For example, many heterogeneous systems exhibit detonation limits that are wider than flammability limits. Such mixtures as ammonium perchlorate–air or some HE–air do not usually support flame at atmospheric pressure, but can detonate when initiated with a proper source [135].

Work performed at the Naval Postgraduate School [96] has demonstrated that very fine aerosols were required in order to support detonation in JP-10–air mixtures (see Table 7). The fine aerosol mixtures were obtained by allowing the original mixture to partially evaporate due to elevated air temperatures *T*. Therefore, the actual mixture detonated at temperature *T* =375 K, which contained about 70% vaporized fuel and the remaining fuel as liquid droplets with SMD of less than 3 μm. The observed detonability limits are shown in Fig. 52. As follows from Fig. 52, to obtain heterogeneous detonation, the laboratory detonation tube should be heated and fuel should be partly prevaporized. Such complex experiments were reported [220].

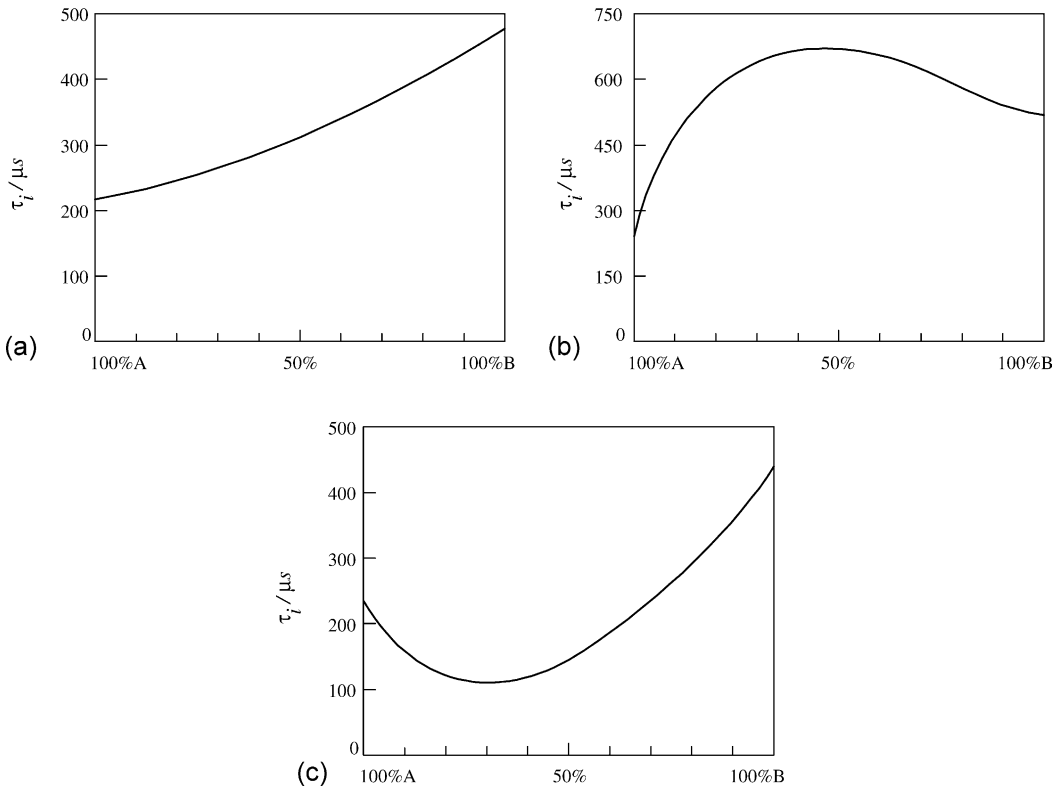

Fig. 51. The effect of additives on ignition delays τ_i of hydrocarbon fuels: (a) isopropyl nitrate (A) with kerosene (B), (b) pentadienyl–tricarbonyl manganese (A) with kerosene (B), and (c) dodecatriene (A) with 1,4-butandyol dinitrate (B) [219].

There exist principal differences between initiation of heterogeneous detonation in a single-pulse (shot) mode and multipulse mode to be implemented in realistic PDEs. When conducting experiments with nonvolatile liquid hydrocarbons in a multipulse mode, the setup is heated up itself during operation, due to considerable heat flux to the wall. The other difference between the processes in realistic PDEs and processes in a laboratory detonation tube operating in a single-pulse mode consists in the existence of a flow of a combustible mixture in front of the detonation wave. Flow turbulence in the DC affects the detonation parameters, and in particular, detonability limits.

In Ref. [137], detonation velocity and detonability limits were measured for mixtures of liquid hydrocarbons in a water-cooled pulse detonation tube described in detail in Section 3 (see Fig. 136). Fuel and oxidizer were injected in the detonation tube separately. A valveless supply system for fuel and oxidizer was used. Preheated liquid fuel was injected in the tube through a nozzle. The oxidizer initial parameters were 1 bar and 20 °C. The temperature of cooling water was usually near 70 °C. The frequency of pulse detonations was 0.5–2 Hz. The maximum operation time was 1 h. Initiation was triggered with an electrical spark with energy of 0.1 J. Detonations of different types of automobile gasoline and jet propulsion (JP) gasoline, as well as *n*-hexane, acetone, and ethanol were studied at initial atmospheric pressure. Air enriched with oxygen was used as oxidizer. Detonation velocities and detonability limits were measured as functions of mixture composition, the degree of air enrichment with oxygen, tube diameter (16, 34, and 36 mm), and tube length (3 and 7 m).

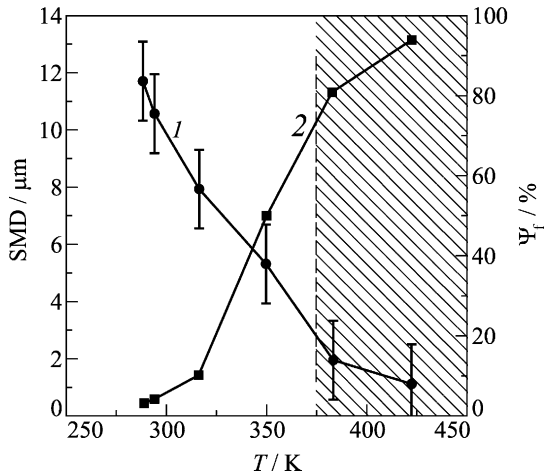

Fig. 52. Observed two-phase requirements for detonating a two-phase stoichiometric JP-10–air mixture in terms of air temperature T, fuel drop SMD (1) and percent of fuel vaporized ψ_f (2) [96]. Detonation was observed in the shaded area.

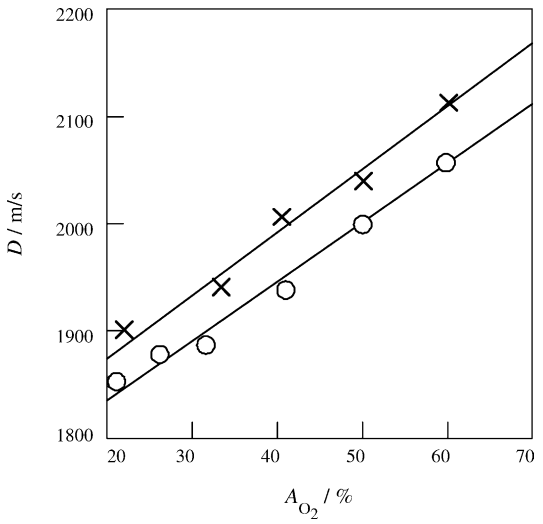

Fig. 53. Measured detonation velocity in stoichiometric mixtures of liquid fuel with oxygen-enriched air in a pulse mode of tube filling and detonation initiation. Crosses correspond to automobile gasoline, circles to *n*-hexane [137].

Fig. 53 shows the dependence of measured detonation velocities on the degree of air enrichment with oxygen, $A_{O_2} = Q_{O_2}/(Q_{O_2} + Q_{N_2})$, where Q_{O_2} and Q_{N_2} are the mass flow rates of oxygen and nitrogen, respectively. As expected, the detonation velocity in oxygen-enriched mixtures is higher than in air mixture.

Significant variation of detonation velocity with the oxidizer-to-fuel ratio α (reciprocal to equivalence ratio, Φ) was observed in the experiments [137]. Decreasing α below a certain value, α_{min}, as well as increasing α above a certain value, α_{max}, resulted in failure of DDT. In this manner, the detonability limits in the device have been found. The detonability limits of several mixtures in terms of α (at $A_{O_2} = 95\%$) are presented in Table 8. It is worth noting that these detonability limits were obtained in a tube with the diameter of 36 mm and length of 7 m. Beyond the limits, the predetonation length might be longer than the length of the tube. In longer tubes, the detonability limits could be wider.

The effect of tube diameter on detonation velocity of two-phase mixtures was studied [158,160,206]. In Ref. [206], the mixture of oxygen with polymodal *n*-decane droplets of diameter ranging from 0.5 to 10 μm was initiated in shock tubes of diameter that was varied from 4.9 to 22.2 mm (see Table 7). The detonation velocity in an *n*-decane–oxygen mixture with an equivalence ratio of 0.65 in a tube of the largest diameter was 2100 m/s, in a tube with $d = 14.2$ mm detonation propagated at 2050 m/s, and in smaller tubes with $d = 8.2$ and 4.9 mm, detonation velocity was 2000 and 1850 m/s, respectively.

Table 8
Measured detonability limits of some hydrocarbons in terms of oxidizer-to-fuel ratio, α, at $A_{O_2} = 95\%$ [137]

Fuel	α_{min}	α_{max}
A-72	0.74	1.20
A-76	0.74	1.20
A-93	0.74	1.10
B-70	0.63	1.25
n-Hexane	0.90	1.20
Ethanol (96%)	0.78	1.00
Acetone	0.75	1.15

In Ref. [158,160], two tubes of different diameters (50.8 and 27 mm) were used to initiate spray detonations of *n*-hexane and *n*-heptane (see Table 7) in air. Clearly, in the tube of smallest diameter the detonation velocity deficit attains 100–200 m/s.

The experimental studies described above can serve as illustrations of a typical behavior of detonation in two-phase media under conditions of intense heat and momentum losses. Unlike gaseous mixtures, heterogeneous mixtures show no abrupt transition from an almost ideal behavior to detonation failure. The detonation velocity in heterogeneous mixtures drops smoothly to much lower values than that in gases, and limiting tube diameters of these mixtures are usually smaller than those that would be expected from the simple 1D theory [98] based on the length of the reaction zone. This is attributed to a peculiar profile of the heat release in heterogeneous mixtures that exhibits an extended tail of the diffusion-controlled burn-down of the fuel, which drastically reduces the sensitivity of the reaction zone length to variations in the flow parameters.

Unfortunately, experimental information on limiting tube diameters in two-phase mixtures is very scarce. Most of the experimental results pertain to variation of the detonation velocity with the tube diameter, rather than to limiting tube diameters.

At the same time, the limiting detonation diameters and effects of tube diameter on detonation velocity of two-phase mixtures can be evaluated on the basis of numerical models of two-phase detonations in shock tubes [216,221]. A comparison of the results of numerical modeling with experiment shows their satisfactory agreement.

2.3.3. Direct initiation

Detonation of a two-phase mixture can be initiated by a number of means. The simplest way is to heat up the mixture to provide a local ignition of the fuel and to wait until deflagration wave develops into detonation. However, in this case the predetonation distance can be too long to obtain build-up of self-supported detonation in any tube or cloud of finite size (this is particularly true for air mixtures in which these distances in smooth tubes may attain hundreds of meters even in gaseous mixtures). Thus, there is a contradiction between the desire of a researcher to obtain as fast detonation initiation as possible and opportunities available.

Both in practical applications and laboratory-scale experiments detonation in heterogeneous mixtures is usually

initiated directly by a shock wave of a given strength, shape and duration. Thus, one should find the critical energy of the shock wave above which detonation in the tested two-phase mixture can be initiated, whereas lower energies are incapable of initiating detonation in two-phase mixtures. The ratio of this critical energy to the corresponding values for gaseous mixtures is a measure of relative susceptibility of two-phase mixtures to detonation initiation by shock waves. For example, the critical initiation energy of stoichiometric aluminium–air mixture in a shock tube is about 3.4 MJ/m^2 for aluminum flake particles and only 0.3 MJ/m^2 for submicron particles [216]. The first value is nearly the same as obtained for propane–air mixtures in shock tubes, i.e. aluminum flake–air suspension in shock tubes has nearly the same detonability as a propane–air mixture.

The evolution of detonation waves in two-phase gas–droplets systems, as well as the initiation energy of spherical, cylindrical, and plane gas–droplets detonations of hydrocarbon fuels with initiators of different energy density (point explosion, HE charge, detonation of reacting gas mixture) were studied numerically [222–225]. It is found from the analysis of the numerical solutions, that there exists a critical energy E_{cr}, such that the explosion dynamics differs considerably for the explosion energy $E_0 > E_{cr}$ and $E_0 < E_{cr}$ (see Fig. 54 [153]). Solid curves in Fig. 54 show the evolution of pressure profile in the case with $E_0 > E_{cr}$. In this case, after initiation the blast wave attains a minimum propagation velocity, $D_{min} < D_{CJ}$. Then, after passing the minimum, the wave velocity starts to increase towards D_{CJ} 'from below'. Dashed curves in Fig. 54 show the case with $E_0 < E_{cr}$. Clearly, there exists a distance, corresponding to a certain shock radius, $r_{s,cr}$, such that at $r_s > r_{s,cr}$ the detonation wave decays. The value of $r_{s,cr}$ decreases with decreasing E_0. The magnitude of E_{cr} depends on the ignition delay and fuel droplet size.

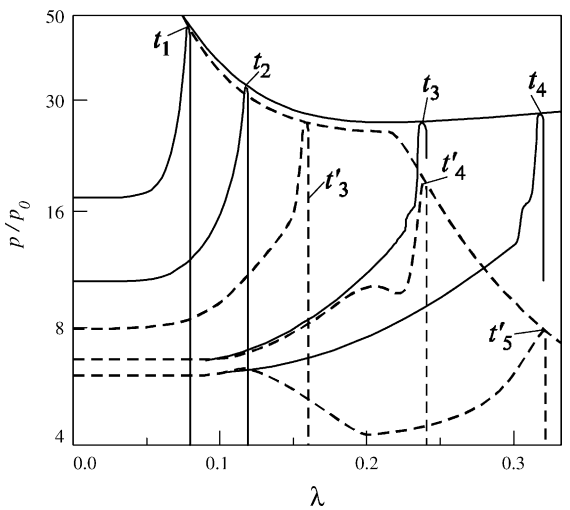

Fig. 54. Predicted explosion dynamics under supercritical (solid curves, time sequence t_1, t_2, t_3, and t_4) and subcritical (dashed curves, time sequence t_1, t_2, t'_3, t'_4, and t'_5) initiation of detonation in gas–droplets mixture; $\lambda = r/\bar{r}$ is the dimensionless distance, $\tau = tu_s/d_0(\rho_l^0/\rho_0)^{0.5}$ is the dimensionless time [153].

Nonmonotonic behavior of unsteady detonation wave velocity is typical for all calculations. Detonation wave attains minimum velocity D_{min} at distance $\lambda_s = r_s/\bar{r} \approx \nu/8$, where $\bar{r} = (E_0/\alpha_\mu p_0)^{1/\nu}$ is the dynamic radius, and, as before, index $\nu = 1$, 2, and 3 stands for planar, cylindrical, and spherical symmetry, respectively. The value of D_{min} decreases monotonically with decreasing point explosion energy and with increasing droplet size in a fuel spray.

Explosion of a fuel spray in gaseous oxidizer contains two independent parameters with the dimension of length: $\bar{r}$ and droplet diameter d_0. In case of polydispersed sprays, droplet diameter d_0 has the meaning of the SMD. The characteristic time for a droplet is $t_d = d_0(\rho_l^0/\rho_s)^{0.5}/u_s$, where ρ_l^0 and ρ_s are the densities of liquid and gas, respectively, and $u_s = D_{CJ}(1 - \rho_0/\rho_s)$ is the gas velocity behind a lead shock wave. For the CJ detonation wave the characteristic length is $\lambda_d = t_d D_{CJ} = d_0(\rho_l^0/\rho_0)^{0.5}/(\sigma^{0.5} - 1/\sigma^{0.5})$, where $\sigma = \rho_s/\rho_0$. To obtain the quantitative dependencies of the minimum velocity D_{min} of a nonsteady detonation wave on the governing parameters $\bar{r}, d_0$, and ν in a two-phase medium, particular calculations were performed in Ref. [153] for spherical, cylindrical and plane geometries.

The analysis of numerical solutions for detonation initiation of monodispersed and polydispersed sprays of liquid fuels in air or oxygen with droplet diameter d_0 =50–700 μm showed, that the critical dynamic radius of direct detonation initiation (by an intense shock wave) is independent of the problem geometry, i.e.

$$\bar{r}(\nu) = \left(\frac{E_\nu}{p_0}\right)^{1/\nu} \approx \text{const} = \bar{r}_{cr}$$

where E_ν is the critical initiation energy relevant to symmetry index ν. Experimental data on initiating liquid hydrocarbon sprays in air by ball and cord charges of condensed explosive correlate well with this equation.

The constancy of $\bar{r}_{cr}$ for different ν is not a strictly proved theoretical conclusion, but it is very useful for estimations. At known initiation energy for some spatial symmetry, it is possible to determine $\bar{r}_{cr}$ and then the initiation energies for the other symmetry as

$$E_\nu \approx p_0 \bar{r}_{cr}^{\nu}$$

Another useful correlation obtained on the basis of numerical solutions is the ratio of $\bar{r}_{cr}$ to the critical radius, $r_{\nu,cr}$, where detonation wave velocity attains its minimum:

$$r_{\nu,cr} \approx \frac{\nu \bar{r}_{cr}}{8}$$

With the help of the two latter equations, it is possible to express the initiation energies per unit area of the wave front

at critical radius for different ν, as:

$$\frac{E_1}{2} = 0.5p_0\bar{r}_{cr}, \qquad \frac{E_2}{2\pi r_{2,cr}} = 0.5p_0\bar{r}_{cr}, \qquad \frac{E_3}{4\pi r_{3,cr}^2} = 0.57p_0\bar{r}_{cr} \tag{11}$$

These values turn out to be close to each other in all the three cases of symmetry.

Unfortunately, only a small portion of experimental data on detonations is related to initiation of fuel–droplets systems. Therefore, the comparison of calculated results with experimental data can be performed only in few cases. For example, in Ref. [226], when initiating detonation of a cylindrical monodispersed spray of kerosene in oxygen (fuel droplet size $d_0 = 400$ μm) by an explosive charge, the value $E_2 \approx 0.34$ MJ/m was obtained.

The experiments were performed in a sector shock tube at controlled fuel concentrations with the mixture equivalence ratio of $\Phi = 0.33$. The calculated values for this case are $0.57 < E_2 < 0.75$ MJ/m. The correlation of calculated and experimental data for gas–droplets systems with the accuracy of a factor of about 2 should be considered as satisfactory, since the kinetic data for heterogeneous ignition exhibit considerable spread.

Two basic points that follow from experimental studies of direct initiation of detonation in gaseous and two-phase mixtures should be emphasized. The first one is greater energies of detonation initiation in heterogeneous mixtures as compared to mixtures of the same fuel in the gaseous state. For example, the minimum energy of detonation initiation in a stoichiometric gaseous propane–air cloud is below 100 g TNT, whereas that for propane fog in air is about 200 g TNT [135]. Qualitatively similar relations are observed in other heterogeneous mixtures, but quantitatively they drastically differ for different particle sizes. Thus, air mixtures of spherical aluminum particles less than 1 μm in diameter have detonability which is close to that of hydrogen–air mixtures, whereas particles 13 μm in diameter do not detonate in air at all, liquid fuel–air mixtures exhibit a similar behavior: in the absence of sufficient amounts of vapor phase, sprays of such fuels as kerosene, diesel fuel, and even gasoline larger than 100 μm fail to detonate in air, while these fuels dispersed to droplets 10 μm in diameter or prevaporized have minimum energies of direct initiation of detonation comparable with those in gases. This observations are substantiated by calculations: Table 9 shows the predicted critical dynamic parameters (critical dynamic radius, $\bar{r}_{cr}$, and critical energies of detonation initiation, E_1, E_2, and E_3) of heterogeneous detonations of stoichiometric benzene–air mixture depending on drop diameter in suspension [153].

The second point is that the relation between the minimum energies of initiation of detonation of heterogeneous mixtures in tubes and unconfined clouds obey the same relation, which follows from the Zel'dovich formula

Table 9
Predicted critical dynamic parameters of heterogeneous detonations of stoichiometric benzene–air mixture depending on drop diameter in suspension [153]

Drop diameter (μm)	r_{cr} (m)	E_1 (MJ/m^2)	E_2 (MJ/m)	E_3 (MJ)
0[a]	2.30	0.24	0.54	1.23
50	3.04	0.31	0.94	2.85
100	3.69	0.37	1.38	5.1
200	4.84	0.49	2.37	11.5
400	6.85	0.69	4.75	32.6
800	10.33	1.05	10.8	111.7
1000	11.94	1.21	14.4	172.4

[a] Zero diameter corresponds to vapor-phase composition.

(see Section 2.2.3). This latter point is very important because it allows one to estimate the minimum energies of initiation of spherical detonation from simple measurements performed in tubes and thus avoid extremely expensive field experiments with large-scale clouds.

In Ref. [210], two-phase *n*-hexane–air and *n*-heptane–air spray detonations were initiated by a powerful electric discharge mounted nearby the closed end of the detonation tube. The tube was 50.8 mm in diameter and 1.5 m long, and the FAM was delivered continuously (during 1 s) into the tube through the 3 mm-diameter nozzle of air-assit atomizer mounted at the closed end. To measure the propagation velocity of shock waves and flames, pressure transducers and ionization probes were installed in three cross-sections of the tube at a distance of 500, 900, and 1300 mm from the discharge electrodes. Fig. 55 summarizes the results of experiments for *n*-hexane with different voltage at the discharge electrodes. It follows from Fig. 55 that increase in voltage to 2000 V shows almost no effect on the flame

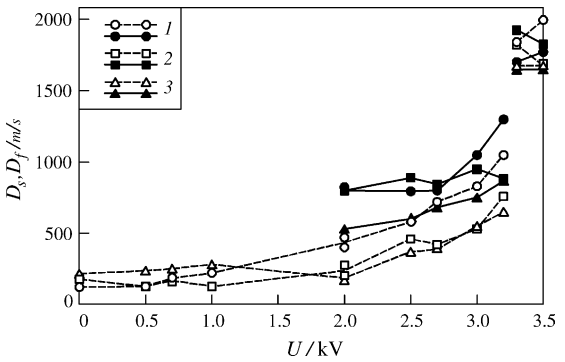

Fig. 55. Measured mean shock wave D_s (solid curves) and flame front D_f (dashed curves) velocities vs. voltage U at the initiating discharge in a series of experiments on direct detonation initiation in a two-phase *n*-hexane–air mixture. Numbers 1–3 denote three successive measuring bases between discharge location and station 500 mm (1), 500 and 900 mm (2), and 900 and 1300 mm (3). Zero voltage corresponds to mixture ignition by the low-energy primary discharge [210]. Tube diameter is 50.8 mm.

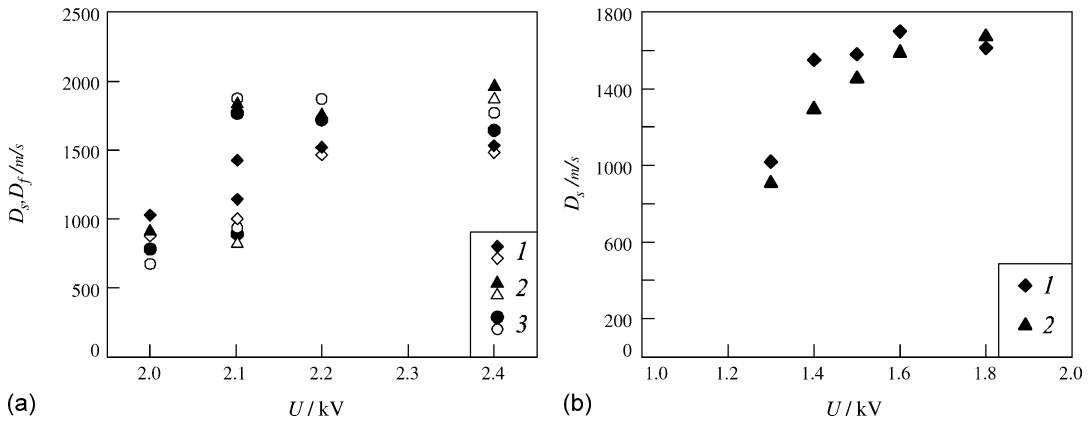

Fig. 56. Measured mean shock wave D_s (solid symbols) and flame front D_f (open symbols) velocities vs. voltage at the initiating discharge in a series of experiments on direct detonation initiation in a two-phase *n*-hexane-air mixture in two tubes of different diameter [160]: (a) d =50.8 mm; numbers 1–3 denote three successive measuring bases between discharge location and station 500 mm (1), between stations 500 and 900 mm (2), and 900 and 1300 mm (3); (b) d =27 mm; numbers 1 and 2 denote two successive measuring bases between stations 125 and 525 mm (1), and 525 and 925 mm (2) downstream the initiating discharge.

propagation velocity. As the voltage exceeds 3300 V, a detonation wave is observed at all measuring stations. In other words, as the ignition energy exceeded 3.3 kJ (estimated energy is based on the rated capacity of the high-voltage capacitor and voltage) direct initiation of detonation in *n*-hexane spray has been obtained. A similar set of experiments has been performed for *n*-heptane. In the test with the discharge voltage of 3300 V, *n*-heptane spray did not detonate. Increase of the ignition energy from 3.3 to 3.7 kJ resulted in direct detonation initiation in *n*-heptane spray.

Further experimental studies of direct initiation of *n*-hexane spray detonation in air have been reported in Ref. [160]. In this paper, the effect of tube diameter on the critical detonation initiation energy has been investigated. In addition to tube 50.8 mm (see Fig. 55), two other tubes of diameter 36 and 27 mm were used. As compared to experiments [210], the igniter configuration was modified to decrease the initiation energy of detonation in the 50.8 mm-diameter tube from 3.3 kJ (as in Fig. 55) to 1.5 kJ. Fig. 56a and b show the dependencies that are similar to that of Fig. 55.

As follows from Fig. 56, a decrease in the tube diameter results in diminishing the critical detonation initiation energy. Thus, almost two-fold decrease in the tube diameter (from 50.8 to 27 mm) resulted in decreasing the critical initiation energy from 1.5 to 0.82 kJ, i.e. almost two-fold. In a small-diameter tube, the minimal voltage required for detonation initiation has decreased from 2100 V in case of Fig. 56a to about 1600 V as in Fig. 56b. At small (near-limit) tube diameter of 27 mm, there is no abrupt change in wave velocity with increasing the energy of initiator.

Experiments similar to those shown in Fig. 55 were made with detonation initiation by two (or three) successively triggered electrical discharges [210]. For this purpose, the second discharge was mounted at a certain distance (100–300 mm) from the first discharge. The experimental procedure encountered a number of steps dealing with 'tuning' a specially designed controller in terms of a preset delay time for triggering the second discharge. The aim of tuning was to obtain a detonation wave at measuring stations 500, 900, and 1300 mm from the first discharge at the lowest

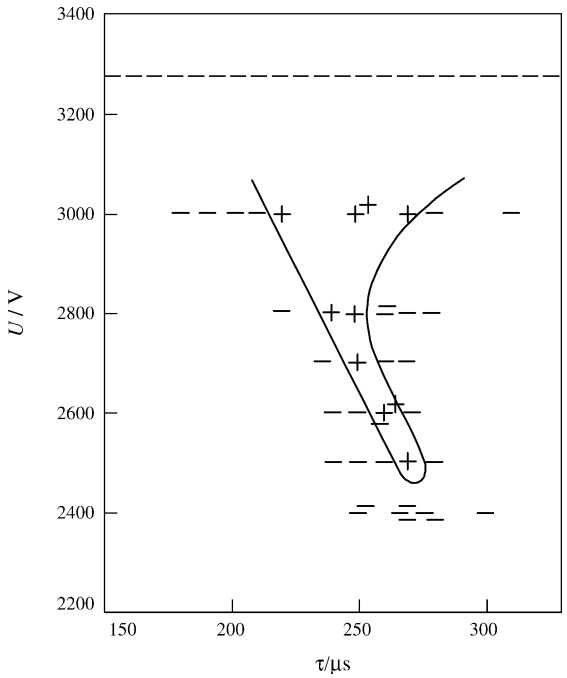

Fig. 57. Measured dependency of detonation initiation energy (in terms of voltage U applied to high-voltage blocks of two igniters with similar capacitance of 300 μF) vs. the delay time τ of the second igniter triggering (counted from activation of first igniter) [210]. Tube diameter 50.8 mm. Dashed line shows voltage required for detonation initiation by a single igniter of capacitance 2 × 300 μF = 600 μF.

possible total ignition energy. Fig. 57 summarizes the results of experiments for *n*-hexane sprays and a distance between the discharges of 200 mm.

The delay time for triggering the second discharge (counted from activation of the first discharge), and the voltage at high voltage blocks of the igniters are plotted along *X* and *Y*-axes, respectively. Plus and minus signs correspond to reliable 'go' and 'no go' detonation conditions reproduced in several similar experiments. It follows from Fig. 57 that there exist resonant conditions for second dicharge triggering in terms of the delay time. The 'width' of the detonation peninsula is about 50 μs at 3000 V and 10 μs at 2500 V. At a fixed delay time, e.g. 270 μs, detonation arises at 2500 V and does not arise at higher voltage (2600–2900 V) that indicates the necessity of careful synchronization of the second discharge triggering with the blast wave generated by the first discharge.

The lowest voltage required for detonation initiation with two successively triggered discharges was 2500 instead of 3300 V required with a single discharge (dashed line in Fig. 57 and abrupt change in shock wave and flame velocities in Fig. 55). This decrease in voltage indicates almost two-fold decrease in the total initiation energy. Thus, the findings of Ref. [210] indicate that (i) there exist resonant conditions for successive triggering of two igniters that have to be met in order to initiate detonation; (ii) the minimal total initiation energy by successively triggered igniters is lower than that required for direct detonation initiation by a single igniter; and (iii) the detonation peninsula at the 'initiation energy vs. triggering time delay' plane is very narrow and indicates the necessity of careful synchronization of successive discharge triggering.

2.3.4. Detonation transition

Similar to gaseous detonations, there exists a critical diameter for transition of two-phase detonation from a duct to unconfined cloud. Unfortunately, these critical diameters are virtually a blank spot both in the theory and experimental studies of heterogeneous detonations. This problem waits for its solution.

One of the recent publications on the topic is that by Kutushev and Shorohova [227]. In this paper, a 2D computational analysis on the possibility to mitigate detonation by adiabatic cooling of a two-phase flow of monofuel particles suspended in air at sudden expansion of the pipeline has been carried out. The geometry of the problem is shown in Fig. 58a. The diagram of Fig. 58b shows the temporal evolution of pressure profiles in the system. Clearly, in this case, detonation is transmitted to the wider tube.

Detailed numerical studies have shown that depending on parameters of the mixture and pipeline, two modes of flame propagation in the wide part of the pipeline are possible, namely, a continuing heterogeneous detonation and detonation failure. The predicted pressure maps during transition of detonation exhibit the features that are very similar to those relevant to gaseous detonations

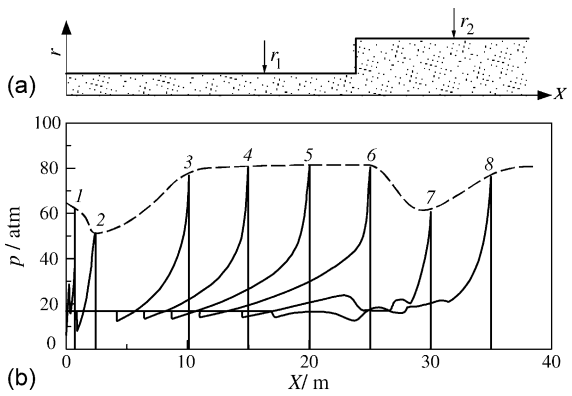

Fig. 58. (a) Schematic of the problem and (b) predicted pressure profiles in a propagating heterogeneous detonation at time t =0.23 ms (1), 1.05 (2), 10.45 (3), 13.83 (4), 17.19 (5), 17.39 (6), 19.47 (7), and 26.11 ms (8). The initial relative mass content of dispersed phase σ_d =3 and initial particle diameter d_0 =40 μm [227].

(irregular Mach reflections, Mach disk formation, etc. (Section 2.2.4)). Fig. 59 shows the predicted critical expansion ratio of the tube cross-section r_2/r_1 vs. particle loading ratio, σ_d (the ratio of particle mass concentration to gas density), at constant particle diameter of d_0 =40 μm. In the region above the curve, detonation fails.

Unconfined spray and dust clouds formed in practice deliberately or due to accidental release of the fuel into air have usually a shape of cylinder or flat slab, therefore, the problem of criticality of detonation of such clouds is acute when assessing the potential hazard of releases. Both field tests and laboratory-scale experiments show that the overwhelming majority of heterogeneous mixtures can detonate only in clouds whose minimum size exceeds 0.5 m (normally 1 m or more). Certainly any active gas-phase or volatile additives to the fuel will significantly reduce both the critical diameter and the initiation energy.

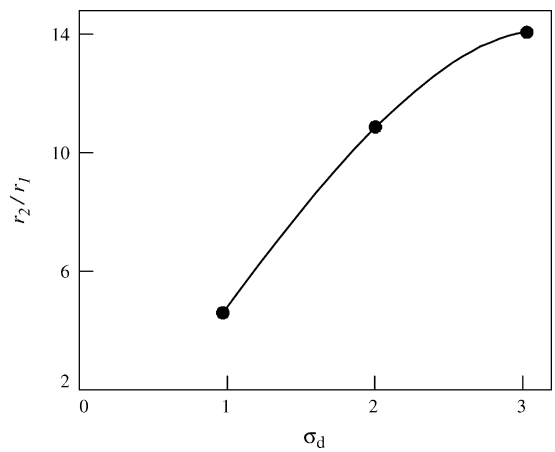

Fig. 59. Predicted critical expansion ratio r_2/r_1 vs. particle loading ratio σ_d at fixed particle diameter d_0 =40 μm [227].

2.3.5. Nonideal detonations

As mentioned above, detonation velocity of two-phase mixtures depends on tube diameter: in wide tubes detonation velocity is usually lower than the ideal CJ velocity, but with small droplets or particles (micron and submicron range) may be rather close to the CJ value, and decreases as the tube diameter decreases due to the losses from the detonation zone to the tube walls, that is, the nonideal character of detonation propagation becomes more and more important with an increase of losses from the detonation zone. For two-phase confined detonations, the list of intrinsic losses given in Section 2.2.5 can be extended as follows:

I. Losses involving nonequilibrium processes in the reaction zone:

- Losses due to nonuniform distribution of the thermodynamic parameters, concentration and velocity fields across a tube;
- Losses caused by turbulence in the core flow;
- Losses induced by nonstationary processes in the reaction zone;
- Losses due to phase transition under the finite difference of concentrations;
- Losses connected with the surface tension forces;

II. Irreversible losses of energy:

- Friction losses involving:
  (a) viscous losses in boundary layers;
  (b) eddy losses due to flow separation on obstacles and on particles;
- Bow shock losses at obstacles and particles;
- Losses arising from divergence of streamlines in the reaction zone;
- Heat losses to the tube walls, obstacles, and dispersed paricles;
- Losses connected with incomplete burning of the combustible mixture and incomplete phase transition.

There are three important discrepancies between the detonation features in gaseous and two-phase systems [202]. An analysis of the experimental data on detonation velocities of two-phase systems shows that low-velocity nonideal regimes can propagate in such systems at the velocity as low as 1000 m/s. Note that this value is much lower than the corresponding value in the gas systems (in smooth tubes), which is about 1700–1800 m/s. This feature is associated with two factors: first, fuel does not burn out completely upstream of the CJ plane and, second, with the hot spot nature of reaction initiation behind the shock wave in the vicinity of droplets or particles which provides short delays of localized ignition events. Indeed, the temperature and oxygen concentration at the stagnation point of larger droplets or particles is higher than in the surrounding flow due to deceleration of the gas flow and formation of bow shocks. However, these low-velocity regimes were observed only in mixtures with large droplets (and predominantly in oxygen mixtures).

The second specific feature of heterogeneous detonation is related to the dependence of detonation velocity on the concentration of liquid fuel. Detonation velocity of a two-phase mixture changes only slightly when the concentration of fuel changes and the detonation velocity deficit relative to the ideal CJ velocity is smaller for leaner mixtures. In gaseous systems opposite trends are observed.

Third, if fuel in a heterogeneous mixture is present both in the gas and condensed phases and if the consumption rate of the gaseous fuel is much faster than that of the condensed one, the detonation velocity and critical parameters in this 'hybrid' mixture is mostly controlled by heat evolution from the gas fuel. These waves may have a peculiar structure. At the first fast heat release stage, the particles serve as heat sinks, but they start burning afterward at a lower rate. Therefore, the overall heat release rate can change its sign in some flow region. Thus, according to gasdynamic equations, in a steady flow, a sonic plane can settle down in this zone. The slow heat release continuing in the supersonic flow downstream of the sonic plane can give rise to a secondary reactive shock wave which follows the primary one. These double-front waves were indeed observed in experiments [228].

The above-discussed processes are similar to nonideal detonation regimes in gases, however, in heterogeneous systems, there is a detonation mode which is inherent only in two-phase mixtures. This is detonation propagating in nonpremixed gas-fuel systems. So far, there is only indirect evidence of detonation-like regimes in such systems in ducts filled with air at atmospheric pressure. Severe explosions in empty pipelines whose walls are coated with liquid fuels and in dusty industrial ducts in some cases show post-effects that could be caused by detonation waves or reaction regimes that are close to detonation. Numerous experimental studies [91,202] demonstrate that the basic features of detonation waves in layered systems are:

1. waves propagate at very low velocities (about $0.5D_{CJ}$);
2. reaction behind the lead shock wave is initiated near the shock wave front due to reflection of transverse shock waves (that are very strong in this case) from the walls and then proceeds in the flame front,
3. wave propagates in the form of regularly repeating explosions;
4. fuel is lifted into the duct volume due to various types of hydrodynamic instability and mixes with the gaseous oxidizer, thereby preparing a premixed layer that actually generates the strong transverse shock waves leading the detonation wave;
5. it should be emphasized that detonation waves of this type propagate only in ducts whose walls are coated with thin fuel layers (less than 1 mm) or covered by a layer of very fine dust particles;

6. energies of direct initiation of such detonation waves are very high, much higher than those of gaseous mixtures;
7. predetonation distances in tubes are larger than in gases and suspensions (more than 10 m even with rather powerful ignition sources);
8. there exist a lean limit of detonation of layered systems, but the rich limit is very high;
9. nobody managed so far to initiate such a detonation regime under unconfined conditions.

2.3.6. Transient deflagration and DDT

In contrast to gaseous mixtures, no publications on systematic studies of DDT in sprays are available in the literature, perhaps, because generation of more or less homogeneous droplet concentration fields in long ducts is a difficult technical problem. Information about DDT processes in ducts whose walls are coated with thin liquid layers or in dusty ducts is more definite and complete, however, these systems are beyond the scope of this review. There are only few publications relevant to DDT processes in suspensions of liquid droplets in oxygen. Webber [229] was, probably, the first to observe amplification of weak shock waves in the course of their propagation through burning sprays, that is, to indicate that there was some mechanism which could be responsible for DDT in sprays. More comprehensive studies [230,231] have demonstrated that transition to detonation within short distances in burning sprays is quite feasible. A mandatory condition for this transition is a weak shock wave that must be sent into a burning spray or spray to be ignited. The study also indicated definitely that it is droplet breakup that is responsible for shock wave amplification.

The experiments were performed in a vertical shock tube equipped with pressure gauges to monitor both the wave velocity and pressure profiles and droplet generator on the tube top. Kerosene drops were injected through nine hypodermic needles 0.6 mm in diameter in oxygen at 1 atm, the average droplet size was 2 mm. The equivalence ratio varied along the tube length from 1.0 near the drop generator to about 0.33 at 1300 mm away from it. The droplet array was ignited after it filled the vertical portion of the tube and then a weak shock wave was generated with a controlled delay by mechanically bursting the diaphragm closing the high-pressure chamber at the tube end opposite to the droplet generator. The Mach number (M) of the shock wave and its duration (Δt) varied in different runs from 1.07 to 1.3 and from 2 to 0.02 ms, respectively. Fig. 60a and b show amplification of a shock wave with $M = 1.16$ spreading in a burning array of droplets at $\Delta t = 1.56$ and 0.125 ms, respectively.

In the first case, the shock amplitude and velocity continuously increased with time from 0.4 to 3.2 atm and from 400 to 600 m/s, respectively. Some profiles show rising pressure behind the shock front (and even formation of a secondary compression wave), which is a result of reaction intensification. At shorter shock pulses, no amplification was observed: the wave either propagated at a constant velocity or decayed.

The results of experiments are summarized in Fig. 61, where they are plotted in the form of dependency of normalized shock overpressure p_s/p_{s0} on distance X_s

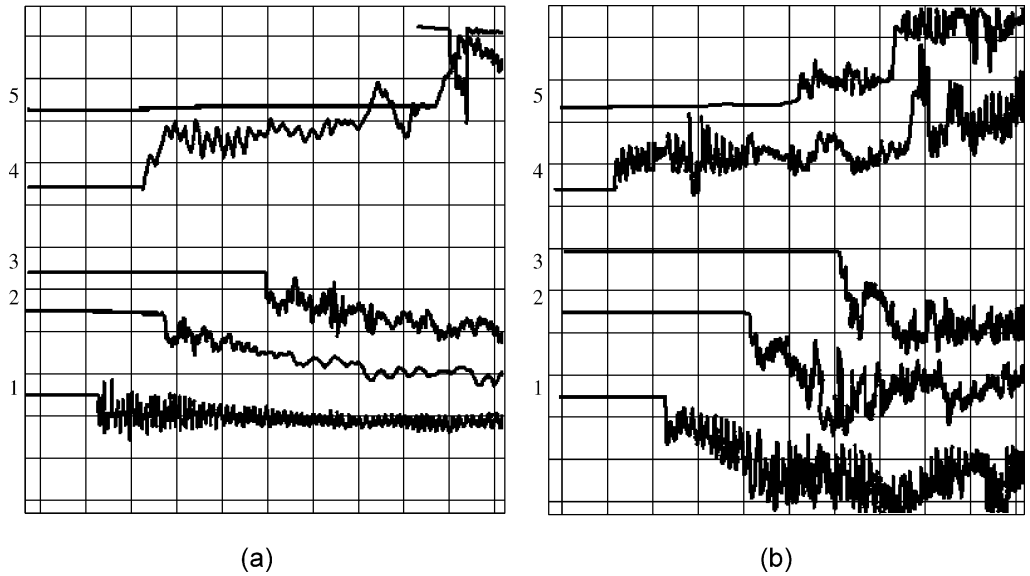

Fig. 60. Pressure recorded by gauges mounted along the tube in which a weak shock wave with $M_0 = 1.16$ spreads through an array of droplets burning in oxygen, the wave duration is 1.56 ms (a) and 0.125 ms (b). The distance of gauges from the triggering one are 240 mm (1), 480 (2), 720 (3), 960 (4), and 1200 mm (5); time scale is 0.25 ms/div for gauges 1, 2, and 3 and 0.1 ms/div for gauges 4 and 5; pressure scale: (a) 0.8, 1.29, 2.08, 4.0, and 5.8 atm/div for gauges 1, 2, 3, 4, and 5, respectively, (b) 0.77, 0.8, 0.83, 0.63, and 0.8 atm/div for the same gauges [230,231].

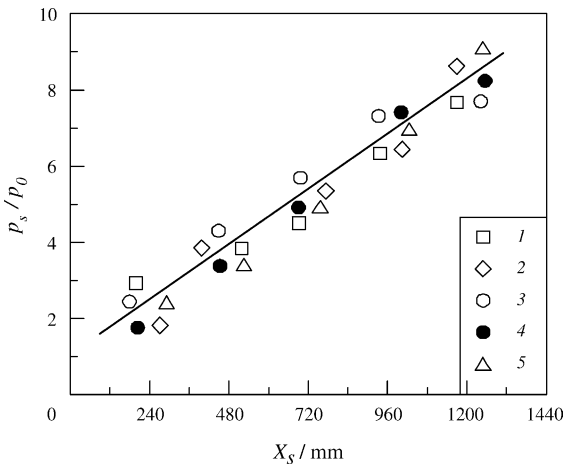

Fig. 61. Shock wave intensity p_s/p_{s0} vs. distance travelled by the wave, X_s; points 1, 2, 3, 4, and 5 correspond to shock waves with $M_0 = 1.11$, 1.14, 1.16, 1.2, and 1.3, respectively [230,231].

travelled by the shock wave, with $p_{s0} = p_s(X_s = 0)$. As seen, the wave amplitude linearly increases with distance, provided the wave duration exceeds a certain value, and the slope of this dependence is virtually independent of the initial wave amplitude. Hence the higher the initial amplitude of the wave and the longer the distance it travels along the burning spray, the closer is the final state of the process to normal detonation. This statement is also supported by Fig. 62, where the time history of the average pressure behind the wave is displayed.

The zero time in the graph pertains to the instant of shock front arrival at the gauge. It should be emphasized that to reveal the characteristic features of the process and to ascertain the mechanism responsible for wave amplification, droplets in Refs. [230,231] were deliberately taken large.

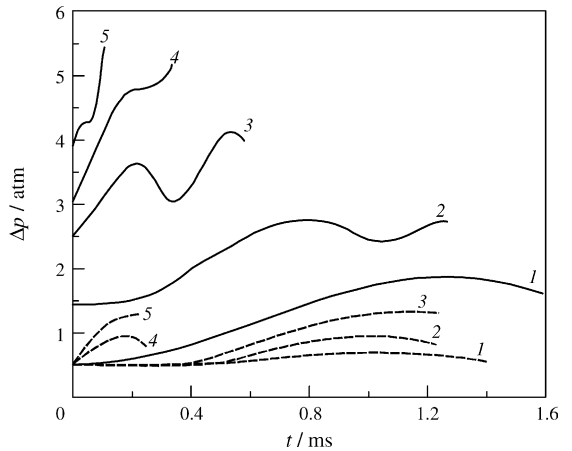

Fig. 62. Time histories of average overpressure Δp recorded by pressure gauges mounted at 240 mm (1), 480 (2), 720 (3), 960 (4), and 1200 mm (5) from the drop generator. Zero time corresponds to the lead shock front. Dashed lines are recorded in the run with the shock wave of short duration Δt [230,231].

Experiments with smaller droplets [232] show that even very short initial waves experience amplification.

Weak shock waves exhibit similar behavior when sent into a nonburning sprays ignited by a permanently operating ignition source after the wave passes over the source. Droplets 2 and 0.5 mm in diameter were injected in this case in nitrogen–oxygen mixtures. The recorded pressure profiles shown in Fig. 63 provide evidence of intense droplet burning that generates secondary compression waves (refer to beams 3 and 4 in Figs. 63a and 63b). Burning arises only when the wave duration and intensity exceed certain critical values.

As the DDT process involves accelerating shock waves, one important issue should be pointed out. Behind shock waves propagating through reactive mixtures with relatively large droplets, the droplets are exposed to a high-velocity flow and experience intense breakup. Fine micromist produced by the breakup process burns at a much higher rate than the parent droplets. There are several breakup modes among which only two are capable of providing an increase in the effective specific area of burning droplets sufficient to support and enhance the shock wave. They are: the so-called stripping and catastrophic modes. The latter mode is observed only in very strong shock waves therefore has nothing to do with the DDT process. Thus, the basic necessary criteria defining the conditions under which weak shock waves can run away to heterogeneous detonation in a burning spray (or in droplet suspensions in hot oxidizing environment) are: (i) Weber number *We* should exceed its critical value defined by inequality $We \geq Re^{1/2}$, where *Re* is the Reynolds number, (ii) characteristic breakup times must be shorter than shock wave duration, and (iii) the secondary droplets must be small enough for their burning times to be shorter than the shock pulse duration.

The other approach to obtain heterogeneous detonation via DDT has been put forward recently [233]. Experimental study has been performed in a 27 mm diameter tube with a turbulizing element in the form of Shchelkin spiral. Fig. 64 shows a schematic of detonation tube with Shchelkin spiral mounted between two discharges. The length of spiral is 460 mm. It is made of steel wire 4 mm in diameter and 18 mm pitch and is installed in tube section 500 mm long.

It is implied that a shock wave generated by first discharge and passed through Shchelkin spiral can be further amplified to detonation intensities by properly tuned triggering of second discharge mounted downstream from the spiral section. The major energy is deposited in the second discharge. To provide precise synchronization of second discharge triggering with shock arrival, a special probe 6 (see Fig. 64) was used. The probe was mounted at a distance of 90 mm upstream from the second discharge. This allowed reliable synchronization of discharge triggering with shock arrival.

Tests with fine *n*-hexane sprays in air at normal conditions with one (first) discharge and Shchelkin spiral have revealed the following. At discharge energies less than 0.1 kJ,

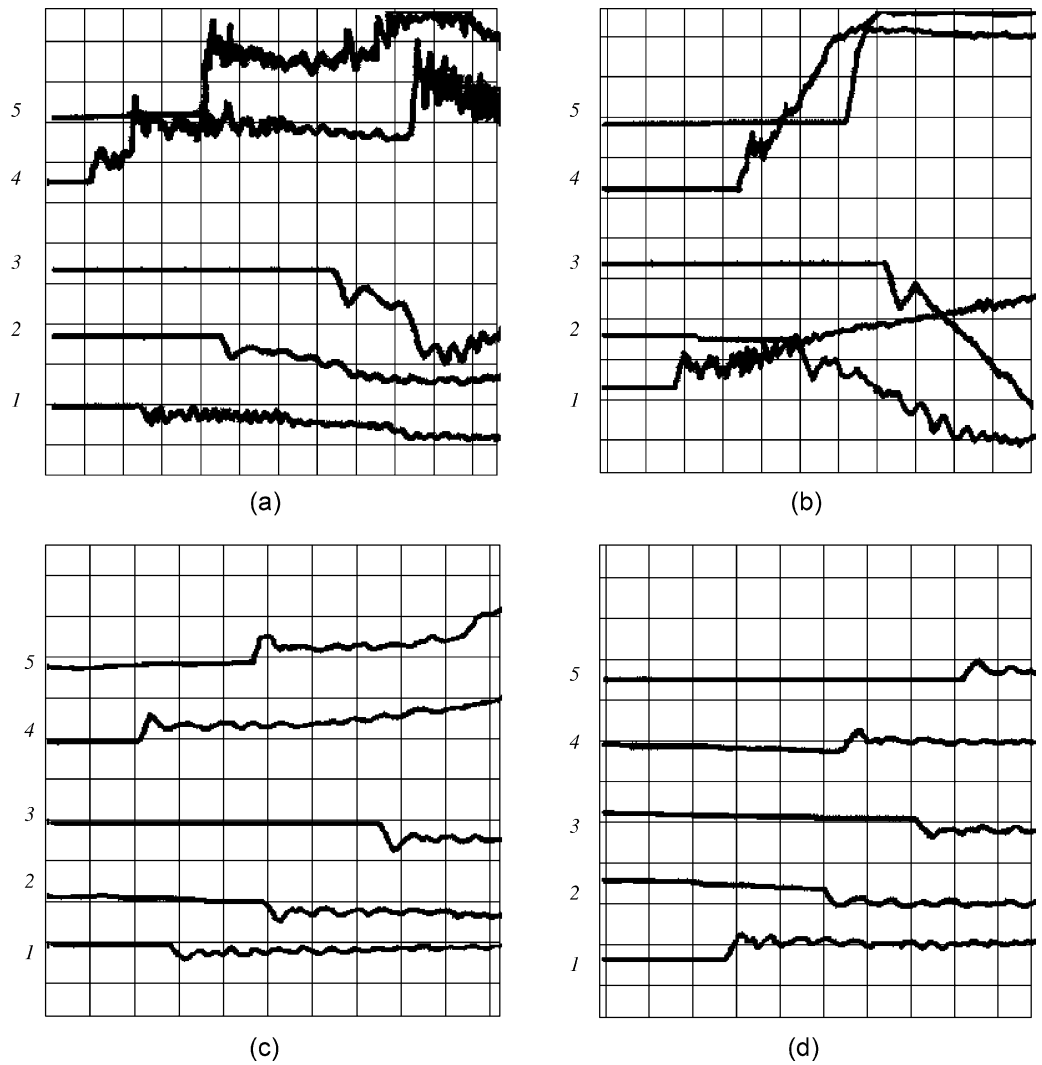

Fig. 63. Pressure–time histories recorded in a tube filled with kerosene droplets ignited only after passage of the shock wave [230,231]. Pressure gauges are mounted at 240 mm (1), 480 (2), 720 (3), 960 (4), and 1200 mm (5) from the drop generator. (a) M_0= 1.16, drop diameter $d = 2$ mm, gaseous mixture $0.5N_2 + 0.5O_2$, time scale 0.25 ms/div, pressure scale 1.2 atm/div for gauges 1 and 2, 1.4 for gauges 3–5; (b) M_0= 1.11, $d = 0.5$ mm, $0.7N_2 + 0.3O_2$, time scale 0.25 ms/div, pressure scale 0.6 atm/div for gauges 1–5; (c) M_0= 1.16, $d = 2$ mm, $0.7N_2 + 0.3O_2$, time scale 0.25 ms/div, pressure scale 1.2 atm/div for gauges 1 and 2, 1.4 for gauges 3–5; (d) $M = 1.16$, $d = 0.5$ mm, $0.5N_2 + 0.5O_2$, time scale 0.25 ms/div, pressure scale 0.7 atm/div for gauge 1 and 1.4 atm/div for gauges 2–5.

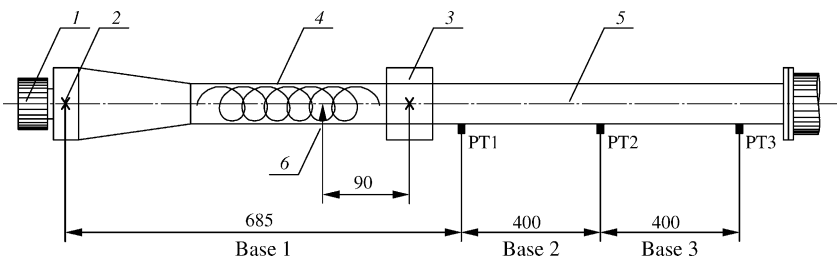

Fig. 64. Experimental setup with 27-millimeter tube and Shchelkin spiral between two discharges [233]: 1—air-assist liquid fuel atomizer, 2—first discharge, 3—second discharge, 4—Shchelkin spiral, 5—tube, and 6—probe; PT1, PT2, and PT3 stand for pressure transducers. Dimensions in mm.

the propagation velocities of compression and combustion waves registered at measuring bases 1–3 were close to the sound speed in air and shock waves did not form. Increasing the discharge energy to 0.1–0.13 kJ led to formation of a shock wave with a propagation velocity of about 910 m/s at measuring base 2 and 770 m/s at measuring base 3. At measuring base 1, the propagation velocity of arising shock waves was close to the sound speed. At higher discharge energies of 0.58–0.62 kJ, the situation changed: shock velocity at measuring base 1 was nearly independent of discharge energy and equal to about 870 m/s, while at measuring bases 2 and 3, the shock velocity decreased to 770–780 and 680–700 m/s, respectively. Clearly, the most efficient amplification of shock waves in the spiral section was attained at discharge energies of 0.1–0.13 kJ—from nearly sound speed to about 910 m/s. These values of first discharge energy were treated as optimal for tests with Shchelkin spiral.

Further experiments were made to check a possibility of amplifying a shock wave exiting from the Shchelkin spiral section by properly tuned triggering of second discharge. In these experiments, the relative capacitance of two discharges, voltage, and time delay of second discharge triggering were varied.

With the setup of Fig. 64, the total initiation energy required for detonation initiation was 0.66 kJ. Fig. 65 shows the measured dependencies of shock wave velocities on the delay time between shock arrival at the probe and second discharge triggering. Clearly, at delay times from 80 to 120 μs, transition to detonation occurs at measuring bases 2 and 3. At total initiation energy of 605 J and below, detonation initiation failed. Delay time of 80 μs can be considered as the optimal value for detonation initiation with two discharges and Shchelkin spiral. Fig. 66 shows the corresponding pressure records at pressure transducers PT1, PT2, and PT3.

Thus, it has been shown that the use of 0.1–0.13 kilojoule discharge in combination with Shchelkin spiral can result in generation of a primary shock wave propagating at the velocity of about 900 m/s in a tube 27 mm in diameter. Such a shock wave can be amplified to detonation by using an additional discharge triggered in phase with shock arrival at its position.

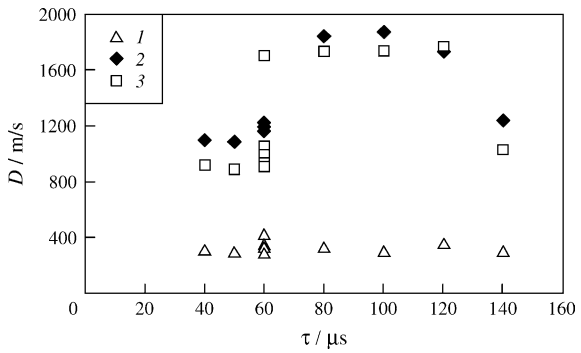

Fig. 65. Measured dependencies of shock wave velocity D in n-hexane spray—air mixture on the delay time τ between shock arrival at the probe and second discharge triggering [233]. Numbers 1, 2, and 3 denote corresponding measuring bases in Fig. 64. At delay times from 80 to 120 μs, transition to detonation occurs at measuring bases 2 and 3.

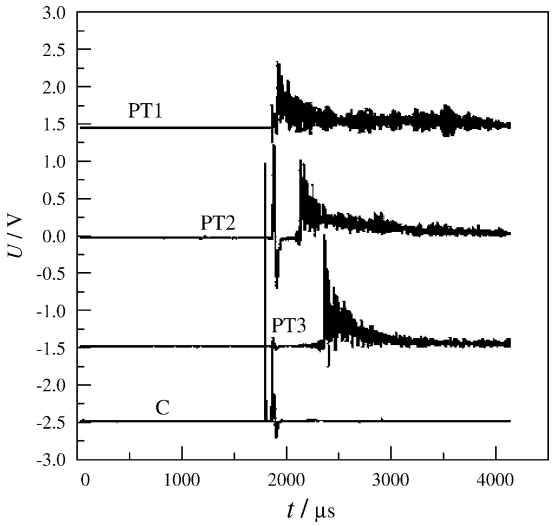

Fig. 66. Pressure records for the experimental run with successful n-hexane spray—air detonation initiation in 27 mm tube of Fig. 64 with second discharge delay time $\tau = 80$ μs [233]. Control channel record (C) shows the instant of second discharge triggering.

2.4. Thermodynamic grounds for detonation cycle

In 1940, Zel'dovich [234] has shown that detonative combustion is thermodynamically more efficient than constant-volume and constant-pressure combustion.

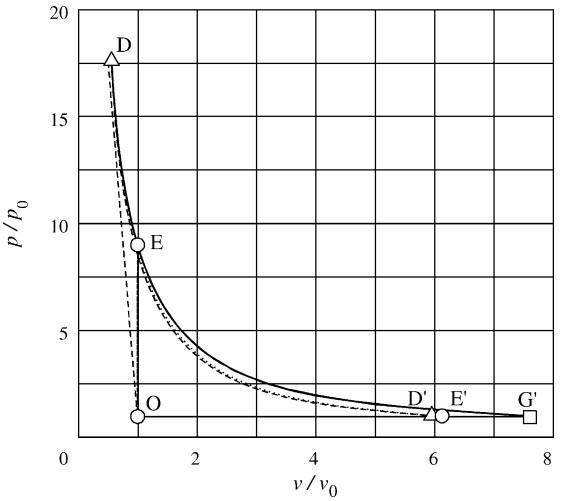

Fig. 67. Thermodynamic cycles with constant-pressure ($OG'O'$), constant-volume ($OEE'O'$), and detonative combustion ($ODD'O'$) with no precompression [235].

This can be readily seen from Fig. 67 that is the pressure (p)–specific volume (v) diagram [235].

Consider as an example the combustion of ethylene–air mixture $C_2H_4 + 3O_2 + 11.28N_2 = 2CO_2 + 2H_2O + 11.28\ N_2$ (quantitatively, Fig. 67 is analyzed below). Assume that the initial thermodynamic state of the reactive mixture corresponds to point O in pressure–specific volume diagram of Fig. 67, i.e. $p = p_0$, $v = v_0$. The thick solid curve is the reactive mixture Hugoniot. Detonative combustion corresponds to the jump from point O to shock Hugoniot (not shown) followed by transition to point D along the Reyleigh line (OD is a piece of that Reyleigh line). At point D, the entropy of combustion products is known to attain a minimum and the corresponding Poisson adiabat is tangent to the reactive Hugoniot. If one assumes that after expansion the combustion products attain the initial pressure p_0, then isentropic expansion from point D proceeds along dotted curve DD' towards point D'. In case of constant-volume combustion, the thermodynamic state of the mixture varies along thin dashed line OE. Further isentropic expansion proceeds along thin dashed curve EE' that terminates at point E'. Finally, constant-pressure combustion results in variation of the thermodynamic state along solid line OG' with point G' representing the final thermodynamic state. Note that points D, E, and G' are located at the same reactive Hugoniot. Clearly, the entropy rise during detonative combustion is minimal, i.e.

$$S_{D'} - S_O < S_{E'} - S_O < S_{G'} - S_O \tag{12}$$

From now on, the constant-pressure, constant-volume, and detonative combustion cycles will be referred to as Brayton, Humphrey, and PDE cycles. The efficiency of thermodynamic cycles $ODD'O, OEE'O$, and $OG'O$ can be readily estimated. At point O, the total specific enthalpy of the reactive mixture is $H_0 = h_0 + q$, where h_0 is the specific thermal enthalpy, and q is the heat effect of combustion. The enthalpy of the combustion products is $H = h$. The work W performed in the cycles is determined as $W = W_e - W_a = H_0 - H = h_0 - h + q$, where W_e is the expansion work and $W_a = p_0(v - v_0)$ is the work against ambient pressure. The efficiency is defined as

$$\chi = \frac{W}{q} = \frac{H_0 - H}{q} \tag{13}$$

For estimations, consider as an example the combustion of ethylene–air mixture $C_2H_4 + 3O_2 + 11.28N_2 = 2CO_2 + 2\ H_2O + 11.28N_2$ with no variation in the mole number. The gas is assumed to obey the ideal gas law at constant specific heats. The combustion heat of ethylene is 316,000 cal/mol (fuel) so that the heat effect of combustion reaction is taken equal to q =22,000 cal/mol (mix). Initial temperature is taken equal to $T_0 = 300$ K and mean mixture specific heats at constant-pressure and at constant-volume are taken, respectively, as $c_p = 11.1$ cal/mol and $c_v = 9.12$ cal/mol, so that $\gamma = c_p/c_v = 1.217$. Corresponding initial mixture properties are taken as: $c_{p0} = 7$ cal/mol and $c_v = 5.02$ cal/mol, so that $\gamma_0 = c_{p0}/c_{v0} = 1.394$. Fig. 67 discussed above is plotted for these values of governing parameters. The reactive Hugoniot in Fig. 67 satisfies the following equation:

$$\frac{p}{p_0} = \frac{\dfrac{\gamma+1}{\gamma-1} - \dfrac{v}{v_0} + \dfrac{2\gamma}{\gamma-1}\dfrac{q}{c_pT_0}}{\dfrac{\gamma+1}{\gamma-1}\dfrac{v}{v_0} - 1} \approx \frac{83.36 - \dfrac{v}{v_0}}{10.09\dfrac{v}{v_0} - 1}$$

As a result of constant-pressure combustion, the temperature, pressure, and specific volume of combustion products at point G' in Fig. 67 are $T_{G'} = T_0 + q/c_p = 300 + 22,000/11.1 = 2282$ K, $p_{G'} = p_0$, and $v_{G'} = 7.6v_0$, giving $H_{G'} = c_{p0}T_0 + c_p(T_{G'} - T_0) = 24,100$ cal/mol. Combustion at constant ambient pressure (without mixture precompression) results in zero thermodynamic efficiency of Brayton cycle, as $H_{G'} = H_0$, i.e.

$$\chi_{p=const} = 0 \tag{14}$$

Constant-volume combustion (point E in Fig. 67) results in temperature $T_E = T_0 + q/c_v = 300 + 22,000/9.12 = 2712$ K, pressure $p_E = p_0T_E/T_0 = (2712/300) = 9.04p_0$, and specific volume $v_E = v_0$. Isentropic expansion of combustion products from p_E to p_0 results in temperature drop from T_E to $T_{E'} = T_E(p_E/p_0)^{-(\gamma-1)/\gamma} \approx 1831$ K and increase in specific volume from v_0 to $v_{E'} = 6.1v_0$, giving $H_{E'} = c_{p0}T_0 + c_p(T_{E'} - T_0) = 19,098$ cal/mol (point E' in Fig. 67). Substituting the value of $H = H_{E'}$ into Eq. (13) one obtains the efficiency of the Humphrey cycle:

$$\chi_{V=const} = \frac{H_0 - H_{E'}}{q} \approx 0.227 \tag{15}$$

At point D in Fig. 67, pressure, temperature, and specific volume of detonation products are estimated as

$$p_D = p_0[1 + \gamma(M_{CJ}^2 - 1)/(\gamma + 1)] \approx 17.61p_0$$

$$T_D = T_0\left(\frac{p_D}{M_{CJ}p_0}\right)^2 \approx 2977\ \text{K}$$

$$v_D = v_0\left(\frac{T_D}{T_0}\frac{p_0}{p_D}\right) \approx 0.563v_0$$

where

$$M_{CJ} = \sqrt{1 + (\gamma+1)q/2c_pT_0} + \sqrt{(\gamma+1)q/2c_pT_0} \approx 5.591$$

is the Mach number of the CJ detonation wave (detonation velocity is 1815 m/s). Isentropic expansion of detonation products from p_D to p_0 results in temperature drop from T_D to $T_{D'} = T_D(p_D/p_0)^{-(\gamma-1)/\gamma} = 1784$ K, and increase in the specific volume from v_D to $v_{D'} \approx 5.95v_0$, giving $H_{D'} = c_{p0}T_0 + c_p(T_{D'} - T_0) = 18,579$ cal/mol. Substituting the value $H = H_{D'}$ into Eq. (13) one obtains the efficiency of the PDE cycle with detonative combustion:

$$\chi_{Detonation} = \frac{H_0 - H_{D'}}{q} = 0.251 \tag{16}$$

Comparing Eqs. (14)–(16) one comes to the following relation between the efficiencies of Brayton, Humphrey,

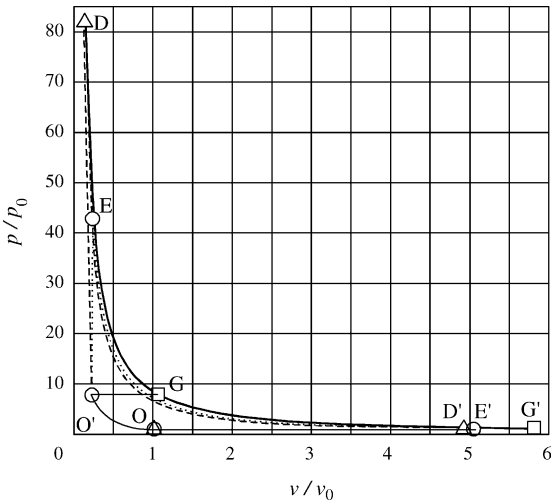

Fig. 68. Thermodynamic cycles with constant-pressure ($OO'GG'O$), constant-volume ($OO'EE'O$), and detonative combustion ($OO'DD'O$) with precompression [235].

and PDE cycles without initial mixture precompression:

$$\chi_{\text{Detonation}} > \chi_{V=\text{const}} > \chi_{p=\text{const}} \tag{17}$$

As $T_{D'} \approx 1784$ K, $T_{E'} \approx 1831$ K, and $T_{G'} = 2282$ K, the relationship (12) between entropy change in processes ODD', OEE', and OG' is now substantiated quantitatively.

Mixture precompression results in the pressure –specific volume diagram of the type shown in Fig. 68 [235].

Assume ideal isentropic compression of initial mixture from state O to state O' with $c_{p0} = 7$ cal/mol, $c_{v0} = 5.02$ cal/mol, and $\gamma_0 = 1.394$. For example, at compression ratio $\pi = p_{O'}/p_0 = 7.82$ (corresponds to ram compression at flight Mach number of 2), the specific enthalpy of the ethylene–air mixture under consideration at point O' is

$$H_{O'} = c_{p0} T_0 \pi^{(\gamma-1)/\gamma} + q \approx 3757 \text{ cal/mol} + q$$

At point O', temperature is $T_{O'} = T_0 \pi^{(\gamma-1)/\gamma} \approx 536.7$ K, pressure $p_{O'} = \pi p_0 = 7.82 p_0$, and specific volume $v_{O'} = v_0(p_0 T_{O'}/p_{O'} T_0) \approx 0.229 v_0$.

Further energy release due to detonative, constant-volume, or constant-pressure combustion results in transition from state O' to state D, E, or G, respectively, located on the reactive Hugoniot:

$$\frac{p}{p_{O'}} = \frac{\dfrac{\gamma+1}{\gamma-1} - \dfrac{v}{v_{O'}} + \dfrac{2\gamma}{\gamma-1}\dfrac{q}{c_p T_{O'}}}{\dfrac{\gamma+1}{\gamma-1}\dfrac{v}{v_{O'}} - 1} \approx \frac{51.638 - 4.367\dfrac{v}{v_0}}{44.614\dfrac{v}{v_0} - 1}$$

which is different from that shown in Fig. 67 as it contains parameters at state O' rather than at state O. Isentropic expansion of combustion products to the ambient pressure p_0 results in new final states D', E', or G', depending on the combustion mode.

At constant-pressure combustion (Brayton cycle $OO'GG'O$), the enthalpy of the combustion products at point G is $H_G = H_{O'}$ resulting in temperature $T_G = T_{O'} + q/c_p = 536.7 + 22,000/11.1 \approx 2518.7$K, pressure $p_G = 7.82 p_0$, and specific volume $v_G = v_0(p_0 T_G/p_G T_0) \approx 1.074\, v_0$. Isentropic expansion of combustion products from p_G to p_0 results in temperature drop from T_G to $T_{G'} = 1745$ K, increase in the specific volume from v_G to $v_{G'} = v_0(p_0 T_{G'}/p_{G'} T_0) \approx 5.818\, v_0$, giving $H_{G'} = 17,172$ cal/mol. The efficiency of cycle $OO'GG'O$ is then equal to

$$\chi_{p=\text{const}} = \frac{H_0 - H_{G'}}{q} = \frac{c_{p0} T_0 + q - H_{G'}}{q} \approx 0.315 \tag{18}$$

Constant-volume combustion (Humphrey cycle $OO'EE'O$) results in temperature $T_E = T_{O'} + q/c_v = 536.7 + 22,000/9.12 = 2949$ K, specific volume $v_E = v_{O'} = 0.229 v_0$, and pressure $p_E = p_{O'}(T_E/T_{O'}) = 7.82 p_0(2949/536.7) \approx 42.95 p_0$. Isentropic expansion of combustion products from p_E to p_0 results in temperature drop from T_E to $T_{E'} = T_E(p_E/p_0)^{-(\gamma-1)/\gamma} \approx 1508$ K, increase in the specific volume from v_E to $v_{E'} = v_0(T_{E'}/T_0) \approx 5.026\, v_0$ and $H_{E'} = c_p T_{E'} \approx 14,538$ cal/mol. Thus, the efficiency of cycle $OO'EE'O$ is:

$$\chi_{V=\text{const}} = \frac{H_0 - H_{E'}}{q} \approx 0.435 \tag{19}$$

At point D, pressure, temperature, and specific volume of detonation products are estimated as

$$p_D = p_{O'}[1 + \gamma(M_{CJ}^2 - 1)/(\gamma+1)] \approx 82.15\, p_0$$

$$T_D = T_{O'}\left(\frac{p_D}{M_{CJ} p_{O'}}\right)^2 \approx 3235 \text{ K}$$

$$v_D = v_0\left(\frac{T_D}{T_0}\frac{p_0}{p_D}\right) \approx 0.131\, v_0$$

where the Mach number of the CJ detonation wave is equal to

$$M_{CJ} = \sqrt{1 + (\gamma+1)q/2c_p T_{O'}} + \sqrt{(\gamma+1)q/2c_p T_{O'}} \approx 4.28$$

which corresponds to detonation velocity of 1859 m/s. Isentropic expansion of detonation products from p_D to p_0 results in temperature drop from T_D to $T_{D'} = T_D(p_D/p_0)^{-(\gamma-1)/\gamma} = 1473$ K and increasing specific volume from v_D to $v_{D'} = v_0(T_{D'}/T_0) \approx 4.912\, v_0$, giving $H_{D'} = c_p T_{D'} = 14,155$ cal/mol. The efficiency of PDE cycle $OO'DD'O$:

$$\chi_{\text{Detonation}} = \frac{H_0 - H_{D'}}{q} = 0.452 \tag{20}$$

Using the same procedure, one can estimate cycle efficiencies for various values of precompression ratio π. Fig. 69 shows the calculated dependencies of $\chi_{p=\text{const}}$ (Brayton cycle), $\chi_{V=\text{const}}$ (Humphrey cycle), and $\chi_{\text{Detonation}}$ (PDE cycle) depending on the compression ratio π [235,236].

Precompression of the reactive mixture increases the efficiency of all cycles under consideration, however,

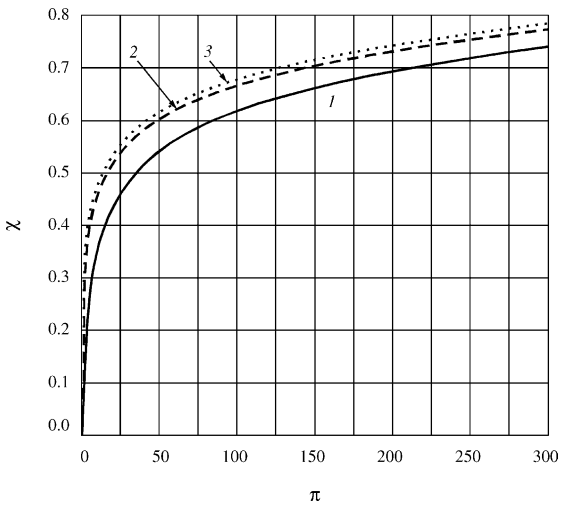

Fig. 69. Predicted thermodynamic efficiency χ of Brayton (1), Humphry (2), and PDE (3) cycles depending on the precompression ratio π [235,236].

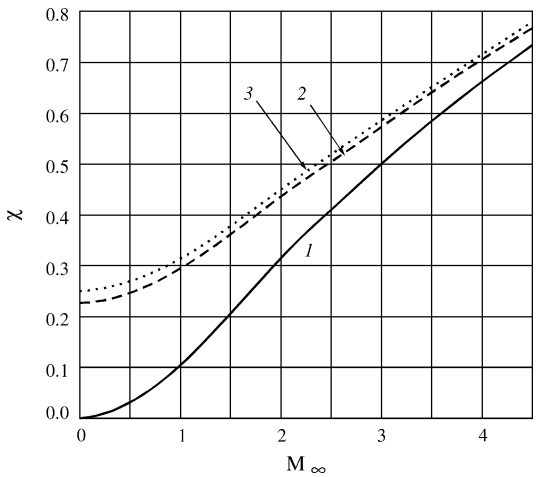

Fig. 70. Predicted dependence of ideal thermal efficiency χ of Brayton (1), Humphrey (2), and PDE (3) cycles on the vehicle flight Mach number M_∞ [235,236].

leaving valid the relationships (12) and (17). With increasing the compression ratio π the difference between thermal efficiencies of the cycles decreases.

Mixture precompression can be attained by using a mechanical compressor and/or by decelerating the flow in a combustor (ram compression). In the latter case, one can readily obtain the relationships between the vehicle flight Mach number M_∞ and ram compression ratio $\pi = \pi_R$, if ideal isentropic compression (without shocks) to stagnation parameters is assumed:

$$\pi_R = \left(1 + \frac{\gamma_0 - 1}{2} M_\infty^2\right)^{\gamma_0/(\gamma_0 - 1)}$$
$$M_\infty = \sqrt{\frac{2}{\gamma_0 - 1}\left(\pi_R^{(\gamma_0 - 1)/\gamma_0} - 1\right)} \quad (21)$$

Fig. 70 shows the dependence of thermal efficiencies of Brayton, Humphrey, and PDE cycles on the vehicle flight Mach number, M_∞ [235,236]. Clearly, in terms of the gain in ideal thermal efficiency, the PDE cycle in an engine with purely ram compression is favorable at flight Mach numbers $0 < M_\infty < 3$, being most favorable at subsonic and transonic flight speeds. At higher M_∞, the difference in ideal thermal efficiencies of the cycles becomes small. The results of Fig. 68 with $\pi = \pi_R = 7.82$ correspond to $M_\infty = 2.0$.

Relatively low absolute thermal efficiencies at transonic flight speeds can be increased by using combined ram and mechanical isentropic compression. In this case, the net compression ratio π can be represented as the product of ram compression ratio $\pi_R = p_R/p_0$ and mechanical compression ratio $\pi_m = p_O/p_R$, i.e. $\pi = \pi_R \pi_m$. Fig. 71 shows the dependencies of ideal thermal efficiencies on π_m at flight Mach numbers 0.8, 2.0, and 3 for PDE and Brayton cycles [235].

Two important observations follow from Fig. 71. First, to attain a thermal efficiency of a PDE with solely ram compression (PDE $\pi_m = 1$), the Brayton-cycle vehicle should be additionally equipped with a mechanical compressor. For example, at flight Mach numbers of $M_\infty = 0.8$, 2.0, and 3.0, the corresponding values of π_m for the compressor are 4.7, 2.9, and 2.3. At compression ratios π_m higher than these values, the Bryton cycle is thermally more efficient than the PDE cycle with solely ram compression. Second, it appears that similar thermal efficiency (e.g. $\chi = 0.45$) is attained in the PDE-based vehicle with $\pi_m = 5.0$ and in the Brayton-cycle vehicle

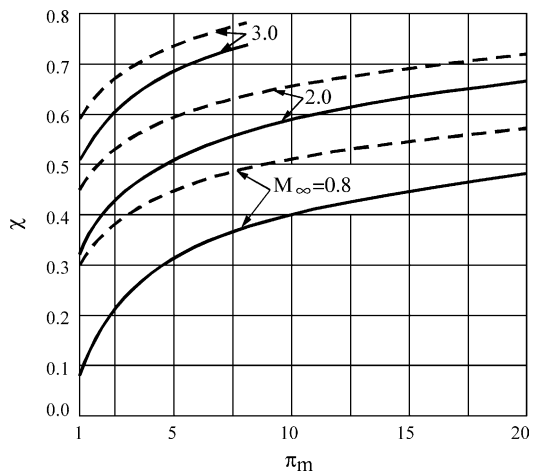

Fig. 71. Predicted dependencies of ideal thermal efficiency χ on mechanical compression ratio π_m at flight Mach number $M_\infty = 0.8$, 2.0, and 3.0 for PDE (dashed curves) and Brayton (solid curves) cycles [235].

with $\pi_m = 15.0$ at flight Mach number of $M_\infty = 0.8$. This means that for attaining the specified thermal efficiency the PDE-based vehicle should be equipped with only low-pressure compressor whereas the Brayton-cycle vehicle should be equipped with both low- and high-pressure mechanical compressors. These findings indicate a great potential advantage of PDE-based propulsion.

It is also instructive to represent thermal efficiencies of the cycles in terms of the temperature ratio $\vartheta = T_{O'}/T_0$ attained due to isentropic mechanical and/or ram compression. The parameter ϑ relates to compression ratio π and flight Mach number M_∞ through the relationships:

$$\vartheta = \pi^{(\gamma_0 - 1/\gamma_0)}, \qquad M_\infty = \sqrt{\frac{2}{\gamma_0 - 1}(\vartheta - 1)} \tag{22}$$

Fig. 72 shows the dependencies of cycle thermal efficiencies in terms of ϑ.

There exists one important implication regarding the detonative combustion cycle that was discussed by Zel'dovich [234]. If one considers detonation products at thermodynamic state D (Fig. 67), their total energy comprising the thermal and kinetic energy exceeds considerably the initial energy of the reactive mixture. As a matter of fact, thermal energy of detonation products at state D is equal to

$$H_D = c_{p0}T_0 + c_p(T_D - T_0) \approx 2100 + 11.1(2977 - 300)$$

$$= 31,815 \text{ cal/mol}$$

that is already 32% higher than $H_0 = 24,100$ cal/mol. In addition, detonation products at state D possess the kinetic energy

$$K_D = \frac{u_D^2}{2} = \frac{1}{2}c_0^2\left[M_{CJ} - \frac{1 + \frac{\gamma}{\gamma+1}(M_{CJ}^2 - 1)}{M_{CJ}}\right]^2 \approx 2.98c_0^2$$

$$\approx 2153 \text{ cal/mol}$$

where $c_0^2 = (\gamma - 1)c_pT_0$ is the squared sound velocity in the reactive mixture at state O. As a result, the total energy of detonation products at state D is the sum

$$H_D + K_D \approx 31,815 + 2153 = 33,968 \text{ cal/mol}$$

that is 41% higher than H_0. The excessive energy at state D is a result of energy redistribution in the detonating charge. The matter detonated previously decelerates and expands thus providing the excessive energy in the newly detonated matter. This means that a part of total energy at state D cannot be used for producing work as it is consumed for continuous 'reproduction' of state D. The calculations relevant to Fig. 67 indicate that only energy equal to $0.251q$ can be ideally transformed into useful work, while $0.749q$ is exhausted and used for the work against external pressure, and the rest $0.41q$ is continuously spent for reproduction of state D.

Calculations of comparative cycle efficiencies with realistic thermodynamics gives qualitatively similar results to those discussed above. Table 10 presents the results of thermodynamic calculations for the stoichiometric ethylene–air mixture at several values of compression ratio $\pi = 1$, 5, 10, 15, and 20. Thermal efficiency of Brayton, Humphrey, and PDE cycles was calculated by using Eq. (13). Two series of calculations are presented in Table 10.

In both series, the heat effect of reaction was taken constant for all the cycles and equal to $q = 22,000$ cal/mol, i.e. similar to the idealized calculations discussed above. In the first series, combustion products were assumed in equilibrium during expansion to pressure p_0, while in the second series, combustion products composition was frozen during the entire expansion process. For the sake of comparison, thermal efficiencies obtained above are also presented in Table 10. It follows from Table 10 that the predicted values of χ are, in general, in a satisfactory agreement with each other. Equilibrium assumption always results in somewhat higher χ values, other conditions being equal. The validity of Eq. (17) is noteworthy.

As detonative combustion shows the values of temperature close to or exceeding 3000 K one could expect a high degree of dissociation in detonation products. This is substantiated by thermodynamic calculations. To take into account this fact, another series of calculations has been conducted. In this series, heat effect of combustion q was calculated as suggested in Ref. [237], i.e. was determined

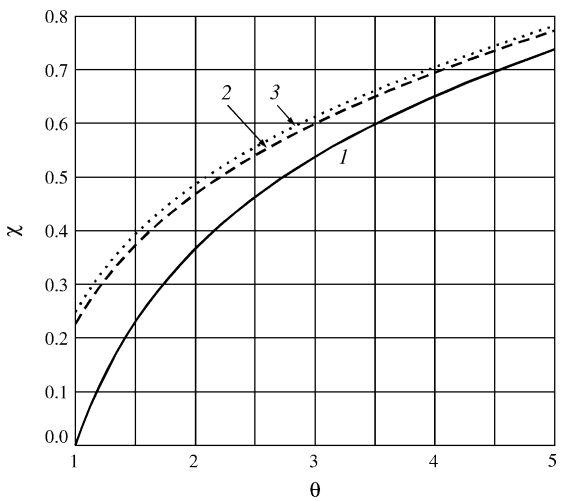

Fig. 72. Predicted dependencies of Brayton (1) Humphry (2), and PDE (3) cycle thermal efficiency χ on temperature ratio ϑ [235].

Table 10
Ideal efficiencies of Brayton, Humphrey and PDE cycles as functions of mixture precompression π [235]

π	Parameter	Brayton	Humphrey	PDE
1	χ (expansion with equil. comp.)	0	0.2544	0.2811
	χ (expansion with frozen comp.)	0	0.2272	0.2332
	χ (const specific heats)	0	0.2274	0.2510
	T_{cp} (K)	2371	2736	2926
	P_{cp} (atm)	1.0	9.3	18.3
	W_{cp} (kg/kmol)	28.387	28.135	27.925
	W_e (kg/kmol)	28.387	28.733	28.751
	S_{cp} (kJ/K/kg)	9.664	9.290	9.246
	$(c_p/c_v)_{eq}$	1.171	1.171	1.172
	$(c_p/c_v)_{fr}$	1.252	1.252	1.253
	$(c_p/c_v)_{ch}$	1.217	1.217	1.217
5	χ (expansion with equil. comp.)	0.2694	0.4294	0.4442
	χ (expansion with frozen comp.)	0.2584	0.3764	0.3704
	χ (const specific heats)	0.2543	0.3925	0.4111
	T_{cp} (K)	2498	2858	3064
	P_{cp} (atm)	5.0	31.6	60.8
	W_{cp} (kg/kmol)	28.407	28.166	27.967
	W_e (kg/kmol)	28.743	28.793	28.795
	S_{cp} (kJ/K/kg)	9.265	8.989	8.949
	$(c_p/c_v)_{eq}$	1.178	1.177	1.178
	$(c_p/c_v)_{fr}$	1.250	1.250	1.251
	$(c_p/c_v)_{ch}$	1.217	1.217	1.217
10	χ (expansion with equil. comp.)	0.3646	0.4847	0.5024
	χ (expansion with frozen comp.)	0.3447	0.4286	0.4190
	χ (const specific heats)	0.3474	0.4578	0.4745
	T_{cp} (K)	2565	2922	3135
	P_{cp} (atm)	10.0	53.9	103.1
	W_{cp} (kg/kmol)	28.405	28.170	27.975
	W_e (kg/kmol)	28.783	28.797	28.797
	S_{cp} (kJ/K/kg)	9.102	8.864	8.825
	$(c_p/c_v)_{eq}$	1.180	1.179	1.180
	$(c_p/c_v)_{fr}$	1.250	1.250	1.251
	$(c_p/c_v)_{ch}$	1.217	1.217	1.217
15	χ (expansion with equil. comp.)	0.4137	0.5170	0.5336
	χ (expansion with frozen comp.)	0.3891	0.4557	0.4438
	χ (const specific heats)	0.3979	0.4946	0.5103
	T_{cp} (K)	2609	2963	3181
	P_{cp} (atm)	15.0	74.0	140.9
	W_{cp} (kg/kmol)	28.401	28.169	27.976
	W_e (kg/kmol)	28.792	28.798	28.798
	S_{cp} (kJ/K/kg)	9.010	8.792	8.754
	$(c_p/c_v)_{eq}$	1.181	1.181	1.182
	$(c_p/c_v)_{fr}$	1.249	1.249	1.250
	$(c_p/c_v)_{ch}$	1.217	1.217	1.217
20	χ (expansion with equil. comp.)	0.4449	0.5385	0.5542
	χ (expansion with frozen comp.)	0.4174	0.4740	0.4605
	χ (const specific heats)	0.4330	0.5208	0.5358
	T_{cp} (K)	2642	2995	3215
	P_{cp} (atm)	20.0	92.8	176.2
	W_{cp} (kg/kmol)	28.396	28.167	27.975
	W_e (kg/kmol)	28.795	28.798	28.798

(*continued on next page*)

Table 10 (*continued*)

π	Parameter	Brayton	Humphrey	PDE
	S_{cp} (kJ/K/kg)	8.946	8.741	8.704
	$(c_p/c_v)_{eq}$	1.182	1.182	1.183
	$(c_p/c_v)_{fr}$	1.249	1.249	1.250
	$(c_p/c_v)_{ch}$	1.217	1.217	1.217

Remark: W_{cp} and W_e are the molecular masses in the combustion products before and after expansion, index cp denotes properties of combustion products before expansion, indices eq, fr, and ch denote parameters obtained in equilibrium, frozen, and constant-specific-heat approximations.

from an energy balance for the overall reaction process:

$$C_2H_4 + 3O_2 + 11.28N_2 = \nu_{CO_2}CO_2 + \nu_{H_2O}H_2O + \nu_{N_2}N_2 + \nu_{H_2}H_2 + \nu_{O_2}O_2 + \nu_H H + \nu_O O + \nu_{OH}OH + \cdots \quad (23)$$

where ν_i is the stoichiometric coefficient of the ith species in equilibrium combustion products. The heat effect is obtained from the relationship

$$q = (h^0_{298})_{fr} - (h^0_{298})_{cp} \quad (24)$$

where $(h^0_{298})_{fr}$ is the sum of standard enthalpies of formation of reactants and $(h^0_{298})_{cp}$ is the sum of standard enthalpies of formation of products in the overall reaction of Eq. (23). Note that this procedure does not take into account recombination processes during expansion of combustion products. The results of calculations of q and the corresponding thermal efficiencies are shown in Table 11. As is seen from Table 11, the heat effect q in PDE cycle is about 12% less than in Brayton cycle. The value of q obtained this way is smaller by about 16% than the value of $q = 22,000$ cal/mol obtained from ethylene combustion heat.

Similar analyses were recently performed in Refs. [238,239] for propane–air and hydrogen–air mixtures of the equivalence ratio from 0.6 to 1.1. It has been shown in Ref. [238] that high temperature of products during detonative combustion leads to dissociation losses that are about 10% higher than during constant-pressure combustion.

2.5. Implementation of the detonation cycle

Two principal schemes of practical implementation of detonation cycle are possible. One applies a concept of fuel combustion in a stabilized detonation front [240]. This concept implies that the approach stream velocity is very high (about the CJ detonation velocity 1600–1800 m/s). The other applies a concept of fuel combustion in repeatedly generated detonation waves traversing the combustion chamber [1–19,241]. In this concept, there are no principal limitations on the approach stream velocity. The thermal efficiency of the ramjet cycle with such a repeated (pulsed) process will evidently depend on the frequency of generation of detonation waves. This device, referred to as a PDE, is the primary focus of this paper.

The PDE comprises:

- the air intake (AI) (diffuser) of cross-section F_1 ensuring continuous inflow (at approach stream velocity u_1) and compression of air from the ambient atmospheric pressure p_1 to a certain stagnation pressure p_2;
- the receiver, where the air passing from the AI is in a stagnant state at pressure p_2;
- a valve-distribution system, which forces air to pass from the receiver to DC(s) in a given time sequence;
- DC of cross-section F_{DC} and length L_{DC}, which consists of one tube or a bundle of identical cylindrical tubes with nozzles at the exit;

Table 11
Ideal efficiencies of Brayton, Humphrey, and PDE cycles as functions of reactive mixture precompression and applying sensitive heat effects of combustion [235]

Pressure (atm)	χ			q (cal/mol)		
	Brayton	Humphrey	PDE	Brayton	Humphrey	PDE
1	0	0.2879	0.3152	18,408	16,968	15,794
5	0.3034	0.4737	0.4957	18,495	17,108	15,971
10	0.4051	0.5394	0.5602	18,467	17,110	15,989
15	0.4580	0.5740	0.5939	18,437	17,096	15,983
20	0.4922	0.5978	0.6167	18,407	17,075	15,963

Remark: Composition of combustion products during expansion is assumed frozen.

- supersonic nozzles with the minimum and exit cross-section areas $F_{\min}$ and F_4, respectively;
- fuel tanks and systems of fuel injection into the DC under a program timed with air injection;
- systems for detonation initiation in the DC.

In the following, indices 1, 2, DC, and 4 correspond to flow parameters at the AI, in receiver, in DC, and at the exit of nozzle, correspondingly.

The operation cycle of a PDE includes the following phases:

1. injection of fuel into the DC and mixing of fuel with incoming air;
2. detonation initiation;
3. mixture burnout in a propagating detonation wave; and
4. expansion of detonation products through a supersonic nozzle.

Subsequent injection of fuel into the DC and mixing of fuel with incoming air starts the new operation cycle. To prevent detonations or shocks from moving outward through the intake, to provide a sufficient time for mixing of fuel with air, and to ensure a controlled inward flow rate of fresh air, a provision is usually made for a mechanical valve. For increasing the PDE performance, preliminary pressurization of air can also be used. To reduce thrust pulsations and noise multitube configurations of PDE are considered that imply the use of phase shift between processes in different tubes.

To get an idea of thrust characteristics of such an engine, we reproduce here the analysis performed by Mitrofanov and Zhdan [242]. Let us consider the ideal process similar to that used in Section 2.4. Air and detonation products are considered as ideal gases with constant ratio of specific heats, γ. Air compression in the AI (without or with compressor), air motion in the DC and expansion of explosion products are assumed isentropic (i.e. without shocks, viscous effects and heat exchange with the walls). The explosion of the FAM is simulated by instantaneous release of energy q per unit mass of air in the DC.

Consider quasi-steady-state, 1D formulation of the problem. Compression of gas in the inlet results in transition from state 1 (approach stream state) to state 2 (receiver) with

$$p_2 = \pi p_1, \qquad \rho_2 = \pi^{1/\gamma}\rho_1, \qquad c_2^2 = \pi^{1-1/\gamma}c_1^2$$

where c is the sound speed.

The flow in the DC is divided into three stages: Stage I—detonation initiation and traversing the DC (valve closed), Stage II—quasi-stationary exhaust of detonation products through the nozzle (valve closed), and Stage III—stationary exhaust of remained detonation products and filling the DC with air (valve open).

Detonation initiation is assumed instantaneous, so Stage I corresponds to the period of detonation traversing the DC. To denote gas parameters at completion of Stage I, index 3 is used. Stage I is approximately modeled as energy release at $\rho_3 = \rho_2$ in DC and pressure rise to the level of p_3 :

$$\frac{p_3}{p_2} = \frac{c_3^2}{c_2^2} = 1 + \gamma(\gamma - 1)\frac{q}{c_2^2}$$

As Stage I is very short as compared to Stages II and III discussed below, the duration of Stage I is assumed zero, i.e. $\Delta t_{\mathrm{I}} = 0$.

Stage II corresponds to quasi-steady-state isentropic gas outflow through the nozzle with chamber pressure $p(t)$ gradually decreasing in time from p_3 to p_2 :

$$\frac{p(t)}{p_3} = \left(\frac{\rho(t)}{\rho_3}\right)^{\gamma} = \left[\frac{c(t)}{c_3}\right]^{2\gamma/(\gamma-1)}$$

so that at time $t = t_{\mathrm{II}}$ (time of Stage II termination)

$$p(t_{\mathrm{II}}) = p_2, \qquad \rho(t_{\mathrm{II}}) = \rho_2(p_2/p_3)^{1/\gamma},$$

$$c(t_{\mathrm{II}}) = c_3(p_2/p_3)^{(\gamma-1)/2\gamma}$$

To obtain the explicit dependencies of pressure, density, and sound speed on time, assume that during Stage II gas outflow velocity in the critical cross-section $F_{\min}$ of the nozzle is critical, i.e. the mass flow is equal to

$$\dot{m}_{\mathrm{cr}}(t) = \rho_{\mathrm{cr}}u_{\mathrm{cr}}F_{\min} = -\left(\frac{2}{\gamma+1}\right)^{(\gamma+1)/2(\gamma-1)}\rho(t)c(t)F_{\min}$$

This results in the differential equation for gas density in the DC:

$$F_{\mathrm{DC}}L_{\mathrm{DC}}\frac{\partial}{\partial t}\left(\frac{\rho(t)}{\rho_3}\right) = -\left(\frac{2}{\gamma+1}\right)^{(\gamma+1)/2(\gamma-1)}\rho(t)c(t)F_{\min}$$

$$= -\left(\frac{2}{\gamma+1}\right)^{(\gamma+1)/2(\gamma-1)}F_{\min}c_3\left(\frac{\rho(t)}{\rho_3}\right)^{(\gamma+1)/2}$$

with the initial condition $\rho(0) = \rho_3$. Solution of this equation is given by

$$\rho(t) = \rho_3(1 + a_{\mathrm{m}}t)^{-2/(\gamma-1)}$$

where

$$a_{\mathrm{m}} = \frac{\gamma-1}{2}\left(\frac{2}{\gamma+1}\right)^{0.5(\gamma+1)/(\gamma-1)}\frac{c_3F_{\min}}{L_{\mathrm{DC}}F_{\mathrm{DC}}}$$

Correspondingly, pressure and sound speed time histories in the combustion chamber at Stage II are given by

$$p(t) = p_3(1 + a_{\mathrm{m}}t)^{-2\gamma/(\gamma-1)}$$

$$c(t) = c_3(1 + a_{\mathrm{m}}t)^{-1}$$

Clearly, the duration of Stage II, $\Delta t_{\mathrm{II}} = t_{\mathrm{II}} - t_{\mathrm{I}}$, is equal to

$$\Delta t_{\mathrm{II}} = \frac{1}{a_{\mathrm{m}}}\left[\left(\frac{p_3}{p_2}\right)^{(\gamma-1)/2\gamma} - 1\right]$$

For obtaining gas parameters at the nozzle exit use the requirement:

$$\frac{p(t)}{p_4(t)} = \frac{p(t_{\mathrm{II}})}{p_4(t_{\mathrm{II}})} = \frac{p_2}{p_1} = \pi \tag{25}$$

which follows from the requirement of constant-speed flight. Then, the gas velocity at the nozzle exit at Stage II, $u_{4,\mathrm{II}}$ (exit Mach number $M_{4,\mathrm{II}}$), which is governed by the energy conservation law

$$u_{4,\mathrm{II}}^2(t) + \frac{2c_4^2(t)}{\gamma - 1} = \frac{2c^2(t)}{\gamma - 1}$$

can be obtained from the following relationship

$$M_{4,\mathrm{II}}^2(t) = \left(\frac{u_{4,\mathrm{II}}(t)}{c_4(t)}\right)^2 = \frac{2}{\gamma - 1}\left[\left(\frac{c(t)}{c_4(t)}\right)^2 - 1\right]$$

$$= \frac{2}{\gamma - 1}(\pi^{(\gamma-1)/\gamma} - 1) = \mathrm{const} \tag{26}$$

At time $t = t_{\mathrm{II}}$, the air valve instantaneously opens. Stage II is followed by Stage III, when the remaining combustion products are pushed out of the chamber by the next portion of air and FAM at constant pressure p_2 and constant velocity of motion of the gases inside the chamber $u_{\mathrm{DC}} \ll c_{\mathrm{DC}}$, where c_{DC} is the characteristic sound speed in the DC at Stage III. Mass flow rate of exhaust is given by

$$\dot{m}_{\mathrm{III}} = \left(\frac{2}{\gamma + 1}\right)^{(\gamma+1)/2(\gamma-1)} \rho(t_{\mathrm{II}}) c(t_{\mathrm{II}}) F_{\min}$$

Therefore, duration of Stage III, $\Delta t_{\mathrm{III}} = t_{\mathrm{III}} - t_{\mathrm{II}}$, is estimated as

$$\Delta t_{\mathrm{III}} = \frac{F_{\mathrm{DC}} L_{\mathrm{DC}} \rho(t_{\mathrm{II}})}{\dot{m}_{\mathrm{III}}} = \frac{\gamma - 1}{2a_{\mathrm{m}}}\left(\frac{p_3}{p_2}\right)^{(\gamma-1)/2\gamma}$$

If the cross-section areas $F_{\min}$ and F_4 are selected such that the nozzle-exit pressure at Stage III is equal to p_1 (i.e. $p_4 = p_1 = \mathrm{const}$) then flow parameters at the nozzle exit are governed by the following relationships:

$$\frac{\rho_4}{\rho_3} = \left(\frac{p_1}{p_3}\right)^{1/\gamma}, \qquad \left(\frac{c_4}{c_3}\right)^2 = \left(\frac{p_1}{p_3}\right)^{(\gamma-1)/2\gamma}$$

At Stage III, the gas velocity at the nozzle exit, $u_{4,\mathrm{III}}$, is governed by the energy conservation law

$$u_{4,\mathrm{III}}^2 + \frac{2c_4^2}{\gamma - 1} = \frac{2c_{\mathrm{DC}}^2}{\gamma - 1} + u_{\mathrm{DC}}^2(t)$$

Due to requirement (25), one obtains:

$$M_{4,\mathrm{III}}^2 = \left(\frac{u_{4,\mathrm{III}}}{c_4}\right)^2 = \frac{2}{\gamma - 1}(\pi^{(\gamma-1)/\gamma} - 1) + \frac{u_{\mathrm{DC}}^2}{c_4^2}$$

After completion of Stage III, the new cycle begins. Thus, the model implies that cycle duration, t_{c}, is equal to

$$t_{\mathrm{c}} = \Delta t_{\mathrm{I}} + \Delta t_{\mathrm{II}} + \Delta t_{\mathrm{III}} \approx \Delta t_{\mathrm{II}} + \Delta t_{\mathrm{III}}$$

Therefore, the operational frequency of the PDE is equal to

$$f = t_{\mathrm{c}}^{-1} \approx (\Delta t_{\mathrm{II}} + \Delta t_{\mathrm{III}})^{-1}$$

Geometrical parameters $F_{\min}, F_4$, and F_{DC} are interrelated by the following formulae:

$$\frac{F_4}{F_{\min}} = \left(\frac{2}{\gamma + 1}\right)^{(\gamma+1)/2(\gamma-1)} \frac{\pi^{(\gamma+1)/2\gamma}}{M_4}$$

$$\frac{F_{\min}}{F_{\mathrm{DC}}} = \left(\frac{2}{\gamma + 1}\right)^{(\gamma+1)/2(\gamma-1)} \left(\frac{c_3}{c_2}\right)^{(\gamma-1)/\gamma} \frac{u_{\mathrm{DC}}}{c_3}$$

$$= \left(\frac{2}{\gamma + 1}\right)^{(\gamma+1)/2(\gamma-1)} \left(\frac{c_3}{c_2}\right)^{1/\gamma} \pi^{-(\gamma-1)/(2\gamma)} \frac{u_{\mathrm{DC}}}{c_1}$$

The latter formula comes from the relationship $L_{\mathrm{DC}} = u_{\mathrm{DC}} \Delta t_{\mathrm{III}}$. If the PDE has a mechanical air compressor, the additional relationship is used to relate flight Mach number M_∞ and the total compression ratio π:

$$\frac{c_1^2 M_\infty^2}{2} + \frac{c_1^2}{\gamma - 1} + \frac{N}{\dot{m}_{\mathrm{ox}}} = \frac{\gamma + 1}{2(\gamma - 1)} c_2^2$$

where $\dot{m}_{\mathrm{ox}}$ is the mass flow of air in the PDE and N is the compressor power.

Thus, the model includes the following governing parameters: γ, c_1, q, π, and u_{DC}. In the calculations [242], the following values of governing parameters were used: $\gamma = 1.4, c_1 = 300$ m/s, $q/c_1^2 = 18.75$, $u_{\mathrm{DC}} = c_1/3$. Fig. 73a shows the predicted pressure variation in the DC of the ideal PDE at $\pi = 10$. Two-dimensional transient simulation of processes in the ideal PDE [242] with similar parameters, based on inviscid flow equations, results in a very similar $p(t)$ curve (see Fig. 73b), indicating that the model described above represents satisfactorily the ideal PDE operation.

It is instructive to estimate the performance of such a PDE. By definition, thrust of the engine, P, and local instantaneous air mass flow through the engine, $\dot{m}_{\mathrm{ox}}$, are given by the formulae:

$$P(t) = F_4\left[\rho_4(t)u_4^2(t) + p_4(t) - p_1\right] - \rho_1 u_1^2 F_1 \ (\mathrm{N})$$

$$\dot{m}_{\mathrm{ox}}(t) = \rho(t)u(t)F \ (\mathrm{kg/s})$$

where F is the local cross-section area of the engine duct.

The thrust and air mass flow averaged over one cycle are given by

$$\tilde{P} = \frac{1}{t_{\mathrm{c}}}\int_0^{t_{\mathrm{c}}} P(t)\mathrm{d}t \approx \frac{1}{t_{\mathrm{c}}}\left(\int_0^{t_{\mathrm{II}}} P(t)\mathrm{d}t + \int_{t_{\mathrm{II}}}^{t_{\mathrm{III}}} P(t)\mathrm{d}t\right)$$

$$= \tilde{P}_{\mathrm{II}} + \tilde{P}_{\mathrm{III}} \ (\mathrm{N})$$

$$\tilde{\dot{m}}_{\mathrm{ox}} = \frac{1}{t_{\mathrm{c}}}\int_0^{t_{\mathrm{c}}} \dot{m}_{\mathrm{ox}}(t)\mathrm{d}t = \dot{m}_{\mathrm{ox},1} = \rho_1 u_1 F_1 \ (\mathrm{kg/s})$$

where $\tilde{P}_{\mathrm{II}}$ and $\tilde{P}_{\mathrm{III}}$ are the contributions of Stages II and III to the cycle-mean thrust $\tilde{P}$. The specific thrust is defined as

$$\tilde{I} = \frac{\tilde{P}}{\tilde{\dot{m}}_{\mathrm{ox}}} \ (\mathrm{m/s})$$

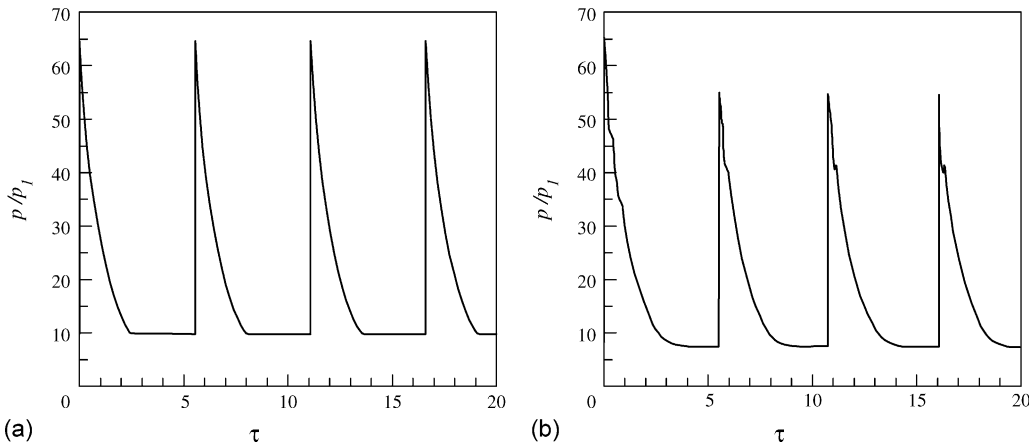

Fig. 73. Predicted dependencies of the dimensionless pressure in the DC on dimensionless time $\tau = t\sqrt{p_1/\rho_1}/L_{DC}$ at $\pi = 10$: (a) analytical model; and (b) 2D calculations [242].

Let us determine the contributions $\tilde{P}_{II}$ and $\tilde{P}_{III}$. Explicitly,

$$\tilde{P}_{II} = \frac{1}{t_c}\int_0^{t_{II}} F_4\rho_4(t)u_4(t)\left[u_4(t) + \frac{p_4(t)}{\rho_4(t)u_4(t)}\right]dt - \frac{1}{t_c}\int_0^{t_{II}} (p_1F_4 + \dot{m}_{ox,1}u_1)dt = \tilde{P}_{II}^{+} - \tilde{P}_{II}^{-}$$

and

$$\tilde{P}_{III} = \frac{1}{t_c}\int_{t_{II}}^{t_{III}} F_4\rho_4(t)u_4^2(t)dt - \frac{1}{t_c}\int_{t_{II}}^{t_{III}} \dot{m}_{ox,1}u_1 dt = \tilde{P}_{III}^{+} - \tilde{P}_{III}^{-}$$

where $\tilde{P}_{II}^{+}$,$\tilde{P}_{II}^{-}$,$\tilde{P}_{III}^{+}$, and $\tilde{P}_{III}^{-}$ denote the corresponding integrals in the above equations. Taking into account Eq. (26), contribution $\tilde{P}_{II}^{+}$ is given by

$$\tilde{P}_{II}^{+} = \frac{1}{t_c}\left(M_4 + \frac{1}{\gamma M_4}\right)\int_0^{t_{II}} \dot{m}_{ox}(t)c_4(t)dt = \frac{2}{\gamma+1}\frac{1}{t_c}\left(M_4 + \frac{1}{\gamma M_4}\right)\frac{\rho_3 c_3 L_{DC}F_{DC}}{\pi^{(\gamma-1)/2\gamma}}\left[1 - \left(\frac{p_2}{p_3}\right)^{(\gamma+1)/2\gamma}\right]$$

Contribution $\tilde{P}_{II}^{-}$:

$$\tilde{P}_{II}^{-} = \frac{1}{t_c}\int_0^{t_{II}} (p_1F_4 + \dot{m}_{ox,1}u_1)dt = (p_1F_4 + \dot{m}_{ox,1}u_1)\frac{t_{II}}{t_c}$$

Contribution $\tilde{P}_{III}^{+}$:

$$\tilde{P}_{III}^{+} = \frac{M_4}{t_c}\int_{t_{II}}^{t_{III}} \dot{m}_{ox}(t)c_4(t)dt = M_4\dot{m}_{ox}(t_{II})c_4(t_{II})\frac{t_{III} - t_{II}}{t_c} = M_4c_4(t_{II})\frac{\rho_3 L_{DC}F_{DC}}{t_c}\left(\frac{p_2}{p_3}\right)^{1/\gamma}$$

Contribution $\tilde{P}_{III}^{-}$:

$$\tilde{P}_{III}^{-} = \frac{1}{t_c}\int_{t_{II}}^{t_{III}} \dot{m}_{ox,1}u_1\,dt = \dot{m}_{ox,1}u_1\frac{t_{III} - t_{II}}{t_c}$$

Using the relationships

$$\frac{F_4}{F_{min}} = \left(\frac{2}{\gamma+1}\right)^{(\gamma+1)/2(\gamma-1)}\frac{\pi^{(\gamma+1)/2\gamma}}{M_4}$$

and

$$\tilde{m}_{ox}t_c = \dot{m}_{ox,1}t_c = \rho_2 L_{DC}F_{DC}$$

one obtains the following formula for the dimensionless mean specific thrust (thrust of the unit mass of air passing through the engine):

$$\frac{\tilde{I}}{c_1} = \frac{2}{\gamma+1}\left(M_{4,II} + \frac{1}{\gamma M_{4,II}}\right)\frac{c_3}{c_2}\left[1 - \left(\frac{c_2}{c_3}\right)^{1+1/\gamma}\right] - \left(\frac{c_2}{c_3}\right)^{1/\gamma}\frac{1}{\gamma M_{4,II}}\frac{\Delta t_{II}}{\Delta t_{III}} + M_{4,III}\left(\frac{c_2}{c_3}\right)^{1/\gamma} - M_1$$

If one takes into account that $M_4 = M_{4,II} \approx M_{4,III}$, the last equation simplifies:

$$\frac{\tilde{I}}{c_1} = \frac{2}{\gamma+1}\left(M_4 + \frac{1}{\gamma M_4}\right)\frac{c_3}{c_2}\left[1 - \left(\frac{c_2}{c_3}\right)^{1+1/\gamma}\right] + M_4\left(\frac{c_2}{c_3}\right)^{1/\gamma}\left(1 - \frac{\Delta t_{II}}{\gamma M_4^2\Delta t_{III}}\right) - M_1$$

Based on the value of $\tilde{I}/c_1$ one can readily obtain the cycle-averaged thrust per unit area of DC cross-section, $\tilde{P}_{ua}$:

$$\frac{\tilde{P}_{ua}}{p_1} = \frac{\tilde{P}}{F_{DC}p_1} = f\frac{c_1\rho_2 L_{DC}}{p_1}\left(\frac{\tilde{I}}{c_1}\right)$$

Table 12 presents the results of calculations for $\tilde{I}/c_1$ for the ideal PDE under consideration. The value of π was specified and varied. The flight Mach number M_∞ was varied from 0 to the value $M_\infty = M_4$ corresponding to solely ram compression of air in an ideal ramjet without a compressor. Analysis of dependencies $\tilde{I}/c_1$ for PDE at $M_\infty = M_4$ on

Table 12
Predicted mean specific thrust of ideal PDE, ramjet and turbojet (TJE) engines (the results of calculations by two-dimensional unsteady model are given in brackets) [242]

π	p_3/p_1	M_4	f (Hz)	$\tilde{I}/c_1$ at $M_\infty \ll 1$		$\tilde{I}/c_1$ at $M_\infty = M_4$	
				PDE	TJE	PDE	Ramjet
2	19.2	1.05	42 (40)	3.87 (3.68)	2.80	2.82	1.76
3	26	1.36	43 (43.5)	4.20 (4.03)	3.46	2.84	2.10
4	32.2	1.56	43.6 (44)	4.44 (4.29)	3.83	2.88	2.27
6	43.8	1.83	44.4 (46)	4.75 (4.61)	4.29	2.92	2.46
10	64.4	2.16	46 (48)	5.11 (4.98)	4.77	2.95	2.61
20	109	2.60	48 (52)	5.55 (5.48)	5.32	2.95	2.72
40	186	3.06	50 (55)	5.97 (6.03)	5.81	2.91	2.75
80	320	3.54	52 (59)	6.38 (6.67)	6.27	2.84	2.73

the compression ratio π for fixed values of q/c_1^2 (Fig. 74) demonstrates a nonmonotonous variation of the mean specific thrust with π. In the range $10 < \pi < 20$, the mean specific thrust for PDE attains maximum.

The obtained performance parameters of the PDE are compared in Table 12 and in Fig. 74 with the ramjet performance:

$$\tilde{I}/c_1 = M_4\left(\sqrt{1+(\gamma-1)\pi^{(\gamma-1)/\gamma}q/c_1^2} - 1\right)$$

calculated under similar idealizations and the same π. It was assumed that in a ramjet, combustion occurs without loss of stagnation pressure. Calculations at $0 \le M_\infty \le 3.6$ and $1 \le \pi \le 80$ show that the performance of PDE is always higher than that of a ramjet and one-spool turbojet engine. This is the most important finding of the analysis. However, with increasing the compression ratio π the advantage of PDE gradually decreases. The other important finding is that in terms of predicted values of $\tilde{I}/c_1$, the results of 2D calculations (corresponding numbers in brackets in Table 12) appear to be within a 5%-discrepancy from the results predicted by the above analytical model. The difference in predicted performance can be attributed to the unsteadiness and nonuniformity of the flow in 2D calculations. Obviously, the corresponding losses can be reduced by nozzle optimization. Such a good agreement of the predictions indicates that the analytical model is based on the adequate phenomenology both qualitatively and quantitatively.

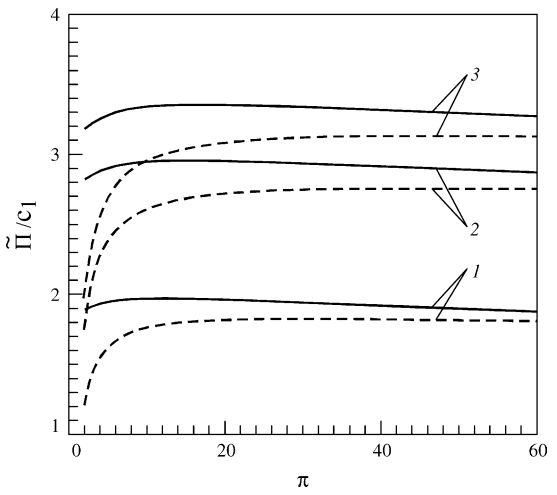

Fig. 74. Predicted dependencies of mean specific thrust $\tilde{I}$ for PDE (solid curves) and Brayton-cycle based ramjet (dashed curves) on compression ratio π at $\gamma = 1.4, c_1 = 300$ m/s, $u_{DC} = c_1/3$. 1—q/c_1^2 =11.11; 2—18.75; and 3—22.22 [242].

Performance predictions by Ma et al. [243] obtained by quasi-one-dimensional and 2D simulation of PDE show qualitatively similar results: The quasi-one-dimensional model overestimates the system performance by about 9% as compared to 2D calculations. In Ref. [243], the 2D simulation of the single-tube PDE shown in Fig. 75 has been performed.

Fig. 76 shows the predicted snapshot of pressure distribution in the PDE under study at time 0.8 ms. At this time instance, the primary shock wave resulting from the detonation wave has moved out of the nozzle and transformed to a weakened bow shock. Other common features, including the formation of an oblique shock train in

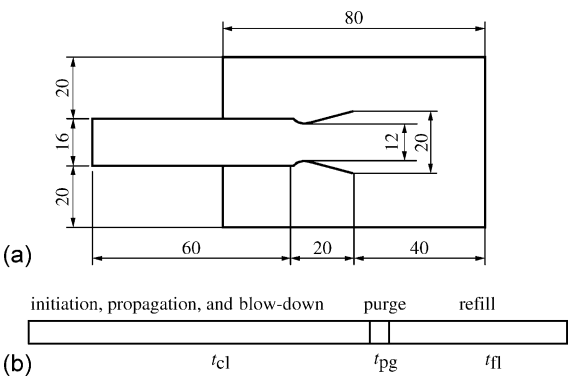

Fig. 75. (a) Two-dimensional computational domain for a single-tube PDE, and (b) operation sequence [243].

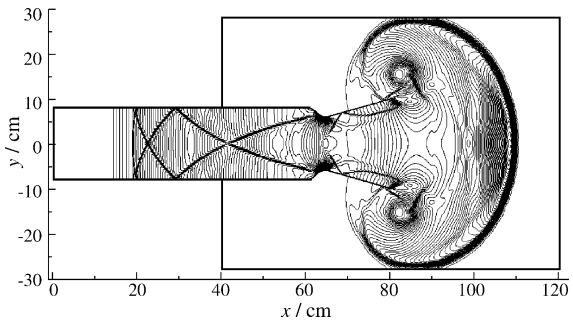

Fig. 76. Predicted snapshot of pressure field in a single-tube PDE at time 0.8 ms; $0 < p < 2.5, \Delta p = 0.025$ atm [243].

the chamber due to shock reflection, the presence of vortices at the nozzle exit due to shock diffraction, and the attachment of secondary shocks onto the vortices, are all clearly seen. In the calculations, the characteristic cycle duration time, t_c, and valve close-up time, t_{close}, were taken 3.0 and 2.1 ms, respectively. The characteristic purge time, t_{purge}, was taken 0.1 ms.

More detailed description of the PDE performance issues is given in Section 2.6.

2.6. Detonation impulse

As the analysis of the PDE performance presented in Section 2.5 is essentially based on the constant-volume rather than detonative combustion, it is instructive to further clarify some performance issues of the idealized PDE by considering a single operation cycle. Following Kailasanath et al. [244], consider an idealized PDE, that is a 20 cm long tube closed at one end and open to the atmosphere at the other. The tube is initially filled with premixed stoichiometric hydrogen–air mixture and a detonation is initiated near the closed end (head-end) of the tube. Since the thrust and other performance measures are usually calculated from the history of the pressure at the head-end of the tube, this parameter is shown in Fig. 77.

The initial high pressure depends on the method used to initiate the detonation. Here, a high-pressure and high-temperature driver is used. When the calculation is initiated, a shock moves towards the open end and expansion waves move toward the closed end. Energy release behind the shock quickly catches up with the shock forming a detonation. The transient effects of the initiation and the transition to detonation are seen to last nearly 100 μs when the pressure at the head-end settles to a value nearly steady at 5.8 atm. This 'plateau' in the pressure history lasts until about 330 μs when the expansion waves from the open end of the tube arrive at the head-end and begin to decrease the pressure. The pressure falls below the 1 atm level around 630 μs. The plateau pressure is an important factor determining the performance. Nicholls et al. [245] estimate

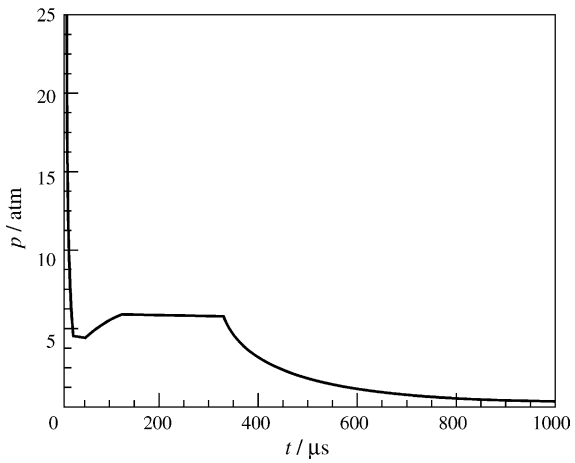

Fig. 77. Pressure history at the closed end of an idealized 20 cm long PDE, operating on stoichiometric hydrogen–air mixture [244].

the value of plateau pressure, p_p, as

$$p_p = p\left(1 - \frac{\gamma - 1}{2}\frac{D_{CJ} - u}{c}\right)^{2\gamma/(\gamma-1)}$$

where all parameters in the right-hand side are taken in the CJ plane and u is the velocity of detonation products in the frame of reference attached to the detonation front.

Since the results of Fig. 77 were obtained from 1D simulations, the difference between the head-end pressure, p, and the ambient pressure, $p_0 = 1$ atm, gives the thrust per unit area, P_{ua},

$$P_{ua}(t) = p(t) - p_0 \tag{27}$$

and the time integral of this quantity, namely,

$$I_{ua} = \int_0^t P_{ua}(t)\mathrm{d}t = \int_0^t [p(t) - p_0]\mathrm{d}t \tag{28}$$

will give the impulse (per unit area), I_{ua}, as a function of time t. This calculation has been done and the results are shown in

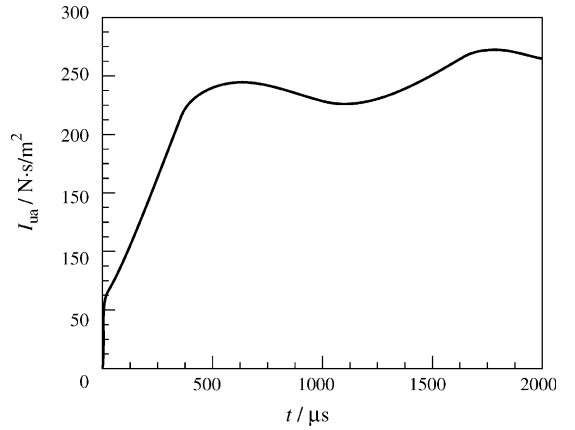

Fig. 78. Predicted time history of the impulse (per unit area of tube cross-section) for an idealized 20 cm long PDE, operating on stoichiometric hydrogen–air mixture [244].

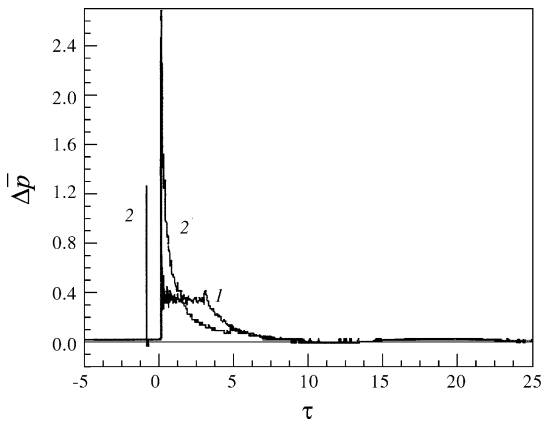

Fig. 79. Measured dimensionless overpressure $\Delta\bar{p}$ vs. dimensionless time τ for different positions of detonation initiation: 1—at the closed end, and 2—at the open end of the tube [9].

Fig. 78. During the first 10 μs, the impulse rapidly rises to a value of about 60 N s/m^2, which is the direct consequence of the high-pressure driver used to initiate detonation. The impulse reaches a value of about 90 N s/m^2 by about 100 μs and then increases nearly linearly to about 200 N s/m^2 by 330 μs. The first peak of 245 N s/m^2 is reached at 630 μs, when the head-end pressure reaches the 1 atm mark. Then, the impulse decreases because the pressure at the head-end of the tube goes below the ambient value $p_0 = 1$ atm, and attains a minimum of about 225 N s/m^2 before increasing again. It increases again because when the pressure within the tube goes below p_0, the gases outside are at higher pressure and rush into the tube creating new compression waves which increase the pressure.

The question arises whether the impulse is dependent on the location of detonation initiation. Desbordes et al. [9] studied this issue experimentally in a single-shot detonation mode. Figs. 79 and 80 show the measured time histories of

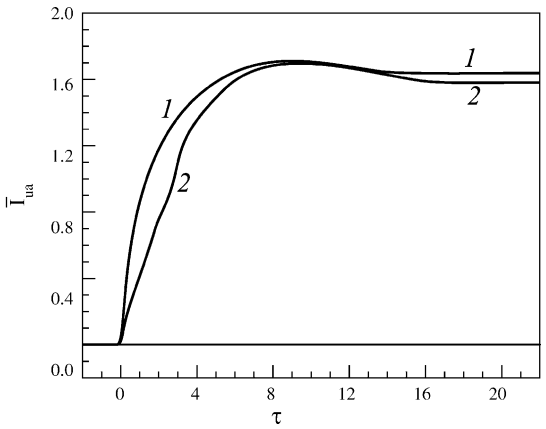

Fig. 80. Measured dimensionless impulse $\bar{I}_{ua}$ (per unit area of tube cross-section) vs. dimensionless time τ for different positions of detonation initiation: 1—at the closed end, and 2—at the open end of the tube [9].

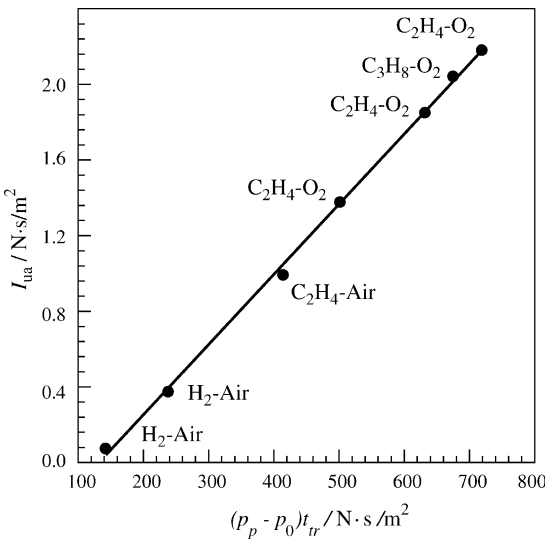

Fig. 81. The generalized dependence for the impulse per unit area I_{ua} obtained from a series of simulations of PDEs operating on different fuels [246].

dimensionless overpressure $\overline{\Delta p}$ and dimensionless impulse $\overline{I_{ua}}$ depending on the position of detonation initiation: at the closed end (curves 1) or at the open end of the tube (curves 2). As a matter of fact, it has been found that the impulse is nearly independent of the direction of detonation propagation.

In Ref. [246], 1D simulations similar to those in Figs. 77 and 78, have been carried out of PDEs in which various other fuel–oxygen and FAMs are detonated. The impulse from the various cases has been normalized using the predicted overpressure $p_p - p_0$ and the 'residence' time of the detonation, t_{tr}, (time it takes the detonation to traverse the tube $t_{tr} = L/D_{CJ}, L$ is the length of the tube). This generalized result is shown in Fig. 81. More than one data point for a mixture indicates data from simulations with different tube lengths. From this generalization one can estimate the impulse from an idealized PDE knowing the plateau pressure, p_p, and the detonation velocity, D_{CJ}. That is, the impulse per unit area is given by:

$$I_{ua} = 4.65(p_p - p_0)t_{tr} \tag{29}$$

The constant of proportionality in this expression is slightly different in various studies [247,248], suggesting some dependence on the details of the particular configuration such as initiators or tube lengths used for deriving the correlation.

Two-dimensional calculations [249] give a good fit to a straight line shown in Fig. 81 and Eq. (29). In Ref. [250], a 2D analysis for an idealized 10 cm long PDE filled with a hydrogen–oxygen mixture was performed with due regard for a detailed kinetic mechanism of fuel oxidation. The calculations were performed at different equivalence ratios: Φ =0.5, 0.75, 1.0, and 1.25. Fig. 82 shows dependencies of

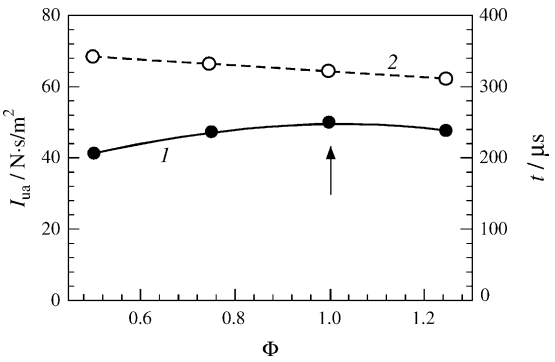

Fig. 82. Predicted impulse per unit area I_{ua} (1) and time t required for combustion and exhaust (2) as a function of equivalence ratio Φ for an idealized 10 cm long PDE operating on hydrogen–oxygen mixture [250]. The impulse has a peak (shown by arrow) for the stoichiometric mixture.

the impulse per unit area, I_{ua}, and the time t required for combustion and exhaust on the equivalence ratio Φ. The impulse has a peak (shown by arrow) for the stoichiometric mixture. In addition to thrust per unit area, P_{ua}, (see Eq. (27)), and impulse per unit area, I_{ua}, (see Eq. (28)), there exist a whole number of other performance parameters, some of which have been already used in Section 2.5. For further discussions, these parameters are defined below:

- Thrust, P (integral of the head-end overpressure over the surface, F, of the thrust wall):

$$P(t) = \int_F P_{ua}(t)\mathrm{d}F = \int_F [p(t) - p_0]\mathrm{d}F$$

measured in N;

- Cycle-averaged thrust, $\tilde{P}$

$$\tilde{P} = \frac{1}{t_c}\int_0^{t_c} P(t)\mathrm{d}t = \frac{1}{t_c}\int_F I_{ua}(t_c)\mathrm{d}F$$

measured in N, where t_c is the cycle duration;

- Cycle-averaged thrust per unit area (thrust density), $\tilde{P}_{ua}$

$$\tilde{P}_{ua} = \tilde{P}/F$$

measured in N/m^2;

- Cycle-averaged mixture mass flow, $\tilde{\dot{m}}$

$$\tilde{\dot{m}} = m/t_c$$

measured in kg/s, where m is the mass of reactive mixture injected in the PDE tube during one cycle,

- Cycle-averaged fuel mass flow, $\tilde{\dot{m}}_f$

$$\tilde{\dot{m}}_f = m_f/t_c$$

measured in kg/s, where m_f is the mass of fuel injected in the PDE tube during one cycle;

- Cycle-averaged oxidizer mass flow, $\tilde{\dot{m}}_{ox}$

$$\tilde{\dot{m}}_{ox} = m_{ox}/t_c$$

measured in kg/s, where m_{ox} is the mass of oxidizer injected in the PDE tube during one cycle.

(Once fuel mass m_f is known, parameters m and m_{ox} are related to m_f through the mixture equivalence ratio, Φ, stoichiometric fuel molar fraction, ψ_f, and molecular masses of fuel, μ_f, and oxidizer, μ_{ox}, as follows:

$$m_{ox} = m_f \frac{\mu_{ox}}{\mu_f \psi_f \Phi}$$

measured in kg;

$$m = m_f + m_{ox}$$

measured in kg);

- Cycle-averaged mixture-based specific impulse, $\tilde{I}_{sp,m}$

$$\tilde{I}_{sp,m} = \frac{\tilde{P}}{\tilde{\dot{m}}g}$$

measured in s;

- Cycle-averaged fuel-based specific impulse, $\tilde{I}_{sp,f}$,

$$\tilde{I}_{sp,f} = \frac{\tilde{P}}{\tilde{\dot{m}}_f g}$$

measured in s;

- Cycle-averaged oxidizer-based specific impulse, $\tilde{I}_{sp,m}$

$$\tilde{I}_{sp,a} = \frac{\tilde{P}}{\tilde{\dot{m}}_{ox} g}$$

measured in s.

For 1D case, these relationships are transformed as:

$$P(t) = P_{ua}(t)F = [p(t) - p_0]F, \qquad \tilde{P} = FI_{ua}(t_c)/t_c$$

$$\tilde{I}_{sp,m} = \frac{FI_{ua}(t_c)}{mg}, \qquad \tilde{I}_{sp,f} = \frac{FI_{ua}(t_c)}{m_f g}, \qquad \tilde{I}_{sp,ox} = \frac{FI_{ua}(t_c)}{m_{ox} g}$$

To calculate these parameters, various approaches have been suggested. For mixture-based $\tilde{I}_{sp,m}$ Desbordes [9] provides the following formula:

$$\tilde{I}_{sp,m} = \frac{K}{g\rho_0 D_{CJ}}\left[p_{CJ}\left(\frac{\gamma+1}{2\gamma}\right)^{2\gamma/(\gamma-1)} - p_0\right]$$

where $K \approx 5.15$ for conventional hydrocarbons and hydrogen–oxygen or air mixtures.

Fig. 83 [250] shows the predicted dependencies of cycle-averaged thrust density, $\tilde{P}_{ua}$, and fuel-based specific impulse, $\tilde{I}_{sp,f}$, on mixture equivalence ratio Φ, that were obtained in calculations presented in Fig. 82. The cycle-averaged thrust density attains a maximum for fuel-rich mixture. However, the fuel-based specific impulse increases as the equivalence ratio decreases. The predicted specific impulse for hydrogen–oxygen mixture of equivalence ratio $\Phi = 0.5$ was found to be about 6000 s.

As shown in Ref. [237] and in Section 2.4, chemical dissociation and recombination influence the estimates of cycle efficiency. Therefore, cycle efficiency could be expected to depend on the proximity of detonation products

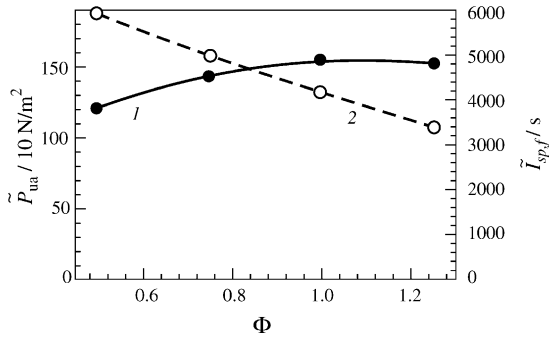

Fig. 83. Predicted cycle-averaged dependencies of thrust density, $\tilde{P}_{ua}$ (1), and fuel-based specific impulse, $\tilde{I}_{sp,f}$ (2), on the mixture equivalence ratio Φ for an idealized 10 cm long PDE operating on hydrogen–oxygen mixture [250].

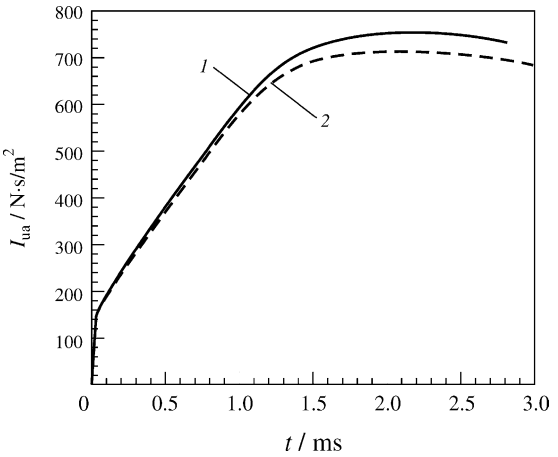

Fig. 84. Chemistry effects on the time histories of the impulse (per unit area) from simulations of a 60 cm long PDE operating on a stoichiometric hydrogen–air mixture [252]. 1—detailed reaction mechanism, 2—2-step overall reaction mechanism.

to thermodynamic equilibrium. In addition, it is important to know whether the use of overall reaction mechanisms and reduced chemical models affects the performance predictions as compared to those obtained by using detailed reaction mechanisms.

Simulations of a hydrogen–air PDE performed in Refs. [101,251] with detailed chemistry, that included the appropriate dissociation and recombination effects implicitly, showed only insignificant effect. However, those simulations were performed for short tubes (10–20 cm in length). It is possible that for longer tubes, where more time is available for the detonation products to undergo recombination reactions before being evacuated from the tube, the result could be more significant. To explore this issue, detonation in tubes of various lengths (10–60 cm) filled with a stoichiometric hydrogen–air mixture initially at 298 K and 1 atm were simulated in Ref. [252] using both a detailed chemistry model as well as a two-step overall chemistry model. The two-step model includes dissociation effects in the shocked flow but assumes that the mixture is chemically frozen at the CJ state. Hence, all further energy addition due to recombination is neglected. The detailed chemistry simulations include these effects. The impulse from simulations of a 60 cm long PDE tube using the two models is shown in Fig. 84. The chemical recombination effects increase the peak impulse by 5.3%. These observations are similar to those made recently in another computational study [239].

Based on the above discussion and closer look at the time history of the head-end pressure (see Fig. 77) one can divide the time history into three distinct stages or regions: initiation, plateau, and relaxation. The first stage is dominated by the method used to initiate detonation and to some extent the details of the transition process. Therefore, it depends on the details of the particular experimental or numerical set-up and the specific test conditions. Attention is usually focused on the second, the plateau region or stage. For the case discussed above, the contribution to the impulse from the plateau region (from about 100–330 μs) is the largest (45%). The third stage describes the relaxation of the plateau pressure to the ambient value. It again depends on the details of the experimental or numerical system configuration.

If the contributions from the initiation and relaxation stages are neglected, one can estimate the performance using just the plateau pressure, p_p, and characteristic time of the process, t_{eff}, given by

$$t_{eff} = t_{tr} + t_{cp}$$

where t_{cp} is the time it takes for the front of the expansion fan to come back to the head-end of the tube ($t_{cp} = L/c_{cp}$, c_{cp} is the sound speed in the combustion products). Calculating this effective time for the case discussed above gives a value of 285 μs. However, because a finite time was needed to form a detonation and establish the plateau pressure, in the actual simulations (see Fig. 77) the effective time was about 230 μs. Note that Nicholls et al. [245] used this simplification assuming that the pressure at the head-end went instantaneously from p_p to the ambient value p_0 once the rarefaction waves reached the head-end. With this assumption, the performance was significantly underestimated.

As mentioned above, the manner in which the detonation is initiated will affect the head-end pressure history and hence the performance. For example, if detonation forms via DDT only at the end of the tube, then the characteristic time is given approximately by

$$t_{eff} \approx t_{cp}$$

as the head-end pressure will be low initially and then rise gradually to the plateau value p_p. However, if direct initiation using a high-pressure driver is used, the head-end pressure is significantly larger than the p_p value initially and then drops down to this value after going through a transition during which it could go below the p_p value as seen in Fig. 77.

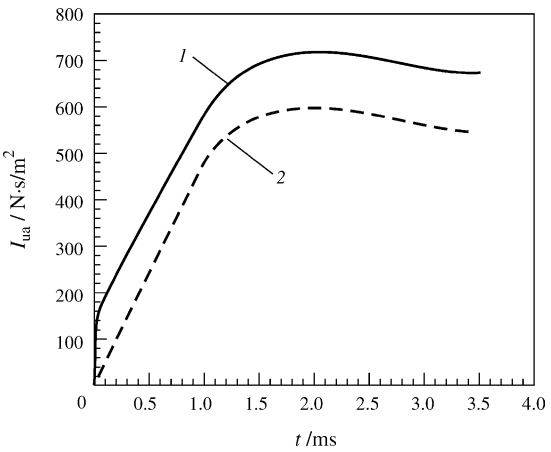

Fig. 85. Predicted effect of initiation energies on the time histories of the impulse (per unit area) from simulations of a 60 cm long PDE operating on a stoichiometric hydrogen–air mixture [252]. 1—high-energy initiator, 2—low-energy initiator.

The effects of parameters used for initiating detonations in simulations have been discussed in detail in Refs. [101,251]. Typically, a high-pressure and high-temperature zone of a certain width near the closed-end of the tube is used for initiating detonations in simulations. A series of overall-chemistry simulations were carried out in Ref. [252] with various temperatures, pressures and zone widths. The predicted impulse from two cases (both for 60 cm long tubes) using a high-energy and a lower-energy initiator is shown in Fig. 85, and the peak values differ by about 17%. A 2 cm zone near the closed end of the tube at 50 atm and 3000 K was used as the high-energy initiator while a 0.2 cm zone at 20 atm and 2000 K was used for the lower-energy initiator. These simulations again emphasize the importance of considering the contribution from initiators in making performance estimates.

Another key factor that affects the performance is the rate at which the pressure relaxes towards the ambient value. In Ref. [244], the effect of this factor was studied by considering a series of 1D numerical simulations where the pressure at the exit plane of the tube is prescribed to relax to the ambient value at different rates. In the analysis, the boundary conditions at the open end of the tube were based on the method of characteristics which ensures that no constrains are imposed on the flow quantities when the outflow is supersonic and enforces the required constraints when the flow becomes subsonic. In the subsonic case, there is a free parameter—characteristic relaxation time—that needs to be specified. Various choices for this parameter result in different rates of relaxation for the pressure at the open boundary.

The predicted pressure histories at the head-end for three different cases (1—very gradual pressure relaxation; 3—abrupt relaxation to constant-pressure at tube exit; and 2—intermediate relaxation rate) are shown in Fig. 86.

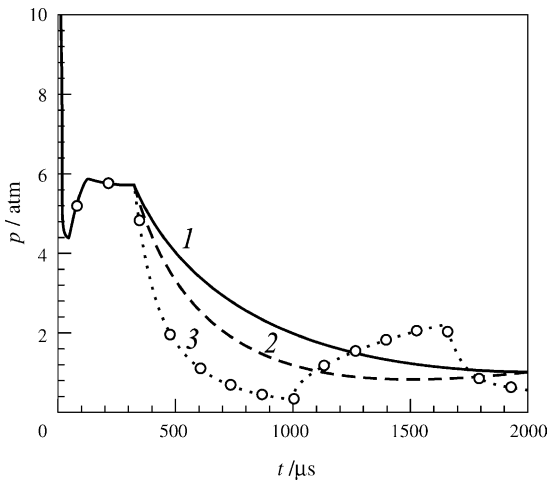

Fig. 86. The predicted time histories of the head-end pressure for three different exit boundary conditions: 1—very gradual pressure relaxation, 3—abrupt relaxation to constant pressure at tube exit, and 2—intermediate relaxation rate. For all cases, a 20 cm long PDE tube is filled with a stoichiometric hydrogen–air mixture [244].

The time evolution of the pressures for the three cases are identical until about 330 μs because the detonation initiation parameters and mixture conditions are identical in the three cases. They begin to differ only when the expansion waves from the open end of the tube reach the head-end. The strength of the expansion waves is different because of the differences in the relaxation process at the open end of the tube. For the slow relaxation process, the pressure reaches the 1 atm mark only by about 2 ms while for the fast relaxation process it reaches that mark by about 630 μs. Clearly, this should have a significant impact on the performance (see Fig. 87).

As seen in Fig. 87, the impulses in the three cases are identical until the effects of the relaxation process at the open

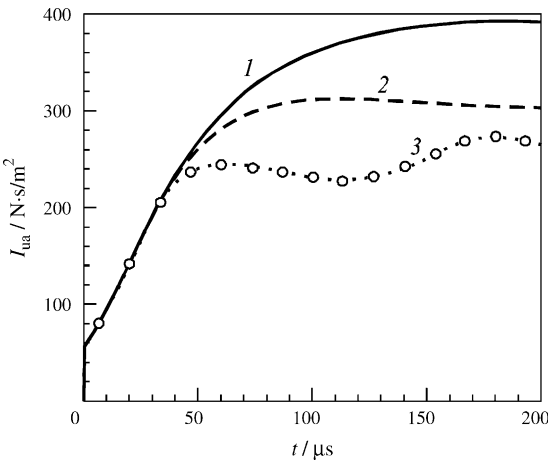

Fig. 87. The predicted time histories of the impulse (per unit area) for three different exit boundary conditions. For other details, see caption for Fig. 86 [244].

end are felt at the head-end. Then, the impulse—time histories differ very much, attaining a maximum value of about 390 N s/m^2 at about 2 ms when relaxation is slow. This peak value is 60% larger than for the fast relaxation condition. These results clearly indicate that the pressure relaxation process at the exhaust end of the PDE tube is an important factor in determining the performance. In practice, different relaxation rates may be attained by suitably tailoring the nozzle shape (see Section 3.15).

As discussed earlier, the plateau pressure can be estimated from the CJ detonation parameters of the specific mixture and initial conditions. Therefore, another approach to modifying the time evolution of the pressure would be to vary the mixture composition along the length of the tube. A special case of this approach would be to partially fill the tube with the reactive mixture and fill the rest of the tube with an inert gas as air. A series of 2D simulations have been conducted in which a 50 cm long tube is filled with a stoichiometric ethylene–air mixture to various fill lengths. Fig. 88 shows the time histories of the impulse for various cases. An interesting observation is that the impulse is not proportional to the amount of fuel fill. When the degree of fill is decreased from 100% (curve 5 in Fig. 88) to 20% (curve 1 in Fig. 88), the peak impulse decreases from 604 to 381 N s/m^2, that is only by 37%. Detailed analysis of these multidimensional simulations [253] shows that the reason for this result is due to the presence of two different sets of expansion waves, one from the fuel–air interface and the other from the exit-end of the tube. When these different sets of expansion waves reach the thrust wall, the pressure decays at different rates because the strength of these expansion waves is different.

The time evolution of the pressure for the various cases is shown in Fig. 89. The two different rates of relaxation are clearly evident in this figure. This result has several

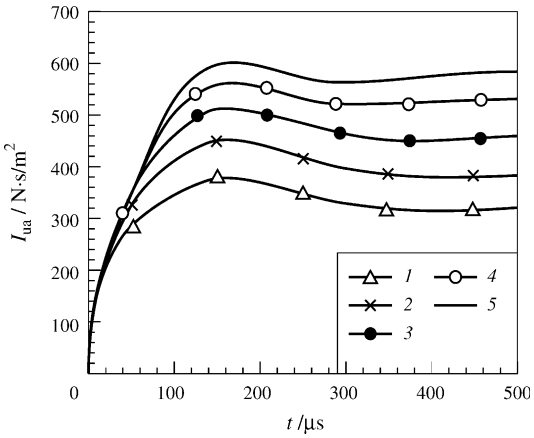

Fig. 88. Effects of partial filling on the time histories of the impulse (per unit area) from a series of 2D simulations of a 50 cm long PDE exhausting into a very large chamber. The section of the PDE filled with a premixed ethylene–air mixture was varied 1—10 cm, 2—20, 3—30, 4—40, and 5—50 cm [244].

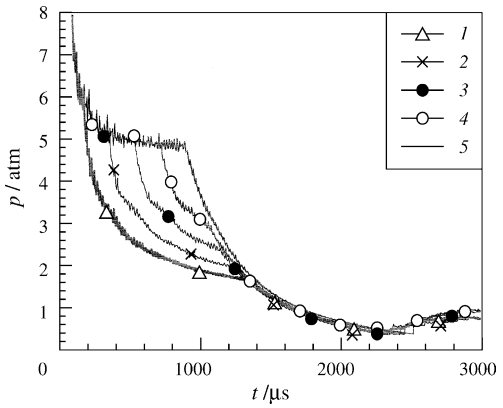

Fig. 89. Effects of partial filling on the time history of the head-end pressure. See caption of Fig. 88 for details [244].

implications. It provides a means of controlling the thrust by controlling the amount of fuel–air fill in the DC. Furthermore, it suggests that a significant performance drop may not occur if during multicycle operations, the tube is not filled completely.

The effect of filling the thrust tube partially with a FAM and filling the rest of the tube with air was also investigated numerically using 2D simulations [252,253]. Two sets of multidimensional numerical simulations have been conducted: (i) a fixed-length PDE tube with fuel sections of varying length, L_f, and (ii) PDE tubes of various lengths, L, with a fuel section of fixed length. As noted before, the interface and exit expansion waves control development of the flow field.

The maximum impulse, $I_{ua,max}$, the fuel-based specific impulse, $\tilde{I}_{sp,f}$, and the mixture-based specific impulse, $\tilde{I}_{sp,m}$, are all shown in Fig. 90 as a function of the ratio, L/L_f. The maximum impulse for a tube of fixed length (1 m) decreases

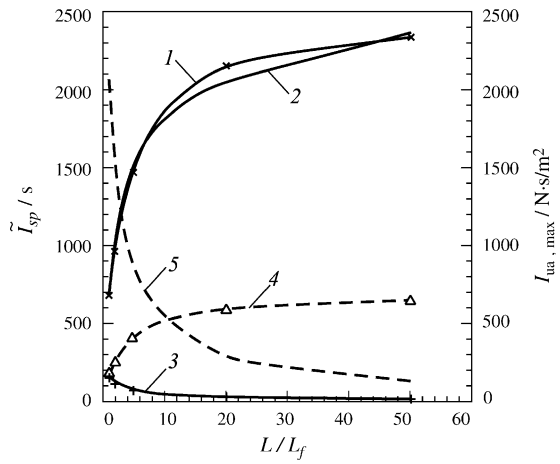

Fig. 90. Effects of partial fuel-fill on various predicted performance parameters [252]. 1—$\tilde{I}_{sp,f}$ (at fixed amount of fuel), 2—$\tilde{I}_{sp,f}$ (at fixed $L = 1$ m), 3—$\tilde{I}_{sp,m}$ (both classes), 4—$I_{ua,max}$ (at fixed amount of fuel), and 5—$I_{ua,max}$ (at fixed $L = 1$ m).

as L/L_f increases because the amount of fuel available for detonation decreases. For a fixed amount of fuel, the maximum impulse increases as L/L_f increases because of the additional shock compression of the air in the tube.

The specific impulses from both sets of simulations collapse onto one curve when viewed as a function of the ratio L/L_f. The fuel-based specific impulse, $\tilde{I}_{sp,f}$, increases with L/L_f, implying that for air-breathing applications, the fuel efficiency of a PDE improves with partial fuel filling. On the other hand, $\tilde{I}_{sp,m}$ decreases with increasing L/L_f indicating that for rocket applications, the fuel efficiency declines with partial fuel filling. Based on these results, a general expression for the fuel-based specific impulse, $\tilde{I}_{sp,f}$, has been derived [254]:

$$\frac{\tilde{I}_{sp,f}}{\tilde{I}^0_{sp,f}} = a - (a-1)\exp\left[-\frac{1}{8}\left(\frac{L}{L_f}-1\right)\right]$$

where $\tilde{I}^0_{sp,f}$ is the fuel-based specific impulse at fully filled conditions ($L/L_f = 1$). The constant a is the asymptotic limit of the benefit multiplier, representing the maximum benefit that can be obtained by partial fuel filling. From the cases simulated, a has a value between 3.2 and 3.5. From Fig. 90, one can also see that most of the benefits of partial fuel filling occurs for L/L_f less than 10. Over this range, the enhancement due to partial fuel filling can be estimated from the simple expression:

$$\frac{\tilde{I}_{sp,f}}{\tilde{I}^0_{sp,f}} = \left(\frac{L}{L_f}\right)^{0.45}$$

The effect of partial fill of a tube on the detonation impulse was examined in Ref. [130]. Fig. 91 shows the set of experimental data [130,255–259] (symbols) on the normalized impulse I_{ua}/I^0_{ua} (where I^0_{ua} is the impulse predicted from the analytical model for the fully-filled conditions) produced by detonation in tubes of constant cylindrical cross-section. Solid line in Fig. 91 corresponds to a semi-empirical model relating the percent of the detonation tube filled with a combustible mixture to the resulting impulse based on experimental and numerical data and simple physical ideas

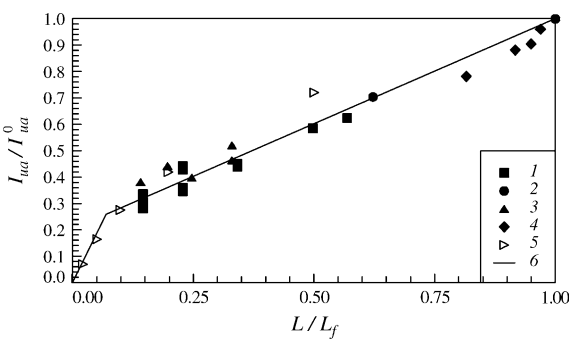

Fig. 91. Normalized impulse vs. percent fill for tubes of constant cylindrical cross-section. Data has been corrected for diaphragm effects [130]. 1—Ref. [255], 2—Ref. [256], 3—Ref. [257], 4—Ref. [258], 5—Ref. [259], and 6—partial fill model [247].

[247]. It follows from Fig. 91 that 5-time decrease in the degree of fill from 100 to 20% results in the decrease in normalized measured impulse by 30–40%, that is in good agreement with 1D calculations of Fig. 88.

There is also the intriguing possibility of enhancing the performance by using by-pass air during the flight. One can envision a situation where the tube is filled only partially with the FAM and by-pass air from the outside is used to fill the rest of the tube. When the detonation reaches the air in the tube, it will degenerate into a shock wave but compression of the air by this shock wave will provide additional thrust and impulse. This enhanced performance can be attained without any additional fuel. Of course, there is a cost for introducing the by-pass air into the tube that must be taken into account.

The above analysis was based on considering a single cycle of an idealized PDE with the initial conditions in the tube corresponding to a certain degree of fill with a premixed FAM. As a matter of fact, the cycle time includes also the time of tube fill. The PDE cycle including the process of filling the tube with premixed hydrogen–oxygen mixture was considered in Ref. [249] based on numerical solving of 2D Navier–Stokes equations for two successive cycles. The first cycle starts at homogeneous conditions, when the mixture has filled a PDE of 30 mm width and length L (L was varied in calculations from 10 to 40 cm). The second cycle was assumed to start immediately after the head-end pressure has decreased to the ambient pressure p_0 due to exhaust of burned products through the open end of the tube. At this instant, fresh hydrogen–oxygen mixture is injected into PDE that still contains a high-temperature burnt gas, by opening two intake ports. Fig. 92 shows the dynamics of tube filling with the fresh reactive mixture in terms of reaction progress variable β. The mixture is injected normal to the lateral wall from the high-pressure reservoir, so that the inflow Mach number is 1.0. The predicted times required for fuel injection, combustion, and exhaust, are shown in the bar graph of Fig. 93 that gives the percentage of each process relative to the total cycle time t_c. The predicted total cycle time t_c is depicted in Fig. 94 as a function of PDE length, L.

It follows from Fig. 93 that none of the times required for all processes in one cycle depend on the PDE length. Moreover, the one cycle time can be estimated, if the PDE length and fuel reservoir pressure are both given: it is closely proportional to the PDE length (see Fig. 94).

It is of interest to compare the specific impulses predicted by 2D numerical calculations with those measured under identical conditions in short tubes where the detonation waves have been proved to propagate in unsteady regimes with velocities lower than the ideal CJ value [260]. Experiments were performed in tubes 100 and 120 mm in diameter of a length varying from 1.2 to 2.5 m. Detonation was initiated by exploding a small amount of a propylene–oxygen mixture. The impulse was measured by the pendulum technique. Deviation of the tube caused by initiator alone was subtracted from the deviation measured

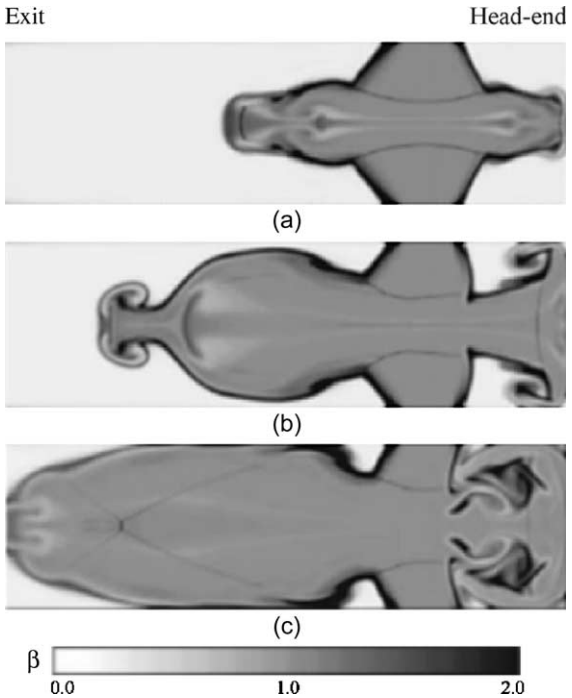

Fig. 92. Predicted distributions of reaction progress variable β in an idealized hydrogen–oxygen PDE after start of fuel injection: (a) 51.4 μs, (b) 96.3, and (c) 153.8 μs [249].

when the tube was filled with a FAM. Measured wave velocities in the tube showed irregular pulsations and were on average well below the CJ values. As seen from Table 13, unsteady detonation waves in experiment produce slightly lower specific impulse than do ideal CJ detonations (compare measured and calculated $\tilde{I}_{sp,f}$ for homogeneous propylene–air and isopropyl nitrate (IPN)), which is not surprising because of losses disregarded in the calculations.

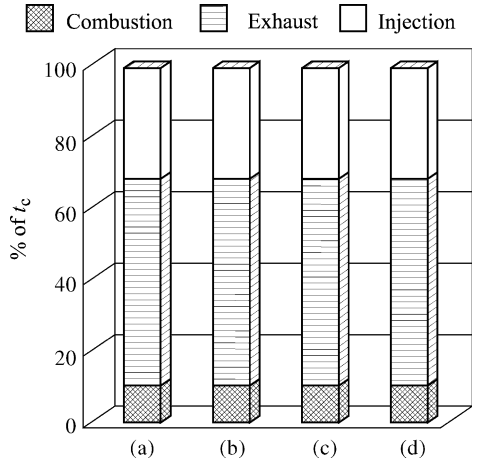

Fig. 93. Duration percentage of particular processes for the four PDEs of different length L: (a) 10 cm, (b) 20, (c) 30, and (d) 40 cm [249].

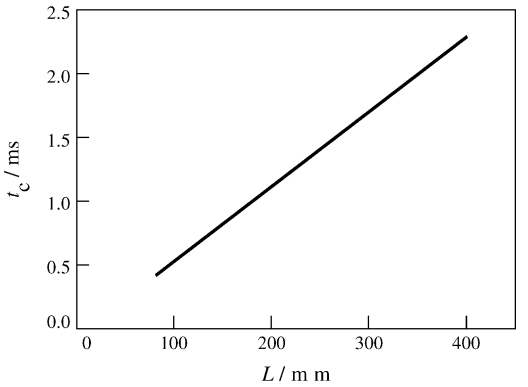

Fig. 94. Predicted total cycle time t_c depending on the PDE tube length L [249].

It should, however, be emphasized that the velocity deficit (as compared to the CJ values) observed in experiment would suggest a significantly greater reduction of the specific impulse, which means that ideal detonation regimes may appear not the best impulse generators.

Table 13 also compares 2D calculations with measurements for another mode of pulsed operation of the same combustor. Instead of filling the tube with a FAM and then detonating it an attempt was undertaken to generate a reactive shock wave and produce impulse by injecting a hot fuel-rich mixture in air. Nitromethane (NM) and IPN were used as the starting fuels, they were partially decomposed in the condensed phase and the products together with unreacted fuel were injected in the tube. The lines NM + Al (injection) and IPN (injection) compare the results of calculations and measurements. The results reveal two interesting findings. First, injection of reacting fuel is not necessarily inferior to detonation in the performance (see initial two lines). On the contrary, calculations show that a significant fraction of the products of NM decomposition leave the combustor unreacted. Hence if mixing were better the impulse produced by jetted NM would be higher. Second, jet mixing with air controls the impulse, calculations demonstrate that only a small fraction of the injected material has time to react with air, which indicates that

Table 13
Comparison of calculated and measured specific impulse [260]

	$\tilde{I}_{sp,f}$ (s) open end (calc.)	$\tilde{I}_{sp,f}$ (s) closed end (calc.)	$\tilde{I}_{sp,f}$ (s) (meas.)
NM + Al (injection)	442	–	150
NM + air (homogen.)	455	495	–
IPN (injection)	241	273	250–300
IPN (homogen.)	671	686	600–700
Propylene + air	1900	1930	1600–1730
Hydrogen + air	4145	–	–

only multiple-jet devices could be efficient. The use of an injector with two orifices slightly shifted along the tube axis increased the measured specific impulse by about 50 s.

Thus, one should admit that the issue of optimal regimes of pulse-engine operation and attainment of their best performance still calls for further thorough studies. Moreover, even performance estimates of the idealized PDE continue to be a controversial issue.

2.7. Operational constraints of pulse detonation engine

It is instructive to indicate the range of operation conditions for the PDE assuming that it is designed for producing thrust for a flying vehicle.

Table 14 shows the estimated variations of the initial (stagnation) pressure p_{20} and temperature T_{20} of the incoming air in the DC, as well as the detonation shock pressure p_s and temperature T_s in a PDE-based supersonic vehicle over the flight Mach number M_∞ range from 1.0 to 2.0, and an altitude (H) ranging from 0 (sea level) to 10 km [117,118].

Also shown in the table are the values of static ambient pressure p_0 and temperature T_0, the isentropic stagnation pressure p_{10}, the coefficient of pressure loss in the shock κ', the coefficient of pressure recovery in the supersonic diffuser χ_{pr}, the speed of sound in a fresh FAM c_{20}, and the Mach number of the detonation wave M_{CJ}. For the estimations, the following relationships were used:

$$p_{10} = p_0\left(1 + \frac{\gamma-1}{2}M_\infty^2\right)^{\gamma/(\gamma-1)}$$

$$p_{20} = \chi_{pr}(M_\infty)\kappa'(M_\infty)p_{10}$$

$$\kappa' = \left(\frac{\gamma+1}{2}\right)^{(\gamma+1)/(\gamma-1)} \times \frac{M_\infty^{2\gamma/(\gamma-1)}}{\left(1+\frac{\gamma-1}{2}M_\infty^2\right)^{\gamma/(\gamma-1)}\left(\gamma M_\infty^2 + \frac{\gamma-1}{2}\right)^{1/(\gamma-1)}}$$

$$T_{20} = T_0\left(1 + \frac{\gamma-1}{2}M_\infty^2\right)$$

$$\rho_{20} = \frac{p_{20}}{RT_{20}}$$

$$c_{20} = \sqrt{\gamma RT_{20}}$$

$$M_{CJ} = D_{CJ}/c_{20}$$

$$\rho_s = \rho_{20}(A + \sqrt{A^2 - B})$$

$$A = \frac{\gamma_s(\gamma-1)(1+\gamma M_{CJ}^2)}{\gamma(\gamma_s-1)(2+(\gamma-1)M_{CJ}^2)}$$

$$B = \frac{(\gamma_s+1)(\gamma-1)M_{CJ}^2}{(\gamma_s-1)(2+(\gamma-1)M_{CJ}^2)}$$

$$p_s = p_{20}\left[1 + \gamma M_{CJ}^2\left(1 - \frac{\rho_{20}}{\rho_s}\right)\right]$$

$$T_s = T_{20}\frac{p_s}{p_{20}}\frac{\rho_{20}}{\rho_s}$$

Table 14
Estimated variations of pressure and temperature in the DC of a PDE-based supersonic vehicle [117]

	M_∞								
	1.0			1.5			2.0		
H (km)	0.0	3.0	10.0	0.0	3.0	10.0	0.0	3.0	10.0
p_0 (bar)	1.0	0.692	0.261	1.0	0.692	0.261	1.0	0.692	0.261
T_0 (K)	288	269	223	288	269	223	288	269	223
p_{10} (bar)	1.89	1.31	0.49	3.67	2.54	0.96	7.82	5.41	2.04
κ'	1.0	1.0	1.0	0.93	0.93	0.93	0.721	0.721	0.721
χ_{pr}	1.0	1.0	1.0	1.049	1.049	1.049	1.157	1.157	1.157
p_{20} (bar)	1.89	1.31	0.49	3.58	2.48	0.94	6.52	4.51	1.7
T_{20} (K)	346	360	268	418	390	323	518	484	401
$\Phi = 1.0, D_{CJ} = 1800$ (m/s)									
c_{20} (m/s)	372	360	328	410	396	360	456	441	401
M_{CJ}	4.84	5.00	5.49	4.39	4.55	5.00	3.95	4.08	4.49
p_s (bar)	53.3	39.4	17.8	83.1	61.8	28.3	122.5	90.4	41.2
T_s (K)	1667	1831	1598	1718	1698	1643	1805	1773	1709
$\Phi \approx 0.6, D_{CJ} = 1600$ (m/s)									
c_{20} (m/s)	372	360	328	410	396	360	456	441	401
M_{CJ}	4.30	4.44	4.88	3.90	4.04	4.44	3.51	3.63	3.99
p_s (bar)	41.6	30.7	13.9	64.8	48.2	22.1	95.6	70.7	32.2
T_s (K)	1434	1570	1364	1488	1466	1409	1578	1548	1478

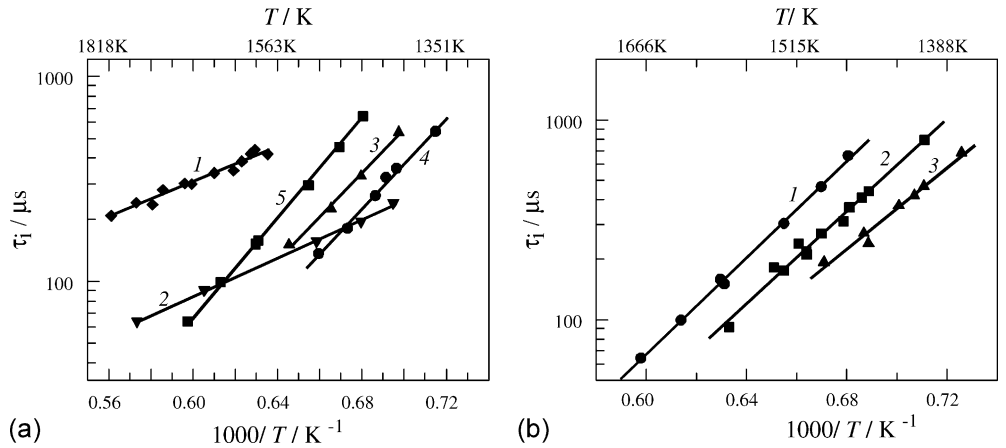

Fig. 95. Measured ignition delay times τ_i of stoichiometric JP-10-O_2 mixtures (diluted with argon) as compared to other hydrocarbons (a) at pressure of 1 bar (1—ethylene (0.2%), 2—ethylene (0.99%), 3—*n*-heptane (0.2%), 4–*n*-decane (0.2%), and 5-JP-10 (0.2%)) and (b) depending on pressure (1—1 atm, 2—2–3 atm, and 3–6 atm) [100,261].

where $\gamma \approx 1.4$ is the specific heat ratio of initial FAM. Two sets of estimated data for c_{20}, M_{CJ}, p_s, and T_s are presented in Table 14: (i) for $D_{CJ} = D_{CJ}(\Phi = 1) = 1800$ m/s and mean $\bar{\gamma} \approx 1.33$ characteristic for stoichiometric hydrocarbon–air mixtures of equivalence ratio $\Phi = 1.0$ at post-shock conditions, and (ii) for $D_{CJ} = D_{CJ}(\Phi = 0.6) = 1600$ m/s and mean $\bar{\gamma} \approx 1.35$ characteristic for the fuel-lean mixtures of equivalence ratio $\Phi = 0.6$ at post-shock conditions. The relationships for ρ_s and p_s have been obtained from the conservation laws within 'two-gamma' approximation.

Examination of Table 14 shows that at Mach number 2.0 the inlet conditions in the DC may range from 520 K and 6.5 bar at sea level to 400 K and 1.7 bar at 10 km. The effect of changing the flight Mach number on the inlet air temperature and pressure may be seen in the range of operation conditions at 10 km, where the inlet conditions in the DC vary from 270 K and 0.5 bar at Mach number 1.0 to 400 K and 1.7 bar at Mach number 2.0. Clearly, according to the data of Table 14, the fuel should detonate within the range of initial temperatures from 270 to 520 K and initial pressures from 0.5 to 6.5 bar.

Other observations come from examining the data for p_s and T_s in Table 14. Depending on the Mach number and flight altitude, the pressure in the leading shock wave is expected to range from 14 to 96 bar for fuel-lean mixtures and from 18 to 122 bar for the stoichiometric composition, while the post-shock temperature changes from approximately 1400 K for the fuel-lean mixture to 1700 K for the stoichiometric composition. Taking into account the dependence of both physical and chemical processes constituting the operation phases of PDE on temperature and pressure, one realizes that special measures should be taken in order to ensure proper timing between repeated detonation initiation and fuel injection. Note that the critical initiation energy and detonability limits depend on the initial temperature and pressure, and on mixture composition (see Sections 2.2.3 and 2.3.3). The humidity of air is also known to affect the fuel detonability [113].

Hanson et al. [100,261] reported their shock-tube measurements of ignition delays of JP-10-O_2–Ar mixtures at various temperatures and pressures. Fig. 95 demonstrates the sensitivity of the ignition delay of JP-10 to pressure and temperature. Decrease in post-shock pressure from 6 to 1 atm results in approximately 3-time increasing of the ignition delay, while the decrease in post-shock temperature from 1600 to 1400 K results in approximately 10-time increasing of the ignition delay. If one takes into account that the characteristic ignition delay in detonation waves is in general less than 100 μs, it is seen that variation of PDE inlet conditions will dramatically influence detonability of JP-10.

To demonstrate how the detonability limits can be estimated for a particular PDE geometry, determine limits for a 4 in. diameter ($d = 0.101$ m) combustor, operating on a stoichiometric FAM, for both ambient static pressure fill conditions and one with backpressurization where the fill pressure is equal to the total pressure recovered at the combustor inlet. The limit can be defined as when the transverse detonation cell size, a, of the mixture (at the particular fill pressure) equals to combustor diameter $a = d = 0.101$ m. Fig. 96 shows the backpressurization case for four flight Mach numbers and a MIL E5007D inlet. As the flight Mach number increases, the total pressure recovered increases and the associated cell size decreases. The detonability limit can therefore be estimated as 15 km at a flight Mach number of 1.6. For a flight Mach number of 1.2, the altitude limit drops to 12 km.

The more limiting case is when a combustor is filled and detonated at the local ambient static pressure. Fig. 97 shows the effects of altitude on cell size and that a limit of only 6 km exists for propane–air with no backpressurization and a 4 in. diameter combustor. The results indicate that some degree of backpressurization will be needed for

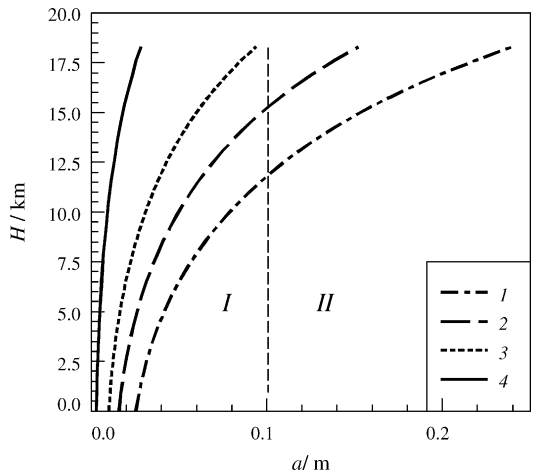

Fig. 96. Estimated detonability limits of a stoichiometric propane–air mixture as a function of flight Mach number M_∞ and altitude H for the case with backpressurization. 1—M_∞ =1.2, 2—1.6, 3—2.0, and 4—3.0. Vertical dashed line corresponds to condition $a = d$−stability limit for detonation in the 4 in. diameter cylindrical combustor. I—detonation, II—no detonation.

air-breathing PDE operation at mid to high altitude situations. The backpressurization can be accomplished by a common nozzle or some type of aeronozzle, which utilizes bypass air dumped transversely into the combustor exit to generate a simulated nozzle.

The existence of detonation limits in terms of pressure, temperature, and mixture composition then dictates the constraints on combustor diameter and mass flow rate. The length of the combustion chamber then determines the combustor volume and overall operating frequency because

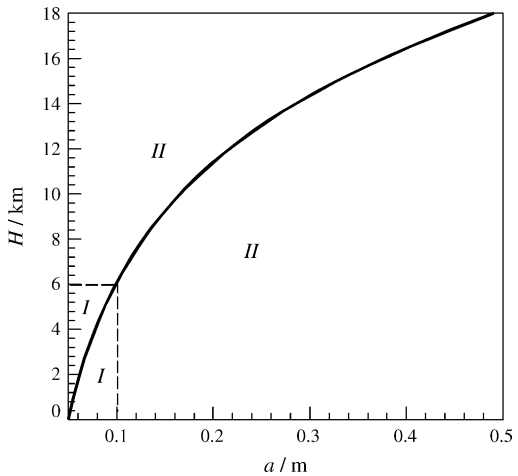

Fig. 97. Estimated detonability limits of a stoichiometric propane–air mixture as a function (implicit) of flight Mach number M_∞ and altitude H for the case without backpressurization. Vertical dashed line corresponds to condition $a = d$–stability limit for detonation in the 4 in. diameter cylindrical combustor. I—detonation, II—no detonation.

of the individual processes that must occur for each cycle. As was demonstrated in Section 2.4, the operating frequency f of a given engine is defined as $1/t_c$, where cycle duration t_c is composed, in general, of five characteristic time intervals: filling Δt_{fl}, purging Δt_{pr}, detonation initiation Δt_{in}, detonation traversing the combustor Δt_{tr}, and exhaust Δt_{ex}, i.e.

$$t_c = \Delta t_{fl} + \Delta t_{pr} + \Delta t_{in} + \Delta t_{tr} + \Delta t_{ex}$$

The dynamic filling and exhaust/purging processes tend to be the longest duration and can be shortened by operating at higher dynamic pressures, but with some upper limit due to filling losses. The length of the combustor and the filling velocity determine the fill time, Δt_{fl}, since the mass flow into the combustor has to traverse the derived combustor length. Practically, this fill rate should occur at no higher than Mach 0.5 for losses to be kept at a reasonable level. The lower time limit for a fill process in a constant-area combustor is therefore Mach 1, but at great expense. A full cycle of the engine, t_c, can then be calculated by summing each characteristic interval and the operating frequency determined as demonstrated in Section 2.4. Since the length, flight dynamic pressure, and operating frequency of a combustor are directly coupled, an optimum will likely exist where performance will be maximized (see e.g. Fig. 74). Practical values are near 100 Hz for a 1 m long combustor operating at an initial pressure of 1 atm, but these frequency limit could be overcome if multiple injection locations are utilized.

It follows from the above discussion that the basic requirement to the PDE fuel is that it should readily detonate with low sensitivity to initial conditions in terms of temperature and pressure. In addition, since the PDE should operate at the lowest possible overall fuel–air ratio and high combustion efficiency, the PDE fuel should exhibit wide detonability limits in terms of mixture composition.

Another requirement to the PDE fuel, which contradicts the above requirements, is avoiding surface ignition of FAM before or after triggering the initiator, or uncontrolled autoignition of FAM due to mixing with residual combustion products. Premature ignition is expected to arise near the hot walls of the DC (at temperatures exceeding 600–800 K), providing that the cycle duration is longer than the autoignition delay of the FAM. In view of it, the PDE fuel should exhibit high resistance to ignition by a hot surface. A particular issue is avoiding premature ignition in the vicinity of the initiator. It is expected that the surfaces located near the initiator and the initiator itself can get very hot during operation, and the abnormal combustion can produce thermal damage in a very short time.

For propulsion applications, the PDE fuel is preferably a liquid hydrocarbon (or other liquid compound) due to high energy density. The requirement of fast mixing of fuel with incoming air implies that the PDE fuel should exhibit high vapor pressure at operation conditions. One of possible solutions is recuperative fuel preheating or prevaporization. The presence in the PDE fuel of nonvolatile hydrocarbons

and additives containing metals and polymeric compounds can promote premature ignition due to their deposit-forming tendency. The deposits are known to produce the thermal isolation effect increasing the wall temperature.

In addition to the fuel detonability requirements mentioned above, a set of vehicle design requirements (low pressure loss, low weight, size constraints, etc.) should be met. Clearly, some of the requirements appear to be quite contradictory, and a sort of compromise must usually be achieved.

3. Design concepts

3.1. Preliminary remarks

This chapter deals with various concepts of PDE that have been evaluated either theoretically or experimentally. Despite of their diversity, their overview can be helpful for better understanding of the existing approaches to implement principles outlined in Sections 2.4–2.6. In some cases, we describe the sequence of operation and provide some technical details of the pulse detonation devices. It is done with intention to provide the reader with examples of possible solutions for numerous problems encountered in the development of practical PDEs. The concepts were differentiated according principles of detonable mixture formation (valved or valveless, uniform or stratified charge), detonation initiation (predetonator, enhanced DDT, shock-booster, resonator, implosion, etc.), and thrust production (detonation or blast wave). Some aspects of inlet and nozzle integration to the PDE combustion chamber, as well as advantages and drawbacks of multitube design are also discussed.

3.2. Valved concepts

Valved PDE concept implies the use of mechanical valves to ensure a controlled (periodic) inward flow rate of fresh air or fuel–oxidizer mixture into the DC, to prevent detonations or shocks from moving outwards from the DC through the inlet, and to provide a sufficient time for mixing of fuel with air. In some PDE configurations, mechanical valves can serve as a thrust wall too.

Several designs with mechanical valves are available in literature. Fig. 98 shows schematically the PDE combustor of Ref. [262]. In this configuration, the PDE has a set of parallel detonation tubes 1 arranged within a drum-like cylinder 2 having outside cylindrical housing 3, front end-wall 4, and back end-wall 5. The detonation tubes are fixed within holes in these two end-walls and extend from one wall to the other, each tube being open at both ends. The tubes are arranged in a group of six circles with the tubes on the outer circle having the largest diameter, and gradually decreasing in diameter to the sixth inner circle of tubes of

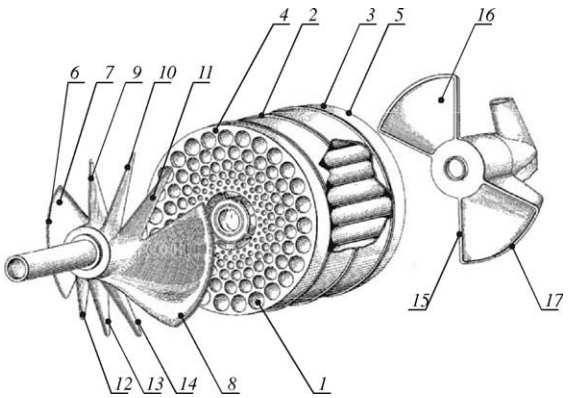

Fig. 98. Perspective view of PDE with mechanical valves [262].

smallest diameter. Arranged to rotate on the face of the front end-wall 4 is inlet rotary valve 6 having two diametrically opposed portions 7 and 8 together with two diametrically opposed groups of fuel inlet headers 9, 10, and 11 in one group, and 12, 13, and 14 in the other. Arranged to rotate at the face of back end-wall 5 is exhaust rotary valve 15 also having two diametrically opposed portions 16 and 17.

Fuel–oxidizer mixture is supplied to the inlet end of the tubes. Liquid fuel is introduced under pressure into a jacket around the detonation tubes where it is preheated by hot portions of the engine. As it emerges from the orifices of the fuel headers 9–11 and 12–14, the high-pressure liquid fuel evaporates and enters the detonation tubes. Simultaneously, air enters the detonation tubes from the front passing around the fuel headers. This fuel–oxidizer mixture passes through the tubes toward the outlet end, thus filling the tubes with the explosive mixture. By proper timing of the inlet and outlet valves the repeated operation of the PDE with detonation initiation, propagation along the tubes, exhaust of detonation products to the ambience, and engine refill is to be attained.

Fig. 99a shows schematically the PDE combustor of Ref. [263] with a disk-shaped mechanical valve (Fig. 99b). In the configuration of Fig. 99a, fuel and oxidizer are supplied to the pulse ignition system 1 from tanks 2 and 3, respectively. The pulse ignition system 1 has a disk-shaped rotary valve 4 (see Fig. 99b) and igniter tubes 5 with spark-plug igniters 6. The igniter tubes are connected to the DCs (not shown). Rotary valve has a flywheel 7 and several ports 8. The flywheel is located inside a stationary valve body 9, sealed on both sides, and is driven by a shaft 10 of electric motor 11. As flywheel rotates, each port 8 rotatingly aligns with oxidizer supply line and an igniter tube 5 is in an open position. As oxidizer enters the igniter tube, fuel is simultaneously released from fuel valve 12 so that the oxidizer mixes with fuel. As flywheel continues to rotate, port 8 sealingly rotates out of alignment with oxidizer supply line causing the igniter tube and the fuel valve to close. Shortly thereafter, spark plug ignites the mixture resulting in detonation formation downstream of the ignition

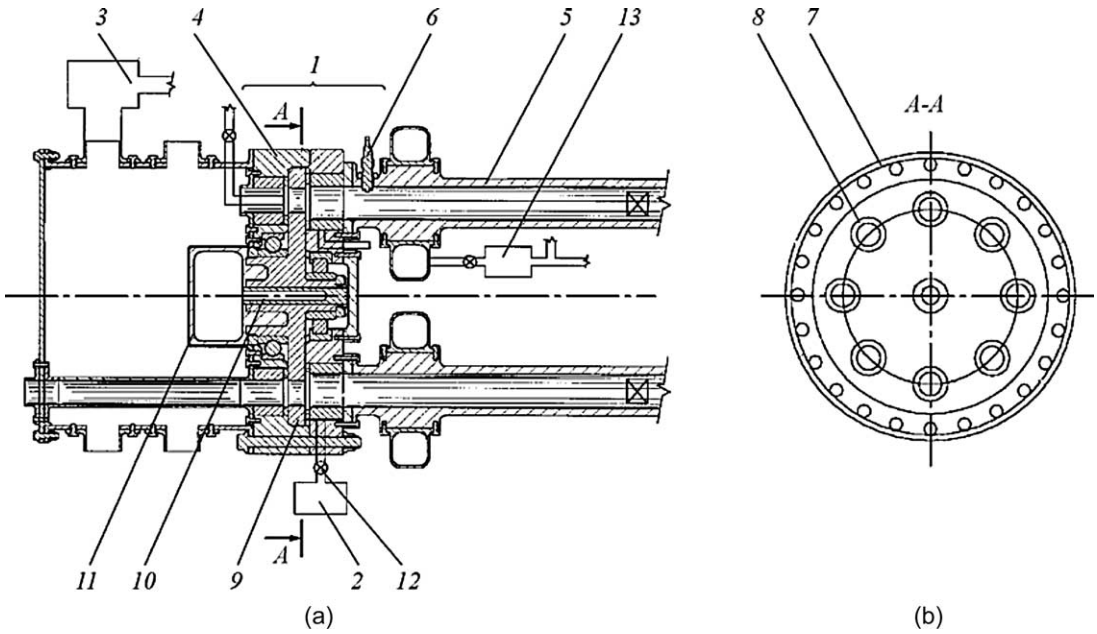

Fig. 99. The PDE combustor (a) of [263] with a disk-shaped mechanical valve (b).

site. The detonation wave propagates down the igniter tube and transmits to the main DC (not shown). It is implied that in operation, pulse ignition system creates a detonation wave in each igniter tube. Detonation wave then moves through the igniter tube to the DC and exits through the open rearward end of the chamber into the ambience. After the detonation, the PDE is purged of residual gases by a special ventilation system 13 utilizing an inert gas and the process is repeated sequentially as described.

A PDE model with a disk-shaped mechanical valve somewhat similar to that shown in Fig. 99 has been tested in Ref. [264]. Fig. 100a shows an exploded cutaway view of the axisymmetric assembly of the PDE prototype. The diffuser 1 of the PDE is designed for flight Mach number of 2.1. The centerbody has a double-cone geometry on the compression side to produce two shock waves that reduce the Mach number to 1.7 ahead of terminal normal shock. Due to further expansion of the post-shock subsonic flow, the flow Mach number at the exit plane of diffuser is decreased to 0.2. Downstream of the diffuser and mechanical intake valve 2, there are six cylindrical ducts 3 distributed evenly along the circumference of a circle. These ducts represent PDE detonation tubes. The simulation of the PDE intake valve operation is done with a flywheel located between the inlet and the PDE ducts. The flywheel 2 (see Fig. 100b) has two contoured cutouts 4 so that at any given time a maximum of four PDE ducts are exposed to the flow and the remaining two are completely covered by the disk. The flywheel blocking the flow is driven by means of shaft 5 passing through the model and rear support 6 as shown in Fig. 100a. The shaft is connected to an external motor. Fig. 101 shows the total cross-sectional area of the PDE ducts exposed to the airflow, F_{DC}, normalized by the diffuser exit area, F_{de}, as a function of rotation angle θ_{rot} during one rotation cycle of the disk resulting in a periodic massflow fluctuation. The figure shows that the opening is

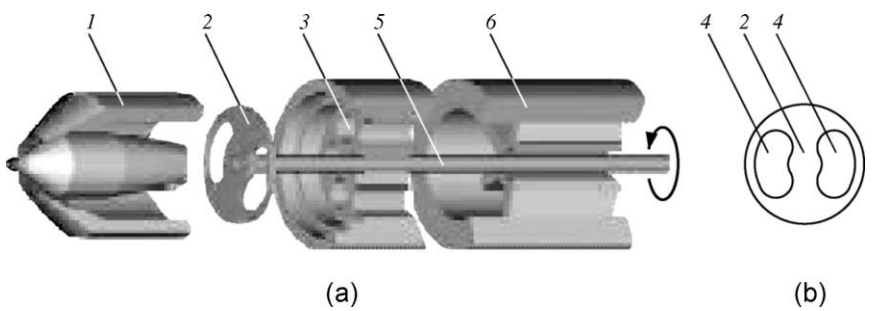

Fig. 100. Exploded cutaway view of the axisymmetric PDE with six detonation ducts at the rear of the diffuser (a) and valve (b) [264]. 1—diffuser, 2—valve, 3—detonation duct, 4—cutouts, 5—shaft, 6—rear support.

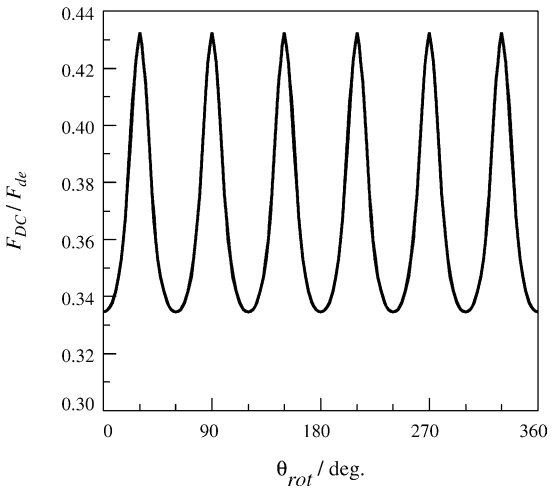

Fig. 101. Airflow cross-section area of the PDE ducts normalized by the diffuser exit area as a function of rotation angle of the flywheel [264]. The total DC area F_{DC} is 64% of the diffuser exit area F_{de}.

33–43% of the diffuser exit area with the disk in place, which can be compared to 64% without the disk. The diffuser capture was designed based on the maximum mass flow at the exit to avoid ingestion of the shocks under all operational conditions. Downstream of the PDE ducts is a cylindrical plenum and channels for exhausting the air downstream into the wind tunnel and the supporting mechanism.

A valved PDE configuration similar to that shown in Fig. 100 has been thoroughly calculated in Refs. [243,265, 266]. Fig. 102 shows the schematic of a supersonic air-breathing PDE with a coaxial, mixed-compression, supersonic inlet and a rotary valve. A system performance analysis of the PDE of Fig. 102 has been conducted for a six-tube, air-breathing PDE operating on a stoichiometric hydrogen–air mixture. The flight altitude is 9.3 km and the freestream Mach number is 2.1. The corresponding stagnation pressure and temperature at the combustor entrance are 2.23 atm and 428 K, respectively. The air mass flow rate is 1 kg/s. The detonation tube measures 60 cm in length and 5.7 cm in internal diameter. The valve opening pattern is assumed to be step-wise, i.e. either fully open or close. Fig. 103 presents the example of pressure–time history at the single tube exit. The cycle frequency in Fig. 103 is 244 Hz.

Fig. 104 shows schematically the PDE combustor of Ref. [267] with conical mechanical valves. In this PDE configuration, fuel and air enter the DC 1 through manifolds 2 and 3, respectively, and through a conical rotary valve 4. The rotary valve is aimed to control receiving a charge of fuel and air. It is equipped with exit chambers 5 (Fig. 104b) for fuel and air and is driven by drive shaft 6, which is connected to motor assembly 7. Towards the exit chambers 5, fuel is supplied through individual fuel ducts that have a finger-shaped cross-section and end with finger-shaped port. The fuel ducts are arranged partially within individual air ducts as shown in Fig. 104b. This arrangement of the exit port is aimed at enhancing fuel–air mixing. The alternative is to use the disk-shaped mechanical valve 4 shown in Fig. 104c. A rear rotary valve 8 is aimed at controlling the discharge of combustion products from the DC into ambient atmosphere through nozzle 9. According to Ref. [267], other valve arrangements are possible, e.g. flapper, fast-acting ball valve, butterfly valve, electrically activated solenoid, etc.).

The other PDE scheme applies mechanical valves in the form of convex spherical elements rigidly secured to their exterior [268]. Fig. 105 shows the sectional view of such a PDE. Spherical inner seal surfaces 1 are mounted to inner housing 2 for rotation therewith. Each inner seal surface is identical to the other, and each comprises a convex spherical element having a bore, which receives inner housing 2. The upstream and downstream edges of the inner seal

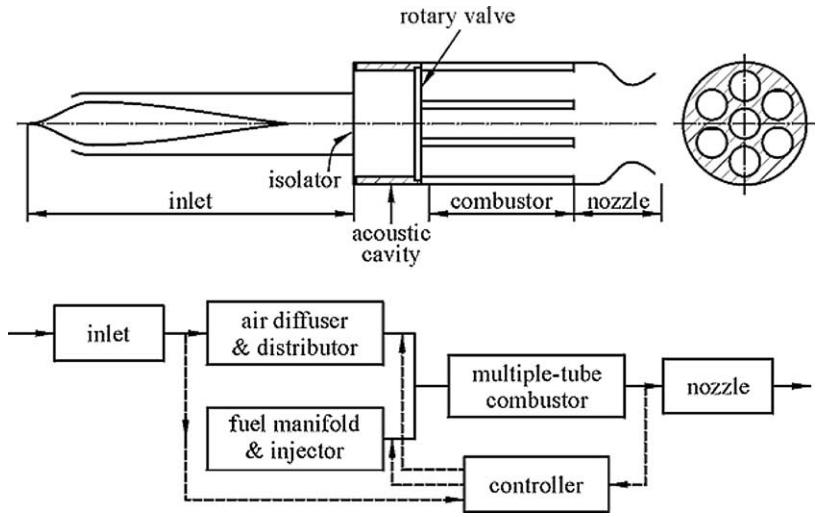

Fig. 102. PDE with coaxial, mixed-compression, supersonic inlet and the scheme of operation control [243,265,266].

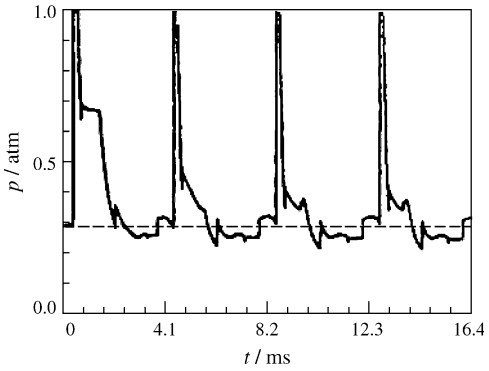

Fig. 103. Time history of pressure at tube exit [265]. Dashed line shows the ambient pressure p_0 =0.29 atm.

surfaces are truncated and abut each other. At least one inner housing port 3 extends from injection chamber 4 radially through the inner housing and through the inner seal surface, terminating at the convex surface.

It is implied that in operation, an exterior power source will rotate shaft 5 to cause gear 6 to rotate the inner housing while outer housing 7 remains stationary. A combustible mixture such as stoichiometrically mixed reactants of fuel and oxidizer flows in inlet 8, and is further mixed as it flows through mixer vane passages 9. Twice per revolution, inner housing ports 3 will align with outer housing ports 10, admitting a combustible mixture to DC 11. Once the inner housing ports rotate slightly past the outer housing ports, igniter 12 will initiate detonation of the combustible mixture in the DC. The arising detonation wave discharges out the jacket 13, creating thrust. A reverberating expansion wave is created by the initial detonation wave. The expansion wave reflects off the end wall 14 and discharges from the rearward end of the jacket, creating additional thrust.

Immediately after but prior to inner housing ports 3 aligning again with outer housing ports 10, purge plate ports 15 will align with ports 16 and purge ports 17. At the time of the detonation, purge plate ports 15 were out of registry with purge ports 17. Inner and outer seals and purge port seals provide a closed upstream end to the DC, preventing any products of the detonation from flowing into plenum 18. Once ports 15 and 16 and purge ports 17 are aligned, air supplied through air inlet 19 will flow through the plenum, through the purge plate ports and the purge ports into the DC. The purge air removes hot products and dilutes trapped reactants from the DC. Immediately thereafter, inner housing ports 3 will align again with outer housing ports 10 and the process will be repeated. The rotational speed of inner housing 2 is selected to create pulses at a rate of approximately 100 cycles per second.

In the scheme of Fig. 105, the spherical seals are expected to provide effective sealing for the high-temperature high-pressure detonations. The sealing should avoid any leakage of high-pressure reactants back into the injection chamber.

In Ref. [269], a device simulating exhaust of a PDE with a mechanical valve somewhat similar to that shown in Fig. 105a has been tested in the supersonic wind tunnel. The device is shown schematically in Fig. 106. A photograph of the test rig is presented in Fig. 107. The objective of the tests was to study the wave pattern in the device, i.e. the starting vortices, the extent of propagation of the wave front, the reflection of the wave from the secondary flowpath walls, and the timing of these events.

Further modification of scheme of Fig. 105 has been suggested in Ref. [270]. Fig. 108 shows the sectional view of the modified valved PDE with separate delivery of fuel and oxidizer in the DC. In this scheme, the flow of oxidizer through one of the passages into the DC and fuel through the other passage reduces the chance of an accidental explosion outside of the DC. A first component of a combustible mixture, such as oxygen or air, is supplied to inner passage manifold 1. A second component of a combustible mixture, such as a hydrocarbon fuel, is supplied to outer manifolds 2. The shaft 3 and drive gear 4 are timed so that ports 5 of inner spherical valves open simultaneously with ports 6 of outer valves. The oxidizer thus flows through inner ports 7 and 5 into annular DC 8. At the same time, gaseous hydrocarbon flows into the DC through outer ports 9 and 6. The two portions of the combustible mixture mix within the chamber.

Once inner ports 7 and 5 and outer ports 9 and 6 close, igniter 10 detonates the combustible mixture. The arising detonation wave propagates along the DC and discharges out the nozzle 11, creating thrust at the end-wall 12.

Immediately after, but prior to inner and outer ports opening again, purge plate ports 13 align with stationary ports 14. At the time of the detonation, the purge plate ports

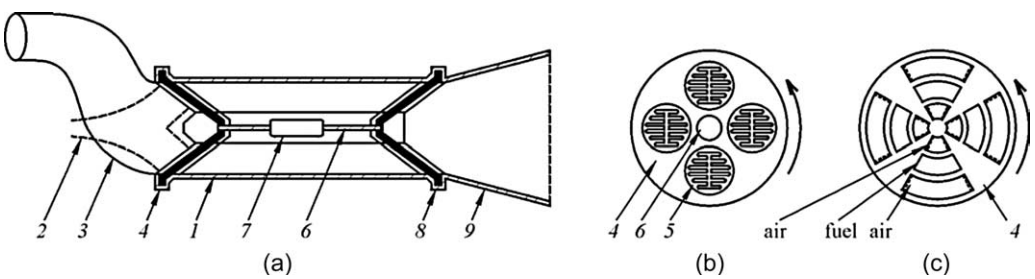

Fig. 104. The PDE combustor (a) of Ref. [267] with conical mechanical valves (b) or disk-shaped valves (c).

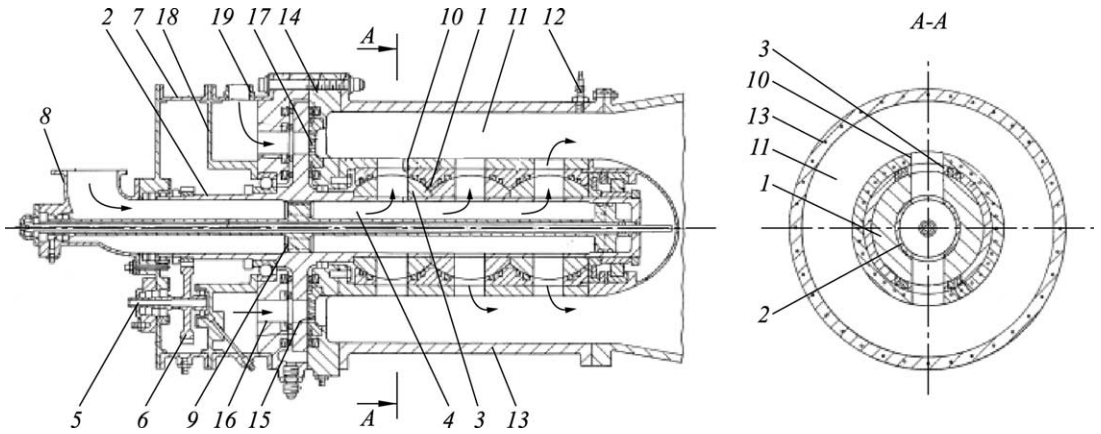

Fig. 105. Sectional views of a valved PDE operating on premixed fuel and oxidizer [268].

are out of registry with the stationary ports. During detonation, inner and outer seals and the upstream end-wall provide a closed upstream end to the annular combustion chamber, preventing any products of the detonation from flowing into plenum 15 through the purge ports 13 and 14. Once these purge ports are aligned, air will flow through the plenum, through the purge ports and into the DC. The purge air removes hot products and dilutes trapped reactants from the DC. Immediately thereafter, inner ports 7 and 5 align and outer housing ports 9 and 6 align to open for repeating the process. The rotational speed of cylinder 16 is selected to create pulses at a rate of approximately 100 cycles per second.

The scheme of Fig. 108 has certain advantages as compared to Fig. 100 as mixing the components of the mixture in the DC adds safety to the apparatus and allows for distributed injection of fuel and oxidizer that reduces the mixing time. One of further modifications of the PDE of Fig. 108 is shown in Fig. 109 [271]. In this configuration, tubular DC 1 is used instead of the annular DC of Fig. 108. Fuel and oxidizer are periodically supplied to different inlet ports 2 distributed along the DC.

Fig. 110 shows the PDE of Ref. [272] with the valve assembly resembling that used in automobile engine. Pulse detonation apparatus of Fig. 110 has a core feed cylinder 1 with inlet ports 2, connected to a purge gas (air), and four outlet ports 3 in the side wall 4. The core feed cylinder is carried rotatably inside an inner sidewall 5 of an annular DC 6. The inner sidewall has four ports 7 positioned to register with the outlet ports 3 twice per revolution of core feed cylinder 1. Motor 8 rotates the core feed cylinder 1 relative to inner sidewall 5. When registered, the purge gas from the core feed cylinder flows into the DC. The DC also has an outer sidewall 9, closed forward wall 10, and open rearward end 11. To introduce gaseous fuel to the DC, there is an external valve assembly 12 mounted to elongated openings 13 in the outer sidewall 9. Shown in Fig. 110a is only one valve assembly, while Fig. 110b shows four valve assemblies spaced equally around the sidewall. Each of the valve assemblies includes a valve housing 14 with valves 15 and valve seats 16 and 17. Each valve has a rod 18 and a spring 19 that urges the valve to the closed or upper position. Each valve housing has two cams 20 aimed at engaging the rods to reciprocate the valves. Cams are driven

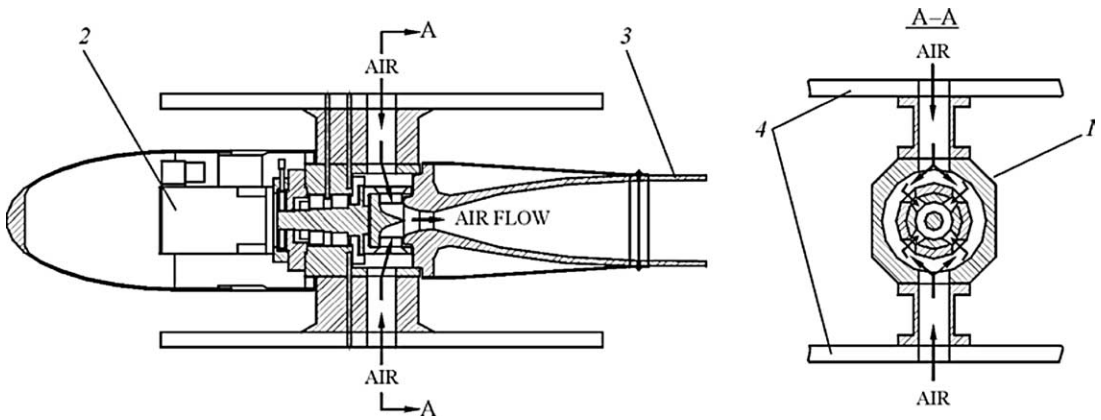

Fig. 106. Cross-sectional views of pulse-valve mechanism 1, motor 2, exhaust nozzle 3, and wind tunnel walls 4 [269].

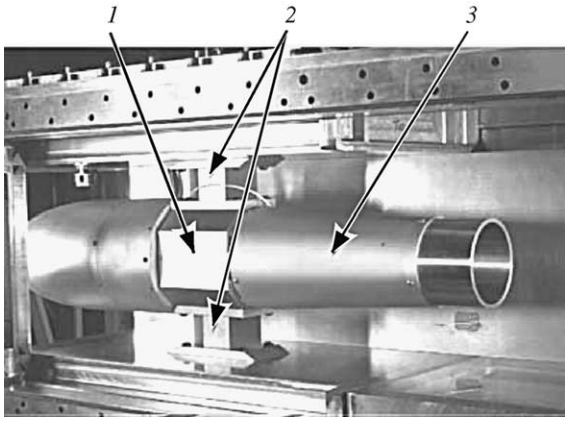

Fig. 107. Pulse valve assembly 1, air inlets 2, and exhaust nozzle 3 mounted in wind tunnel [269].

by sprockets 21, which, in their turn, are driven by chains 22. There are two supply manifolds 23 and 24 that are in communication with the intakes of the valve seats.

In operation, motor 8 will rotate core feed cylinder 1 relative to DC 6. Chains are driven to rotate cams. Cams open the valve seats 16, 17 causing the delivery of fuel–oxidizer mixture into the DC. At the same time that the cams open the valve seats, ports 3 and 5 will be out of registry, sealing ambient purge air in the core feed cylinder from entering the DC. After filling the DC with fuel–oxidizer mixture, valve seats 16, 17 will be closed due to rotation of cams and the core feed cylinder ports 3 will be closed due to the rotational position of the core feed cylinder. At this time, igniter 25 will ignite the explosive mixture causing detonation. The detonation wave propagates along the DC and discharges to the ambience through the open end 11. After the arising expansion wave decreases the pressure in the DC to a certain level, the continuous rotation of the core feed cylinder causes the ports 3 and 7 to register inducing the purge air to enter the DC and blow the residual burned gases from the chamber. The ports 3 will then rotate out of alignment with ports 7 and the cycle described above will be repeated.

Multivalve schemes of Figs. 105 and 108–110 have obvious advantages in terms of a possibility to use stratified explosive charges in PDEs. More specifically, they allow arranging the explosive charge composition in the DC in such a way that a readily detonable mixture is placed in the vicinity to igniter, while the rest of the chamber can receive the charge of decreasing detonability. In this case, the detonation wave initiated in the sensitive mixture will transmit to the less sensitive mixture in accordance with observations described in Section 2.2. The use of stratified explosive charge is one of the most promising approaches that is discussed in detail in Section 3.6 below.

A practical pulse detonation device with a mechanical valve has been reported in Ref. [273]. The schematic of the device and the dimensions of the lab-scale test tube are shown in Fig. 111a and b, respectively. The device is fed with a gasoline–air mixture from a V-shaped automobile engine 1 (see Fig. 111a) while a part of it works as a compressor preparing the mixture. This type of feeding was chosen to meet the requirement of applying the device for drilling purposes. Other applications like propulsion will certainly need different principles of mixture formation. Through reverse valve 2 of the automobile type, the combustible mixture is delivered into the ignition chamber 3, 100 mm in diameter. The mixture is ignited by the standard spark plug 4. The standard automobile igniting unit 5 needs a power supply of 12 V.

The operation principle of the device of Fig. 111a is as follows. After filling the device with the FAM, the igniter 4 is activated. The pressure rise caused by combustion closes valve 2 and pushes the mixture into prechamber 6 that serves as an additional turbulizing element. Detailed studies of the effect of such a prechamber on DDT has been reported in Refs. [273,274]. Further flame acceleration and transition to detonation takes place in the pack of seven tubes 7 (each 25 mm in diameter) connected with prechamber 6. The use of seven tubes, arranged as shown in Fig. 111a (cross-section A–A), instead of a single tube of a wider cross-section is due to the fact the DDT process takes a shorter distance in tubes of smaller diameter. An overdriven detonation wave in the tubes arises at a distance of

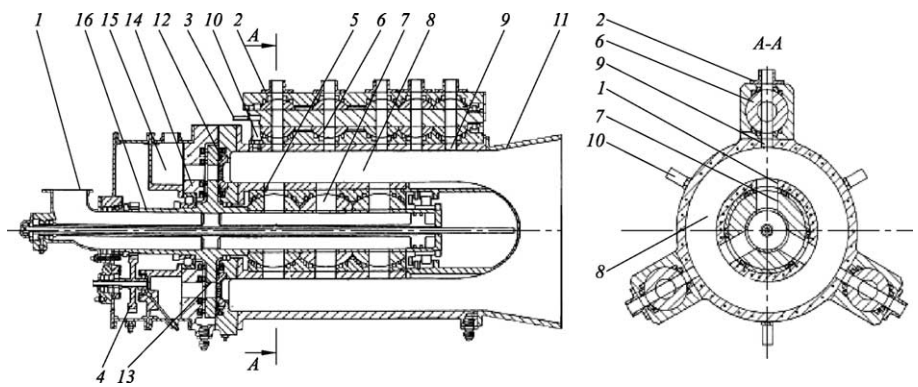

Fig. 108. Sectional views of a valved PDE with separate delivery of fuel and oxidizer in the annular DC via manifolds 1 and 2 [270].

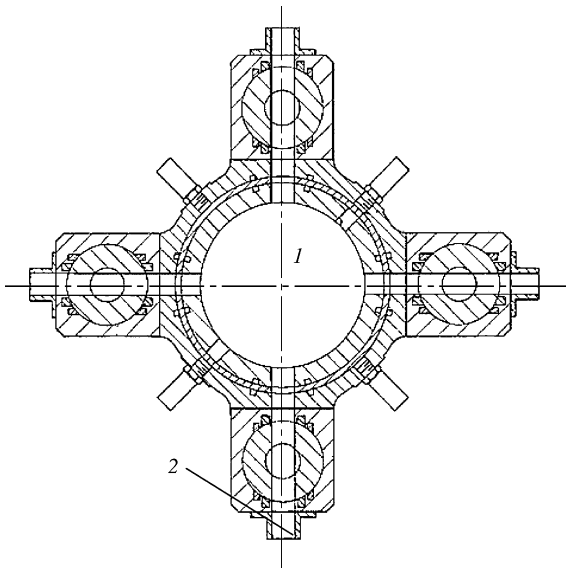

Fig. 109. Sectional view of the PDE with mechanical valves and separate delivery of fuel and oxidizer in the tubular DC 1 via inlet ports 2 [271].

2–3 m, depending on the mixture composition and initial conditions. Then the detonation wave slows gradually down to the CJ regime.

The onset of detonation took place in all seven tubes nearly at the same distance from the prechamber. To minimize the divergence in predetonation lengths, orifices were made in the adjacent walls of the tubes to provide free access of hot combustion products from one tube to another.

Using of the device of Fig. 111a for drilling purposes required the maximal intensity for the reflected wave. Investigations of wave reflections at different stages of DDT showed [275] that the maximal rates of loading were obtained upon reflection of overdriven detonation waves. Thus, the length of the device had usually the limit of 3 m to operate in the mode of overdriven detonation waves. Nevertheless, the device proved to be reliable in operating with longer tubes (up to 7 m).

The frequencies of detonation wave generation in the device of Fig. 111a varied from 5 to 10 Hz, depending on the length of the device and the power of the feeding compressor. The slowest stage of the cycle is refilling of the device with a fresh mixture, therefore refill was the limiting process that determined the pulse frequency. The maximum frequency of 10 Hz was achieved in a device with tubes 3 m long.

Lab-scale experiments were made in the tube shown in Fig. 111b. In Fig. 111b, 1 is the ignition chamber, 2 is the turbulizing prechamber, 3 is the optical section (25×25 mm square cross-section), 4 is the ignition device, 5 is the reverse valve, 6 is the piezoelectric pressure transducer. Gasoline–air mixtures with gasolines of different ON (76 and 92) were detonated. The experiments showed that the predetonation length was shorter for gasoline of ON 76. Increasing the mixture temperature from 20 to 70 °C resulted in shortening of the predetonation length and time.

Reported in Ref. [276] are the results of tests of the four-tube, valved, research PDE shown in Fig. 112. The research engine design is based upon the automobile cylinder head valve system, shown in Fig. 113. Valving and tube mount systems have been redesigned to permit higher frequency operation, quick valve system and detonator tube configuration change-outs, and eliminate fatigue problem areas. As the operating conditions of PDE's are somewhat similar to internal combustion engines, many of the components can be shared. By driving the overhead cams with an electric motor, the four valves in each of the four cylinders can be

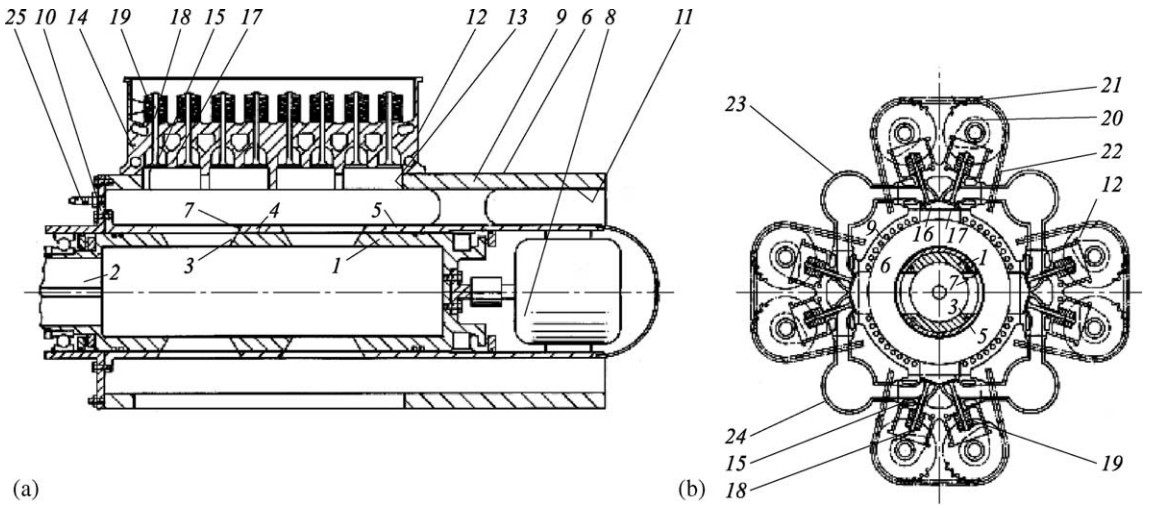

Fig. 110. Schematic of PDE using the valve assembly resembling that of automobile engine [272]. (a) PDE with one valve assembly, (b) PDE with four valve assemblies spaced equally around the sidewall.

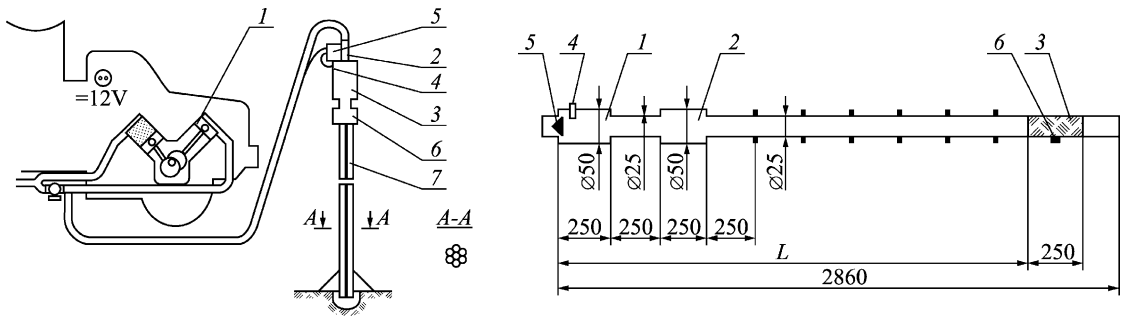

Fig. 111. (a) Schematic of the pulsed detonation device with a mechanical valve fed by gasoline–air mixture from an automobile engine. The cross-section A-A shows a pack of seven detonation tubes; (b) schematic of the experimental detonation tube with a mechanical valve [273]. Dimensions in mm.

made to operate at between 0.5 and 40 Hz. Many different detonator tube configurations are possible and interfaces are available including single and multiple tube configurations with tubes ranging from 20 to 150 mm in diameter and various lengths; 0.3–2 m being typical. Provisions for lubrication, cooling, ignition, and fuel delivery are integral to the cylinder head/intake manifold assembly.

The two intake valves in each cylinder, visible in Fig. 113, are used to feed premixed air and fuel into detonation tubes, which are attached to an adapter plate secured by the head bolts. In the configuration of Fig. 112, the head and detonation tubes are installed horizontally, and the intake valves are the upper pair in Fig. 113. Cold air flows through the exhaust valves in reverse as a purge gas to buffer hot products from igniting the next incoming charge and to convectively cool the inside of the detonation tube walls.

The research PDE of Fig. 112 is operated premixed, minimizing mixing and stratification issues. To obtain detonation with the weak ignition source (spark plug), the enhanced DDT concept is used (see Section 3.5). The large pop-off valves and check valves visible in Fig. 112 are some of the precautions used to prevent catastrophic failure in the event of an engine backfire through the premixed intake section. The detonation tubes can be run at 90° out of phase. The main combustion air and purge air lines contain ball valves for each detonation tube feed system so that the engine can be run with one tube, two tubes 180° out of phase, or all four tubes. A rotary position sensor is adapted to the intake camshaft to provide both an index of the valve timing sequence and the relative position of the valves. This signal serves as the master timing signal for the ignition and data acquisition systems.

An eight-channel igniter/fuel injection control box is triggered off the rotary position sensor. Separate control of each detonation tubes igniter and/or fuel injector can be accomplished with this system. Vapor fuels are premixed with the combustion air via a separate critical flow nozzle and flow control system. Due to the high noise levels associated with PDE testing, all controls and data acquisition are performed remotely from an isolated control

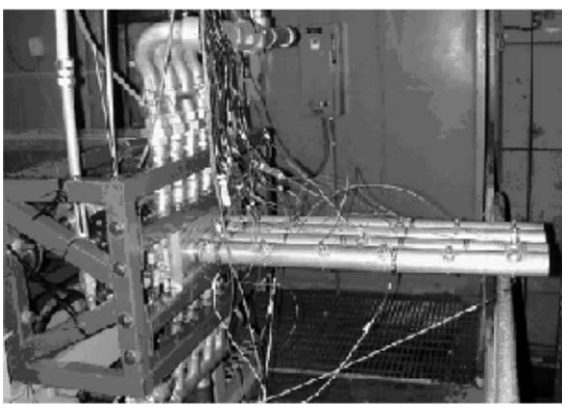

Fig. 112. Four-tube research PDE installed on a damped thrust stand. The upper manifold supplies premixed fuel and air; the lower manifold provides purge cycle of clean, unfueled air [276].

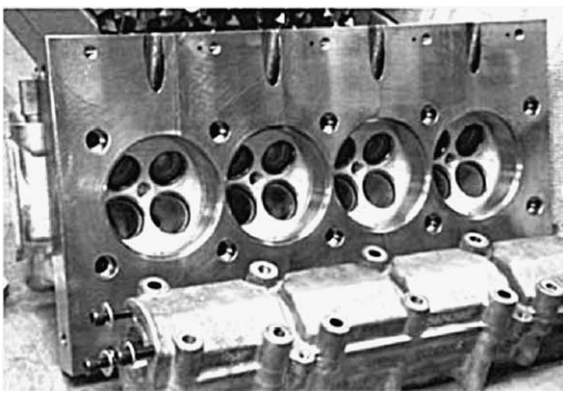

Fig. 113. PDE valve assembly based on the automobile cylinder-head valve system. Each of the four tube positions contains two intake valves (the upper pairs) and two exhaust valves, which are currently used for purge cycles (the lower pairs of valves). The stock igniter location (smaller central hole between four valves) is typically used for ignition [276].

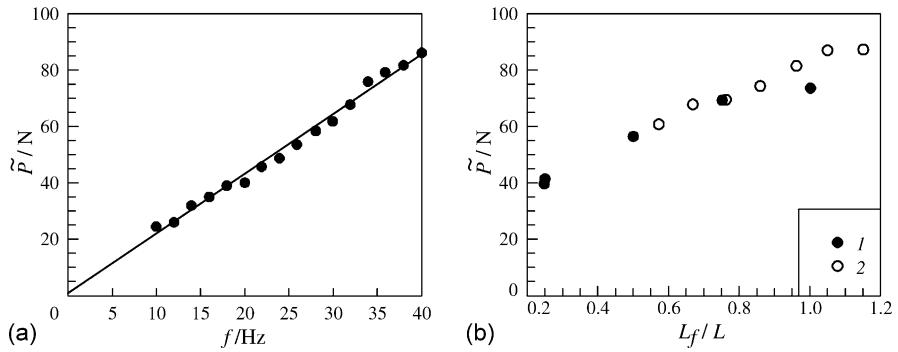

Fig. 114. (a) Measured thrust $\tilde{P}$ vs. frequency f, and (b) thrust $\tilde{P}$ vs. tube fill fraction for hydrogen–air (1) and ethanol–air (2) mixtures [276].

room. Further details on the research facility and engine are available elsewhere [277,278].

The research engine of Fig. 112 has been run in multitube mode, demonstrating both two-tube operation 180° out of phase and four tube operation 90° out of phase. A wide variety of frequencies have also been demonstrated indicating the simple linear scaling of thrust $\tilde{P}$ vs. frequency f as shown in Fig. 114a. This data also demonstrates the accuracy of the thrust measurements, as the deviation from the linear dependence is ± 2.2 N. Such thrust measurements have been demonstrated with the current system down to 13 N but the accuracy and thrust range can be varied with configuration changes.

In addition to frequency alterations, thrust modulation may also be accomplished via variation of the length of the tube L_f filled with a detonable mixture. Via volumetric flow control, the tube fill fraction L_f/L was varied with the resulting impact upon thrust measured as shown in Fig. 114b. Similar results were observed with both hydrogen and liquid fuels. Fill fractions $L_f/L > 1$ typically result in a cloud of combustible mixture around the end of the detonator tube that does not contribute to the thrust. Fill fractions $L_f/L < 1$ result in a detonation driving either purge cycle and/or products from the previous cycle. This results in the same effect as a bypass ratio in a turbofan engine, in that a bigger mass is moved at a lower change in velocity with resultant gains in efficiency.

3.3. Valveless concepts

Valveless PDE concepts imply continuous or intermittent supply of propellants (fuel and oxidizer) to the DC without using mechanical valves.

Fig. 115 shows an example of the PDE without mechanical valve [279]. The PDE comprises DC 1, manifold 2 providing the supply of oxidizer and manifold 3 providing the supply of fuel, fuel and oxidizer tanks (sources) 4 and 5, initiating means 6, means 7 for cooling the fuel and oxidizer manifolds, and manifold 8 having control means for feeding an inert gas. The pressure in the fuel and oxidizer sources is maintained constant and different (e.g. for the sake of definiteness, the oxidizer pressure is higher than that of fuel). In operation, fuel and oxidizer are fed into the DC in which they are mixed to form an explosive mixture. After activating the initiator 6, the detonation wave forms and traverses the DC. The pressure of detonation products is substantially higher than the initial pressure in the chamber and in the admission manifolds. Therefore, the products are expelled into manifolds 2 and 3 and are cooled by the cooling means 7. The speed and depth of products penetration into the manifolds depend on the pressure differentials between DC and the corresponding tanks (sources). As the pressure in the DC diminishes due to the outflow of the detonation wave into the ambience through the open end of the chamber, the direction of the flow in the manifold of the tank with higher pressure (oxidizer) is reversed. Further reduction of pressure results in the change of the direction of flow in the manifold attached to the tank with lower pressure (fuel). The detonation products cooled in the manifolds 2 and 3 flow back to the DC to form a buffer zone. Moreover, after the high-pressure manifold is free of the detonation products, the oxidizer begins to flow into the DC and, when mixed with the cooled detonation products, additionally cools the products. After the low-pressure manifold is also free of the detonation products, fuel starts to flow into the DC and mix with oxidizer to form the explosive composition.

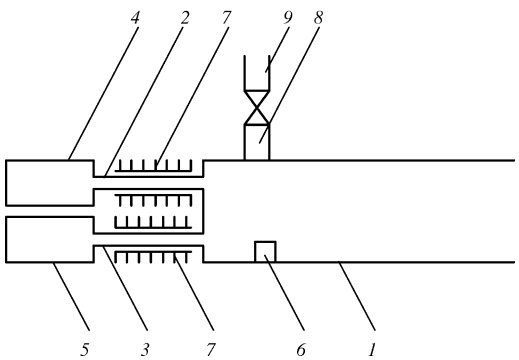

Fig. 115. Valveless PDE with separate delivery of fuel and oxidizer in the DC 1 via wide manifolds 2 and 3 [279].

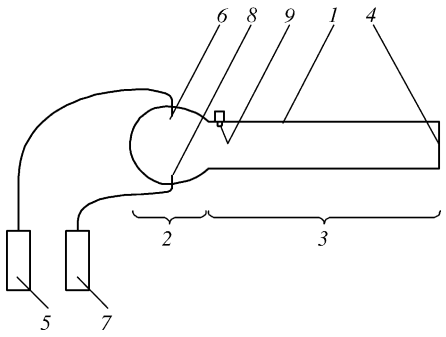

Fig. 116. Schematic of the valveless PDE with separate delivery of fuel and oxidizer in the DC 1 via small orifices 6 and 8 [280].

Now, the fuel–oxidizer mixture is separated from hot detonation products left in the chamber after the preceding cycle by the buffer zone consisting of the detonation products cooled significantly to avoid premature ignition of the fresh charge. If the cooling means applied are insufficient to avoid the premature ignition of the new charge, additional means can be used to feed inert gas, such as nitrogen, into the DC. In this case, nitrogen is fed into the DC through manifold 8 in the zone adjacent to the oxidizer and fuel manifolds after every detonation cycle.

A simple valveless scheme of PDE that is somewhat similar to that shown in Fig. 115 has been suggested in Ref. [280]. Fig. 116 shows the schematic of the PDE. The PDE has a DC 1, which is comprised of the first, widened, portion 2 and a second, straight, portion 3. The DC is open at one end 4. Fuel from fuel tank 5 is introduced into portion 2 through an injection orifice 6. Oxidizer from a second source tank 7 is introduced into portion 2 through an injector orifice 8. The fuel and oxidizer gases mix within portion 3 of the DC. After the gases become suitably mixed and fill both portions 2 and 3 of the detonation tube, initiation energy is introduced at point 9. Detonation of gases causes the formation of a detonation wave traversing through the DC. The overpressure created by detonation stops the flow of fuel and oxidizer into tube 1 at injection orifices 6 and 8 as long as the pressure in tanks 5 and 7 is less than the pressure of detonation products. As the detonation wave traverses the full length of the DC, the pressure in the chamber decreases and drops below the pressure in tanks 5 and 7. Once it happens, the filling of the DC with fuel and oxidizer resumes. At this point in time, the system has undergone a complete cycle and is beginning the next cycle.

Practical implementation of the schemes suggested in Refs. [279,280] (see Figs. 115 and 116) has been performed in Ref. [281]. The operational principle of the pulse device tested is shown in Fig. 117. Similar to Ref. [279], the essence of the principle is in creating the separating gas volume between the fresh combustible mixture and hot detonation products. The operation cycle starts from filling the DC 1 (see Fig. 117a) with fresh mixture 2 of fuel and oxidizer delivered separately via feed manifolds 3 and 4, respectively. Ignition of the mixture by electric spark 5 results in combustion followed by transition to detonation, which propagates towards the DC open end filling the DC with combustion products 6 (Fig. 117b). The pressure inside the DC increases above the pressure inside fuel and oxidizer feed manifolds. Combustion products penetrate into the feed lines and interrupt the flow of fuel and oxidizer to the chamber (gasdynamic valves are closed!). After the detonation wave reaches the DC open end, the rarefaction wave propagates into the combustion products. At a certain time, this rarefaction wave reaches the contact boundary between the combustion products and fuel and oxidizer inside the corresponding feed manifolds and terminates the expansion of the combustion products into the feed manifolds (see Fig. 117c) (gasdynamic valves are open1). After this moment, all gases propagate towards the DC open end. Uncontrolled ignition of the fresh combustible mixture 2 is prevented by the 'cold' combustion products 7 cooled in the feed lines (Fig. 117d). Thereafter, the DC is filled with fresh combustible mixture 2 again and the cycle is repeated.

After ignition of the combustible mixture, the following characteristic times of processes contribute to cycle duration t_c:

t_{in}	detonation formation;
t_{tr}	detonation traversing the DC;
t_e	period of adiabatic expansion of combustion products from the DC;
t_{cp}	period of outflow of combustion products from the fuel and oxidizer feed manifolds; and
t_{fl}	period of DC filling with the combustible mixture.

Thus, the operation frequency depends on the following basic parameters: DC length, L_{DC}, its diameter, d_{DC}, length of the fuel and oxidizer feed manifolds, L_{fd}, their diameter, d_{fd}, pressure inside the feed manifolds, p_{fd}, the type of fuel and oxidizer and oxidizer-to-fuel ratio, α. Based on these parameters, one can estimate the maximum operation frequency of the device.

For a propane–air mixture in a DC of constant cross-section with $L_{DC} = 1$ m, $d_{DC} = 16$ mm, six (6) feed tubes for fuel and oxidizer with $d_{fd} = 6$ mm and $L_{fd} = 6$ m, the estimated values of characteristic times are listed in Table 15 with t_{Σ} and f_{max} denoting the total time and maximum frequency, respectively. For the DC of variable cross-section, 1.71 m^3 in volume, with a diameter of the outlet opening 16 and 25 mm, the characteristic times of the cycle and maximum pulse frequency are presented in Table 16. The stoichiometric mixtures $CH_4 + 2O_2$, $2H_2 + O_2$, and H_2 + air were considered. The pressure in feed manifolds was equal to 0.3 MPa. It follows from Table 15 that characteristic times t_e, t_{cp}, and t_{fl} are the longest. They amount to 99% of the total cycle duration at low frequencies (<4 Hz) and 74% at high frequency of 92 Hz. Thus, reduction of these characteristic times is expected to be the most promising approach to increasing the maximum

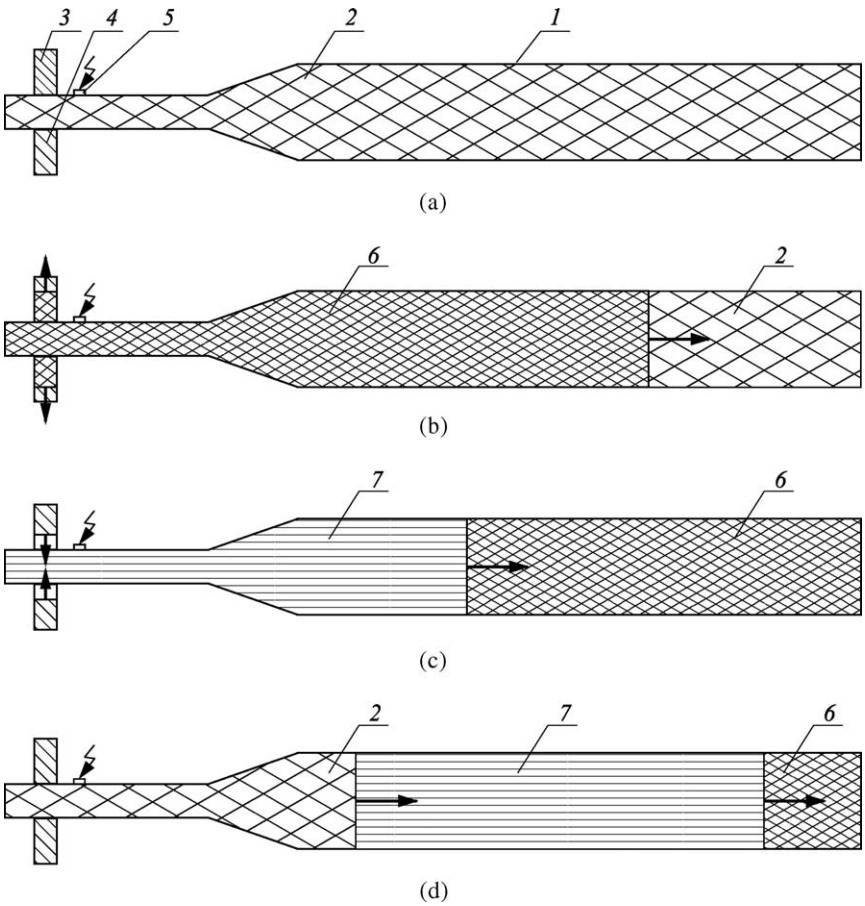

Fig. 117. Operation cycle of a DC in Ref. [281]: 1—DC, 2—fresh combustible mixture, 3,4—fuel and oxidizer feed manifolds, 5—spark plug, 6—hot combustion products, and 7—cold combustion products.

operational frequency, f_{max}. The maximum operation frequency can be increased by increasing the total cross-section area of the fuel and oxidizer feed manifolds and by increasing the pressure inside the manifolds. However, it is impractical to increase f_{max} significantly by these means because the volume of cooled combustion products decreases and their temperature increases, which may lead to ignition of the combustible mixture by the detonation products of the previous cycle.

For DC of a variable cross-section, the time of adiabatic expansion of the combustion products, t_e, becomes important as its value decreases with an increase in the outlet diameter d_{DC}. Heating of DC walls by detonation products is another factor limiting the operation frequency. In Ref. [281], during operation, an intense heat flux from the combustion products to the DC walls was detected. The flux depends mostly on the temperature of the products and detonation frequency. Depending on the cooling and

Table 15
Influence of pressure inside feed manifolds, p_{fd}, on the characteristic times determining the PDE cycle frequency [281]

p_{fd} (kPa)	t_{in} (ms)	t_{tr} (ms)	t_e (ms)	t_{cp} (ms)	t_{fl} (ms)	t_Σ (ms)	f_{max} (Hz)
2.5	1.1	0.3	1.42	132	91.2	226	4.25
294	1.1	0.3	1.42	3.33	4.66	10.86	92

Table 16
Estimated characteristic times and pulse frequencies for several PDE configurations [281]

Mixture	t_{in} (ms)	t_{tr} (ms)	t_e (ms)	t_{cp} (ms)	t_{fl} (ms)	t_Σ (ms)	f_{max} (Hz)
$d_{DC} = 16$ (mm)							
$CH_4 + 2O_2$	1.0	1.25	6.6	9.40	16.9	35.0	28.6
$2H_2 + O_2$	1.0	1.07	5.3	7.50	11.3	26.5	37.7
H_2 + air	1.0	1.55	8.0	9.20	14.9	35	28.6
$d_{DC} = 25$ (mm)							
$CH_4 + 2O_2$	1.0	1.25	2.7	4.70	6.9	20	50.0
$2H_2 + O_2$	1.0	1.07	2.2	3.80	4.6	13	76.7
H_2 + air	1.0	1.55	3.3	4.65	6.1	17	58.8

operating conditions, the temperature of DC walls changes and can become higher than the self-ignition temperature of the mixture. The latter can result in transition of detonative combustion to the conventional deflagration mode. With the DC of $d_{DC} = 16$ mm, the heat loss to the wall was about 40% of the chemical energy released at $f = 1$ Hz and up to 28% at a few dozens of hertz. The end section of the DC exhibits a 1.5-fold more stressed thermal state than the head section. At frequencies above 3 Hz, the wall temperature of DC with natural cooling reaches the self-ignition temperature of the combustible mixture (stoichiometric methane–oxygen mixture) and uncontrolled spontaneous ignition takes place. In this case, DC walls must be forced cooled.

Another example of the valveless PDE approach has been described in Ref. [96]. The experimental setup of Ref. [96] includes a direct-connect air facility and the actual PDE (see Fig. 118a and b). The direct-connect facility operates at airflow rates of up to 1.3 kg/s and provides the engine with air inlet temperatures of up to 425 K. The air is heated by a hydrogen vitiator 1 (see Fig. 118a) with make-up oxygen and a maximum outlet temperature of 725 K. The vitiator outlet is connected via three-way valve 2 to the engine inlet 3 through a 6.35 cm diameter flex hose. The main combustor 4 is 127 mm in diameter and 1830 mm long. The engine is mounted on two slide rails 5 to allow for thrust measurements using load cell 6. The engine geometry is shown in Fig. 119 with exploded views of selected areas.

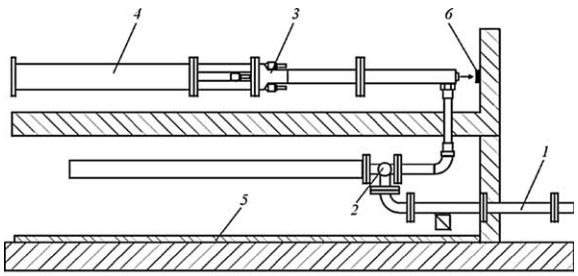

(a)

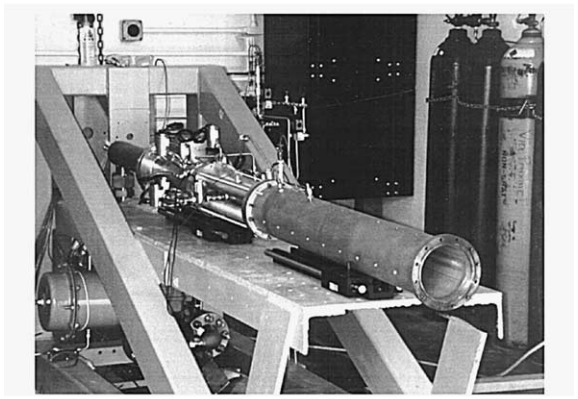

(b)

Fig. 118. (a) Experimental layout of a PDE and (b) test cell view of experimental setup [96]. 1—vitiator, 2–3-way valve, 3—inlet manifold, 4—main combustor, 5—slide rails, and 6—load cell.

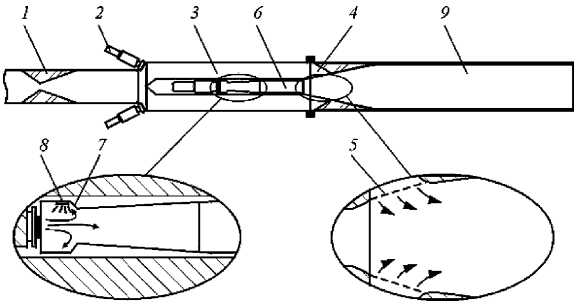

Fig. 119. PDE geometry [96]. 1—outlet choke, 2—fuel injector, 3—fuel/air arms, 4—plenum, 5—perforated cone segment, 6—pre-detonator, 7—ramp, 8—spark plug, and 9—main combustor.

The engine inlet choke 1 isolates the vitiator from pressure oscillations in the main combustor and allows for redundant metering of the vitiated airflow. Fuel is injected by four air-blast injectors 2 just after the inlet choke and is allowed to mix completely with the air while flowing through 38 mm diameter inlet arms 3 with lengths of 450 mm. The atomizers produce sprays with very low SMD values (7–10 μm) over a wide range of flow rates. The inlet arms discharge into a plenum region 4 where the mixture is directed to flow through a perforated cone segment 5 in order to provide increased turbulence, mixing, and partial acoustic isolation. The porosity of the cone was varied between 15 and 40%. The predetonator 6 is composed of a head-end cavity region to aid in confinement and utilize a rearward-stepped diffusion ramp 7 to increase turbulence levels and prevent fuel adhesion to the walls. The predetonator is 38 mm in diameter and 203 mm long (resulting in 1% total combustor volume) and is operated with a JP-10–oxygen mixture at an equivalence ratio of 1.25. Spark plug 8 is used to ignite the reactive mixture in the predetonator. The predetonator is located on the combustor axis and discharges into the main combustor 9 at the same location as the four fuel–air inlet arms. This geometry was determined to provide the most rapid and reliable generation of a detonation wave in a JP-10–oxygen aerosol [282]. Although the length of only 170 mm is required for the detonation to form, a total length of 25 cm is used to allow the wave to reach a steady propagation velocity. Direct transition of the detonation wave from the predetonator to the main combustor is generally observed.

With the setup shown in Figs. 118 and 119, the repeated detonation of a homogeneous FAM (e.g. ethylene–air) as well as two-phase JP-10–oxygen and JP-10–air mixtures was obtained. For two-phase JP-10–air mixture, the maximum operation frequency achieved was 10 Hz. It is important to mention that the device of Fig. 118 operates on a continuous air flow and, in case of JP-10–air mixture, on fully or partly vaporized aerosols possessing SMD values below 3 μm and a fuel vaporization degree of at least 70%.

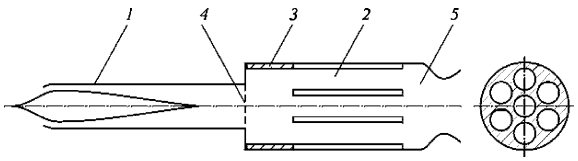

Fig. 120. Valveless scheme of PDE with a coaxial, mixed-compression, supersonic inlet [265,283]. 1—inlet, 2—DC, 3—acoustic cavity, 4—isolator, and 5—nozzle.

The observed head-end pressures for the continuous airflow geometry appeared to be approximately 30–35% below a comparable closed head-end system. The slightly longer blow down process after a cycle may be exploited in a PDE based on this principle to provide additional thrust.

The valveless scheme of PDE with a continuous airflow through the coaxial, mixed-compression, supersonic inlet, shown in Fig. 120 has been thoroughly evaluated in Refs. [265,283]. This configuration is similar to the valved configuration of Fig. 102, however, the mechanical rotary valve has been removed. As the communication between the inlet 1 and DC 2 is now open, periodic detonation initiation in the DC tubes generates pressure waves that propagate upstream from the combustor through the acoustic cavity 3 and perforated isolator 4, decay, and interact with the inlet flow. As a result of pressure wave reflections, the flow in the inlet diffuser exhibits oscillations. These oscillations either propagate downstream to the DC and nozzle 5 in the form of acoustic waves or are convected downstream with the mean flow in the form of vorticity and entropy waves and further reinforce the unsteady motions in the DC. A feedback dynamic loop is thus established between the inlet and combustor. In more details, the combustor–inlet interaction is discussed below in Section 3.14.

A valveless PDE scheme with a continuous airflow is described in Ref. [284] within a combined-cycle concept. It is implied that prior to switching to the pulse-detonation propulsion the vehicle has been accelerated by the other propulsion devices to a speed comparable with the CJ detonation velocity. The engine duct comprises inlet, mixing chamber, DC, and nozzle. The operation process of such a PDE is controlled by periodic changes in fuel supply into the supersonic flow. Once the fuel is supplied, the detonation wave propagates upstream. When fuel supply is terminated, the detonation wave decays to the shock wave and is convected downstream. The new cycle starts from supplying the next portion of fuel into the DC. The engine needs to be started only once. The performance of such a device has been compared with alternatives such as subsonic ramjet and scramjet.

Somewhat similar to the PDE of Fig. 120 is the valveless PDE concept studied in Refs. [285,286]. The schematic of the PDE is shown in Fig. 121. The air-breathing PDE contains common inlet 1, multiple DCs 2, hydrogen manifolds 3, and the common nozzle 4. An individual DC comprises a subsonic inlet 5, a set of hydrogen pylons with

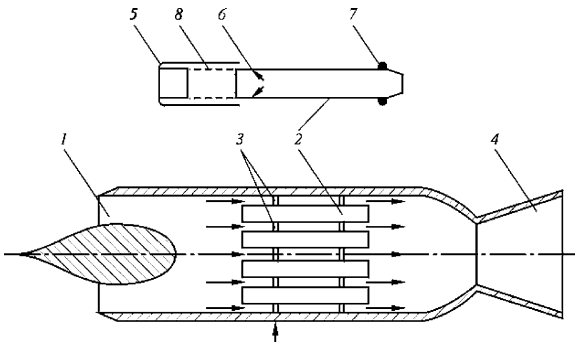

Fig. 121. Schematic of a multitube valveless PDE [285,286]. 1—common inlet, 2—DC, 3—hydrogen manifolds, 4—common nozzle, 5—subsonic inlet, 6—hydrogen injectors, and 7—igniter.

injectors 6, and igniter 7 located at the rearward end of the DC. Similar to Fig. 120, there is a provision for a tube section 8 with perforated walls (isolator) located upstream from the hydrogen injectors. The perforated section is aimed at attenuating a shock wave propagating upstream into the inlet. The total area of perforation orifices exceeds the DC cross-section area to efficiently attenuate the shock wave. Contrary to Fig. 120, in the schematic of Fig. 121 the pack of DCs is cooled with the airflow coming through the gaps between the tubes. The operation cycles of individual detonation tubes can be shifted in phase to ensure high operation frequency.

So far, the experimental and computational studies of the operation process in a single detonation tube have been performed in Refs. [285,286]. Calculations with continuous hydrogen supply revealed that hot combustion products entrained by the shock wave moving upstream can ignite the fresh hydrogen supplied by injectors and form a stabilized turbulent diffusion flame in the vicinity of hydrogen pylons. To reinitiate detonation, it is necessary to temporarily stop hydrogen supply. If hydrogen supply is terminated simultaneously with detonation initiation, the diffusion flame does not form. When, after exhaust of hot products, hydrogen supply is triggered again, the detonation cycle can be readily reinitiated.

3.4. Predetonator concept

Predetonator concept implies the use of a two-step detonation initiation process in the DC, namely, the use of an additional, highly sensitive reactive mixture contained in a tube of small diameter and readily detonated by a source of low energy, and transmitting the obtained detonation wave into the larger-diameter DC containing considerably less sensitive reactive mixture. The small-diameter tube is referred to as predetonator. To achieve direct detonation initiation with low energy (e.g. with standard spark plugs), additional oxidizer (e.g. oxygen) and/or high sensitive fuel (e.g. hydrogen, ethylene) are required, as well as the predetonators of small diameter should be used. In addition,

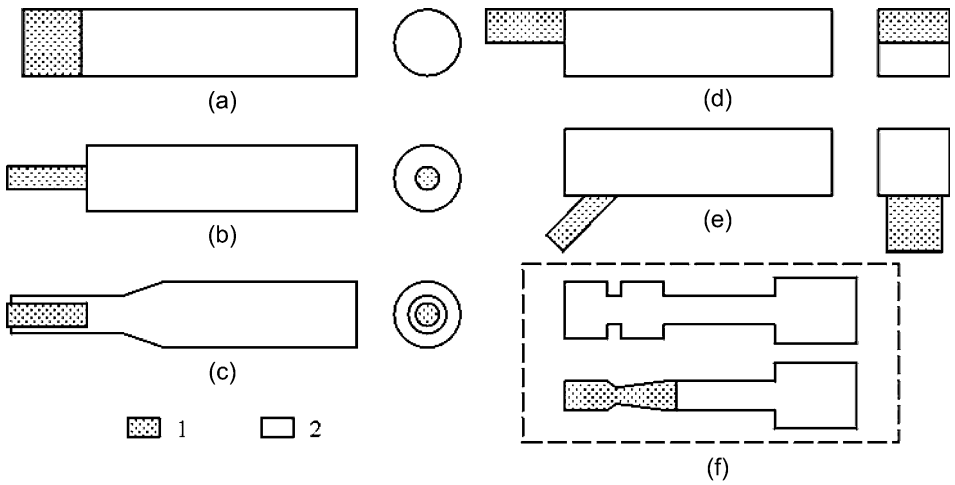

Fig. 122. Examples of predetonator concepts [290]. 1—fuel–oxygen mixture, 2—fuel–air mixture.

particular measures are needed to successfully transmit the detonation from the predetonator to the main DC. Detonation transmission from the small tube to the main chamber has been discussed in Sections 2.2.5 and 2.3.5. It is known to be easier if it is combined with local focalization devices, multiple transmission points with focalization, and with a special design for smooth transition [9]. The basic ideas that support these techniques are as follows:

1. overdriven detonations are known to be transmitted with reduced critical tube diameter [287];
2. transmission of detonation from a tube into a larger volume is enhanced by placing a central circular blockage (BR of 50%) which creates implosion followed by an intense explosion [288];
3. an adapted diverging cylinder reducing expansion between the two media helps to obtain successful transmission [289];
4. presence of composition gradient in the sense of more energetic to less energetic mixture can help detonation initiation and transmission [173].

Various initiator concepts exist and can vary from coaxial designs to transverse or splitter plate concepts just to name a few. Most concepts operate on fuel–oxygen mixtures while others utilize a blend of oxygen-enriched air as the oxidizer. Although the use of oxygen provides excellent reliability, repeatability, and a vary rapid ignition event, the minimization of the oxygen required is of paramount importance since it is treated as 'fuel' for specific impulse $\tilde{I}_{sp}$ and specific fuel consumption calculations and directly reduces the overall system performance. Another problem is that an oxygen source or generator will be required for air-breathing applications resulting in additional weight and system complications.

Thus, efficient coupling between an initiator and the larger DC is of high importance. Some examples of initiator designs are shown in Fig. 122, but many more exist at the concept level. Concept (a) simply involves the use of an oxygen-fuel 'plug' at the head-end of a DC. This concept has been shown to work well, but often requires the use of a substantial amount of oxygen. Initiator concepts (b) and (c) utilize a smaller combustor which 'transmits' a fuel–oxygen detonation wave into a larger combustor containing the FAM. Concept (b) possesses a solid back wall at the diffraction plane while concept (c) allows the wave to diffract initially to slightly larger diameter, but with less confinement than in (b). Concepts (d) and (e) are two that have been explored on a limited scale computationally and little work exists in the open literature. The last concepts depicted as caption (f) are examples of hybrid designs, which may use wall shaping/confinement and/or shock reflection/focusing to promote the generation of a detonation wave. Both concepts could also be used solely with air as the oxidizer, but would likely be limited in operational frequency, reliability, and also require additional axial length for the DDT process to occur.

The lower initiator depicted in Fig. 122f is representative of the actual predetonator in use today in Ref. [290]. The actual PDE operates with predetonator as discussed in Section 3.4 (see Figs. 118 and 119). The latest reported geometry of the air-breathing PDE is shown in Fig. 123 [291].

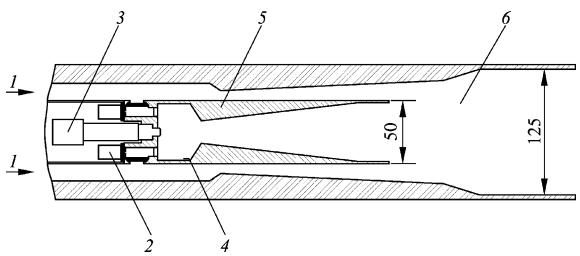

Fig. 123. Air-breathing PDE with predetonator [291]. 1—fuel–air mixture supply, 2—oxygen supply, 3—JP-10 injector, 4—igniter, 5—predetonator, and 6—main combustor. Dimensions in mm.

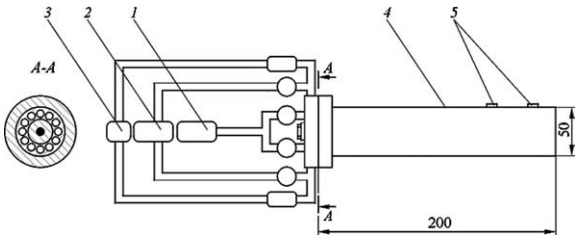

Fig. 124. Predetonator for the valveless PDE [291]. 1—fuel, 2—oxygen, 3—air, 4—DC, and 5—pressure transducers. Dimensions in mm.

The design of the predetonator is shown in Fig. 124. It is claimed that such a predetonator will allow for the PDE operation frequency up to 100 Hz. The geometry shown in Fig. 124 operates on a combination of fuel 1, oxygen 2, and air 3. A small amount of bypass air is allowed to flow through the predetonator 4 in order to purge the combustion products in between cycles. The fuel–oxygen mixture is then rapidly injected into the manifold which momentarily disrupts the air flow through the predetonator and is rapidly initiated. So far, this predetonator has been evaluated up to 50 Hz operating on ethylene/oxygen and propane/oxygen mixtures due to limitations with the ignition system. Pressure–time histories registerd by pressure transducers 5 mounted at the predetonator exit have revealed excellent repeatability as shown in Fig. 125 [291].

As mentioned in Section 2.7 the surfaces located near the initiator and the initiator itself can exhibit high thermal loads during operation. As an example substantiating this statement, Fig. 126 shows the thermal imaging of the predetonator after 5 s operation time (200 cycles at a frequency of 40 Hz) [291]. Such studies were performed to determine critical cooling areas which will require cooling in the actual PDE.

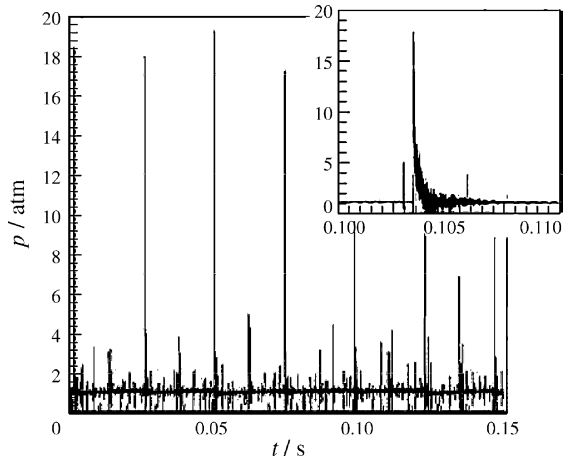

Fig. 125. Operation of propane–oxygen predetonator of Fig. 124 at frequency 40 Hz [291].

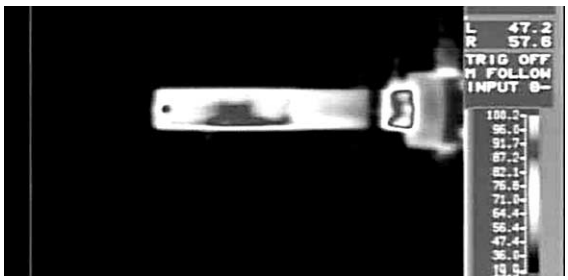

Fig. 126. IR image of predetonator after 200 cycles at frequency of 40 Hz [291].

3.5. Enchanced DDT concept

Enchanced DDT concept implies the use of various passive means to promote DDT and obtain a detonation wave in the main DC with the working mixture ignited by a low-energy source. The means to promote DDT include inserting regular or irregular obstructions (like Shchelkin spiral, orifice plates, etc.) or diverging-contracting sections in the tube, designing shock-focusing end-walls, etc.). When the concept is applied to marginally sensitive FAMs, there is often a need in using an initiating tube—a tube of a relatively small diameter filled with DDT enhancing means, as DDT is more efficient in small tubes. In this case, the detonation wave arising in the initiating tube should be transmitted to the main chamber. Contrary to the predetonator concept discussed in Section 3.4, the initiating tube is filled with the working FAM.

Fig. 127 shows the calculated snapshots of pressure and temperature contours in a PDE chamber equipped with diverging-contracting sections [292]. The detonation wave travels from left to right. The plots are shown at the time when the detonation wave has just exited from the DC. It is clear that the flow field is completely different from the detonation structure in the smooth-walled tube (see Fig. 6 in Section 2.2.1) in which triple points are the salient features.

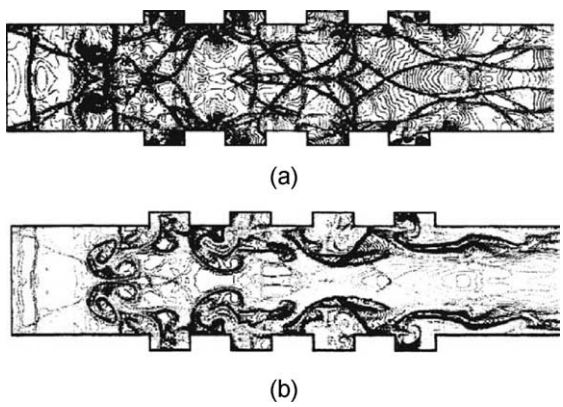

Fig. 127. Calculated snapshots of pressure (a) and temperature (b) contours in a detonation tube equipped with the diverging-contracting sections [292].

Instead, a very complex flow pattern occurs, including reflected and interacting shock waves, and local high and low pressure and temperature regions near cavities. Moreover, the cavities along the walls behave as flame holders and local hot spots to support chemical activity.

In Ref. [276], high speed digital imaging was used to study the impact of obstacles such as the Shchelkin spiral on the DDT (see Fig. 128). By utilizing an optically clear polycarbonate detonator tube, flame acceleration and formation of hot spots may be observed in Fig. 128. Obtained at 18,000 frames per second, these images depict the classical micro-explosion formation of a DDT event, the detonation and retonation propagation, as well as the expansion process during tube blow down.

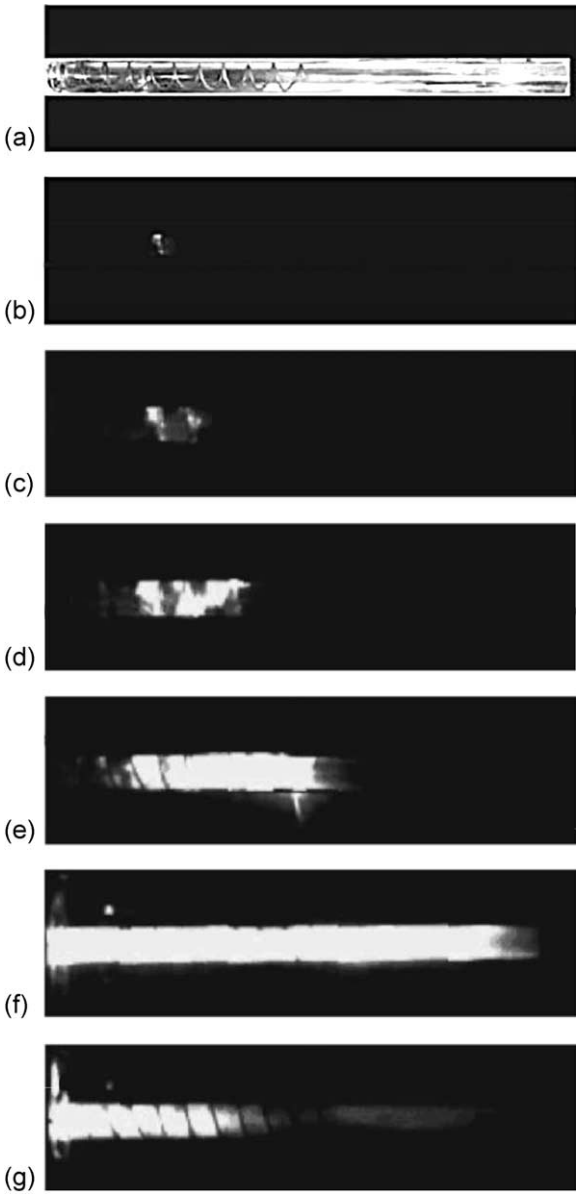

Fig. 128. High-speed digital imaging of DDT process with the Shchelkin spiral in polycarbonate tube. (a) Still of polycarbonate tube with Shchelkin spiral, (b) formation of hot spot, (c) formation of multiple hot spots, (d) micro-explosion, (e) DDT event, (f) subsequent right running detonation and left running retonation, and (g) left running expansion wave during blow down process [276].

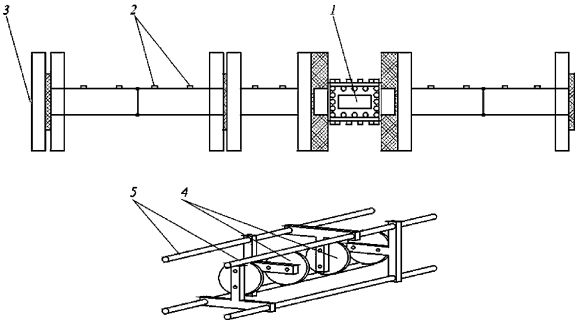

Fig. 129. Optically accessible square pulse-detonation tube, and obstacle configuration [293]. 1—window 44 × 100 mm^2, 2—ports for pressure transducers and photodiodes, 3—igniter, 4—obstacle, and 5—rods.

Pulse detonation devices utilizing the enhanced DDT concept have been attracted much attention as they do not require energetic initiators like a predetonator. Below we consider three examples of actual PDEs applying an enhanced DDT concept.

One of the pulse devices has been tested in Ref. [293]. The DDT experiments were carried out in a 1.71 m long square tube with 45 × 45 mm cross-section, giving length-to-diameter ratio of 38 as shown in Fig. 129. The detonation tube incorporates four interchangeable sections including an optically accessible section 1, pressure transducers and photodiode ports 2, and igniter 3. The obstacles 4 used for DDT enhancement consist of flat plates mounted in a helical pattern as shown in Fig. 129, similar to a Shchelkin spiral. Obstacles are mounted on four rods 5 positioned inside the tube using T-shaped supports. Spacers placed between the obstacles dictate the obstacle pitch. The obstacles are structurally robust to withstand detonation impulses, easily reconfigured to facilitate rapid design optimization and accessible to optical diagnostics.

For multicycle experiments, the oxidizer (air) and fuel were injected to the detonation tube and dynamically mixed using an impinging jet injector of the type shown in Fig. 130 [180]. The design of this injector is based on conventional rocket injector designs for achieving rapid mixing. The injector assembly, which includes a spark plug mounting arrangement, adds 60 mm to the length of the detonation tube. The propellant flows for multicycle operation are controlled by solenoid valves with opening and closing times of approximately 3 ms.

In the tube of Fig. 129 with the injector of Fig. 130, multicycle operation at repetition rates up to 20 Hz was achieved [293]. A typical series of detonation events obtained using high-speed pressure transducers are shown

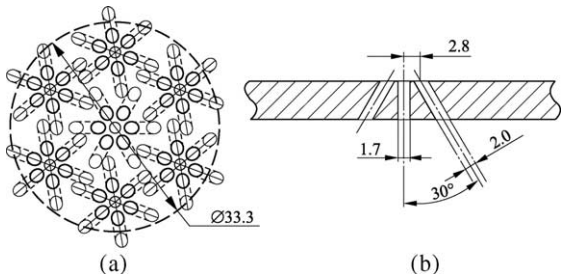

Fig. 130. Top view (a) and cross-section (b) of the impinging injector for pulse-detonation experiments [180]. The fuel is injected along the center holes with surrounding oxidizer holes. Dimensions in mm.

in Fig. 130 for the ethylene–air mixture of equivalence ratio 1.2 at a 10 Hz repetition rate. The variation in the baseline in Fig. 131 (dashed line) is due to the heating of the pressure transducer during operation. The inverting time between detonation events has been purposefully removed to allow displaying of the full set of detonations with reasonable time resolution.

As an indication of the reproducibility of the velocity profile of the detonation wave as it propagates down the tube, Fig. 132 provides a comparison between five different detonations of a forty-one pulse series. A comparison with the results relevant to a single shot is also shown. Clearly, multicycle operation shows slightly higher velocities in the DDT transition region between 0.4 and 0.6 m downstream of the injector. Nevertheless, the transition to a CJ detonation occurs at about the same location, that is 1 m downstream of the injector.

As mentioned above, operation of the 45 mm square tube of Fig. 129 was limited to repetition rates of 20 Hz. For rates higher than 20 Hz and sometimes even at 20 Hz depending on the valve timing, intermittent behavior in terms of achieving detonations on each cycle was observed. It has

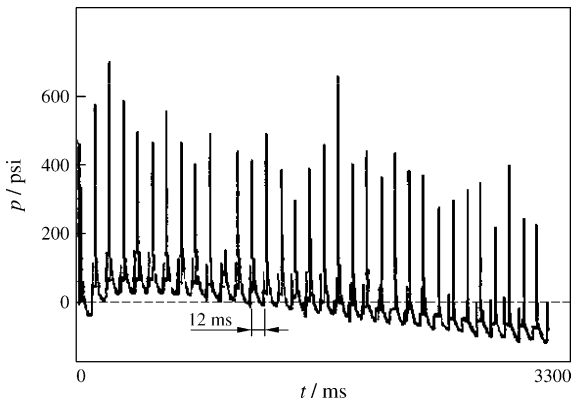

Fig. 131. Pressure profiles under multicycle operation at 10 Hz for the $1.2C_2H_4 + 3CO_2 + 3.76N_2$ mixtures at an equivalence ratio of 1.2 for the pressure transducer located 1.2 m from the injector face. Only individual pressure profiles are shown (12 ms duration) that are spaced by 100 ms from each other [293].

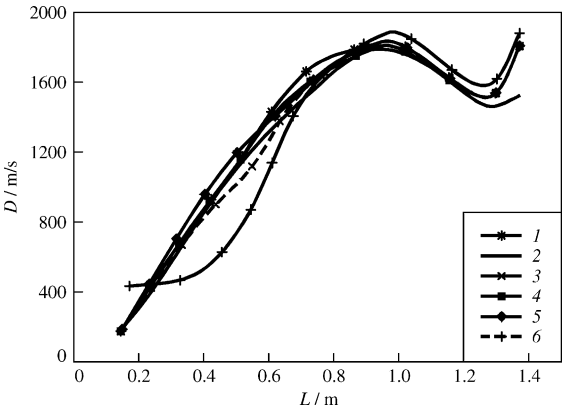

Fig. 132. Compression wave velocity as function of distance from the injector face for various individual pulses under multicycle and single-shot PDE operation [293]. 1—pulse No. 2, 2—No. 10, 3—No. 20, 4—No. 30, 5—No. 41, and 6—single shot.

been found that, when a failure to detonate the mixture occurs, combustion is observed to persist between cycles near the injector face and consumes new propellant mixture. The occurrence of the cycle-to-cycle variations that led to DDT failure was explained by trapping of hot products behind the obstacles at high repetition rates. These findings highlight the need for careful design and characterization of obstacle geometry and its effects.

The experimental facility of Fig. 129 was also used for studying a possibility to detonate propane–air mixture of equivalence ratio 1.2. Detonations of propane were not observed despite the use of several arrangements for the obstacles that had proven successful for the ethylene–air studies. The reason for this inability to observe detonation in the case of propane was attributed to the fact that the 45 mm square tube is smaller than the cell size for propane, which is approximately 50 mm. To alleviate this problem, a larger round tube (105 mm diameter) has been used [180]. In a larger tube, to detonate ethylene–air mixture there was a need in using the predetonator 33.3 mm in diameter and 2.031 m long (with obstacles) fed with the same mixture, and the 216 mm long transition cone with a 10° divergence angle. Moreover, it was necessary to install a shock-focusing obstacle at the exit of the transition section (see Fig. 35 in Section 2.4).

The other pulse detonation device utilizing the enhanced DDT concept has been already considered above (see e.g. Fig. 111 [273]). This device is essentially based on the configuration shown in Fig. 133 [274]. The device of Fig. 133 allows one to vary the length of turbulizing chambers used for DDT enhancement in the attached ducts (see Fig. 111a in Section 3.4). The side walls of chambers 1 and 2 have a thread on the inner surface. This makes it possible to screw cylindrical plates 3 and 4 more or less deep into the chambers thus varying the volume. After filling the device with a fuel (gasoline vapor)–air mixture through reverse valve 6 and igniting it by means of spark plug 5,

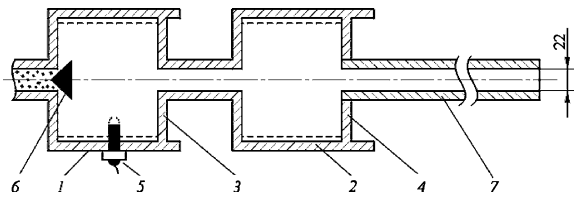

Fig. 133. Schematic of a gas-fueled pulse detonation device operating on enhanced DDT concept [274]. 1,2—chambers, 3,4—cylindrical plates, 5—spark plug, 6—reverse valve, and 7—DC.

mixture starts to burn. The gas flow induced by flame expansion gets highly turbulized due to geometry of the device and gives rise to a toroidal vortex in chamber 2. The vortex causes drastic acceleration of the turbulent flame on its entering chamber 2. Subsequent expansion of the combustion products into DC 7 produces a piston effect thus enhancing flame acceleration and promoting DDT in the DC. Cylindrical plate 4 being moved down to the bottom of chamber 2 allows investigating the DDT process in a DC with only one turbulizing chamber 1. Detailed investigations made it possible to optimize the design of the device to obtain the shortest possible DDT length and time.

In addition to the effect of geometry, the effect of initial temperature of FAM on the DDT time and length has been studied. In experiments, three characteristic time and length scales were distinguished: (i) the time (length) of shock wave formation ahead of the flame, t_s, (L_s), (ii) the earliest time (length) of detonation onset in a hot spot, t_{hs}, (L_{hs}), and (iii) the time (length) of detonation wave overtaking the lead shock and entering the undisturbed mixture as an overdriven detonation, t_{OD}, (L_{OD}) Fig. 134a [274] shows the measured dependencies of these characteristic times and the corresponding lengths (L) on the initial temperature of a stoichiometric mixture of gasoline vapor–air (gasoline of ON 72 was used) within the temperature range from 290 to 350 K.

As is evident from Fig. 134a, all the characteristic times decrease with temperature, while the predetonation lengths remain nearly constant, though a slight decrease is noteworthy. Fig. 134b shows the measured velocity of the leading pressure wave at T_0 =290 K. Curve 1 corresponds to gasoline of ON 72, whereas curve 2 is relevant to gasoline of ON 92. The increase in the gasoline ON brought to a 15–20% increase in the predetonation length. Another result of the experiments: at low temperatures, the DDT process was more stable for fuel-rich ($\Phi = 1.1$) mixtures, while at $T_0 > 320$ K the DDT in fuel-lean mixtures ($\Phi = 0.9$) was also very stable.

A similar variable-geometry pulse detonation device operating on heterogeneous FAM is shown in Fig. 135 [294]. In this device, gaseous oxidant is delivered through valve 3, liquid fuel is atomized by atomizer 4, and the mixture is ignited by spark plugs 5. Experiments showed that using air at ambient temperature as an oxidant did not allow the onset of detonation after ignition. Preheating of fuel and replacing air by Diesel engine exhaust gas containing 18% of oxygen brought to a stable repetitive onset of detonation with a frequency of up to 10 Hz (limited by the time necessary to refill the device). The use of a static reverse valve 3 based on a principle of hydrodynamic damping made the device free of moving parts and, therefore, highly reliable.

The third example of actual pulse detonation device utilizing the enhanced DDT concept is that developed and tested in Ref. [295]. This device has been already discussed in Section 3.3 as it applies the valveless concept. A schematic of a liquid-fueled pulse detonation device is shown in Fig. 136. The device comprises the assembly of several segments placed in water-cooling jacket 1. There are two initiating tubes 2 and 3 (16 and 22 mm in diameter, respectively) connected through transition cone 4; main DC 5 (83 mm in diameter) connected to tube 3 through transition cone 6, and transition cone 7 used to connect the main chamber to the optional exhaust tube 40 mm in diameter. Fuel (automobile gasoline) and air are supplied separately through manifolds 8 and 9 located

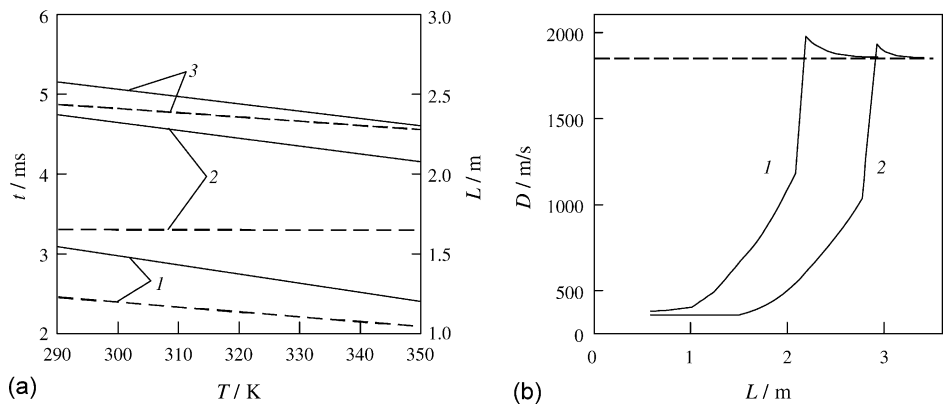

Fig. 134. Measured dependencies of the predetonation characteristics on the initial temperature [274]. (a) Predetonation time (solid curves) and length (dashed curves): 1—t_s, 2—t_{hs}, 3—t_{OD}; (b) time histories of pressure wave velocity at T_0 =290 K: 1—gasoline of ON 72, 2—gasoline of ON 92. Dashed line corresponds to CJ detonation velocity.

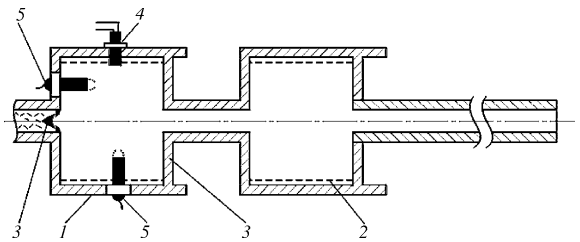

Fig. 135. Liquid–fuel pulse detonation device operating on enhanced DDT concept [294]. 1,2—chambers, 3—valve, 4—liquid–fuel atomizer, and 5—igniter.

near the end-wall of initiating tube 2. Fuel is kept in the fuel tank (not shown) and pressurized with gaseous nitrogen. Mass flow rates of fuel and air are measured by rotameters. Prior to injection into the initiating tube, fuel can be preheated in an electrical heater. The heater is designed in such a way that before injection the fuel passes through the annular gap between the facility wall and the electrically heated outer wall that is thermally insulated from the surrounding water jacket. To ignite the FAM in initiating tube 2, standard spark plug 10 is used that is fed from a regular automobile electronic ignition system. The facility is cooled with water circulating in a closed-loop jacket with an automobile radiator blown through with air. The temperature of water in the cooling jacket is controlled with a regular automobile cooling system. Heat flux in the facility walls is measured by a calorimeter. The main chamber is equipped with piezoelectric pressure transducers and ionization gauges, 11.

To start the facility, air is supplied first to obtain the mass flow rate required for repetitive operation of the facility at 2 Hz. With this mass flow rate, the whole volume of the facility can be refilled with fresh air. Then fuel, preheated up to about 70 °C, is delivered to tube 2 through the atomizer shown in Fig. 137. As the fuel inlet port is located downstream of the air inlet port, the atomizer design ensures airflow through nozzle 1 and through annular gap 2 between the nozzle and tube wall 3. The former flow assists to spray the fuel supplied through manifold 4, while the latter flow avoids deposition of fuel films and drops on the tube walls. Initially, the fuel is preheated by means of the electrical heater.

The initial ignition frequency is established at 10 Hz. At these conditions, only one-fifth of the facility volume can be filled with FAM. Due to DDT (enhanced with obstructions), detonation wave forms in the initiating tube. The detonation wave first traverses the part of the facility filled with the fresh FAM and then decays in the products of the preceding cycle. When the walls of the facility are heated so that the temperature of the cooling water attains 60 °C, the ignition frequency is gradually reduced to 2 Hz. The electrical heater for fuel preheating is then turned off and further preheating of fuel is achieved by its contact with the hot walls of the facility. The temperature of cooling water is then allowed to increase to 70–80 °C and is supported at this level by a control unit including temperature sensor, air ventilator, and cooling radiator. After attaining a steady-state operation conditions, the facility operates at 2 Hz for several hours. Monitoring of pressure and ionization current in various locations of the main chamber indicates that the facility operates with repetitive detonations. In the experiments, no restrictions in increasing the operation frequency of the facility was revealed. As a matter of fact, with methane–oxygen mixture, a frequency of 92 ± 1 Hz was attained at the facility [281].

3.6. Stratified-charge concept

Stratified-charge concept implies controlled injection of propellants into the PDE DC aimed at formation of the explosive charge with variable spatial sensitivity to

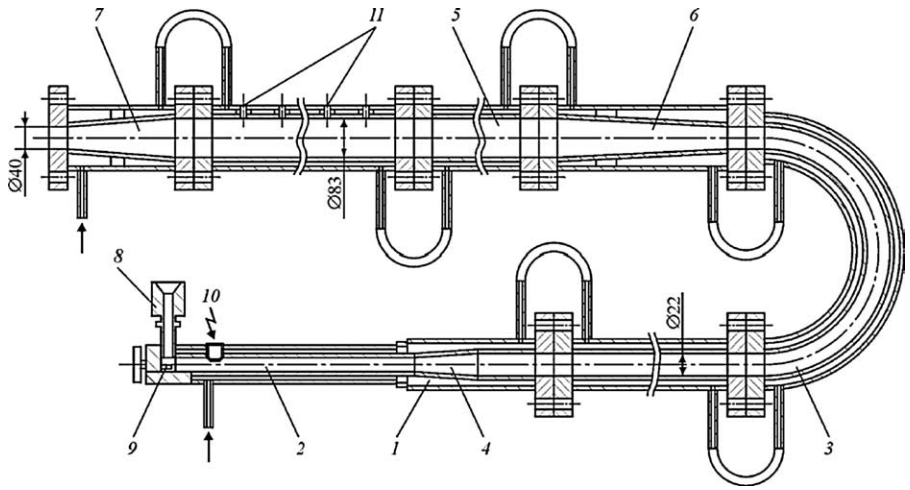

Fig. 136. Schematic of water-cooled liquid-fueled pulse detonation device [295]. Arrows show water ports in the water-cooling jacket 1. Fuel and oxidizer are injected in the DC separately through manifolds 8 and 9. Dimensions in mm.

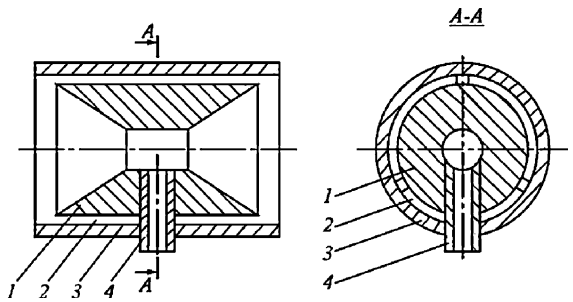

Fig. 137. Fuel atomizer used in the facility of Fig. 136 [295]. 1—nozzle, 2—annular gap, 3—tube wall, and 4—fuel manifold.

detonation. Stratified explosive charge can be obtained by proper timing of fuel and/or oxidizer valves, by controlled distributed injection of fuel and/or oxidizer along the DC, or by various geometrical means creating a proper vortical structures in the tube.

One example of applying the stratified-charge concept has been reported elsewhere [209,296] and is shown in Fig. 138a. The facility is a 5.8 m long tube of inner diameter 100 mm. It is made of 56 modules each 100 mm long. Each module features four tapped holes separated by 90°. Two opposite holes are fit with fuel injectors (see Fig. 138b), other two holes can be fit with a plug, an ionization detector or a pressure transducer. The top flange has been equipped with a fuel delivery system that can be used to supply various stoichiometries and fuel–oxidizer combinations (e.g. acetylene–oxygen) in near-plug-flow conditions. This permits the top of the tube to be used as an initiator section. In operation with liquid fuel, the top four modules in the tube do not inject liquid fuel while the remaining modules are outfitted with automobile-type fuel injectors. Initiation of spray detonation in the facility is achieved using an incident gaseous detonation wave. The top section of the detonation tube is filled with a stoichiometric mixture of ethylene and oxygen immediately prior to firing the fuel injectors. The fuel injectors are then fired. After a predetermined delay period, a plasma jet in the top flange is fired, which causes the gas mixture to rapidly transition to detonation. This detonation wave meets and propagates through the two-phase region, where the overdriven velocity quickly decays to a level sustainable by the spray detonation.

The distributed injection system of Fig. 138 is very flexible to provide a controlled mixture composition along the tube. In such a system, capability of detonation to transition from the sensitive portion of mixture to the marginally sensitive portion will be governed by the phenomena discussed in Section 2.6.

3.7. Dual-fuel concept

The dual-fuel concept implies that the liquid-fueled air-breathing PDE operates on two liquid fuels that are delivered to the DC by means of controlled distributed

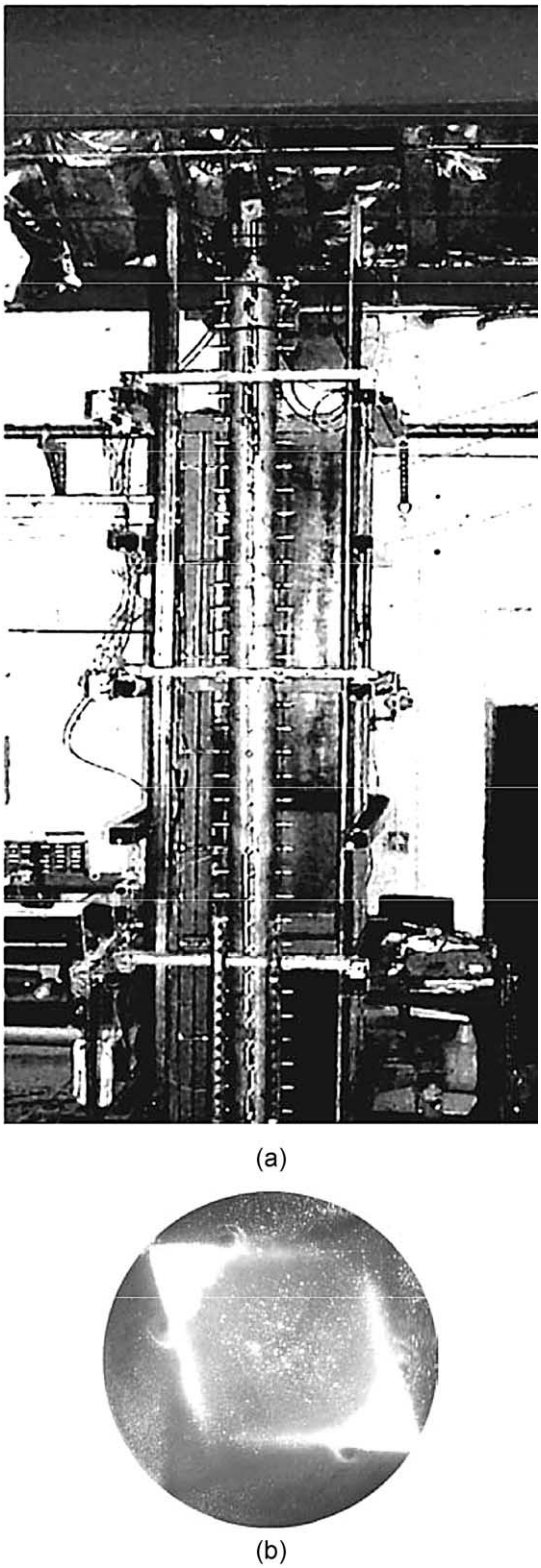

Fig. 138. (a) Modular detonation facility applying the stratified-charge concept, and (b) opposed injection configuration [209,296].

injection and in situ mixing with each other and with air. The fuels are supposed to exhibit essentially different reactivity in terms of ignition delays, burning rates, and sensitivity to detonation. On the one hand, the dual-fuel concept can be considered as the analog to the predetonator concept (see Section 3.4), as it implies the use of a two-stage detonation initiation process. On the other hand, this concept is close to the stratified-charge concept of Section 3.6 as it applies controlled distributed injection of propellants. Nevertheless, there are principal differences between the concepts. Contrary to the predetonator concept, the dual-fuel concept applies two fuels and one oxidizer (air) rather than two oxidizers (air and oxygen) and one fuel. As a result, with the dual-fuel configuration, the vehicle weight constraints can be minimized. Moreover, the dual-fuel concept avoids the use of a second DC (predetonator). Contrary to the stratified-charge concept, the dual-fuel concept applies distributed injection of different fuels rather than one fuel. In view of it the flexibility of the dual-fuel concept in terms of controlling the sensitivity of propellant to detonation can be significantly higher.

The grounds for the dual-fuel concept, first considered in Refs. [95,117,118], follow from the analysis presented in Section 2, as it is hardly possible that a standard JP fuel could meet the PDE requirements (see Section 2.4) of high detonability at variable flight conditions in terms of flight Mach number and altitude, on the one hand, and low reactivity at temperatures less than or about 800 K relevant to the premature ignition phenomenon on the other hand. With using two fuels, a readily detonable compound should be distributed closer to an initiator, and the less sensitive compound—in the rest of the DC. This implies that distributed injection of both fuels along the DC followed by their in situ mixing could be applied, e.g. as shown in Section 3.2. The other practical solution is to mix the fuels in different proportions immediately prior to injection to the DC. In this case, detonation of emulsified fuels with variable content of sensitive compound could be applied. In view of it, a number of problems arise dealing with detonability of fuel blends and emulsions within the wide range of pressure, temperature, and mixture composition. The most intricate problems are:

- controlling a local fuel–air ratio in the vicinity of the initiator to ensure robust initiation of detonation at variable conditions;
- controlling fuel distribution along the DC to ensure a desired detonability and sensitivity to premature ignition; and
- maintaining a desired overall fuel–air ratio in the course of repeated detonation initiation.

Various dual-fuel systems can be considered including gas and liquid fuels (e.g. hydrogen–JP fuel, ethylene–JP fuel, etc.) or only liquid fuels. As an example, consider a liquid-fueled dual-fuel system containing JP kerosene and concentrated aqueous solution of HP [95]. JP kerosene and HP are the conventional liquid propellants in aerospace applications. General information on physical and chemical properties of JP fuels is available elsewhere [297]. Detailed description of HP applications in various types of propulsion devices can be found [298–300].

JP kerosene can be considered to made up of approximately 79% high *n*-alkanes, 10% cycloalkanes, and 11% aromatics [301]. Gas chromatographic analysis of products shows four principal compounds: decane $C_{10}H_{22}$, dodecane $C_{12}H_{26}$, trimethylbenzene C_9H_{12}, and butylcyclohexane $C_{10}H_{20}$ [302]. Thus, JP kerosenes can be approximately modeled by a mixture of *n*-alkanes. Density of JP kerosenes varies from 760 to 810 kg/m^3 at normal atmospheric conditions. Kerosenes usually exhibit high boiling temperature (above 450–500 K) and therefore have low vapor pressure; heat of combustion is about 43–44 MJ/kg.

At normal conditions, HP is a liquid with density 1440 kg/m^3 and boiling temperature of 423.3 K. In pure HP, 47% by weight of the substance is available as oxygen. This oxygen can be used for enhancing combustion of JP kerosene in air. In addition, HP is the exothermically decomposing compound with a substantial heat release (about 5.4 MJ/kg) in the course of its decomposition to water and oxygen. HP is usually applied in the form of concentrated aqueous solutions. In the absence of contaminating catalysts and in clean containers made of noncatalytic materials, HP is known to be a stable substance. However, the intrinsic stability of HP is affected by various impurities. In practice, decomposition of HP is minimized during storage or use by the addition of stabilizers counteracting the effect of catalytic impurities or container surfaces. Highly concentrated aqueous solutions of HP are stabilized by sodium stannate, oxine, phosphates, etc. The required amount of stabilizers is very small (fractions or units of ppm). Containers for storage and transportation of concentrated HP are usually made of high-purity aluminum, Teflon, or Pyrex glass. HP solutions with the percentage of H_2O_2 less than 95–96% do not support a propagating condensed-phase detonation at normal conditions, even with powerful initiation and strong confinement. The condensed-phase detonation velocity in aqueous solutions containing 96–100% H_2O_2 is about 6500 m/s [298]. At atmospheric pressure, vapors containing 26% vol. or more HP can be exploded by a spark, by contact with catalytically active materials initially at room temperature, or by noncatalytic materials (like aluminum) that are at temperatures of about 420 K and higher [298].

The schematic of the PDE operating on a dual-fuel concept is shown in Fig. 139 [117]. The PDE comprises supersonic diffuser 1, mechanical valve 2, igniter 3, DC 4, fuel injectors 5, and nozzle 6. The operation cycle of the PDE of Fig. 139 includes four principal stages discussed above: (i) controlled distributed injection of liquid fuels by means of injectors 5 into the DC 4 and mixing of the fuels

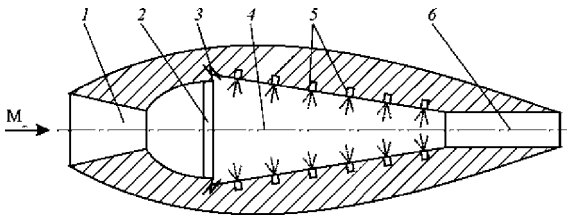

Fig. 139. Schematic of the PDE operating on a dual-fuel concept: 1—supersonic diffuser, 2—mechanical valve, 3—igniter, 4—detonation chamber, 5—fuel injectors, and 6—nozzle [117].

with incoming air, (ii) detonation initiation by igniters 3, (iii) mixture burnout in a propagating detonation wave, and (iv) expansion of detonation products through nozzle 6 to the ambient atmosphere. Subsequent filling of the DC with air and fuel components starts a new operation cycle. In principle, a provision should be made for a mechanical (e.g. rotary) valve to prevent detonations or shocks from moving outwards through the intake, to provide a sufficient time for mixing of fuel with air, and to ensure a controlled inward flow rate of fresh air. Valveless approaches of Section 3.3 can also be applied.

As the dual-fuel air-breathing PDE under consideration implies the use of liquid sprays of JP kerosene and HP, it is important to know thermodynamic properties of the multi-phase, multicomponent mixture containing JP fuel, aqueous solution of HP, and air at high temperature and pressure relevant to propulsion applications. In particular, it is important to ensure a sufficient content of JP fuel and HP in the vapor phase prior to detonation initiation. Liquid–vapor phase equilibrium for such systems is still the problem that is unsolved theoretically due to the lack of properly substantiated equations of state for most of liquids and dense vapors. For the system at hand, several promising approaches have been suggested in Ref. [303]. Based on the equations of phase equilibrium for individual components, *n*-tetradecane, HP, and water, written in the form

$$p_{\mathrm{f}}(T) = [(7.5324 \times 10^5 T)^{1/8} - 10.8801]^8$$

$$p_{\mathrm{HP}}(T) = [(2.6566 \times 10^6 T)^{1/8} - 12.5302]^8$$

$$p_{\mathrm{w}}(T) = [(2.8836 \times 10^6 T)^{1/8} - 12.4575]^8$$

(where T is temperature in K, and p is the pressure in atm, and indices f, HP and w denote fuel, HP and water, respectively) and validated up to the corresponding critical points, the equation for the total pressure of the multi-component system has been obtained. It is worth noting that the ideal solution approximation for obtaining the vapor-phase concentrations does not generally hold. For example, for the binary two-phase HP–water system the activity coefficients can be several times less than unity, in particular at small molar fractions of water (case of interest for propulsion).

If the required vapor-phase concentrations of JP fuel and HP are attained during stage (i) of the dual-fuel PDE operation, then the detonation initiation energy is primarily affected with the vapor-phase content. As predicted in Ref. [95], the critical initiation energy of a dual-fuel vapor-phase mixture can be significantly lower than that for the JP fuel–air mixture. For example, in terms of the critical initiation energy, with the admixture of 5% (vol.) and 20% (vol.) of HP vapor, the vapor-phase stoichiometric JP fuel–air mixture was shown to be equivalent to stoichiometric ethylene–air and hydrogen–air mixtures, respectively. The effect of water vapor on the critical initiation energy of the dual-fuel system is shown in Fig. 140. According to Fig. 140, the critical initiation energy E_3 of direct detonation initiation for the gaseous mixture containing *iso*-octane and air in stoichiometric composition with 20% vapor admixture of 85% concentrated aqueous solution of HP, is about 7 kJ. It is considerably less (by a factor of 1500!) than the critical initiation energy for stoichiometric *iso*-octane–air mixture. As the effect of water available in highly concentrated aqueous solutions of HP (up to 90–95%) is insignificant, Fig. 140 demonstrates that the dual-fuel system under consideration can be considered as a promising propellant for PDE.

The analysis similar to that made in Refs. [95,117,118, 303] can be performed for other dual-fuel compositions for searching promising candidates for PDE propulsion.

3.8. Shock-booster concept

One of the most challenging problems encountered in the development of PDE is detonation initiation in FAMs at distances that are feasible for propulsion applications.

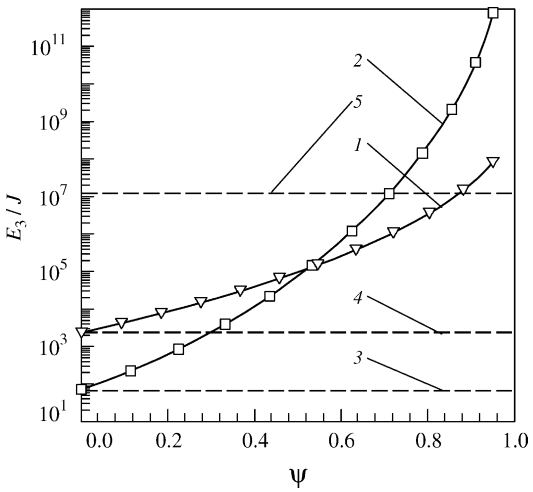

Fig. 140. Critical initiation energy for spherical detonations E_3 as a function of molar fraction of water ψ in the aqueous solution of HP for dual-fuel systems *iso*C_8H_{18}–air—20% ($(1-\psi)H_2O_2 + \psi H_2O$) (1) and *iso*$C_8H_{18}$–air—60% ($(1-\psi)H_2O_2 + \psi H_2O$) (2). Horizontal dashed lines 3, 4, and 5 correspond to the initiation energies in the systems with $\psi = 0$ and 60% H_2O_2, 20% H_2O_2, and 0% H_2O_2, respectively [95].

As is well known (see Sections 2.2.3 and 2.3.3), detonation occurs via a transient stage of strong coupling between the shock wave and the shock-induced reaction in the explosive medium.

Fundamentally, no matter how the energy is deposited into the post-shock flow: spontaneously, due to shock-induced chemical reactions, or by means of inducing chemical reactions with an external energy source. In the former approach, due to a highly activated nature of exothermic chemical reactions in FAMs, shock waves of high amplitudes and proper durations are required to ensure the coupling. Such shock waves can be obtained by means of exploding HE charges with a mass exceeding 20–30 g. The latter approach implies the use of an external energy source to artificially induce exothermic reactions closely behind a relatively weak shock wave in order to stimulate the strong coupling. Clearly, in this case, the external energy source should be distributed rather than concentrated and should provide pulse or continuous coupling of energy deposition with a propagating shock wave.

A PDE concept based on accelerating an initially weak shock wave with an in-phase external ignition of reactive mixture will be referred to as the 'shock-booster concept' according to Refs. [158,210].

Originally, the idea of using external sources to drive detonation belongs to Zel'dovich and Kompaneets [98]. They have shown theoretically that motion of an ignition source in a compressible reactive mixture at the characteristic detonation velocity would result in formation of a self-sustaining detonation in a long run. To model the moving ignition source, Zel'dovich and coworkers [93,164] considered the nonuniformly preconditioned reactive mixture, implying that the initial gradient of autoignition delay time will produce a similar effect. As a matter of fact, it has been proved computationally that temperature and composition nonuniformities in the reactive mixture preconditioned to autoignition may result in spontaneous onset of detonation. Thibault et al. [94] reported their 1D numerical study of the situation when the external energy source traveled at a constant velocity in an inert compressible medium. It has been proved that the strength of the shock wave arising in the medium depends on the energy source velocity and attains a maximum value when this velocity approaches the characteristic detonation velocity based on the specific energy (per unit mass of gas) deposited by the source, i.e. substantiated the original idea of Zel'dovich and Kompaneets computationally. Later, Yoshikava et al. [163] extended the analysis to take into account coupling between the moving energy source and the shock wave. Lee and Moen [304] have suggested the SWACER mechanism and applied it to qualitatively explain the experimental findings in photochemical initiation of detonation [305], detonation initiation by injecting hot turbulent jets into explosive mixture [161], and 'explosion in the explosion' phenomenon during DDT [306].

In Refs. [158,159], the experimental studies on a possibility to efficiently accelerate a weak shock wave by in-phase triggering of distributed external energy sources (electrical discharges) in the course of shock wave propagation along the tube filled with nonreactive or reactive mixture have been described. Fig. 141 shows their experimental setup. A detonation tube is 2 in. (51 mm)

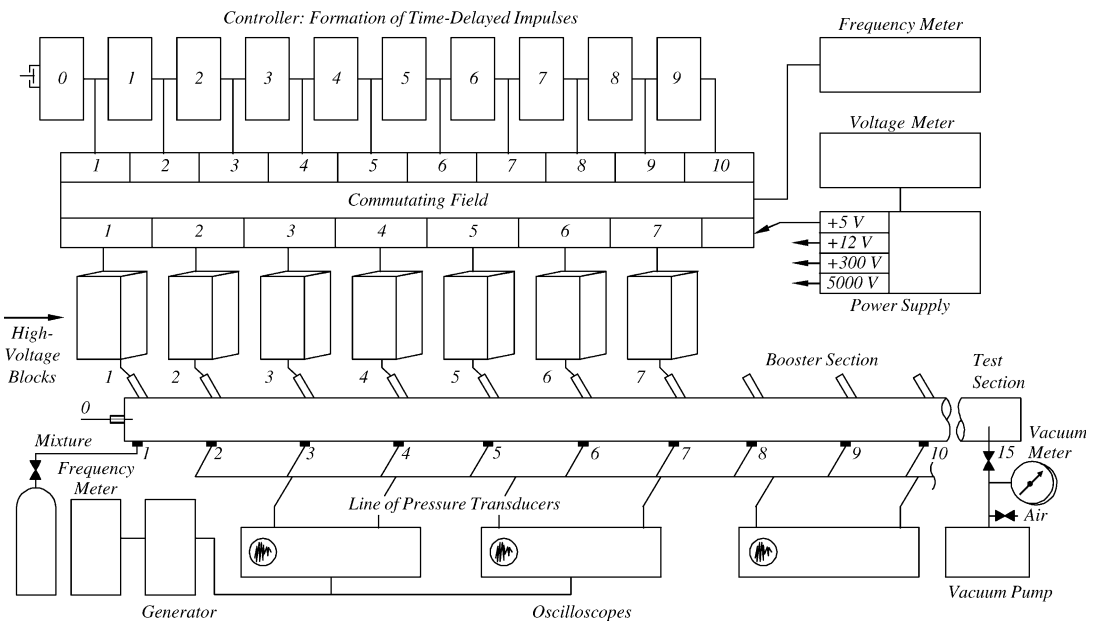

Fig. 141. Experimental setup for testing a shock-booster PDE concept, implying acceleration of a relatively weak shock wave to detonation intensities by in-phase triggering of electrical dischargers mounted along the detonation tube [158,159].

in inner diameter and 1.5 m long with closed ends. The tube comprises a booster section 1.0 m long and test section 0.5 m long connected by means of a flange. The booster section is equipped with 11 lateral ports for electrical igniters and 1 port for the aft igniter, 10 pressure transducers, and the opening for feeding a test mixture. The lateral ports for igniters are flush mounted to the tube at an angle of 45° as shown in Fig. 141. The axial distance between successive lateral igniters is 100 mm. The test section is equipped with ports for pressure transducers and ionization probes, and the opening for evacuating the tube. The distance between successive ports for the pressure transducers is 100 mm.

Three types of igniters were applied allowing one to produce electrical discharges of various duration and intensity. Igniters of type I are the prechamber-type igniters with replaceable nozzles of different diameter connecting a prechamber with the booster section. Type II igniters comprise the copper central electrode and the isolated coaxial copper cylinder with the discharge gap of 1.5 mm. The igniters of type III were also made of copper and encountered thicker discharge gaps (up to 2.5 mm). Contrary to igniters of type I, igniters of types II and III were inserted into the tube to position a tip of the electrode 15 mm from the nearest tube wall. Each igniter is fed independently with an individual high-voltage capacitor (see Fig. 141). The characteristic rated capacity was 100 μF. The discharge triggering time is controlled with a controller. The controller provides time-delayed impulses to successively trigger, via the commuting field, the individual high-voltage blocks of the igniters with a preset time delay. The time delay could be varied within a wide range (from 50 to 500 μs). The discharge intensity of each igniter is controlled by the capacitor voltage. The following values of capacitor voltage were used: 1500, 2100, 2300, and 2500 V. The duration of energy deposition of type-I igniters was determined by the prechamber nozzle diameter (2, 4, and 8 mm) and attained a value of several milliseconds for the smallest nozzle. The duration of energy deposition of type-II and III igniters was less than 80–100 μs. The high-voltage lines were properly grounded to avoid the interference with the measurement signals. The data acquisition system comprised oscilloscopes, frequency meters and a PC.

All experiments were performed at atmospheric pressure of 0.1 MPa and ambient temperature of 292–297 K. As test mixtures, three compositions were used: (i) pure air, (ii) stoichiometric propane–oxygen-enriched air (C_3H_8–$(O_2 + 3N_2)$), and (iii) stoichiometric propane–air (C_3H_8–$(O_2 + 3.76N_2)$).

The experimental procedure encountered a number of steps dealing with ‘tuning’ the controller in terms of the preset delay times for triggering the successive electrical discharges. The aim of the tuning was to obtain a blast wave of the highest possible velocity in the nearest downstream measuring base in the booster, other conditions being constant.

The tube was evacuated and filled with the test mixture. After triggering the aft igniter and lateral igniter in cross-section 1 (CS1), the shock wave velocity was measured between CS2 and CS4. Based on this velocity, a first approximation for the time delay of triggering the discharge in CS2 was obtained for the next run. This time delay was preset in the controller. The next run encountered time-delayed triggering of the aft igniter, igniter in CS1 and the igniter in CS2. By using the pressure transducers in CS3 and CS5, the shock wave velocity at this new section of the tube was then measured. In the subsequent runs, by varying the time delay of discharge triggering in CS2, the best conditions for shock wave amplification in terms of the velocity between CS3 and CS5 were obtained.

The next step was aimed at finding the best timing for triggering the igniter in CS3 to obtain the shock wave of the highest velocity between CS4 and CS6, keeping fixed the best triggering time of igniter in CS2. This procedure was continued until all available igniters were tuned in such a way that the shock wave was amplified at a maximum rate. In some cases, information on transformation of the shock wave pressure profile was additionally taken into account in choosing the optimum timing for triggering the corresponding igniter.

At each stage of the procedure, several runs were performed to collect the statistics on the reproducibility of the results. It has been found that the results were satisfactorily reproducible both in air and in the reactive mixtures.

Fig. 142 shows the distance–time diagram that summarizes the results of experiments relevant to shock wave amplification in the stoichiometric C_3H_8–air mixture.

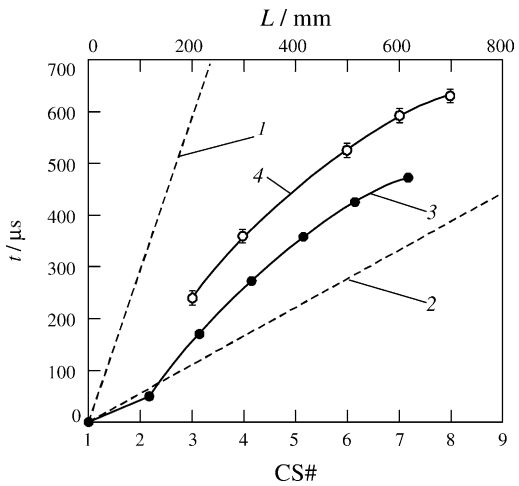

Fig. 142. Experimental distance–time diagram of shock wave amplification in the stoichiometric C_3H_8–air mixture. Detonation occurs after cross-section CS 7 [158,159]. 1—slope 342 m/s, 2—slope 1800 m/s, 3—triggering timing of igniters in various CSs, and 4—shock wave arrival timing.

The characteristic capacitor voltage in this series was 2500 V. Dashed lines 1 and 2 in Fig. 142 correspond to the characteristic values of sound and detonation velocities, 342 and 1800 m/s, respectively. Solid circles and curve 3 correspond to the optimized preset times of igniter triggering. Open circles and curve 4 approximately correspond to shock wave arrival times to booster cross-sections. Clearly, in CS8, at a distance L of about 0.6–0.7 m from the aft igniter, the detonation-like process is achieved in the booster when all available igniters are triggered in one run. This wave propagates at the velocity of about 1800 m/s in a test section as detected by the corresponding pressure transducers and ionization probes.

In a special set of runs, the optimized sequence of igniter triggering times was purposefully changed to study the sensitivity of the phenomenon to wrong timing. For example, triggering of the igniter in CS4 with the delay of 320 μs rather than with the optimized value of 270 μs in experiments of Fig. 142 resulted in failure of detonation initiation. Similar results were obtained when the triggering times of other igniters were shifted by 50 μs from their optimized values. These findings indicate that the phenomenon under study exhibits a resonant behavior.

Thus, it has been proved that the use of a sequence of relatively weak igniters with properly tuned triggering times allows one to initiate detonation in a premixed hydrocarbon–air mixture at distances as short as 0.6–0.7 m in a 51 mm diameter tube with smooth walls, i.e. at length-to-diameter ratio of 12–14. The initial (registered) shock wave Mach number in these cases was as low as 2.0–2.5. It has been found that for attaining the highest rates of shock wave amplification, the igniters should be triggered prior to the arrival of a shock wave to the igniter location. For the conditions of Fig. 142, the average advance time in triggering the igniters attains 80–100 μs, i.e. the value correlating with the estimated discharge duration. In the C_3H_8–air mixture, the shock wave velocity was gradually increasing from 850 ± 12 to 1767 ± 25 m/s by successive triggering of igniters in CS1 to CS7. Between CS11 and CS14, the shock wave propagated at the velocity of 1770 ± 25 m/s. In all series of experiments with successful detonation initiation, the igniters of type II and III were used. In all tests with prechamber igniters of type I, detonation initiation was failed, apparently due to relatively long duration of energy deposition.

Two important findings of the experiments should be emphasized. First, each discharge in the sequence deposits the energy that is much less than the energy required for direct detonation initiation by a single initiator. Second, the total initiation energy of detonation by means of successive triggering of electrical discharges is less than the critical energy of direct detonation initiation by a single initiator. The total (theoretical) energy of discharges required for detonation initiation in propane–air mixture under conditions of Fig. 142 is estimated as $E_t = (nCU^2/2)/(\pi d^2/4) = 1.68\ \mathrm{MJ/m^2}$, where n is the total number of capacitors (11), C is the rated capacitance (100 μF), U is the voltage (2500 V), and d is the tube diameter (51 mm). The value of 1.68 MJ/m^2 is close to the value of 3 MJ/m^2 reported [134] for the critical detonation initiation energy in a stoichiometric propane–air mixture. Contrary to experiments described above, plane detonations in Ref. [138] were initiated by three sorts of HE sources: liquid NM with diethylamine, plasticized HE, and a spiral of a detonating cord. As the efficiency of conversion of electrical energy into the production of blast waves is usually low [307] (about 10%) as compared to the corresponding efficiency of HE, current results can be treated as the evidence of a decrease in the total critical detonation initiation energy. As a matter of fact, successive triggering of discharges results in multiple reflections of blast waves that could promote detonation initiation. In this case, there should be a difference between the flow patterns with distant and near location of neighboring electric discharges.

Further experiments were made with liquid fuels (*n*-hexane, *n*-heptane, etc.), [160,210]. Fig. 143 shows the schematic of the liquid-fueled experimental setup with air-assist atomizer 1 mounted at the left end of the DC. The DC

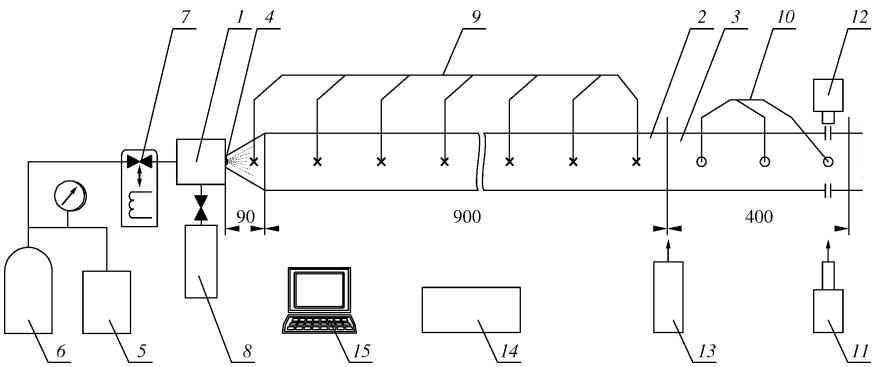

Fig. 143. Sketch of liquid-fueled experimental setup applying shock-booster concept [160,210]. 1—air-assist atomizer, 2—booster section, 3—test section, 4—cone, 5—compressor, 6—bottle, 7—solenoid valve, 8—fuel tank, 9—igniters, 10—pressure transducers and ionization gauges, 11—laser, 12—optical system, 13—droplet sizing unit, 14—controller, and 15—PC. Dimensions in mm.

comprises booster section 2 and test section 3. As in gas-fueled experiments, the detonation tube is 51 mm in inner diameter and 1.5 m long. The atomizer is attached to the test tube via the expanding cone nozzle 4. The right end of the tube is connected to atmosphere via the detonation arrester (damper)—a big steel barrel with a packing made of metal ribbon.

The air supply system comprises compressor 5, bottle 6, and air solenoid valve 7. The liquid supply system consists of the pressurized fuel tank 8 and the fuel solenoid valve. The air bottle and fuel tank are pressurized to preset pressure values before each run. When the solenoid valves are activated, air and fuel are directed to atomizer 1 that provides the entire mixture flow rate through the DC. Pulse flow duration is about 1 s.

Booster section 2 is equipped with multiple lateral ports for 'booster' igniters 9, pressure transducers, and ionization gauges. The aft igniter is located inside the cone nozzle. The first lateral igniter is mounted 100 mm downstream from the aft igniter. The distance between successive lateral igniters is 100 mm. The test section is equipped with lateral ports for pressure transducers and ionization gauges 10, diode laser 11 and optical system 12 to control tube fill with the two-phase mixture. Droplet sizing unit 13 is installed between the booster and test sections.

A specially designed digital controller 14 (based on a PC 15) controls opening and closing of air and fuel solenoid valves, as well as triggering of the aft igniter and lateral igniters.

Some results of the experiments at the facility of Fig. 143 have already been discussed in Section 2.3.3. It has been proved that shock-booster concept can be efficiently applied for initiating two-phase detonations. The schematic of a liquid-fueled PDE based on the shock-booster concept is shown in Fig. 144. The PDE comprises the air assist atomizer 1 which provides very fine fuel drops (about 5 μm in diameter), igniter 2 mounted in the chamber of optimized shape with transition cone 3, shock-booster section 4 aimed at shock wave acceleration to detonation intensities, and a detonation transition cone 5 aimed at transitioning of the detonation wave to main combustor 6. It is implied that the main combustor receives continuously the FAM via an external duct. In the schematic of Fig. 144, the detonation initiation device plays the role of the predetonator. However, in contrast to other predetonator concepts (see Section 3.4) this predetonator operates on the same fuel and oxidizer as those used in the main combustor. Also, contrary to enhanced DDT concepts of Section 3.5, the predetonator of Fig. 144 applies a smooth-walled DC rather than a DC heavily blocked with obstructions like Shchelkin spiral, etc. One of the disadvantages of the predetonator under consideration is the need in a relatively powerful energy source to ensure shock wave amplification in the booster. In view of it, some combinations of shock-booster and enhanced DDT concepts have been proposed recently [233] which minimize the energy requirements.

3.9. Shock-implosion concept

Shock-implosion PDE concept implies the use of the imploding shock wave to initiate detonation in the PDE DC. The schematic of a PDE based on this concept is shown in Fig. 145 [308]. The PDE includes four major parts: inlet 1, DC 2, discharge electrodes 3, and outlet 4. In operation, the combustible mixture entering the DC is first ignited by a standard spark plug in the front section of the DC or by the contact with the residual combustion products from the previous cycle. After ignition, the turbulent flame propagates in the DC. When the turbulent flame impinges on electrodes 3 that are connected to an energy storage capacitor, the powerful electric discharge is activated. Electrodes 3 are made with a Rogowsky profile that eliminates electric field enhancement near the electrode edges. The arising 'collar', ring-type electrical discharge creates converging shock waves in the combustible mixture, leading to detonation initiation. The rest of the reactive mixture is burned in the detonation wave that traverses chamber 2.

The shock implosion PDE concept can employ both valved and valveless schemes of Sections 3.2 and 3.3. It is important that the energy of combustion of one cycle is much higher than the electrical energy delivered by the electric discharge creating the detonation. The photograph of an actual experimental facility is shown in Fig. 146. The operational frequency reported in Ref. [308] is 148 Hz. Note that measured overpressures in the chamber, reported so far, are considerably lower than those relevant to detonation waves.

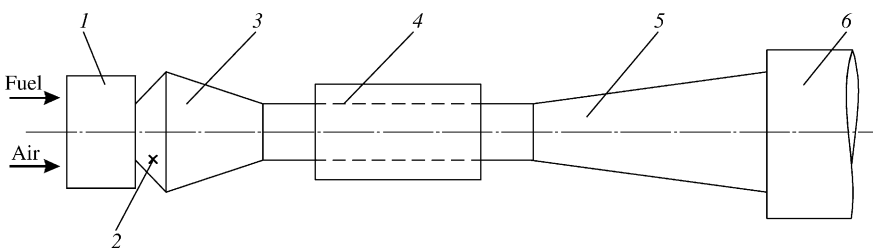

Fig. 144. Schematic of PDE based on a shock-booster concept [160]. 1—air-assist atomizer, 2—igniter, 3—transition cone, 4—booster section, 5—detonation transition cone, and 6—main combustor.

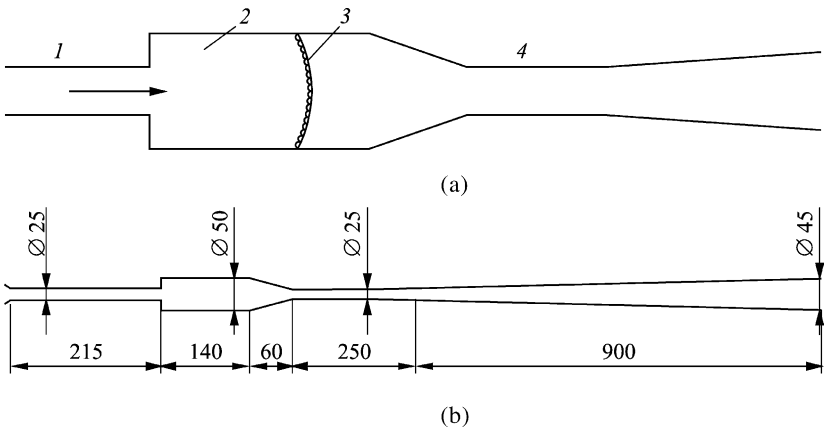

Fig. 145. Schematic of a PDE applying the shock implosion concept [308]. 1—inlet, 2—DC, 3—discharge electrodes, and 4—outlet. Dimensions in mm.

3.10. Pulse-reinitiation concept

Pulse-reinitiation concept suggested in Ref. [281] implies the use of pulse-reinitiated overdriven detonations, rather than CJ detonations, for producing thrust. Fig. 147 shows the schematic of the pulse DC used in Ref. [281]. Actually, the chamber of Fig. 147 is the same as that discussed in Section 3.5 (see Fig. 136) except for the attachment of optional working section 6 to exit transition cone 5 lacking in the configuration of Fig. 136. In operation, oxidizer and fuel are supplied separately into a long narrow tube 2. For igniting the combustible mixture and controlling the frequency of detonation waves, a special ignition unit 1 is used. It includes a spark plug and an electronic ignition system similar to that used in automobiles. It tube 2, obstacle-assisted DDT occurs.

Tube 2 is connected to the main chamber 4 through transition cone 3. The facility has the following dimensions: Tube 2 is 16 mm in diameter and 3 m long, main chamber 4 is 65 mm in diameter and 1 m long, the angle of transition cone 3 is 16°, and the angle of transition cone 5 is 40°.

The pulse-reinitiation mode of operation is realized when the detonation wave arising in tube 2 decays in the diverging transition cone and then recovers in the converging transition cone. Experimental studies of this mode were conducted with a methane–oxygen mixture under normal initial conditions. Fig. 148 shows schematic representation of the processes relevant to pulse-reinitiation mode (in the bottom) and the corresponding distance–time diagram. The components of the combustible mixture are introduced into initiating tube and mixed there. Diameter and length of the initiating tube are selected so that stationary detonation forms in it within time t_1. An additional requirement to the diameter of the initiating tube is that the detonation wave, as it passes through the diverging transition cone and enters the main chamber, decouples into a shock wave and flame front (time t_2). As the decoupled wave system propagates towards and through the cylindrical main chamber, separation between the shock wave and flame front increases (time t_3). In the converging transition cone, the shock wave undergoes Mach reflection and the gas is compressed and self-ignites (time t_4), resulting in detonation reinitiation and formation of retonation and overdriven detonation waves. Then, the overdriven detonation enters the working tube, propagates through the fresh combustible mixture with the gradual velocity drop and exits into ambience. The pressure and temperature of the products of this detonation wave are higher than those of the CJ detonation in the initiating tube. The general pattern of the process is to some extent similar to that observed in tubes with sudden contraction and expansion of their cross-section [274,275].

Experiments with the PDE of Fig. 147 in the pulse-reinitiation mode were conducted with a methane–oxygen mixture, $CH_4 + 2\alpha O_2$ at pulse frequency of 0.5–2 Hz. The pulse-reinitiation mode of operation was found to exist within the concentration limits $1.4 \leq \alpha \leq 1.8$. Fig. 149 compares the measured evolution of the detonation velocity in the working tube for two cases: (i) successful detonation transition from the initiating tube into the main chamber

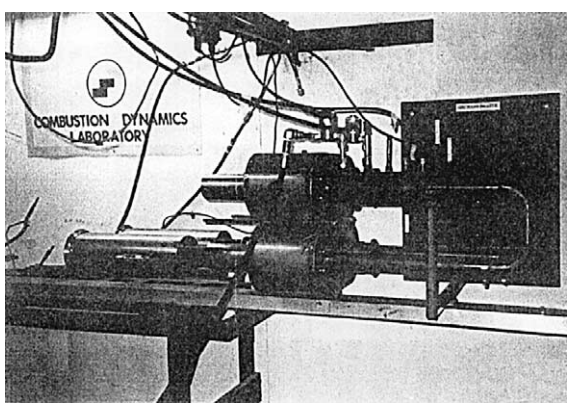

Fig. 146. A general view of the twin PDE assembly [308].

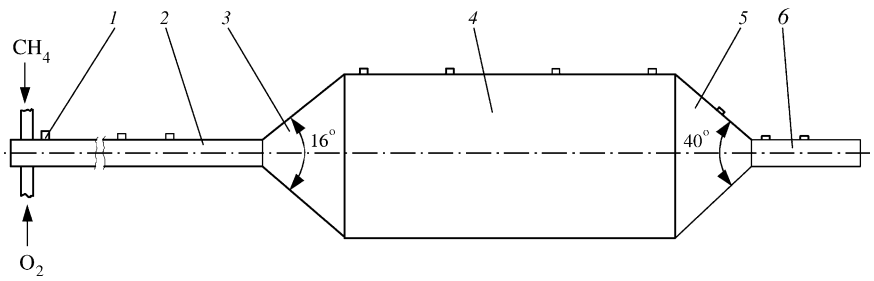

Fig. 147. Pulse detonation chamber of variable cross-section [281]. 1—igniter, 2—tube, 3—transition cone, 4—main chamber, 5—transition cone, and 6—detonation tube.

(curve 1), and (ii) detonation decay in the diverging transition cone and reinitiation in the converging transition cone (curve 2). In both modes, the overdriven detonation propagates in the working tube with wave velocity decaying to the CJ velocity (dashed line 3). Clearly, the velocity, D, of the reinitiated overdriven detonation (or overdrive degree, D/D_{CJ}) is considerably higher, and thus the corresponding pressure and temperature of the detonation products are higher. According to Ref. [281], the PDE implementing unsteady overdriven detonations could exhibit higher performance than the PDE operating on CJ detonations. Although being intuitively quite reasonable, this implication, however, has been substantiated neither by thermodynamic calculations nor by direct thrust measurements.

Note that there are several ways to obtain overdriven detonation in PDE [309]. As the first example refer to Gavrilenko et al. [310]. Consider a DC of a constant cross-section initially filled with an explosive mixture. To obtain the overdriven detonation wave, a portion of inert gas is issued into a middle part of the DC. After detonation initiation at the chamber inlet, the detonation wave propagating along the DC meets the layer of the inert gas that results in detonation decay. The resulting shock wave compresses the explosive mixture downstream from the inert layer, giving rise to mixture self-ignition and detonation reinitiation. After the reinitiated detonation catches up with the leading shock wave, the overdriven detonation arises in the initial mixture. Its velocity drops gradually as shown in Fig. 150a.

The second example is a DC of variable cross-section equipped with a converging transition cone (or wedge) connecting large- and small-diameter DCs (similar to Fig. 147). The overdrive degree at the inlet to the small-diameter DC depends on the cone (or wedge) angle φ and the relation between the initial and final cross-section areas [311]. The dependencies of this quantity on the cone (and wedge) angles are shown in Fig. 150b. The maximum overdrive degree obtained in the experiments is close to 1.7.

The third example is shown in Fig. 151. The device for obtaining an overdriven detonation consists of two chambers: the bigger upper chamber 1, and smaller lower chamber 2. The chambers are connected through a special turbulizer 3 and filled with an explosive gas mixture. Flame is initiated at the top of chamber 1 by igniter 4. The flame propagates downward and compresses the initial gaseous mixture in the two chambers due to the expansion of burned gases. During flame propagation through turbulizer 3, DDT occurs and the mixture in chamber 2 detonates at elevated

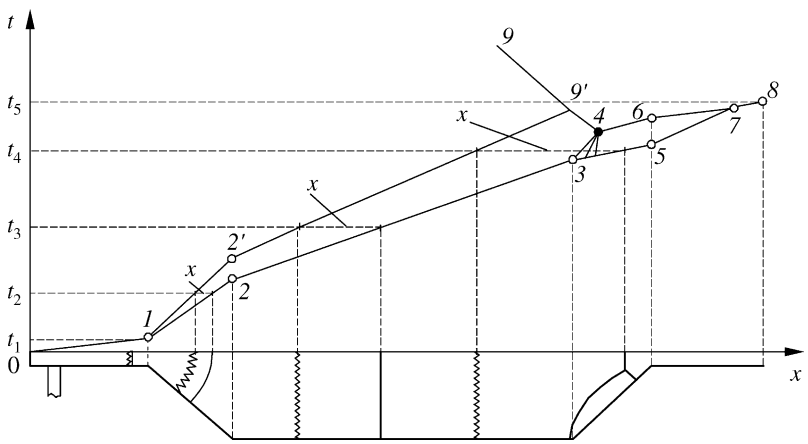

Fig. 148. Distance–time diagram of processes relevant to pulse-reinitiation mode of PDE operation: 1,2—shock wave, 1,2′—combustion front, Δx is the distance between the shock wave and flame front, 1,2,3,5,7—shock wave, 1,2′,9′—flame front, 9′,9—retonation wave, 4,6,7,8—secondary detonation wave, 7,8—overdriven detonation [281].

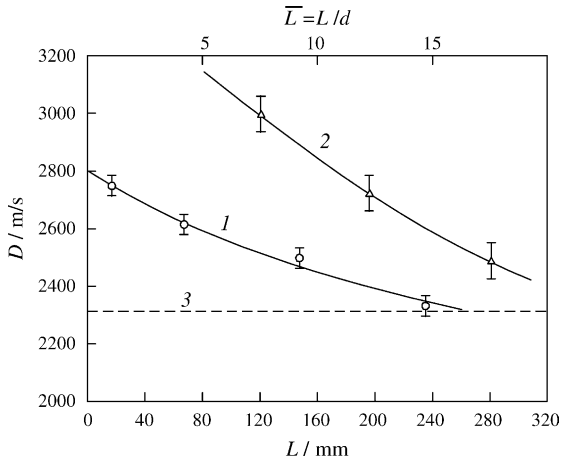

Fig. 149. Detonation wave velocity in a working tube for two cases: 1—detonation transmitted from the main chamber, and 2—detonation reinitiated in the converging transition cone, 3—CJ detonation velocity for stoichiometric methane–oxygen mixture [281].

pressure and density. The process can be controlled by changing the sizes of chambers and by choosing proper gas components of the explosive mixture. Clearly, application of this procedure in PDE requires the use of the rear valve (see e.g. Figs. 98 and 104 in Section 3.2).

3.11. Pulse-blasting concept

Pulse-blasting PDE concept implies the use of pulse blast waves rather than CJ or overdriven detonations for producing thrust. As was shown above, the development of a PDE employing CJ or overdriven detonations brings about serious problems. Among these problems are: (i) filling of the DC with air and fuel within a very short time period, (ii) provision of nearly perfect mixing between the components (which is needed because detonation can be initiated and propagates within quite a narrow equivalence ratio range), (iii) preevaporation of liquid fuels (experiments show that such fuels as kerosene cannot be detonated in a duct if the vapor phase pressure in the mixture is insufficient), (iv) initiation of detonation within short distances available in engines (apart from the necessity of very large energy inputs for direct initiation of detonation or special measures speeding up the DDT process, steady CJ detonations in real engines would hardly be attained, and, finally, (v), limiting diameter of detonation which rapidly increases as the ambient pressure drops (e.g. at 0.25 bar, propane–air mixtures cannot detonate in tubes less that 150 mm in diameter). Thus, if even all the above-listed problems are successfully solved, the burning regime in the PDE chamber is inevitably unsteady.

Pulse-blasting PDE concept suggested in Ref. [312] allows one to avoid the aforesaid difficulties and, at the same time, seems to be as efficient as detonation-based concepts. In the pulse-blasting concept, mixing and reactive shock generation are combined in a single process. This is done by injection of a preconditioned fuel in the main chamber filled with air. Preconditioning means preheating of the fuel to a temperature that would provide its fast spontaneous reaction with the ambient air. If the pressure in the jet is high enough to drive a strong blast wave at the initial stage of discharge that would be supported at later stages by the fuel reaction within the mixing layer, the burning process would be similar, at least to some extent, to detonation.

The schematics of experimental facilities used for substantiating the pulse-blasting concept are presented in Fig. 152a and b [312]. The setup of Fig. 152a comprises a steel tube 1 (3 m long and 120 mm in diameter), and special injector 2 (thick-walled steel cylinder) screwed in the end flange 3. The opposite tube end is open. The tube is equipped with five pressure gauges to monitor the blast wave velocity and pressure profiles. Distances between the gauges are: $l_0 = 250$ mm, $l_1 = l_2 = 505$ mm, and $l_3 = l_4 = 500$ mm. Liquid NM in an amount of 4–9 g with small additives of Al powder (0.3 or 0.5 g) is poured in the injector closed with diaphragm 4. The mixture is ignited with a pyrotechnic primer 5. The injector diameter-to-length ratio is varied from 1/5 to 1/12 to find an optimal value at

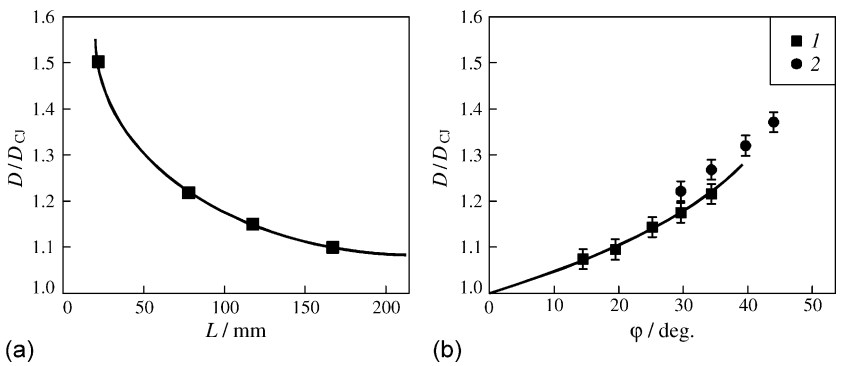

Fig. 150. Velocities of overdriven detonations obtained in a DC of constant cross-section (a) [310], and in a chamber with the diverging transition wedge (1) or cone (2) (b) [311].

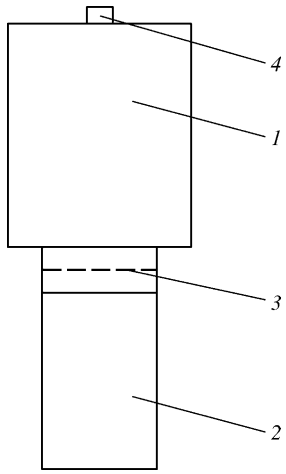

Fig. 151. Two-chamber device for obtaining overdriven detonations: 1—combustion chamber, 2—DC, 3—turbulizer for fast DDT, and 4—igniter [309].

which the blast wave velocity and pressure amplitude are the greatest.

In as much as NM contains too much of oxygen in its molecule and the heat of its combustion in air is low, in a special set of tests IPN was used as a fuel. IPN cannot be ignited with a primer therefore it is ignited either by gradually heating the injector until self-ignition occurs or rapidly admitting the liquid in the preheated injector. Experiments with self-ignition are conducted in a setup shown in Fig. 152b

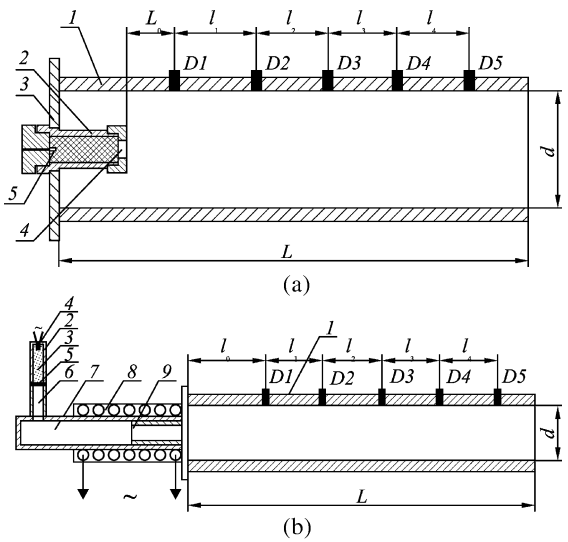

Fig. 152. (a) Schematic of the experimental setup for studying propagation of reactive shock waves produced by injection of hot fuel into a combustion chamber [312]: 1—tube, 2—injector, 3—flange, 4—diaphragm, and 5—igniter. (b) Experimental apparatus in which propellant is self-ignited in the injector [312]: 1—tube, 2—container, 3—propellant, 4—igniter, 5—diaphragm, 6—channel, 7—injector, 8—heater, and 9—orifice. D1 to D5 denote pressure gauges.

comprising a steel tube 1 (1.35 m long and 95 mm in diameter), container 2 with propellant 3, primer 4, separating diaphragm 5, channel 6 connecting container 2 with injector 7, electrical heater 8,and injection orifice 9. The tube is equipped with five pressure gauges. Distances between the gauges are: $l_0 = 300$ mm, $l_1 = 225$ mm, $l_2 = 230$ mm, $l_3 = 225$ mm, and $l_4 = 225$ mm.

To assess the efficiency of the devices to produce thrust, the shorter tube of Fig. 152b is suspended and the impulse is measured by the pendulum technique. Since the measured impulse depends on the discharge conditions, the efficiency of heterogeneous jets in producing impulse is assessed in comparative tests in which experiments with heterogeneous jets are compared with detonation of homogeneous mixtures. Detonation in homogeneous mixtures is initiated by detonating a small volume of a stoichiometric propylene–oxygen mixture in the chamber attached to the tube instead of injector. The impulse produced by the initiator is measured in a run where the tube is filled with air and subtracted from the impulse measured in runs with a FAM present in the tube.

The saturated vapor pressure of IPN is too low to allow preparing a stoichiometric IPN–air mixture in the tube. Moreover, IPN is easily adsorbed by the tube walls. Therefore detonated was a lean mixture and the actual IPN concentration was estimated by the average measured detonation velocity using a calculated dependence of the CJ detonation velocity on fuel concentration.

In experiments with NM, the highest blast wave velocities (up to 1400 m/s) and pressure of about 30 atm were observed at injector diameter-to-length ratios, d/L, ranging between 1/12 and 1/8. At smaller d/L ratios, only low-velocity regimes (with velocities of about 600 m/s) were observed. The representative pressure records in the facility of Fig. 152a are shown in Fig. 153. In Fig. 153a, the average blast wave velocity drops gradually between pressure gauges D1–D5, attaining the highest value of 1260 m/s between gauges D1 and D2. In general, the blast wave parameters measured near the injector are the highest because the amount of NM is insufficient to make a stoichiometric mixture with air in the tube. To increase the amount of fuel to its stoichiometric content, 1.8 cm^3 of kerosene (JP type) was poured on the diaphragm closing the injector. Typical pressure records for this case are shown in Fig. 153b. As seen in Fig. 153b, the blast wave velocity between gauges D1 and D2 in this case increased to 1390 m/s. Pressure profiles in Fig. 153 indicate the presence of reaction of the injected material with air as the generated blast waves exhibit long duration of the compression phase.

Fig. 154 shows the pressure records of the blast wave generated in the facility of Fig. 152b upon injection of preheated and partly burned IPN (3.5 g). The initial amount of IPN in this case is stoichiometric, and the charge is initiated by means of gradual preheating the injector. The pressure records indicate that only a small fraction of

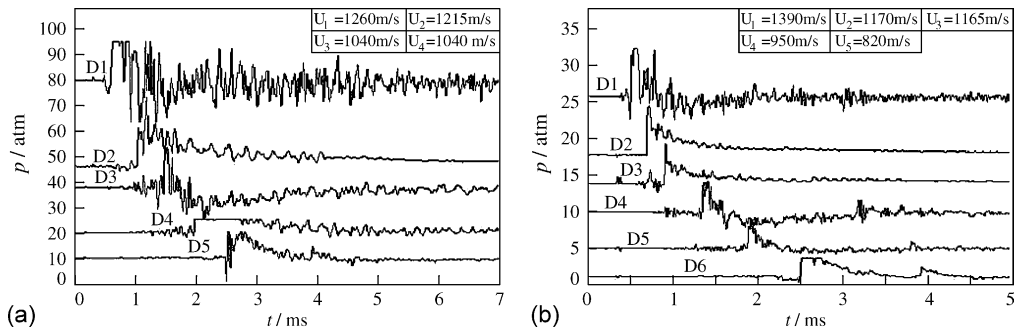

Fig. 153. Representative pressure records of the blast waves generated in the facility of Fig. 152a upon injection of (a) reacting jet initially containing NM (8 cm^3) and Al (0.5 g); and (b) reacting jet initially containing NM (4 cm^3), Al (0.2 g) and kerosene (1.8 cm^3) [312].

the injected fuel reacts with air and mostly near the injector (blast velocity between gauges D1 and D2 is 1125 m/s).

Measured values of the fuel-based specific impulse for IPN jets are much lower than those for homogeneous detonation. To understand the reason why the impulse produced by homogeneous IPN–air mixtures is about twice as high as the impulse generated by IPN jets, a set of numerical computations was made. As computations show, the major reason is incomplete burning of the injected material caused by fast expansion of the jet and formation of a plug flow at the beginning of the tube. Thus, the mixing layer area is reduced to the jet head only, therefore the major fuel fraction is not oxidized in air. This indicates that, on the one hand, the jet expansion should be restricted, and on the other, the jet must be split in several smaller jets to drastically enhance the mixing process keeping the jet velocity at a high level. This can be done either by confining the jet in a tube of a smaller diameter with perforations to eject the propellant and products of its decomposition into the main chamber as the jet spreads through the smaller tube or by injecting the decomposition products through several orifices distributed over the chamber. The mixing can be also enhanced with turbulizing obstacles.

The most important finding that follows from the computations is that the impulse produced by a NM jet is nearly equal to that of the gas-phase detonation of NM, in spite of the fact that only a small fraction of the jet material is oxidized by air. This is attributed to the longer pressure pulses resulting from the lesser energy left in the reaction products, higher density and velocity of the fluid discharged from the tube as compared to the detonation wave issuing from the tube.

The pulse-blasting concept eliminates most of the difficulties inherent in PDEs, namely, the jet initiates the reaction, so that the initiation problem is no longer critical. High-pressure jets can be generated by self-igniting (in a preheated volume) or igniting with a spark either a liquid monopropellant rich in the fuel component and injecting the partially reacted material in air or a small amount of a monopropellant to inject the products of its decomposition together with a conventional hydrocarbon fuel. The same applies to fuel pre-evaporation and detonation limits, because the injected material is preheated and reacts with air with no limitations. The combustion chamber needs refilling with air only, which is much easier to arrange than to fill it with a FAM. As to the essentially unsteady nature of the flow, it is, as mentioned above, inevitable in any short combustion chambers. The only problem left is mixing, but its solution requires other approaches than those in the case of detonation of premixed components.

The most promising approach to improving performance of the aforementioned combustion chambers is to use multijet fuel injection distributed along the chamber length. Indeed as both experiment and computations show changing the injector design (attaching to it a perforated tube) and placement (mounting it near the open chamber end and reversing the injection direction) resulted in an increase of the specific impulse for IPN to 511 s.

3.12. Multitube schemes

Multitube schemes allow one to control thrust, operation frequency, and thrust vector. Most of the PDE schemes considered above can be readily extended to multitube

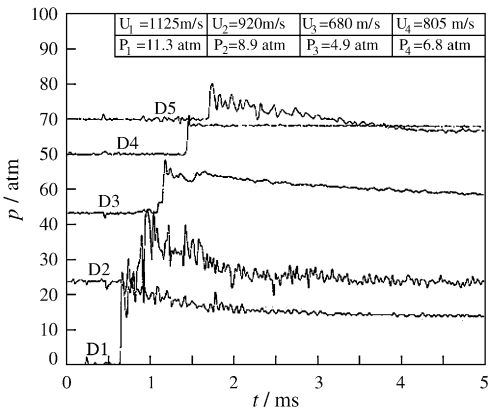

Fig. 154. Representative pressure records of the blast waves generated in the facility of Fig. 152b upon injection of a reacting jet initially containing IPM (3.5 g) [312].

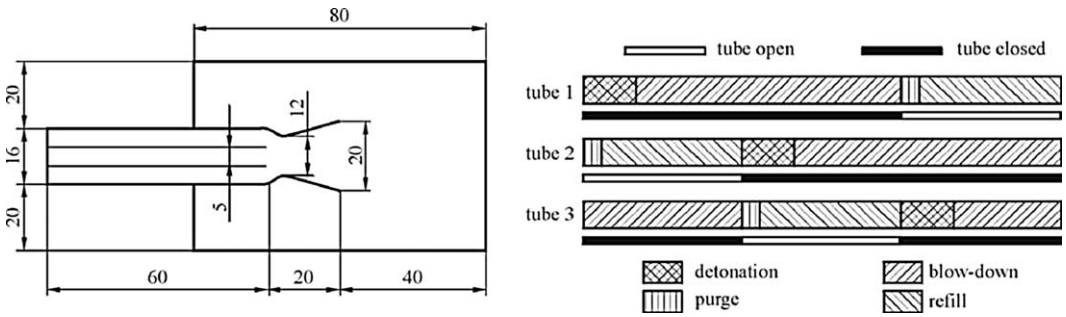

Fig. 155. (a) Computational domain for multitube PDE, and (b) operation sequence [266]. Dimensions in cm.

configurations. In addition to the study of single-tube PDE system dynamics, much effort was made to investigate the intricate combustion and gasdynamic processes in multitube pulse detonation combustors.

Consider, as a specific example, the results of a computational study of a PDE combustor consisting of three detonation tubes connected downstream with a common convergent–divergent nozzle [243,266]. This configuration helps preserving the chamber pressure during the blow-down and refilling stages, and consequently improves the propulsive performance of the engine.

Fig. 155 shows the computational domain (a) and the adopted operation sequence of the tubes (b) [266]. The PDE tubes of Fig. 155 are 60 cm long and 5 cm in diameter. Each PDE tube operates on the stoichiometric hydrogen–air mixture with frequency f =333 Hz. Fig. 156 presents the time evolution of the predicted density-gradient field within one cycle of operation. Initially, the bottom tube is partially filled with a reactive mixture. After initiation detonation propagates downstream (Fig. 156a), and eventually degenerates to a nonreacting shock wave. The resultant shock wave then proceeds further downstream, diffracts at the exit

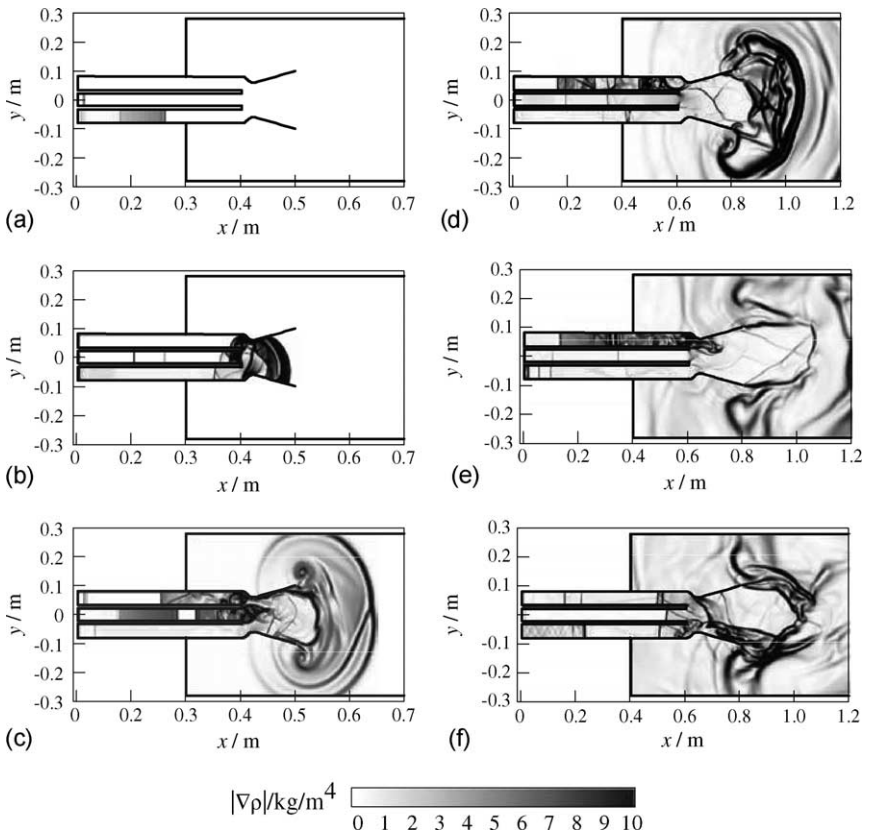

Fig. 156. Time evolution of density-gradient field during first cycle of operation. (t_c = 3 ms, t_{close} = 2.1 ms) [266]: (a) t = 0.15 ms, (b) 0.60 ms, (c) 1.15 ms, (d) 1.60 ms, (e) 2.15 ms, and (f) 2.60 ms.

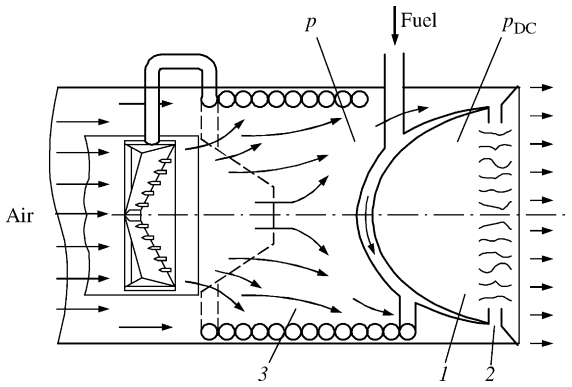

Fig. 157. General schematic of the resonator PDE [313]: 1—resonator, 2—annular nozzle, and 3—reactor; p and p_{DC} are the pressures in the reactor and resonator, respectively.

of the tube, reflects on the inner walls, and causes complex waves propagating upstream into all the three detonation tubes and downstream into the nozzle (see Fig. 156b). During this period, the middle tube undergoes the purging and refilling processes. After one-third cycle period, detonation is initiated and propagates in the middle tube while the top tube begins to purge burnt gases and refill fresh mixtures (Fig. 156c). The detonation wave then degenerates to a shock wave after passing through the interface between the reactant and purged gases. Further interactions between the shock wave and the local flowfield result in a complex flow structure as shown in Fig. 156d. After another one-third cycle period, detonation is initiated and propagates in the top tube (Fig. 156e) and the new cycle begins (Fig. 156f).

Stable cyclic operation is reached at the fifth cycle. The cycle-averaged specific impulse $\tilde{I}_{sp,f}$ and specific thrust $\tilde{I\!I}$ obtained are 3279 s and 830 m/s, respectively. They are about 5% higher than those achieved by the single-tube PDE, demonstrating the improvement by implementing a multitube design.

In another configuration, the length of the detonation tube decreases to 45 cm, leaving a free volume of 15 cm long between the detonation tubes and the nozzle. The flowfield exhibits a structure similar to the case without free volume. The cycle-averaged specific impulse $\tilde{I}_{sp,f}$ and specific thrust $\tilde{I\!I}$ are 3156 s and 800 m/s, respectively, which are slightly (5%) lower than those of the previous case. It should be noticed that there may exist lateral thrust in the vertical direction for multitube PDEs due to their unsymmetric operations. The present triple-tube PDE may produce a maximum lateral thrust of 1000 N per 1 kg/s air mass flow rate, thereby causing unnecessary vibration of the vechile. This undesired effect can be harnessed by introducing the concept of tube pair. Each tube pair includes two detonation tubes, which are located at symmetric positions and operate synchronously in time, to diminish the lateral thrust.

3.13. Resonator concept

The resonator PDE concept implies the use of a gasdynamic resonator cavity to provide autoperiodic supply and detonative combustion of a reactive mixture. Fig. 157 shows the schematic of the resonator PDE [313]. The PDE comprises resonator 1, annular nozzle 2, and reactor 3. Resonator 1 is a spherical semiclosed cavity with a cut in the vicinity of which annular nozzle 2 is installed. In operation, compressed air is supplied to reactor 3 through the inlet. In the reactor, where liquid fuel (JP kerosene) is properly decomposed and partially oxidized, homogeneous exothermically active FAM of required composition is prepared. The FAM enters annular nozzle 2 and resonator cavity 1 in the form of the imploding supersonic jet, producing the gas curtain in the cavity (see Fig. 158a). At the instant when the imploding supersonic jet reaches the resonator axis area, a complicated shock wave pattern forms. For simplicity, in Fig. 158b it is presented in the form of a single shock wave. The combustible mixture is then compressed twice by this shock wave and by the subsequent reflected wave (Fig. 158c). The shock wave reflected from the resonator spherical surface is focused in some area (named ‘focus’ in Fig. 158c) filled with the preconditioned FAM. The pressure and temperature in this area rise to values sufficient to ignite the mixture and produce the detonation kernel. The reaction zone moves towards the thrust wall as a detonation wave (Fig. 158d). The detonation wave interacts with the resonator wall

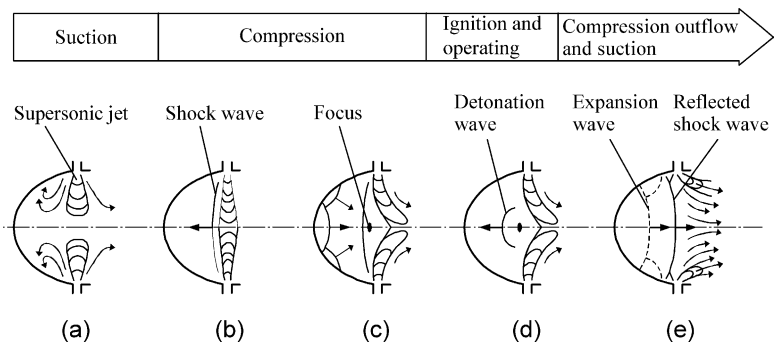

Fig. 158. Schematic presentation of the operation process in the resonator PDE [313].

(thrust wall) producing thrust. Then, after reflection of the detonation wave, the jet curtain is disintegrated and the detonation products expand to the ambience (Fig. 158e). The expansion process provides suction of a new portion of the combustible mixture into the resonator cavity, and the new operation cycle starts.

The results of testing of the resonator thruster were reported elsewhere [313]. Fig. 159 presents time histories of pressure, p, in the reactor (in front of the annular nozzle, see Fig. 157) and in the resonator cavity, p_{DC}, as well as thrust P. The diameter of the resonator cavity outlet cross-section in the test model was 70 mm, and the ratio of the outlet cross-section area of the resonator to the throat cross-section area of the annular nozzle was equal to 4.0. As follows from Fig. 159, pressure in the cavity is higher than the pressure in the reactor. Instantaneous p_{DC}/p values attain 6–10 and even more, while the thrust attains the values of 2000 N. Oscillation frequency measured in the resonator cavity was 24–25 kHz. This corresponds to the acoustic range for the designed cavity geometry and the temperature of combustion products of 2500–2600 K. Cold tests of the model under the same pressure at the inlet were accompanied with high-frequency autooscillations, however, their frequency was about 7.5 kHz.

3.14. Inlets

In air-breathing PDEs, the inlet is aimed at continuous and stable supply of airflow at a rate required for efficient operation of combustor under various flight conditions. In addition, the design of the PDE inlet should provide the lowest possible pressure loss under oscillating back pressure caused by upstream propagation of periodic disturbances from the combustion chamber.

To study the PDE inlet aerodynamics and its response to downstream disturbances, a series of numerical simulations of a model inlet has been conducted in Ref. [283]. Fig. 160 shows the inlet configuration. The freestream conditions have a Mach number of 2.0, total pressure of 2.64 atm, and total temperature of 546 K.

Fig. 161 presents the pressure contours at three different back pressures p_b/p_0: 0.6729 (a), 0.7103 (b), and 0.7477 (c). With these values of back pressure, the engine operates under supercritical conditions. The airflow passing through a complicated shock system is adjusted to the axial direction and becomes subsonic behind the terminal normal shock S. The response of the inlet shock system to downstream disturbances is simulated by imposing periodic pressure oscillations (with amplitude up to 10% of back pressure and frequencies in the range of 0.5–1.0 kHz) at the exit plane. Fig. 162 shows the predicted evolution of terminal shock location, X_s, for various downstream disturbances having different frequencies and amplitudes. The terminal shock exhibits a larger excursion at lower frequencies at a fixed amplitude (compare curves 1 and 2) and higher amplitude at a fixed frequency (compare curves 2 and 3). Moreover,

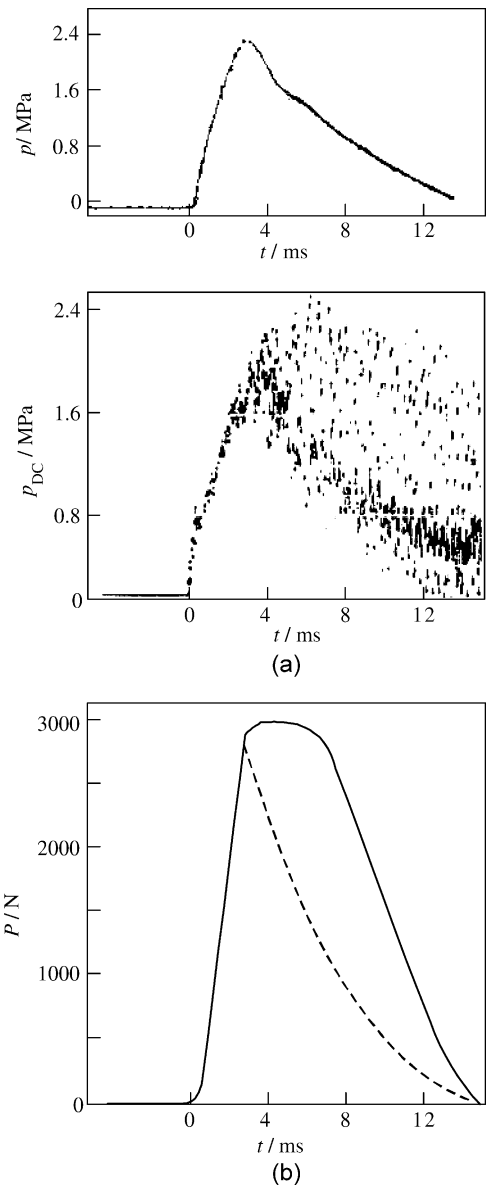

Fig. 159. Measured time histories of pressure in reactor (a), pressure in resonator cavity (b), and thrust (c) [313]. Dashed curve corresponds to standard Laval nozzle.

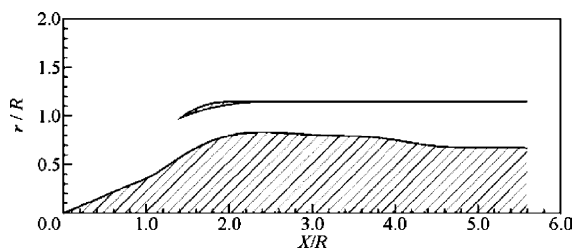

Fig. 160. Configuration of a mixed-compression supersonic inlet with $R = 34$ mm [283].

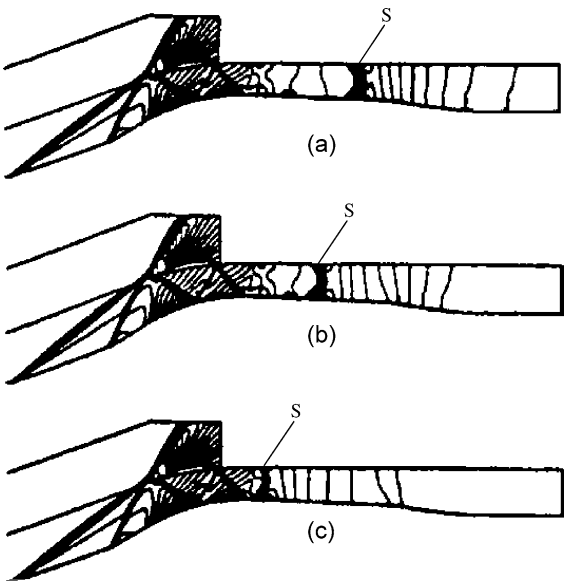

Fig. 161. Steady-state pressure contours with different back pressures, p_b/p_0: 0.6729 (a), 0.7103 (b), and 0.7477 (c). *S* stands for the terminal normal shock [283].

lower frequency and higher amplitude disturbances tend to displace the terminal normal shock farther upstream, that is, make the device more vulnerable to inlet instability. At large-amplitude oscillations the shock can eventually get pushed out of the inlet [314].

The processes described above apply to both single-tube and multitube PDE schemes. Multitube PDE schemes often apply a common inlet (see e.g. Figs. 99, 100, 102, 104, 111, 120, and 121). As a result of repeated detonation initiation in various tubes and their refilling with air, the common inlet will experience unsteady operation with nonsymmetrical disturbances of back pressure. In the PDE schemes with and without mechanical valves, the oscillating back pressure will affect the operation of the inlet including the potential

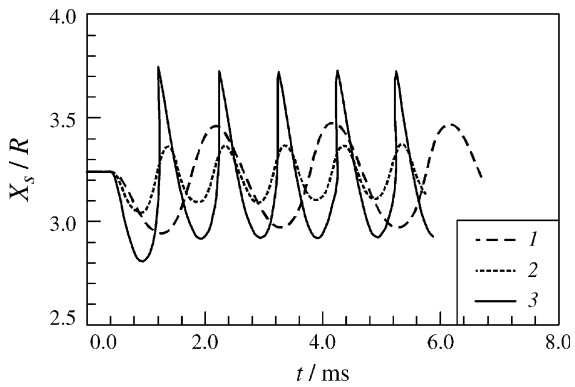

Fig. 162. Instantaneous shock locations, X_s, in a mixed-compression supersonic inlet at different amplitudes and frequencies of back pressure oscillations [283]: 1—$A = 0.05p_b$ and $f = 500$ Hz, 2—$A = 0.05p_b$ and $f = 1000$ Hz, and 3—$A = 0.1p_b$ and $f = 1000$ Hz.

of hummershock and unstarting of the inlet [315]. If a single inlet is used as a plenum for multiple detonation tubes, the back pressure is then expected to have a reduced effect on the inlet flow field. However, the spillage from a closing valve into an adjacent opening valve may affect the combustor operation.

Theoretical studies [316] of the characteristic times involved show that the time required to transfer air between adjacent tubes in the valved multitube PDE is of the order of 10 μs which is significantly shorter than the time required to form the hummershock (of the order of 10 ms). Therefore, the concept of a plenum inlet supplying air to multiple DCs can be feasible for practical PDEs.

To simulate operation of a multitube PDE inlet, a particular experimental study has been performed in Ref. [315] with the model inlet shown in Fig. 163. In the model inlet, the exit plane was nonuniformly excited in a sinusoidal manner (at frequency up to 50 Hz) both in space (spanwise direction) and in time. The amplitude of the pressure oscillations was also varied. This was achieved by blocking the exit with four plunging pistons mounted on a camshaft having a phase difference of 90° between two adjacent cams. Each set of pistons offered a different blockage at the exit (up to 83%), thus varying considerably the amplitude of excitation as compared to calculations [283,314]. The degree of pressure oscillations increased with increasing blockage and decreased with increasing excitation frequency. Despite the large blockage, the model inlet of Fig. 163 started and remained started for all test conditions described. The pressure oscillations inside the inlet were confined to downstream of the throat and no adverse effects were observed on the flow field upstream of the throat.

3.15. Nozzles

Nozzle is aimed at improving the propulsive performance of a PDE. In addition, as the nozzle affects the flow dynamics in the PDE combustor, it may determine the timing

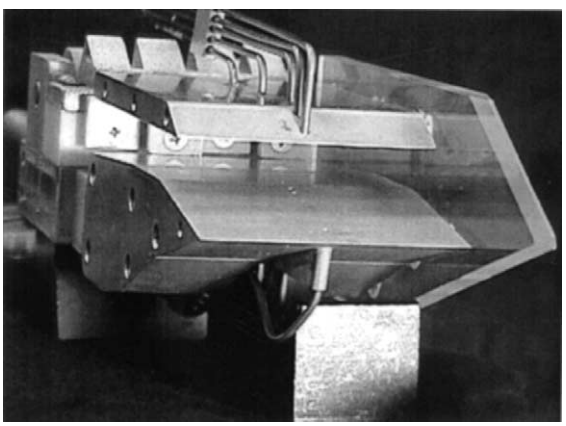

Fig. 163. A 10°, 12 cm long inlet model designed for PDE operation at flight Mach number 2.0. Throat height is 1.2 cm [315].

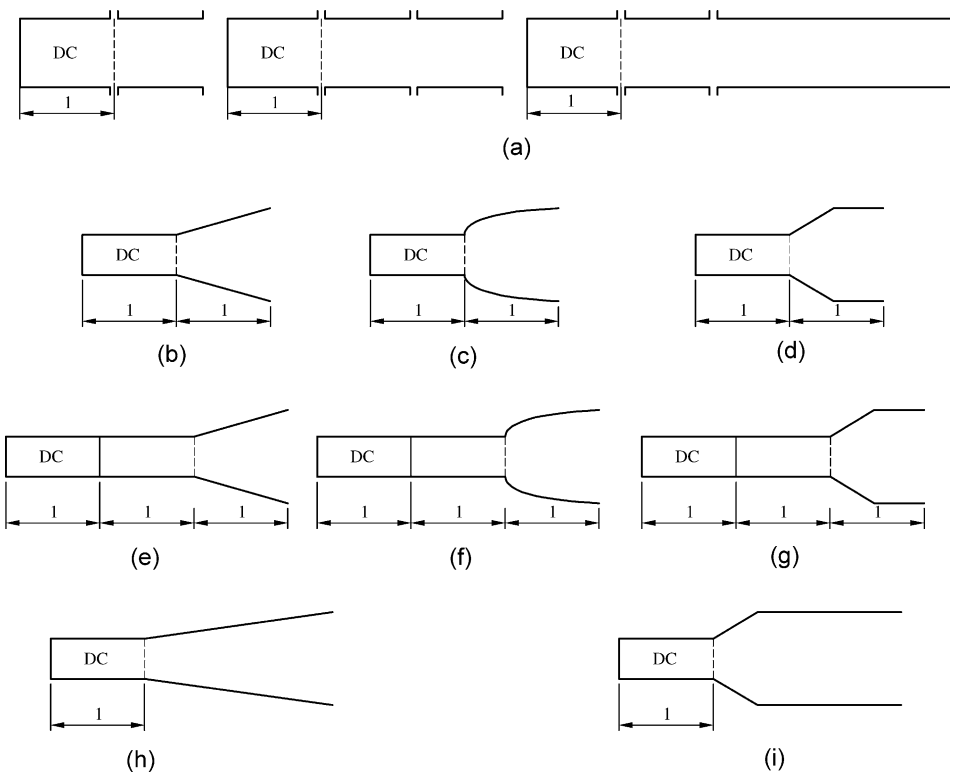

Fig. 164. Nozzles tested in Ref. [318]: (a) cylindrical, (b) diverging, (c) bell-shaped, (d) composite, and (e) to (i) elongated composite. Unity stands for the length normalized by the DC length.

of various gasdynamic processes such as purging, refilling, etc. Contrary to nozzles of steady-flow engines, PDE nozzles operate at essentially unsteady conditions and their design and optimization require consideration of the whole operation process. When a detonation wave approaches the open end of the PDE tube the high-pressure detonation products have a considerable expansion potential. Attachment of a nozzle to the end of the detonation tube makes it possible to gradually expand the gases and decrease the rate of pressure drop in the tube, thus increasing a cycle thrust. On the other hand, attachment of the nozzle results in increasing the length of the engine and thereby decreasing the operation frequency. Theoretically, the effects of nozzle was studied [12,243,244,266,283,317]. It has been found that nozzles indeed can increase the thrust.

A detailed experimental study of the nozzle effect on the single-pulse performance of a PDE DC has been reported in Refs. [318,319]. The DC comprises a cylinder 50 mm in internal diameter and of length L_{DC} closed at one end with a rigid flange (thrust wall) and open at the other end. Prior to filling the DC with a stoichiometric ethylene–oxygen mixture, the open end of the DC was covered with a destroyable milar film 12 μm thick. Detonation in the DC is either directly initiated by an exploding wire source (with energy of about 30 J), or obtained via the use of a 100 mm long, 12 mm-diameter predetonator.

Various nozzles were attached to the open end of DC: cylindrical (Fig. 164a), diverging (Fig. 164b), bell-shaped (Fig. 164c), and composite (Fig. 164d), as well as elongated composite nozzles of Fig. 164e–i. Configuration of Fig. 164a involves the DC with $L_{DC} = 65$ mm and a cylindrical nozzle of the same internal diameter as the DC but of different length $B = L_{nz}/L_{DC}$, where L_{nz} is the nozzle

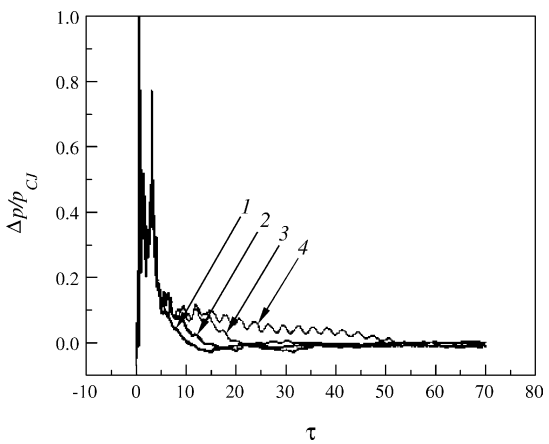

Fig. 165. Thrust wall dimensionless overpressure-time records measured with cylindrical nozzles of different length: 1—$B = 0$, 2—0.69, 3—1.8, and 4—5.7 [318].

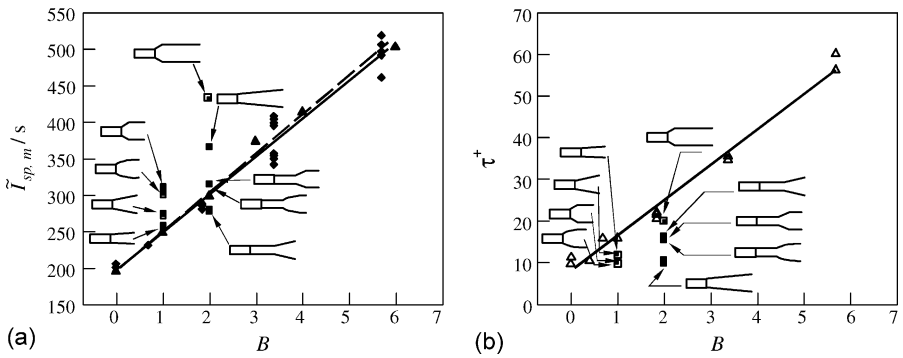

Fig. 166. (a) Summary of measured mixture-based specific impulse: triangles—[257], dashed line—fit for data of Ref. [257] for cylindrical nozzles; other symbols—Ref. [318], solid line—fit for data of Ref. [318] for cylindrical nozzles; (b) summary of measured duration of the positive overpressure at the thrust wall, τ^+, for nozzles of various configurations: triangles—cylindrical nozzles [318], solid line—fit for data of [318] for cylindrical nozzles, other symbols—nozzles of other configurations shown in Fig. 164.

length; B ranging from 0 (no nozzle) to 5.7. Typical dimensionless pressure-time records for different B are shown in Fig. 165. Overpressure is normalized to the CJ pressure, p_{CJ}, and time is normalized to L_{DC}/D_{CJ}. As the cylindrical nozzle controls and limits the expansion of detonation products in comparison to free direct expansion into atmosphere, thrust increases with B. Measured mixture-based specific impulse $I_{sp,m}$ increases linearly with B (see in Fig. 166a and b solid and dashed lines—fits of experimental data for cylindrical nozzles of Ref. [257,318], respectively).

Configurations of Fig. 164b–i involve the DC with $L_{DC} = 100$ mm and $B = 1$ and 2. Diverging nozzles of Fig. 164b differ by the cone half-angle, υ, which is varied from 0° (cylindrical nozzle) to 18°. Fig. 166a and b summarize the results of measurements of the mixture-based specific impulse, $\tilde{I}_{sp,m}$, and the dimensionless duration of the positive overpressure at the thrust wall, τ^+, with nozzles of various configurations [319]. Clearly, the composite nozzle of Fig. 164d is the most efficient for the shortest configuration ($B = 1$). Elongated composite nozzle of the same type is also the most efficient at $B = 2$. For noncylindrical nozzles, the duration of positive overpressure is always less than for cylindrical nozzles, however, composite nozzles lead to slightly higher τ^+ than diverging nozzles of other types. Note that the use of diverging nozzles can be accompanied with an increase of the vehicle drag due to increase in the frontal area.

In a multitube configuration, the nozzle flow pattern becomes very complex. Fig. 167 shows the results of 2D calculations reported in Ref. [243]. Due to unsymmenric flow field in the nozzle a lateral thrust will exist as mentiond in Section 3.12. Moreover, nozzle durability issues can become critical.

3.16. Active control

Fig. 168 depicts the schematic of a PDE operating on the ethylene–oxygen mixture [100]. The PDE is periodically filled with the mixture using finite-volume supply tanks of oxygen 1 and ethylene 2 and via valves 3 and premixer 4. After filling the DC, ignition is triggered by igniter 5 at the closed end leading to detonation wave 6 initiation and propagation towards the open end. To optimize fuel consumption and maximize PDE performance, an active control scheme is applied. The active control of the PDE operation process is based on the diode-laser ethylene sensor. The diode laser 7 is modulated across the C_2H_4 combination band Q-branch near 1.62 μm.

At the beginning of the experiment, supply gas valves 3 are open. When fuel is detected at the tail end of the PDE tube using sensor 8, a control signals produced by controller 9 are sent to close the mixture filling valves and fire the igniter. After a fixed-duration cooling cycle, the control scheme is repeated until the gas supply tanks have emptied.

Fig. 169a shows the results of gas filling duration for this set of experiments. As the supply tanks are depleted, the control scheme adjusts the filling duration to ensure full tube fills. As seen in Fig. 169b, this active control maintains constant impulse compared to fixed valve timing.

Similarly, the ethylene-based control system was used to actively control the spark timing of the ethylene–oxygen predetonator tube shown in Fig. 124. When ethylene is detected at the tail end, a signal is sent to actuate the igniter ensuring full tube fills and minimizing wasted fuel. As shown in Fig. 170, the missing peaks in the equivalence ratio histories are due to detonation failure resulting from pulse-to-pulse-interference. The actively controlled spark is able to reduce this performance-degrading behavior.

3.17. Rocket pulse detonation propulsion

There exist two distinct categories of chemical propulsion engines: air-breathing engines that use ambient air, and rocket engines that use the oxidant carried onboard a flying vehicle. The pulse detonation technology in propulsion can in principle be applied to both categories. Let us consider a possible scheme of the rocket engine applying pulse detonations [320]. Fig. 171 shows a simplified

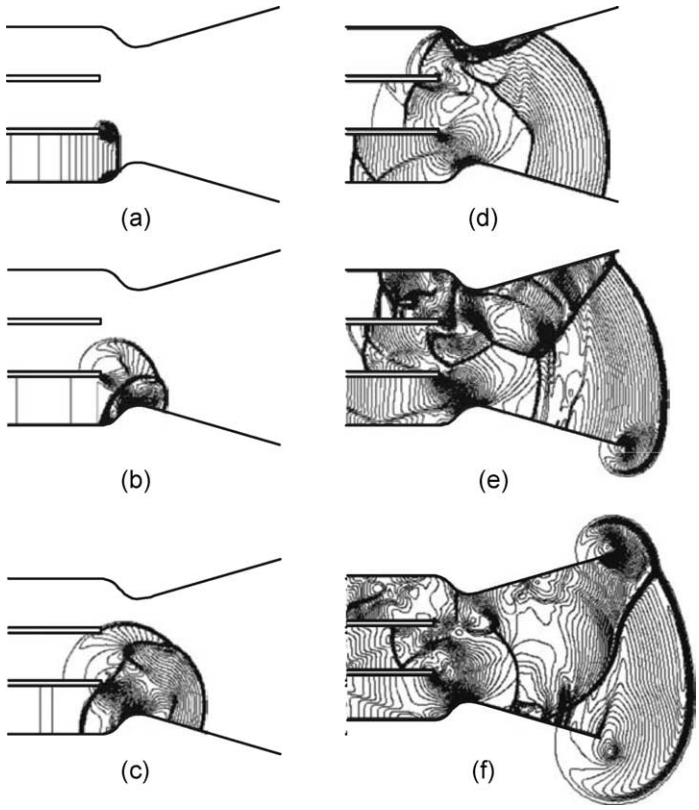

Fig. 167. Snapshots of pressure field showing flow development in a nozzle after the detonation wave enters the common nozzle from the lower tube. The PDE schematic and parameters are similar to that shown in Fig. 155 [243,266]: (a) $t = 0.40$ ms, (b) 0.45 ms, (c) 0.50 ms, (d) 0.60 ms, (e) 0.70 ms, and (f) 0.80 ms.

schematic of a pulse detonation rocket engine (PDRE). The engine comprises six cylindrical DCs 1 each having inlet end 2 and outlet end 3. The outlet ends are in fluid communication with nozzle 4 that directs the thrust vector produced from the detonation products expelled from chambers 1. Inlet ends 2 are supplied with fuel and oxidizer, each supplied through a fuel/oxidizer manifold 5 in fluid communication with a series of fast-acting flow-metering fuel valves 6 and oxidizer valves 7. The fuel/oxidizer manifold 5 is in fluid communication with fuel tank 8 and oxidizer tank 9, both stored onboard the vehicle propelled by the rocket engine. Cycle hardware 10 (e.g. gas generator, expander, staged combustion, as well as other equipment) may be needed to supply the fuel and oxidizer from tanks 8 and 9 to manifold 5 at suitable conditions of pressure and temperature.

In operation, fuel is supplied to the fuel valves while oxidizer is supplied to the oxidizer valves. The valves timing is controlled by an onboard processor. After passing the valves, fuel and oxidizer are injected into the DCs in a proper stoichiometry and ignited by igniters. After ignition, a detonation wave forms that traverses the DC and expels the combustion products through the nozzle. It is then possible, by proper timing of the valves, to create a buffer zone between the expelling hot exhaust gas and a fresh fuel–oxidizer charge, e.g. in the form of a fuel-rich zone. Such a buffer zone will then be followed by the fresh fuel–oxidizer charge that will be detonated by triggering the igniter at the subsequent cycle.

The PDRE of Fig. 171 can be supplied with the regenerative cooling system to preheat fuel prior to injecting into the DC. It can operate with simultaneous firing of all the detonation tubes or in a predetermined sequence of firing the tubes.

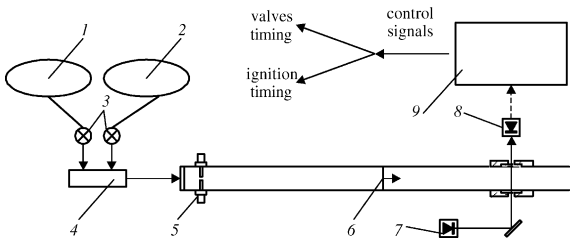

Fig. 168. Schematic of ethylene-based active control scheme applied to PDE [100]: 1—oxygen tank, 2—ethylene tank, 3—valves, 4—mixer, 5—igniter, 6—detonation wave, 7—1.62 μm diode laser, 8—detector, and 9—controller.

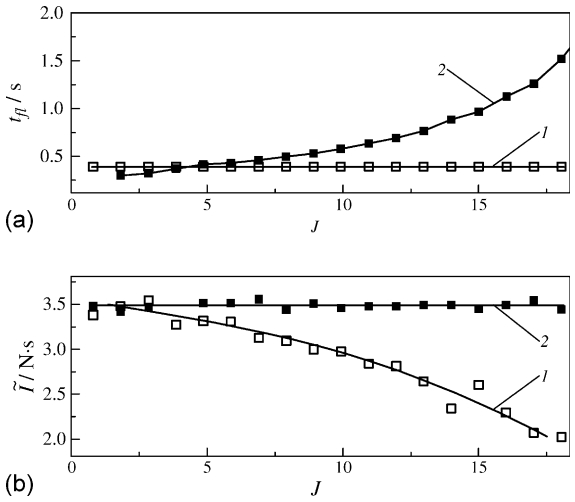

Fig. 169. Active control experiments to realize full tube fills in a research PDE: (a) variation of fuel fill duration with the pulse number J, and (b) cycle impulse for the cases of fixed valve opening duration (no control) (1) and variable opening due to active control (2) [100].

As follows from Section 2.4, the thermodynamic efficiency of the PDRE cycle will depend on the operation pressure. It is expected that at high chamber pressure the PDRE cycle will have no significant advantages against the constant-pressure rocket motor cycle. However the PDRE cycle allows for a considerable decrease in the chamber pressure to attain the same thermodynamic efficiency as that attained in a standard rocket motor. This advantage may result in decreasing the requirements to cycle hardware (turbopumps, etc.) power and in less fuel consumption rates.

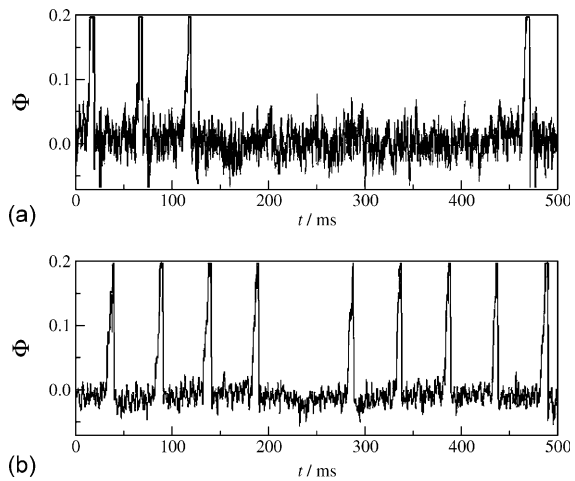

Fig. 170. Results of active control experiments at the predetonator of Fig. 124 running on ethylene–oxygen mixture with a continuous air purge. The equivalence ratio at the tail end is shown for (a) fixed spark timing (no control) and (b) actively controlled spark timing using the fuel diagnostic [100].

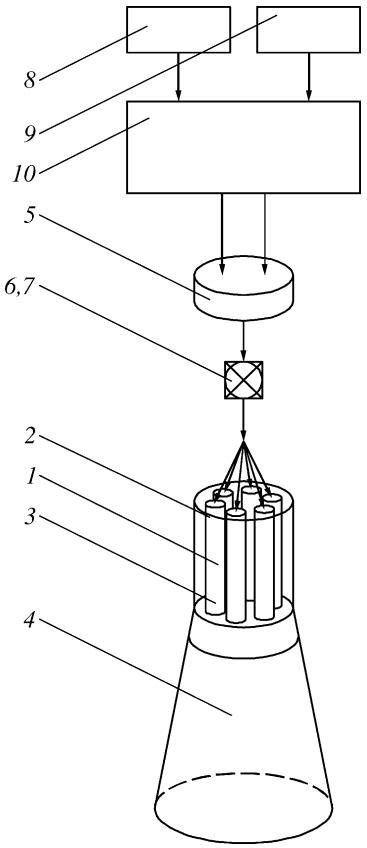

Fig. 171. (a) Schematic of main components of a PDRE [320]: 1—cylindrical DCs, 2—inlet, 3—outlet, 4—nozzle, 5—fuel/oxidizer manifolds, 6,7—fuel/oxidizer valves, 8—fuel tank, 9—oxidizer tank, and 10—cycle hardware (turbopump, etc.).

4. Concluding remarks

The material discussed above reflects the state-of-the art in the new, rapidly developing, area of science and technology that is the pulse detonation propulsion. Nowadays, it is absolutely clear that there is no fundamental constrains in applying repeatedly propagating confined detonations for producing thrust. Thermodynamic efficiency of pulse detonation thrusters is considerably higher than that of other conventional thrusters based on combustion, particularly at subsonic flight at relatively low altitudes. In view of it, both air-breathing and rocket propulsion seem to receive a chance of getting a long-expected breakthrough in efficiency, and, as a consequence, in increased range, payloads, etc. The additional benefits of an ideal PDE are: simplicity of design and low weight.

Existing idealized schemes of PDEs imply perfect premixing of fuel and oxidizer, steady-state initial conditions in the DC, localized instantaneous detonation initiation, thermodynamically equilibrium pressure, temperature and composition of detonation products in a planar,

constant speed, classical CJ detonation, and an adapted ideal nozzle. Idealized schemes of air-breathing PDE, in addition, imply perfect inlets with full pressure recovery and infinitely-fast-response mechanical valves. With this in mind, it is natural to pose a question: "Do the theoretical advantages of PDEs preserve in realistic conditions or the idea of PDE is condemned to be just the usual kind of castles in the air?" A well-known example is a two-stroke piston engine that, theoretically, is supposed to have a doubled power as compared to the four-stroke engine. As a matter of fact, due to various imperfections, the actual gain in power is only about 50%, while fuel consumption grows by 15–20% as compared to the four-stroke counterpart. Moreover, due to more stringent thermal loading of the piston, the durability issues become critical. Nevertheless, the two-stroke engine has found a number of applications, e.g. in low-speed ship propulsion, high-speed diesels, etc.

To definitely answer the above question, the up-to-date knowledge is still scanty. The reader can perceive it looking through Section 2 of this paper. First of all, the detonation phenomenon—the kernel of the PDE operation cycle—is not completely understood yet. Most of existing knowledge on fuel detonability is based on empirical and computational findings for academic systems comprising light hydrocarbons (methane, acetylene, ethylene, etc.) as fuel, oxygen as oxidizer, and argon as diluent. Confined fuel–air detonations were studied, with some exceptions, only for light gaseous hydrocarbons. A number of empirical rules and guides exist to estimate the critical initiation energy, as well as the limiting and critical tube diameter of detonation. All these rules and guides are based on the mean size of the detonation cell—a footprint of the propagating detonation on the smoked foil surface. It happened in the detonation physics that the cell size became a merit of detonation, and is considered as a kind of 'phlogiston' released during explosion. It is getting disappointing that a growing number of publications operate with the cell size rather than with the intrinsic characteristics of reaction kinetics in detonations. As the detonation cell structure is quite irregular for practical gaseous explosive systems and depends on many parameters (pressure, temperature, mixture composition, tube diameter, wall roughness and acoustic properties, etc.), no wonder that the relevant literature is quite controversial. As for the confined detonation of fuel sprays, i.e. heterogeneous FAMs containing fuel drops or particles, the actual structure, mechanism, and kinetics of heat evolution is still vague.

Further research is evidently needed to clarify pros and cons of the PDEs. Imperfections inherent to PDEs can be readily marked. Because of rigorous safety regulations, it is hardly possible that perfectly premixed fuel and air will be utilized in practical devices. Just the other way about, injection of fuel sprays in the PDE combustion chamber should be considered as the standard approach. In view of it, the whole spectrum of problems critical for other concepts of chemical propulsion comes into play. Obviously, various techniques for mixing enhancement used in chemical propulsion could be directly implemented in PDEs. However, as the operation cycle of PDE is transient and the time available for mixing is very short as compared with the steady-state analogs, these techniques can simply fail. Thus, mixing enhancement can become a crucial issue.

Another issue calling for more thorough studies is combustor filling with FAM or air. Achievement of efficient thrust requires closed head of the combustor which impedes the filling process. Therefore, some special design solution not inherent in conventional air-breathing engines should be looked for. As the operation requirements imply high-frequency of detonation pulses the time available for combustor filling should be short and the rate of recharging could become unreasonably high.

According to all accounts, the detonation initiation issue is the most challenging. The idealized PDE performance is obtained based on the assumption that detonation is initiated and attains the CJ parameters in the immediate vicinity to the thrust wall. As a matter of fact, it takes quite a long distance for detonation to build up after triggering it with a low-energy source in the fuel–oxidizer mixture. It is worth noting that this is particularly important for PDE concepts with separate supply of fuel and oxidizer. Clearly, as the development of detonation takes a finite time and length, the thrust and specific impulse produced in a single cycle will be different from those obtained in idealized calculations and experiments with highly sensitive fuel–oxygen mixtures.

Deflagration-to-detonation transition is presently considered as one of the most promising approaches to initiate detonation in PDE. In spite of the fact that qualitatively the DDT phenomenon is sufficiently well understood, there are no prognostic theories so far which would allow predicting the predetonation length and time and pressure evolution at the thrust wall. In view of it, there is a need for computer codes comprehensively validated by experiments and allowing for modeling noninstantaneous detonation initiation via DDT and unstable modes of predetonation flame propagation in a detonation tube.

Based on weight and volume constraints, the reasonable length of the PDE combustion chamber should not exceed few meters. This implies that obtaining detonation via DDT is problematic for combustion chambers of large diameter. Among the promising approaches applicable to both large- and small-diameter (e.g. predetonator) chambers are the use of (i) strong reactive shocks generated by high-pressure jets rather than detonations for producing thrust, (ii) coherent energy deposition in external sources distributed both in space and time, and (iii) shock focusing. These interesting concepts need further experimental substantiation under realistic conditions.

Critical phenomena occurring during detonation transmission from a predetonator to the PDE combustion chamber are well studied both experimentally and computationally for gaseous systems. Such studies are very important for better understanding the mechanism of

detonation reinitiation due to collision of the decaying shock waves with the side wall of the combustor and/or with the shock-focusing obstacles.

For PDE applications, there is a need for experimental and computational data on critical properties of detonations under realistic operating conditions, i.e. at subsonic and supersonic flight conditions (flight Mach number from zero to 3–4) at various altitudes. Although the primary attention should be paid to detonations of sprays of standard aviation fuels (JP-8, JP-10), critical detonation properties of other liquid fuel candidates can also be of interest for particular applications. As detonability of regular aviation fuels is usually very low, various approaches to detonate such fuels with least energy requirements have been suggested in literature. These approaches can be either passive or active.

Passive approach implies the use of various chemical additives to the fuel or fuel preconditioning by its partial oxidation, decomposition, etc. and, in fact, leads to the replacement of the original fuel with its surrogate. Partial fuel preevaporation is a mandatory approach for low-volatility fuels. Experimental studies indicate that small additives (several volume percent) are capable of decreasing the ignition delay of the evaporated fuel behind a shock wave no more than by a factor of 2–3. This decrease can result in at most one order of magnitude decrease in the critical energy of detonation initiation. Fuel preconditioning can also lead to some increase in its detonability.

Active approach implies the use of various means promoting detonation of the original fuel. Among active approaches, DDT is the most efficient in terms of initiation energy but requires long distances and times for detonation build-up. Little reliable data on DDT of fuel sprays is available in literature that makes it difficult to rely on this approach when designing actual PDEs. Transmission of a developed detonation wave from a sensitive fuel–oxidizer mixture to the marginally sensitive FAM in the main combustor of PDE is another example of the active approach. In this case, detonation in the sensitive mixture can be readily initiated by a relatively weak initiator. Then the problem of detonating the fuel in the chamber is replaced by the problem of successfully transmitting the detonation from sensitive to marginally sensitive mixture. This approach is much more elaborate than the DDT approach, therefore most of actual PDEs apply the predetonator concept. Nevertheless, there is a lack of knowledge on detonation transmission for fuel sprays at conditions mentioned above.

Thus, to our belief, the problem of detonation initiation in close-to-practical PDEs with homogeneously mixed FAMs approaches its successful solution. In view of it, the problems of organizing efficient filling of the combustor and nearly-perfect mixing become crucial. Unfortunately, these issues are not properly tackled so far.

Other important problems not relevant to combustion per se but worth to be mentioned are noise and vibration, fatigue durability, heat transfer, the choice of optimal nozzle designs and operation control. They have to be thoroughly studied before designing real PDEs.

This review deliberately confines itself to PDE used for flying vehicles but no less important is the use of the PDE concept for producing energy in on-surface stationary power plants. Some of the aforementioned difficulties can obviously be obviated such as combustor filling and mixing, as size and weight restrictions are not crucial any longer in these devices.

Acknowledgements

Since several years, the US Office of Naval Research (ONR) sponsors the fundamental research on detonations with implication of further use of the new knowledge in the development of PDEs. To make the effort more efficacious, ONR collaborates with other research sponsoring agencies, such as the Russian Foundation for Basic Research, in organizing international meetings of specialists and disseminating the scientific results worldwide. As mentioned in the Introduction, a number of subject-oriented books were issued based on this collaboration. We are grateful to Prof. S. Zhdan who kindly provided us with the notes of late Prof. V. Mitrofanov which became a basis of Section 2.5. We also thank Prof. C. Brophy for useful discussions.

References

[1] Eidelman S, Grossman W. AIAA Paper 92-3168 1992.
[2] Bussing T, Pappas G. AIAA Paper 94-0263 1994.
[3] Eidelman S, Yang X, Lottati Z. AIAA Paper 95-3877 1995.
[4] Bussing T, Pappas G. In: Murthy SNB, Curran ET, editors. Progress in astronautics and aeronautics series. Washington, DC: AIAA Inc; 1996. p. 165.
[5] Eidelman S. AIAA Paper 97-2740 1997.
[6] Kailasanath K. AIAA Paper 99-1067 1999.
[7] Roy GD. ISABE Paper 99-7127 1999.
[8] Kailasanath K. AIAA Paper 2001-0474 2001.
[9] Desbordes D, Daniau E, Zitoun R. In: Roy G, Frolov S, Netzer D, Borisov A, editors. High-speed deflagration and detonation: fundamentals and control. Moscow: Elex-KM Publ; 2001. p. 177–92.
[10] Kailasanath K. AIAA Paper 2002-0470 2002.
[11] Eidelman S, Grossmann W, Lottati I. J Propulsion Power 1991;7(6):857–65.
[12] Cambier J-L, Tegner JK. J Propulsion Power 1998;14(4): 489–98.
[13] Kailasanath K. AIAA J 2000;38(9):1698–708.
[14] Roy G, Frolov S, Kailasanath K, Smirnov N. Advances in experimentation and computation of detonations. Moscow: Enas Publ; 1998.
[15] Roy G, Frolov S, Netzer D, Borisov A, editors. Control of detonation processes. Moscow: Elex-KM Publ; 2000.
[16] Roy G, Frolov S, Santoro R, Tsyganov S, editors. Advances in confined detonations. Moscow: Torus Press; 2002.

[17] Roy G, Frolov S, Kailasanath K, Smirnov N, editors. Gaseous and heterogeneous detonations: science to applications. Moscow: Enas Publ; 1999.
[18] Roy G, Frolov S, Netzer D, Borisov A, editors. High-speed deflagration and detonation: fundamentals and control. Moscow: Elex-KM Publ; 2001.
[19] Roy G, Frolov S, Santoro R, Tsyganov S, editors. Confined detonations and pulse detonation engines. Moscow: Torus Press; 2003.
[20] Lyle Cummins JrC. Internal fire. Lake Oswego, Oregon: Carnot Press; 1976.
[21] Berthelot M. Compt Rend Acad Sci, Paris, Fr 1870;71: 619–25. see also p. 667–77 and 709–28.
[22] Berthelot M. Annal Chim Phys, 4e Ser 1871;23:223–73.
[23] Berthelot M. Compt Rend Acad Sci, Paris 1881;93:18–22.
[24] Berthelot M, Vieille P. Compt Rend Acad Sci, Paris 1882;94: 101–8. 822–3.
[25] Berthelot M, Vieille P. Compt Rend Acad Sci, Paris 1883;95: 151–7.
[26] Mallard E, Le Chatelier H. Compt Rend Acad Sci, Paris 1881;93:145–8.
[27] Mallard E, Le Chatelier H. Ann Mines 1883;8(4):274–568.
[28] Rankine WJM. Philos Trans R Soc London 1870;277–88.
[29] Hugoniot H. J De l'Ecole Polyt Cahier 1887;57:1–97.
[30] Mikhelson VA. PhD Dissertation. Imperial Moscow University Publication; 1890.
[31] Mikhelson VA. Sci Bull Imperial Moscow Univ, Phys Math Ser 1893;10:1–92.
[32] Chapman DL. Philos Mag, 5th Ser 1899;47(284):90–104.
[33] Jouguet E. Comp Rend Acad Sci, Paris, Fr 1904;140:1211.
[34] Jouguet E. J Math Pures Appl, 6e Serie 1905;1:347–425.
[35] Bauer PA, Dabora EK, Manson N. In: Kuhl AL, Leyer J-C, Borisov AA, Sirignano WA, editors. Dynamics of detonations and explosions: detonations Progress in astronautics and aeronautics ser. 133. 1991. p. 3–18.
[36] Manson N, Dabora EK. In: Dynamic aspects of detonations. Kuhl AL, Leyer J-C, Borisov AA, Sirignano WA, editors. Progress in astronautics and aeronautics series 153. 1993. p. 3–42.
[37] Hinshelwood CN, Williamson AT. Reaction between hydrogen and oxygen. 1934. London.
[38] Semenov NN. Chain reactions. Leningrad: Goskhimtekhizdat Publ; 1934.
[39] Campbell C, Woodhead DW. J Chem Soc 1926;128: 3010–21.
[40] Sokolik AS. Combustion and detonation in gases. Leningrad: Gosizdat Publ, USSR; 1934.
[41] Ricardo HR. SAE J 1922;10:300–12.
[42] Nernst W. Zeitschrift VDI 1905;49:1426–31.
[43] Voinov AN, Sokolik AS. Izvestiya USSR Acad Sci 1937;1: 137.
[44] Lewis B, von Elbe G. Combustion, flames and explosions of gases, 1st ed. Cambridge University Press; 1951. (2nd ed, Academic Press; 1951).
[45] Rakipova KhA, Troshin YaK, Shchelkin KI. J Tech Phys 1947;17:1397–408.
[46] Zel'dovich YaB, Roslovsky AI. Doklady USSR Acad Sci 1947;57:365–8.
[47] Ferrie F, Manson N, Proceedings of the 4th Symposium (International) on Combustion, Williams and Wilkins; 1953. p. 486–94.
[48] Shchelkin KI. Combustion and detonation in gases. Moscow: Voenizdat; 1944.
[49] Zel'dovich YaB. J Exp Theor Phys 1940;10(5):543–68.
[50] Von Neumann J. OSRD Rep 1942;549.
[51] Doering W. Annal Phys, 5e Folge 1943;43:421–36.
[52] Zel'dovich YaB. J Exp Theor Phys 1942;12:389–406.
[53] Taylor GI. Proc R Soc London 1950;A200:235–47.
[54] Zeldovich Ya B, Kogarko SM, Simonov NN. Sov J Tech Phys 1956;26(8):1744.
[55] Gelfand BE, Frolov SM, Nettleton MA. Progr Energy Combust Sci 1991;17:327–71.
[56] Frolov SM. In: Combustion, detonation, shock waves. Merzhanov AG, Frolov SM, editors. Proceedings of Zel'dovich Memorial, vol. 1. Moscow: Enas Publ; 1995. p. 266–72.
[57] Voinov AN. Doklady USSR Acad Sci 1950;125–8.
[58] Voitsekhovsky BV. Doklady USSR Acad Sci 1957;114: 717–20.
[59] Denisov YuN, Troshin YaK. Doklady USSR Acad Sci 1959; 125:110–3.
[60] Oppenheim AK, Stern RA, Procedings of the 7th Symposium (International) on Combustion, London: Butterworths; 1959. p. 837–59.
[61] Shchelkin KI, Troshin Ya K. Gasdynamics of combustion. Moscow: USSR Academy Science Publishers; 1963.
[62] Urtiev PA, Oppenheim AK. Proc R Soc London 1966;A295: 13–21.
[63] Strehlow RA. Combust Flame 1968;12(2):81–101.
[64] Vasil'ev AA, Mitrofanov VV, Topchiyan ME. Combust, Explosion, Shock Waves 1987;3(5):109–31.
[65] Saytsev SG, Soloukhin RI, Proceedings of the 8th Symposium (International) on Combustion, Baltimore: Williams and Wilkins; 1962. p. 344–7.
[66] Vermeer DJ, Meyer JW, Oppenheim AK. Combust Flame 1972;18:327–36.
[67] Borisov AA, Kogarko SM. Doklady USSR Acad Sci 1963; 149(3):623–5.
[68] Borisov AA. Astronaut Acta 1974;1(7–8):909–14.
[69] Borisov AA, Kogarko SM, Lyubimov AV. Zh Prikl Mekh Tekhn Fiz 1960;3:175–82.
[70] Zaidel RM. Doklady USSR Acad Sci, Phys Chem Sect 1961; 136:1142–5.
[71] Erpenbeck JJ. Phys Fluids 1962;5:604.
[72] Fickett W, Wood WW. Phys Fluids 1966;9:903.
[73] Taki S, Fujiwara T, Proceedings of the 18th Symposium (International) on Combustion; 1980. p. 1671–81.
[74] Oran E, Boris JP, Young T, Flanigan M, Burks T, Picone M, Proceedings of the 18th Symposium (International) on Combustion; 1980. p. 1641–9.
[75] Markov VV. Doklady USSR Acad Sci 1981;258(2):314–7.
[76] Borissov AA, Sharypov OV. In: Dynamic structure of detonation in gaseous and dispersed media. Borissov AA, editor. Fluid mechanics and its application series, vol. 5. Dordrecht: Kluwer Academic Publishers; 1991. p. 27–49.
[77] Meyer JW, Urtiew PA, Oppenheim AK. Combust Flame 1970;14:13–20.
[78] Oppenheim AK. Laser cinematography of explosions. Courses and lectures no. 100 of the international center for mechanical sciences. Udine: Springer.
[79] Oppenheim AK. Philos Trans R Soc London A 1985;315: 471–508.

[80] Babkin VS, Kozachenko LS. Zh Prikl Mekh Tekhn Fiz 1960; 3:165–71.
[81] Kozachenko LS, Babkin VS. Doklady USSR Acad Sci 1960; 131(3):591–3.
[82] Lee JHS, Knystautas R, Freiman A. Combust Flame 1984;56: 227–39.
[83] Zeldovich YB, Borisov AA, Gelfand BE, Frolov SM, Mailkov AE. Dynamics of explosions. In: Kuhl A, Bowen JR, Leyer J-C, Borisov AA, editors. Progress in astronautics and aeronautics series, vol. 114. New York: AIAA; 1988. p. 211–31.
[84] Mitrofanov VV, Soloukhin RI. Doklady USSR Acad Sci 1964;159(5):1003–6.
[85] Pawel D, Van Tiggelen P, Vasatko H, Wagner H. Gg Combust Flame 1970;15:173.
[86] Matsui H, Lee JHS, Proceedings of the 17th Symposium (International) on Combustion; 1978. p. 1269–80.
[87] Bull DC. Trans J Chem Eng 1979;57:21.
[88] Desbordes D. In: Dynamics of explosions. Kuhl A, Bowen JR, Leyer J-C, Borisov AA, editors. Progress in astronautics and aeronautics series, vol. 114. New York: AIAA; 1988. p. 170–85.
[89] Moen I, Donato M, Lee JHS, Knystautas R, Proceedings of the 18th Symposium (International) on Combustion, Waterloo, Canada; 1980.
[90] Bach GG, Knystautas R, Lee JHS, Proceedings of the 13th Symposium (International) on Combustion; 1970. p. 1097–110.
[91] Dabora EK, Weinberger LP. Acta Astronaut 1974;1(3/4): 361–72.
[92] Borisov AA, Gelfand BE, Gubin SA, Proceedings of the 13th Symposium (International) on Combustion, Pittsburgh, PA: The Combustion Institute; 1970. p. 1171–7.
[93] Zel'dovich YaB, Librovich VB, Makhviladze GM, Sivashinski GI. Astronaut Acta 1970;15:313–21.
[94] Thibault PA, Yoshikava N, Lee JH. 1978 Fall Technical Meeting of the Eastern Section of the Combustion Institute, Miami Beach, FL. 1978.
[95] Frolov SM, Basevich VYa, Vasil'ev AA. In: Roy G, Frolov S, Netzer D, Borisov A, editors. High-speed deflagration and detonation: fundamentals and control. Moscow: Elex-KM Publ; 2001. p. 315–32.
[96] Brophy CM, Netzer DW, Sinibaldi J, Johnson R. In: Roy G, Frolov S, Netzer D, Borisov A, editors. High-speed deflagration and detonation: fundamentals and control. Moscow: Elex-KM Publ; 2001. p. 207–22.
[97] Thermochemical Equilibrium Program (TEP). Carson City, NV: Sofware and Engineering Associates, Inc.
[98] Zel'dovich YaB, Kompaneets AS. The theory of detonation. Moscow Gostekhizdat Publ; 1955.
[99] Borisov AA, Melnichuk OI, Kasimov AR, Khasainov BA, Troshin K Ya, Kosenkov V. Chem Phys Rep 1996;15(4):603.
[100] Hanson RK, Mattison DW, Ma L, Davidson DF, Sanders ST. In: Roy GD, Gupta AK, editors. Proceedings of the 15th ONR Propulsion Meeting, College Park, MD; 2002. p. 155–60.
[101] Kailasanath K, Patnaik G. Proc Combust Inst 2000;28: 595–601.
[102] Soloukhin RI. Shock waves and detonations in gases. Baltimore, MD: Mono Book Corp; 1966.
[103] Oran ES. In: Roy G, Frolov S, Kailasanath K, Smirnov N, editors. Gaseous and heterogeneous detonations: science to applications. Moscow: Enas Publ; 1999. p. 97–120.
[104] Hanana M, Lefebvre MH, Van Tiggelen PJ. In: Roy N, Frolov K, Kailasanath S, Smirnov G, editors. Gaseous and heterogeneous detonations: science to applications. Moscow: Enas Publ; 1999. p. 121–30.
[105] Voitsekhovsky BV, Mitrofanov VV, Topchiyan ME. Structure of the detonation front in gases. Izd Sib Branch Acad Sci USSR, Novosibirsk 1963.
[106] Gamezo VN, Desbordes D, Oran ES. Combust Flame 1998; 116:154–65.
[107] Kailasanath K, Oran ES, Boris JP, Young TR. Combust Flame 1985;61:199–209.
[108] Pintgen F, Austin JM, Shepherd JE. In: Roy G, Frolov S, Santoro R, Tsyganov S, editors. Advances in confined detonations. Moscow: Torus Press; 2002. p. 68–72.
[109] Manson N. Comp Rend 1946;222:46.
[110] Boa-The Chu, Proc Symp Aerothermochem Evanson; 1956. pp. 95–111.
[111] Campbell C, Lovell P, Boyd TA. Ind Eng Chem 1928;20: 1045.
[112] Campbell C, Lovell P, Boyd TA. Ind Eng Chem 1931;23(26): 555.
[113] Owen K, Coley T, Automotive fuels handbook, Warrendale, PA: SAE Inc; 1990. p. 108.
[114] Bach GG, Knystautas R, Lee JH, Proceedings of the 12th Symposium (International) on Combustion, Pittsburgh, PA: The Combustion Institute; 1967. p. 665.
[115] Agafonov GL, Frolov SM. Russ J Phys Combust Explos 1994;28(2):189.
[116] Sokolik AS. Selfignition, flame and detonation in gases. Israel Program for Scientific Translation, Jerusalem; 1963.
[117] Frolov SM, Basevich VYa, Belyaev AA, Neuhaus MG. In: Roy G, Frolov S, Kailasanath K, Smirnov N, editors. Gaseous and heterogeneous detonations: science to applications. Moscow: Enas Publ; 1999. p. 311–30.
[118] Frolov SM, Basevich VYa. AIAA Paper No. A99-34130 1999.
[119] Strehlow RA, Engel CD. AIAA J 1969;7(3):492–6.
[120] Trotsyuk AV. In: Roy G, Frolov S, Kailasanath K, Smirnov N, editors. Gaseous and heterogeneous detonations: science to applications. Moscow: Enas Publ; 1999. p. 331.
[121] Oran ES. In: Merzhanov AG, Frolov SM, editors. Combustion, detonation, shock waves. Proceedings Zel'dovich Memorial, vol. 1. Moscow: Enas Publ; 1995. p. 228–47.
[122] Oran ES, Weber JW, Stefaniw EI, Lefebvre MH, Anderson JD. Combust Flame 1998;113:147–63.
[123] Penyazkov OG. In: Roy G, Frolov S, Santoro R, Tsyganov S, editors. Advances in confined detonations. Moscow: Torus Press; 2002. p. 73–9.
[124] Borisov AA, Gelfand BE, Loban' SV, Mailkov AE, Khomik SV. Chem Phys Rep 1982;1(6):848.
[125] Pawel D, Vasatko H, Wagner H-Gg. Report AF EOAR 67-49 1967.
[126] Tieszen SR, Stamps DW, Westbrook CK, Pitz WJ. Combust Flame 1991;84(3):376–90.
[127] Auffret Y, Desbordes D, Presles HN. Shock Waves 2001;11: 89–96.
[128] Von Guhlmann K, Push W, Wagner H-Gg. Ber Bunsen-Ges Phys Chem 1966;70(2):143–8.
[129] Jost W, Wagner H-Gg. Report AF-71-2146 1973.
[130] Shepherd JE, Austin J, Jackson S, Cooper M, Pintgen F, Chao T, Lieberman D. In: Roy GD, Gupta AK, editors.

Proceedings of the 15th ONR Propulsion Meeting, College Park, MD: University of Maryland; 2002. p. 161–6.
[131] Austin JM, Shepherd JE. Combust Flame 2004. Accepted for publication.
[132] Borisov AA, Mel'nichuk OI, Kasimov AR, Khasainov BA, Troshin KYa, Kosenkov VV. J Phys IV 1995;5:C4-129.
[133] Zamansky VM, Borisov AA. Prog Energy Combust Sci 1992;18:297–325.
[134] Borisov AA, Kosenkov VV, Mailkov AE, Mikhalkin VN, Khomik SV. In: Kuhl AL, Leyer J-C, Borisov AA, Sirignano WA, editors. Dynamic aspects of detonations. Progress in astronautics and aeronautics series, vol. 153.; 1993. p. 153.
[135] Borisov AA. Private communications.
[136] Borisov AA, Mailkov AE, Kosenkov VV, Aksenov VS. In: Kuhl AL, Leyer J-C, Borisov AA, Sirignano WA, editors. Dynamics of detonations and explosions: detonations. Progress in astronautics and aeronautics series, vol. 133.; 1991. p. 268–78.
[137] Baklanov DI, Gvozdeva LG, Scherbak NB. In: Roy G, Frolov S, Santoro R, Tsyganov S, editors. Advances in confined detonations. Moscow: Torus Press; 2002. p. 225–30.
[138] Borisov AA. In: Roy GD, Frolov SM, Kailasanath K, Smirnov NN, editors. Gaseous and heterogeneous detonations: science to applications. Moscow: Enas Publ; 1999. p. 3–24.
[139] Troshin YaK. Doklady USSR Acad Sci 1979;247(4):887.
[140] Korobeinikov VP. Tasks of the theory of point explosion in gases. Moscow: Nauka; 1973.
[141] Levin VA, Markov VV. Sov J Phys Combust Explosion 1975;11(4):623–33.
[142] Levin VA, Markov VV, Osinkin SF. Combust, Explosion, Shock Waves 1995;31(2):91–5.
[143] Vasil'ev AA. Near-critical modes of a gas detonation. Russia: Novosibirsk; 1995.
[144] Vasil'ev AA. Proceedings of the 28th Fraunhofer ICT-Conference. Germany: N. Eisenreith; 1997: p. 50/1–14.
[145] Vasil'ev AA. Combust, Explosion, Shock Waves 1978; 14(3):154–5.
[146] Vasil'ev AA, Nikolaev YuA, Uljanitsky VYu. Combust, Explosion, Shock Waves 1979;15(6):94–104.
[147] Vasil'ev AA, Grigorjev VV. Combust, Explosion, Shock Waves 1980;16(5):117–25.
[148] Vasil'ev AA, Nikolaev YuA. Acta Astronaut 1978;5: 983–96.
[149] Zhdan SA, Mitrofanov VV. Combust, Explosion, Shock Waves 1977;21(6):98–103.
[150] Mitrofanov VV. Combust, Explosion, Shock Waves 1983; 19(4):169–74.
[151] Benedick WB, Guirao CM, Knystautas R, Lee JH. In: Bowen JR, Leyer J-C, Soloukhin RI, editors. Dynamics of explosion. Progress in astronautics and aeronautics series, vol. 106.; 1986. p. 181–202. New York.
[152] Westbrook CK, Urtiew PA, Proceedings of the 19th Symposium (International) on Combustion, Pittsburgh, PA: The Combustion Institute; 1982. p. 615–23.
[153] Vasil'ev AA, Zhdan SA, Mitrofanov VV. In: Roy GD, Frolov SM, Kailasanath K, Smirnov NN, editors. Gaseous and heterogeneous detonations: science to applications. Moscow: Enas Publ; 1999. p. 25–38.
[154] Vasil'ev AA, Nikolaev YuA, Ulyanitsky VYu. Combust, Explosion, Shock Waves 1977;13(3):404–8.
[155] Carlson GA. Combust Flame 1973;21:383.
[156] Bull DC, Elsworth JE, Hooper G. 6th ICDERS, Stockholm; 1977.
[157] Borisov AA, Mailkov AE, Mel'nichuk OI. Chem Phys Rep 1997;16(10):1823.
[158] Frolov SM, Basevich VyA, Aksenov VS. In: Roy GD, Mashayek F, editors. Proceedings of the 14th ONR Propulsion Meeting, Chicago, IL: University of Illinois at Chicago; 2001. p. 202.
[159] Frolov SM, Basevich VYa, Aksenov VS. J Propul Power 2003;19(4):573–80.
[160] Frolov SM, Basevich VYa, Aksenov VS, Polikhov SA. In: Roy GD, Frolov SM, Santoro R, Tsyganov S, editors. Confined detonations and pulse detonation engines. Moscow: Torus Press; 2003. p. 157–74.
[161] Knystautas R, Lee JHS, Moen I, Wagner H-Gg, Proceedings of the 17th Symposium (International) on Combustion, Pittsburgh, PA: The Combustion Institute; 1979. p. 1235–45.
[162] Murray SB, Moen IO, Thibault PA, Knistautas R, Lee JHS, Sulmistras A. In: Kuhl AL, Leyer J-C, Borisov AA, Sirignano WA, editors. Dynamics of detonations and explosions: detonations. Progress in astronautics and aeronautics series, vol. 133. Washington, DC: AIAA; 1991. p. 91–117.
[163] Yoshikava N, Thibault PA, Lee JH. 1979 Spring Technical Meeting of the Canadian Section of the Combustion Institute, Kingston, Ontario; 1979.
[164] Zel'dovich YaB, Gelfand BE, Tsyganov SA, Frolov SM, Polenov AN. In: Kuhl A, Bowen JR, Leyer J-C, Borisov AA, editors. Dynamics of explosions. Progress in astronautics and aeronautics series, vol. 114. New York: AIAA; 1988. p. 99.
[165] Frolov SM. D.Sc. Thesis; 1992.
[166] Rose M, Uphoff U, Roth P. In: Roy G, Frolov S, Kailasanath K, Smirnov N, editors. Gaseous and heterogeneous detonations: science to applications. Moscow: Enas Publ; 1999. p. 51–64.
[167] Fischer M, Pantow E, Kratzel T. In: Roy G, Frolov S, Kailasanath K, Smirnov N, editors. Gaseous and heterogeneous detonations: science to applications. Moscow: Enas Publ; 1999. p. 197–212.
[168] Edwards DH, Thomas GO, Nettleton MA. J Fluid Mech 1979;95:79.
[169] Dremin AN, Trofimov VS, Proceedings of the 10th Symposium (International) on Combustion, Pittsburgh, PA: The Combustion Institute; 1965. p. 893.
[170] Thomas GO, Williams RL. Shock Waves 2002;11(6): 481–92.
[171] Schults E, Shepherd J. Explosion dynamics laboratory report FMOO-1. Pasadena, CA: Ins. Techn 2000.
[172] Vasil'ev AA. D.Sc. Dissertation. Novosibirsk.
[173] Desbordes D, Lannoy A. In: Kuhl AL, Leyer J-C, Borisov AA, Sirignano WA, editors. Dynamics of detonations and explosions: detonations. Progress in astronautics and aeronautics series, vol. 133. New York: AIAA; 1991. p. 170–86.
[174] Vasil'ev AA. Combust, Explosion, Shock Waves 1988; 24(2):118–24.
[175] Murray SB, Thibault PA, Zhang F, Bjerketvedt D, Sulmistras A, Thomas GO, Jenssen A, Moen IO. In: Roy G, Frolov S, Netzer D, Borisov A, editors. High-speed deflagration and detonation: fundamentals and control. Moscow: Elex-KM; 2001. p. 139–62.

[176] Teodorczyk A, Lee JH, Knystautas R. In: Kuhl AL, Leyer J-C, Borisov AA, Sirignano WA, editors. Dynamics of detonations and explosions: detonations. Progress in astronautics and aeronautics series, vol. 133. New York: AIAA; 1991. p. 223–40.
[177] Oran ES, Jones DA, Sichel M. Proc R Soc A London 1992; 436:267–97.
[178] Oran ES, Boris JP. In: Kuhl AL, Leyer J-C, Borisov AA, Sirignano WA, editors. Dynamic aspects of detonations. Progress in astronautics and aeronautics series, vol. 153. Washington, DC: AIAA; 1993. p. 241–52.
[179] Brophy CM, Sinibaldi JO, Netzer DW, Kailasanath K. In: Roy G, Frolov S, Santoro R, Tsyganov S, editors. Advances in confined detonations. Moscow: Torus Press; 2002. p. 271–4.
[180] Santoro RJ, Lee S-J, Conrad C, Brumberg J, Saretto S, Lecat P, Pal S, Woodward RD. In: Roy G, Frolov S, Santoro R, Tsyganov S, editors. Advances in confined detonations. Moscow: Torus Press; 2002. p. 243–9.
[181] Thomas GO, Satton P, Edwards DH. Combust Flame 1991; Flame.
[182] Van Tiggelen P. In: Roy G, Frolov S, Santoro R, Tsyganov S, editors. Advances in confined detonations. Moscow: Torus Press; 2002. p. 65–7.
[183] Kuznetsov M, Dorofeev SB, Efimenko AA, Alekseev VI, Bretung W. Shock Waves 1997;7:297–304.
[184] Kuznetsov M, Alekseev V, Matsukov I. In: Roy G, Frolov S, Santoro R, Tsyganov S, editors. Advances in confined detonations. Moscow: Torus Press; 2002. p. 60–4.
[185] Strehlow RA, Adamczyk AA, Stiles RJ. Astronaut Acta 1972;17:509.
[186] Hemeryk L, Lefebvre MH, Van Tiggelen PJ. In: Roy G, Frolov S, Netzer D, Borisov A, editors. High-speed deflagration and detonation: fundamentals and control. Moscow: Elex-KM Publ; 2001. p. 81–96.
[187] Williams FA. Combustion theory. Massachusetts: Addison-Wesley; 1965.
[188] Podgrebenkov AL, Gelfand BE, Kogarko SM, Borisov AA. Doklady USSR Acad Sci 1969;184(4):883.
[189] Kuznetsov M, Alekseev V, Matsukov I. In: Roy G, Frolov S, Santoro R, Tsyganov S, editors. Advances in confined detonations. Moscow: Torus Press; 2002. p. 26–30.
[190] Frolov SM. PhD Thesis; 1987.
[191] Ishii K, Shimizu Y, Tsuboi T, Weber M, Olivier H, Gronig H. In: Roy G, Frolov S, Netzer D, Borisov A, editors. Control of detonation processes. Moscow: Elex-KM Publ; 2000. p. 104–9.
[192] Smirnov NN, Nikitin VF, Boichenko AP, Tyurnikov MV, Baskakov VV. In: Roy G, Frolov S, Kailasanath K, Smirnov N, editors. Gaseous and heterogeneous detonations: science to applications. Moscow: Enas Publ; 1999. p. 65–94.
[193] Kuan TS, Lindstedt RP, Vaos EM. In: Roy G, Frolov S, Santoro R, Tsyganov S, editors. Confined detonations and pulse detonation engines. Moscow: Torus Press; 2003. p. 17–40.
[194] Kerampran S, Desbordes D, Veyssiere B. In: Roy G, Frolov S, Tsyganov S, editors. Advances in confined detonations. Moscow: Torus Press; 2002. p. 16–21.
[195] Veyssiere B, Arrigoni M, Kerampran S. In: Sochet I, editor. J Phys IV. Proceedings of the 4th Symposium (Internatinal) on Hazards, Prevention, and Mitigation of Industrial Explosions, 12(7). EDP Science Publ; 2002. p. 265–71.
[196] Higgins AJ, Pinard P, Yoshinaka AS, Lee JHS. In: Roy G, Frolov S, Netzer D, Borisov A, editors. High-speed deflagration and detonation: fundamentals and control. Moscow: Elex-KM Publ; 2001. p. 45–62.
[197] Achasov OV, Penyazkov OG. In: Roy G, Frolov S, Netzer D, Borisov A, editors. High-speed deflagration and detonation: fundamentals and control. Moscow: Elex-KM Publ; 2001. p. 31–44.
[198] Vasil'ev AA. In: Roy G, Frolov S, Santoro R, Tsyganov S, editors. Advances in confined detonations. Moscow: Torus Press; 2002. p. 31–5.
[199] Achasov OV, Krivosheyev PN, Penyazkov OG, Sevrouk KL, Zhdanok SA. In: Roy G, Frolov S, Santoro R, Tsyganov S, editors. Advances in confined detonations. Moscow: Torus Press; 2002. p. 109–12.
[200] Peraldi O, Knystautas R, Lee JHS. Proceedings of the 21st Symposium (International) on Combustion. 1986. p. 1629–37.
[201] Chue RS, Lee JHS, Scarinci T, Papyrin A, Knystautas R. In: Kuhl AL, Leyer J-C, Borisov AA, Sirignano WA, editors. Dynamic aspects of detonations. Progress in astronautics and aeronautics series, vol. 153. Washington, DC: AIAA; 1993. p. 270–82.
[202] Mitrofanov VV. Theory of detonations in heterogeneous media. Novosibirsk: Novosibirsk University Press; 1988.
[203] Eckhoff RK. Dust explosions in the process industries, 2nd ed. Oxford: Butterworth-Heinemann; 1997.
[204] Dabora EK, Ragland KW, Nicholls JA. Astronaut Acta 1966; 12(1):9–16.
[205] Pierce TN, Nicholls JA. Astronaut Acta 1972;17(4–5):703.
[206] Bowen JR, Ragland KW, Steffes FJ. Proceedings of the 13th Symposium (International) on Combustion. Pittsburgh, PA: The Combustion Institute; 1976. p. 1131–9.
[207] Pinaev AV. Combust, Explosion, Shock Waves 1978;1: 81–9.
[208] Edwards CF, Knappe BM. In: Roy GD, Strykowski PJ, editors. Proceedings of the 13th ONR Propulsion Meeting; 2000. p. 146–51.
[209] Knappe BM, Edwards CF. In: Roy GD, Gupta A, editors. Proceedings of the 15th ONR Propulsion Meeting, College Park, MA: University of Maryland; 2002.
[210] Frolov SM, Basevich V, Ya , Aksenov VS, Polikhov SA. In: Roy G, Frolov S, Santoro R, Tsyganov S, editors. Advances in confined detonations. Moscow: Torus Press; 2002. p. 150–7.
[211] Zhang F, Greilich P, Groenig H. Shock Waves 1992;2(2): 81–8.
[212] Ingignoli W, Veyssiere B, Khasainov BA. In: Roy GD, Frolov SM, Kailasanath K, Smirnov NN, editors. Gaseous and heterogeneous detonations: science to applications. Moscow: Enas Publ; 1999. p. 337–50.
[213] Papavassiliou J, Makris A, Knystautas R, Lee JHS, Westbrook CK, Pitz WJ. In: Kuhl AL, Leyer J-C, Borisov AA, Sirignano WA, editors. Dynamic aspects of explosion phenomena. Progress in astronautics and aeronautics series, vol. 154. Washington, DC: AIAA; 1993. p. 148–69.
[214] Wolanski P, Lee B, Sichel M, Kauffman CW, Nicholls JA. In: Bowen JR, Manson N, Oppenheim AK, Soloukhin RI, editors. Dynamics of shock waves, explosions, and

detonations. Progress in astronautics and aeronautics series, vol. 94. New York, NY: AIAA; 1984. p. 241–63.
[215] Peraldi O. These de Docteur-Ingeneur. Poitiers, France: E.N.S.M.A.; 1985.
[216] Borisov AA, Khasainov BA, Veyssiere B, Saneev EL, Khomik SV, Fomin IB. Chem Phys Rep 1991;10(2):250–72.
[217] Tulis AJ, Sumida WK, Heberlein DC, Patel DL, Egghart H, Proceedings of the 5th Colloquium (International) on Dust Explosion, Pultusk, Poland; 1993. p. 391–400.
[218] Khasainov BA, Veyssiere B. In: Dynamic aspects of detonations. Kuhl AL, Leyer J-C, Borisov AA, Sirignano WA, editors. Progress in astronautics and aeronautics series, vol. 153. Washington, DC: AIAA; 1993. p. 447–61.
[219] Borisov AA, Gelfand BE, Timofeev EI, Tsyganov SA, Khomik SV. In: Flames, lasers, and reactive systems. Bowen JR, Manson N, Oppenheim AK, Soloukhin RI, editors. Progress in astronautics and aeronautics series, vol. 88.; 1983. p. 239–51.
[220] Akbar R, Thibault PA, Harris P. AIAA Paper No. 2000-3592. 2000.
[221] Gladilin AM, Grigorov AI, Sagidullin GG. Detonation processes in two-phase media. Moscow: Nedra; 1991.
[222] Mitrofanov VV, Pinaev AV, Zhdan SA. Acta Astronaut 1979;6(3/4):281–96.
[223] Zhdan SA. Combust, Explosion, Shock Waves 1981;17(6): 105–11.
[224] Zhdan SA. Abstracts of the 8th ICDERS, Minsk, USSR. 1981.
[225] Voronin DV, Zhdan SA. Combust, Explosion, Shock Waves 1984;20(4):112–6.
[226] Nicholls JA, Bar-Or R, Gabrijel Z, et al. AIAA J 1979;288:4.
[227] Kutushev AG, Shorohova LV. In: Roy GD, Frolov SM, Santoro R, Tsyganov S, editors. Advances in confined detonations. Moscow: Torus Press; 2002. p. 161–6.
[228] Veyssiere B, In: Bowen JR, Mansion N, Oppenheim AK, Soloukhin RI, editors. Dynamics of Shock Waves, explosions and detonations. AIAA progress in astronautics and aeronautics, vol. 94; 1984. p. 264–76.
[229] Webber WT, Proceedings of the 8th Symposium (International) on Combustion, Baltimore: Williams and Wilkins; 1960.
[230] Borisov AA, Gelfand BE, Gubin SA, Kogarko SM, Podgrebenkov AL. J Prikl Mekh Tekhn Fiz 1970;1:163–73.
[231] Borisov AA, Gelfand BE, Gubin SA, Kogarko SM, Podgrebenkov AL. Doklady USSR Acad Sci 1970;190(3):621–4.
[232] Webber WT, Cramer FB. Proceedings of the 10th Symposium (International) on Combustion. New York: Academic Press; 1965.
[233] Frolov SM, Basevich VYa, Aksenov VS, Polikhov SA. J. Propulsion and Power, 2004; 20(6).
[234] Zel'dovich YaB. J Tech Phys 1940;10(17):1455–61.
[235] Frolov SM, Barykin AE, Borisov AA. Adv Chem Phys 2004; 23(3):120–9.
[236] Frolov SM. Zh Tyazheloe Mashinostroenie (J Heavy Ind) 2003;9:19–22.
[237] Povinelli LA. NASA/TM-2001-211080; 2001.
[238] Heiser WH, Pratt DT. Propulsion Power 2001;18(1).
[239] Povinelli LA, Yungster S. NASA/TM-2002-211575; 2002.
[240] Nicholls JA, Dabora EK, Proceedings of the 8th Symposium (International) on Combustion, Pittsburgh, PA: The Combustion Institute; 1962. p. 644–55.
[241] Roy GD. AIAA Paper No. A99-34128 1999.
[242] Mitrofanov VV, Zhdan SA. In: Roy G, Frolov S, Santoro R, Tsyganov S, editors. Confined detonations and pulse detonation engines. Moscow: Torus Press; 2003. p. 177–84.
[243] Ma F, Choi J-Y, Wu Y, Yang V. In: Roy G, Frolov S, Santoro R, Tsyganov S, editors. Advances in confined detonations. Moscow: Torus Press; 2002. p. 231–4.
[244] Kailasanath K, Patnaik G, Li C. In: Roy G, Frolov S, Netzer D, Borisov A, editors. High-speed deflagration and detonation: fundamentals and control. Moscow: Elex-KM Publ; 2001. p. 193–206. p. 193–206.
[245] Nicholls JA, Wilkinson HR, Morrison RB. Jet Propulsion 1957;27(5):534–41.
[246] Kailasanath K. In: Roy G, Frolov S, Santoro R, Tsyganov S, editors. Advances in confined detonations. Moscow: Torus Press; 2002. p. 207–12.
[247] Wintenberger E, Austin J, Cooper M, Jackson S, Shepherd JE. AIAA Paper No. 2001-3811 2001.
[248] Falempin F, Bouchaud D, Forrat B, Desbordes D, Daniau E. AIAA Paper No. 2001-3815 2001.
[249] Fujiwara T, Kawai S. In: Roy G, Frolov S, Santoro R, Tsyganov S, editors. Advances in confined detonations. Moscow: Torus Press; 2002. p. 213–20.
[250] Miyasaka T, Fujiwara T. In: Roy G, Frolov S, Santoro R, Tsyganov S, editors. Advances in confined detonations. Moscow: Torus Press; 2002. p. 267–70.
[251] Kailasanath K, Li C, Patnaik G. AIAA Paper 99-2634 1999.
[252] Kailasanath K, Li C, Cheatham S. In: Roy G, Gupta A, editors. Proceedings of the 15th ONR Propulsion Meeting, College Park, MD: University of Maryland; 2002. p. 191–6.
[253] Li C, Kailasanath K, Patnaik G. AIAA Paper No. 2000-0314 2000.
[254] Li C, Kailasanath K. AIAA Paper 2002-0610 2002.
[255] Falempin F, Bouchaud D, Forrat B, Desbordes D, Daniau E. AIAA paper 2001-3815 2001.
[256] Cooper M, Jackson S, Austin JM, Winenberger E, Shepherd JE. AIAA paper 2001-3812 2001.
[257] Zhdan SA, Mitrofanov VV, Sychev AI. Combust, Explosion, Shock Waves 1994;30(5):633–57.
[258] Zitoun R, Desbordes D. Combust Sci Technol 1999;144: 93–114.
[259] Li C, Kailasanath K. AIAA Paper 2000-3592 2000.
[260] Borisov AA, Mailkov AE, Sumskoi SI, Shamshin IO, Barykin AE, Komissarov PV, Silakova MA, Elshin RN. In: Roy G, Frolov S, Santoro R, Tsyganov S, editors. Advances in confined detonations. Moscow: Torus Press; 2002. p. 158–60.
[261] Hanson RK, Jenkins TP, Davidson DF, Sanders ST. In: Roy GD, Strykowski PJ, editors. Proceedings of the 13th ONR Propulsion Meeting, Minnesota, MN: University of Minnesota; 2000. p. 140–5.
[262] Bollay W. United States Patent 2,942,412; June 28, 1960.
[263] Winfree DD, Hunter LG. United States Patent 5,937,635; August 17,1999.
[264] Mullagiri S, Gustavsson JPR, Segal C. In: Roy GD, Mashayek F, editors. Proceedings 14th ONR Propulsion Meeting. Chicago, IL: University of Illinois at Chicago; 2001. p. 131–42.
[265] Yang V, Wu YH, Ma FH. In: Roy GD, Mashayek F, editors. Proceedings of the 14th ONR Propulsion Meeting, Chicago, IL: University of Illinois at Chicago; 2001. p. 165–70.

[266] Ma F, Choi J-Y, Wu Y, Yang V. In: Roy G, Frolov S, Santoro R, Tsyganov S, editors. Confined detonations and pulse detonation engines. Moscow: Torus Press; 2003. p. 219–34.
[267] Bussing TRA. United States Patent 5,513,489; May 7, 1996.
[268] Hunter LG. Jr., Louis G, Winfree Don D. United States Patent 5,546,744; August 20, 1996.
[269] Fernandez R, Slater JW, Paxson DE. In: Roy G, Frolov S, Santoro R, Tsyganov S, editors. Advances in confined detonations. Moscow: Torus Press; 2002. p. 264–70.
[270] Hunter LG Jr, Louis G, Winfree DD. United States Patent 5, 557,926; September 24, 1996.
[271] Winfree DD, Hunter Jr. United States Patent 5,615,548; April 1, 1997.
[272] Hunter LG, Jr, Winfree DD. United States Patent 5,579,633; December 3, 1996.
[273] Smirnov NN, Nikitin VF, Boichenko AP, Tyurnikov MV, Baskakov VV. In: Roy G, Frolov S, Kailasanath K, Smirnov N, editors. Gaseous and heterogeneous detonations: science to applications. Moscow: Enas Publ; 1999. p. 65–94.
[274] Smirnov NN, Nikitin VF, Tyurnikov MV, Boichenko AP, Legros JC, Shevtsova VM. In: Roy G, Frolov S, Netzer D, Borisov A, editors. High-speed deflagration and detonation: fundamentals and control. Moscow: Elex-KM Publ; 2001. p. 3–30.
[275] Smirnov NN, Panfilov II, Tyurnikov MV, Berdyugin AG, Dushin VR, Presnyakov YuP. J Hazardous Mater 1997;53: 195–211.
[276] Schauer F, Stutrud J, Bradley R, Katta V, Hoke J. Confined detonations and pulse detonation engines. Moscow: Torus Press; 2003. p. 275–90.
[277] Hancock RD, Gord JR, Shouse DT, Schauer FR, Belovich VM, Roquemore WM. Proceedings of the International Test and Evaluation Association (ITEA) Conference. 1999.
[278] Schauer F, Stutrud J, Bradley R. AIAA paper No. 2001-1129 2001.
[279] Valaev AA Zhimerin DG, Mironov EA, Popov VA. United States Patent 3,954,380; May 4, 1976.
[280] DeRoche M. United States Patent 5,800,153; September 1, 1998.
[281] Baklanov DI, Gvozdeva LG, Scherbak NB. In: Roy GD, Frolov SM, Netzer DW, Borisov AA, editors. High-speed deflagration and detonation: fundamentals and control. Moscow: Elex-KM Publ; 2001. p. 239–50.
[282] Brophy C, Netzer D. Proceedings of the 14th ISABE Symposium, Florence, Italy 1999.
[283] Yang V. In: Roy GD, Strykowski PJ, editors. Proceedings of the 13th Propulsion Meeting, Minneapolis, MN: University of Minnesota; 2000. p. 184–9.
[284] Alexandrov VG, Kraiko AN, Reent KS. In: Roy G, Frolov S, Netzer D, Borisov A, editors. High-speed deflagration and detonation: fundamentals and control. Moscow: Elex-KM Publ; 2001.
[285] Remeev NKh, Vlasenko VV, Khakimov RA, Ivanov VV. Chem Phys Rep 2001;20(7):119–29.
[286] Remeev N, Kh , Vlasenko VV, Khakimov RA, Ivanov VV. In: Roy GD, Frolov SM, Santoro RJ, Tsyganov SA, editors. Advances in confined detonations. Moscow: Torus Press; 2002. p. 238–42.
[287] Desbordes D, Vachon M. In: Bowen JR, Leyer C-J, Soloukhin RI, editors. Dynamics of explosions. Progress in astronautics and aeronautics series, vol. 106. Washington, DC: AIAA; 1986. p. 131–43.
[288] Moen IO, Sulmistras A, Thomas GO, Bjerketvedt D, Thibault PA. In: Bowen JR, Leyer C-J, Soloukhin RI, editors. Dynamics of explosions. Progress in astronautics and aeronautics series, vol. 106. Washington, DC: AIAA; 1986. p. 120–30.
[289] Thomas GO, Edwards DH, Lee JHS, Knystautas R, Moen IO, Wei YM. In: Bowen JR, Leyer C-J, Soloukhin RI, editors. Dynamics of explosions. Progress in astronautics and aeronautics series, vol. 106. Washington, DC: AIAA; 1986. p. 144–54.
[290] Brophy CM, Sinibaldi JO, Netzer DW, Kailasanath K. In: Roy G, Frolov S, Santoro R, Tsyganov S, editors. Confined detonations and pulse detonation engines. Moscow: Torus Press; 2003. p. 59–72.
[291] Brophy CM, Sinibaldi JO, Netzer DW. In: Roy G, Mashayek F, editors. Proceedings of the 14th ONR Propulsion Meeting, Chicago, IL: University of Illinois at Chicago; 2001. p. 171–6.
[292] Yu STJ. In: Roy GD, Mashayek F, editors. Proceedings of the 14th ONR Propulsion Meeting, Chicago, IL: University of Illinois at Chicago; 2001. p. 219–24.
[293] Conrad C, Watts J, Lee S-Y, Woodward RD, Pal S, Santoro RJ. In: Roy G, Mashayek F, editors. Proceedings of the 14th ONR Propulsion Meeting. Chicago, IL: University of Illinois at Chicago; 2001. p. 143–53.
[294] Smirnov NN, Nikitin VF, Boichenko AP, Tyurnikov MV, Kulchitsky AV. In: Roy G, Frolov S, Netzer D, Borisov A, editors. Control of detonation processes. Moscow: Elex-KM Publ; 2000. p. 212–5.
[295] Baklanov DI, Gvozdeva LG, Scherbak NB. In: Roy G, Mashayek F, editors. Proceedings of the 14th ONR Propulsion Meeting, Chicago: University of Illinois at Chicago; 2001. p. 189–94.
[296] Knappe BM, Edwards CF. In: Roy GD, Mashayek F, editors. Proceedings of the 14th ONR Propulsion Meeting, Chicago, IL: University of Illinois at Chicago; 2001. p. 124–30.
[297] Goodner EM, Hydrocarbon fuels, London: Macmillan; 1975.
[298] Schumb WC, Satterfield CN, Wentworth RL. Hydrogen peroxide. New York/London: Reinhold/Chapman & Hall; 1955.
[299] Seryshev GA. Chemistry and technology of hydrogen peroxide. Leningrad: Chemistry Publ; 1984.
[300] Cheung WS, Tilston JR. Proceedings of the 14th ISABE, Florence, Italy. ISABE Paper 99-7278; 1999.
[301] Gueret C, Cathonnet M, Boettner JC, Gaillard F. Proceedings of the 23rd Symposium (International) on Combustion. Pittsburgh, PA: The Combustion Institute; 1990. p. 211.
[302] Sochet I, Pascaud J-M, Gillard P. J Phys IV 2002;12(7): 429–35.
[303] Frolov SM, Kuznetsov NM. In: Roy GD, Gupta A, editors. Proceedings of the 15th ONR Propulsion Meeting, College Park, MD: University of Maryland; 2002. p. 211–8.
[304] Lee JHS, Moen IO. Progr Energy Combust Sci 1980;6(4): 359.
[305] Lee JH, Knystautas R, Yoshikawa N. Acta Astronaut 1978; 5(11–12):971–82.
[306] Oppenheim AK, Introduction to gasdynamics of explosions, courses and lectures, No 48, International Center for Mechanical Sciences, Wien: Springer; 1972.

[307] Nettleton MA. Gaseous detonations: their nature, effects and control. London: Chapman & Hall; 1987.
[308] Korobeinikov VP, Markov VV, Semenov IV, Pedrow PD, Wojcicki S. In: Roy G, Frolov S, Netzer D, Borisov A, editors. High-speed deflagration and detonation: fundamentals and control. Moscow: Elex-KM Publ; 2001. p. 289–302.
[309] Mitrofanov VV. In: Roy G, Frolov S, Kailasanath K, Smirnov N, editors. Gaseous and heterogeneous detonations: science to applications. Moscow: Enas Publ; 1999. p. 181–96.
[310] Gavrilenko TP, Krasnov AN, Nikolaev YuA. Combust, Explosion, Shock Waves 1982;18(2):127–31.
[311] Gavrilenko TP, Prokhorov ES. Combust, Explosion, Shock Waves 1981;17(6):121–5.
[312] Borisov AA. In: Roy G, Gupta A, editors. Proceedings of the 15th ONR Propulsion Meeting, College Park, MD: University of Maryland; 2002. p. 219–24.
[313] Levin VA, Nechaev JN, Tarasov AI. In: Roy G, Frolov S, Netzer D, Borisov A, editors. High-speed deflagration and detonation: fundamentals and control. Moscow: Elex-KM Publ; 2001. p. 223–38.
[314] Bierdon BT, Adamson TC. AIAA J 1988;26(11):1336–45.
[315] Mullagiri S, Segal C. In: Roy G, Frolov S, Netzer D, Borisov A, editors. High-speed deflagration and detonation: fundamentals and control. Moscow: Elex-KM Publ; 2001. p. 263–72.
[316] Pegg RJ, Couch BD, Hunter LG. AIAA Paper No. 96-2918 1996.
[317] Eidelman SX, Yang G, Lottati Z. AIAA Paper No. 98-3877 1998.
[318] Daniau E, Zitoun R, Couquet C, Desbordes D. In: Roy G, Frolov S, Netzer D, Borisov A, editors. High-speed deflagration and detonation: fundamentals and control. Moscow: Elex-KM Publ; 2001. p. 251–62.
[319] Canteins G, Franzetti F, Zitoun R, Desbordes D, Daniau E. In: Roy G, Frolov S, Santoro R, Tsyganov S, editors. Confined detonations and pulse detonation engines. Moscow: Torus Press; 2003. p. 291–304.
[320] Bussing TRA. United States Patent 5,873,240; February 23, 1999.